

**SYNTHESIS OF NANOCOMPOSITE GLASS-LIKE FILMS CONTAINING
SEMICONDUCTOR NANOCRYSTALS AND NOBLE BIMETALLIC
COLLOIDS BY SOL-GEL ROUTE AND THEIR CHARACTERISATION**

**Dissertation
zur Erlangung des Grades
des Doktors der Ingenieurwissenschaften (Dr.-Ing.)
der Naturwissenschaftlich-Technischen Fakultät III
Chemie, Pharmazie und Werkstoffwissenschaften
der Universität des Saarlandes**

**von
Ganesh Suyal**

**Saarbrücken
2002**

Tag des Kolloquiums: 15.03.2002

Dekan: Herr Prof. Dr. R. Hempelmann

Berichterstatter: Herr Prof. Dr. H. Schmidt
Herr Prof. Dr. W. F. Maier

To My Parents

ABSTRACT

Two type of glasses are currently of interest and being studied extensively. One is a glass doped with semiconducting nanocrystals while the other type is doped with noble metal colloids. In addition to their applications in non-linear optics, the first type glasses can also be seen as future optical filters and the second type of glasses can be used as coloured glasses. Therefore the present work was carried out with an objective of synthesising nano-composite glass like thin films containing semiconductor nanocrystals and mixed- and alloy- noble bimetallic colloids using the sol-gel process.

The sol-gel process has successfully been used for the synthesis of nanocomposite thin films containing $\text{CuCl}_x\text{Br}_{1-x}$ ($x = 0 - 1$) nanocrystals. Copper could be stabilised as Cu^+ forming an acid soluble halocuprate complex in solution, in the presence of acetonitrile. These complexes decompose during heat treatment and form copper halide nanoparticles. The formation of acid soluble halocuprate complexes like CuX_2^- and CuX_3^{2-} ($X = \text{Cl}, \text{Br}$) and their decomposition during the heat treatment to CuCl and CuBr was confirmed by the UV-VIS spectroscopy, XRD measurements and HR-TEM analysis. For the synthesis of $\text{CuCl}_x\text{Br}_{1-x}$ ($x > 0 < 1$) nanoparticles in thin films stepwise substitution of chloride by bromide ions was carried out successfully.

The sol-gel process has also been applied for the synthesis of nanocomposite thin films containing alloy and mixed colloids of Ag / Au and Ag / Cu in thin films. Structural and chemical analysis of alloy and mixed nanoclusters in silica matrix was performed by means of UV-VIS spectroscopy, HR-TEM and EDX. UV-VIS spectroscopy has successfully been applied to differentiate between alloy- and phase separated mixed-mixed colloids of gold and silver.

Thin films containing Ag-Au alloy colloids showed one absorption peak. The position of the peak shifts continuously from the absorption maxima of silver (410 nm) to the absorption maxima of gold (530 nm) with an increasing molar ratio of gold. This allows the tuning of the absorption band (and hence the colour) using glass like films containing nanosized alloy colloids. The absorption spectra of Ag / Au mixed colloids on the other hand show two peaks corresponding to the plasmon peak of gold and silver. UV-VIS spectra of Ag / Cu alloy colloids showed two plasmon peaks for the molar ratio of $\text{Ag} / \text{Cu} > 4 : 1$, corresponding to Ag and Cu plasmon resonance. This was due to the limited miscibility of silver and copper in bulk. The theoretical absorption spectra for the alloy- and mixed- colloids of Ag / Au and Ag / Cu were also calculated using Mie theory and a good agreement was found between theoretical and measured spectra.

KURZFASSUNG

Zwei Arten von Gläsern liegen im Schwerpunkt des aktuellen Interesses und werden zur Zeit intensiv untersucht. Dies sind zum einen dotierte Gläser mit halbleitenden Nanopartikeln und solche mit Edelmetallkolloiden. Zusätzlich zu ihren Anwendungen in der nichtlinearen Optik kann man die mit Halbleiterkolloiden dotierten Gläser dabei als zukünftige optische Filter ansehen. Edelmetallkolloidhaltige Gläser können als farbige Beschichtungen verwendet werden. Gegenstand dieser Arbeit war daher die auf dem Sol-Gel-Prozeß basierende Herstellung von nanokomposithaltigen glasartigen Beschichtungen, welche halbleitende Nanopartikel sowie gemischte und legierte Kolloide zweier Edelmetalle enthalten.

Der Sol-Gel-Prozeß konnte erfolgreich zur Herstellung dünner Nanokomposit-Beschichtungen mit inkorporierten $\text{CuCl}_x\text{Br}_{1-x}$ -Nanokristallen ($x = 0-1$) angewandt werden. Dabei gelang es, Kupfer durch einen säurelöslichen Halocuprat-Komplex als Cu^+ in acetonitrilhaltiger Lösung zu stabilisieren. Diese Komplexe zersetzen sich unter der thermischen Verdichtung der Beschichtungen und bilden dabei Kupferhalogenid-Kolloide. Die Bildung von säurelöslichen Halocuprat-Komplexen wie CuX_2^- and CuX_3^{2-} ($x = \text{Cl, Br}$) und ihre thermische Zersetzung zu CuCl bzw. CuBr konnte mit Hilfe von UV-VIS-Spektren, röntgendiffraktometrischen Messungen sowie HR-TEM-Analysen gezeigt werden. $\text{CuCl}_x\text{Br}_{1-x}$ -Nano-partikel konnten erfolgreich durch die schrittweise Ersetzung von Chlorid durch Bromid hergestellt werden.

Der Sol-Gel-Prozeß wurde außerdem zur Herstellung dünner Nanokomposit-Beschichtungen angewandt, welche legierte bzw. gemischte Ag / Au- und Ag / Cu-Kolloide enthielten. An den dabei in der silicatischen Matrix entstandenen Ag / Au- und Ag / Cu-Nano-clustern wurden strukturelle und chemische Analysen in Form von UV-VIS-Spektren, HR-TEM-Aufnahmen und EDX-Spekten durchgeführt. Die UV-VIS-Spektroskopie konnte dabei erfolgreich zur Unterscheidung von legierten Gold- und Silber-Kolloiden gegenüber phasenseparierten gemischten Kolloiden angewandt werden.

Beschichtungen mit legierten Ag/Au-Kolloiden zeigen lediglich eine Absorptionsbande, deren Lage sich kontinuierlich mit abnehmendem Ag / Au Verhältnis vom Silber (410 nm) zum Absorptionsmaximum von Gold (530 nm) verschiebt. Dieses Verhalten erlaubt das Einstellen der Lage der Absorptionsbande und damit der Farbe der glasartigen Beschichtungen. Dagegen zeigen Beschichtungen mit gemischten Ag / Au-Kolloiden zwei Peaks, welche mit der Plasmonbande von Silber bzw. Gold korrelieren. Legierte Ag / Cu-Kolloide mit einem Ag / Cu-Molverhältnis > 4 zeigen im UV-VIS-Spektrum ebenfalls zwei Plasmonbanden, deren Lage jeweils mit der Ag- bzw. Cu-Plasmonbande übereinstimmt. Dies wird durch die begrenzte Löslichkeit von Silber und Kupfer im Bulkmaterial verursacht. Die theoretischen Absorptionsspektren für legierte und gemischte Ag / Au- und Ag / Cu- Kolloide wurden außerdem mit Hilfe der Mie-Theorie berechnet. Dabei konnte eine hinreichende Übereinstimmung zwischen den theoretischen und gemessenen Absorptionsspektren erzielt werden.

ACKNOWLEDGEMENTS

I gratefully acknowledge Professor Helmut Schmidt who gave me the opportunity of working in his group and carry out this research work in outstanding conditions.

In particular I wish to thank my supervisor, Dr. Martin Mennig for his guidance, availability, constant enthusiasm and fruitful suggestions and discussions, which helped me to work my way through this research.

I would like to express my sincere thanks to the following persons:

Dr. U. Werner and Mrs. Haettich for carrying out the HR-TEM investigations.

Dr. Claudia-Fink Straube for her support and invaluable discussions.

My brother Dr. Navin Suyal, who constantly helped me during my Ph.D., without whose support it would have been difficult for me to complete this work.

My sincere thanks to all my colleagues in lab and at the INM, for all their support and providing a great atmosphere to work.

I would like to thank all my personal friends and colleagues for their understanding, co-operation, help, friendship, company and love. My special thanks are due to my friends Habib, Harish, Nicole, Ingo, Thomas and Doris for their support and nice company during my stay in Germany.

Finally I thank my family for encouraging me during these years of studies. Last but not least, I specially wish to thank my wife Prabha for her constant support, patience and for filling my life with joy.

CONTENTS **I**

I INTRODUCTION **1**

II OPTICAL NANO-COMPOSITES: THE STATE OF THE ART **4**

2.1 Synthesis of copper halide containing bulk glasses	5
2.2.2 <i>Copper halide containing glasses by sol-gel route</i>	10
2.2.3 <i>Thin films containing CuCl - CuBr mixed crystals</i>	12
2.2 Bimetallic particles in solution and glasses	15
2.2.1 <i>Synthesis of monometallic noble metal colloids in thin films</i>	17
2.2.2 <i>Synthesis of Bimetallic Particles in Solution</i>	19
2.2.3 <i>Bimetallic particles in thin films</i>	29
2.3 Objective of the present work	32

III EXPERIMENTAL **33**

3.1 Material Used	33
3.2 Synthesis of the sols from GPTS and TEOS	34
3.3 Synthesis of nanocomposite thin films containing CuX (X = Cl, Br) nanoparticles	35
3.3.1 <i>Synthesis of thin films containing CuCl nanoparticles</i>	35
3.3.1.1 Synthesis of copper free reference sol	35
3.3.1.2 Synthesis of sol containing copper and chloride	35
3.3.1.3 Synthesis of thin films containing copper chloride nanoparticles	36
3.3.2 <i>Synthesis of thin films containing CuBr nanoparticles</i>	37
3.3.2.1 Synthesis of sol containing copper and bromide	37
3.3.2.2 Synthesis of nanocomposite thin films containing copper bromide	37
3.3.3 <i>Synthesis of nanocomposite thin films containing CuCl_xBr_{1-x} (x = 1-0) nanoparticles</i>	38
3.4 Synthesis of nanocomposite thin films containing bimetallic colloids of Ag / Au and Ag / Cu	39
3.4.1 <i>Alloy- and mixed- colloids from Ag / Au system</i>	39
3.4.1.1 Synthesis of Ag / Au Alloy colloids in thin films	39
3.4.1.1.1 <i>Synthesis of colloidal gold sol in aqueous solution</i>	40

3.4.1.1.2 <i>Synthesis of SiO₂ sol containing silver</i>	40
3.4.1.1.3 <i>Synthesis of PbO-SiO₂ sol containing silver</i>	40
3.4.1.2 Synthesis of Ag / Au mixed colloids in thin films	42
3.4.2 <i>Alloy and mixed- colloids from Ag / Cu system</i>	44
3.4.2.1 Synthesis of Ag / Cu alloy colloids in thin films	44
3.4.2.2 Preparation of Ag / Cu mixed colloids in thin films	46
IV CHARACTERISATION METHODS	49
4.1 Apparatus Used	49
4.2 UV-VIS Spectroscopy	49
4.3 X-Ray Diffraction Studies	50
4.4 Transmission Electron Microscopy	51
4.5 Differential Thermal Analysis and Thermogravimetry	51
4.6 Spectroscopic Ellipsometry	51
4.7 Profilometry	52
V RESULTS AND DISCUSSIONS	53
5.1 Synthesis and characterisation of thin films containing CuX (X = Cl, Br) nanoparticles	53
5.1.1 <i>CuCl nanoparticles</i>	53
5.1.1.1 UV-VIS spectroscopic characterisation	54
5.1.1.2 The effect of GPTS / TEOS ratio on the formation of CuCl nanoparticles	55
5.1.1.3 The evolution of CuCl nanoparticles as a function of heat treatment	56
5.1.1.4 X-ray diffraction characterisation	58
5.1.1.4. <i>Study of evolution of CuCl nanoparticles using X-ray diffraction analysis</i>	59
5.1.1.5 Effect of post heat treatment on the samples containing CuCl nanoparticles	62
5.1.2 <i>Thin films containing CuBr nanocrystallites</i>	65
5.1.2.1 UV-VIS characterisation	65
5.1.2.1.1 <i>Study of the evolution of CuBr nanoparticles in thin films using UV-VIS spectroscopy</i>	65
5.1.2.1.2 <i>Temperature dependence of Z_{1,2} and Z₃ exciton peaks of CuBr nanoparticles in thin films</i>	68
5.1.2.2 X- ray diffraction characterisation	70

5.1.2.2.1	<i>Study of the evolution of CuBr nanoparticles using X-ray diffraction analysis</i>	72
5.1.2.3	Effect of post heat treatment on the films containing CuBr nanoparticles	73
5.1.3	<i>HR-TEM characterisation</i>	75
5.1.4	<i>Thin films containing $CuCl_xBr_{1-x}$ ($x = 0-1$) nanoparticles</i>	78
5.1.4.1	Stepwise substitution of chloride by bromide ions	78
5.1.4.2	UV-VIS spectroscopic study of the sequential substitution of Cl^- by Br^-	78
5.1.4.3	Comparison of the absorption spectra of CuCl and CuBr	79
5.1.4.4	Study of sequential substitution of Cl^- by Br^- using XRD analysis	82
5.1.5	<i>Summary and Conclusion</i>	84
5.2	Synthesis and characterisation of nanocomposite thin films containing bimetallic colloids of Ag / Au and Ag / Cu	86
5.2.1	<i>Ag / Au system: Thin films containing alloy- and mixed-colloids</i>	86
5.2.1.1	Alloy colloids	86
5.2.1.1.1	<i>Synthesis of colloidal gold particles in solution</i>	87
5.2.1.1.2	<i>Calculation of colloidal turnover of Au colloids in aqueous solution</i>	87
5.2.1.1.3	<i>UV-VIS spectroscopic study</i>	90
5.2.1.1.4	<i>Calculation of theoretical spectra of Ag / Au alloy colloids</i>	94
5.2.1.1.5	<i>Change in absorption peak positions as a function of temperature</i>	95
5.2.1.1.6	<i>DTA-TG Investigations</i>	103
5.2.1.1.7	<i>HR-TEM characterisation of thin films containing Ag / Au alloy colloids</i>	106
5.2.1.1.8	<i>X-ray diffraction characterisation of thin films containing Ag / Au alloy colloids</i>	109
5.2.1.2	Mixed colloids	111
5.2.1.2.1	<i>UV-VIS spectroscopic studies</i>	112
5.2.1.2.2	<i>Calculation of theoretical absorption spectra of Ag / Au mixed colloids</i>	120
5.2.1.2.3	<i>Effect of the tin content of float glass on the formation of mixed colloids</i>	121
5.2.1.2.4	<i>Effect of pre-heat treatment of float glass substrates on the formation of Ag / Au mixed colloids</i>	124
5.2.1.2.5	<i>HR-TEM characterisation</i>	126
5.2.1.2.6	<i>X-ray diffraction characterisation</i>	128
5.2.1.3	Summary and conclusion	129
5.2.2	<i>Ag / Cu system: Thin films containing alloy- and mixed-colloids</i>	131
5.2.2.1	Alloy colloids	131

5.2.2.1.1	<i>Synthesis of colloidal silver containing sol</i>	131
5.2.2.1.2	<i>Calculation of colloidal turnover of Ag colloids in solution</i>	132
5.2.2.1.3	<i>Synthesis of Ag / Cu alloy colloids</i>	133
5.2.2.1.4	<i>UV-VIS spectroscopic studies</i>	134
5.2.2.1.5	<i>Calculation of theoretical absorption spectra of Ag / Cu alloy colloids</i>	137
5.2.2.1.6	<i>HR-TEM characterisation</i>	138
5.2.2.1.7	<i>X-ray diffraction characterisation</i>	141
5.2.2.2	Mixed colloids	143
5.2.2.2.1	<i>UV-VIS spectroscopic studies</i>	143
5.2.2.2.2	<i>Calculation of absorption spectra of Ag / Cu mixed colloids</i>	145
5.2.2.2.3	<i>HR-TEM characterisation</i>	147
5.2.2.2.4	<i>X- ray diffraction characterisation</i>	150
5.2.2.3	Summary and Conclusions	151
VI CONCLUDING REMARKS		153
VII APPENDIX		155
VIII REFERENCES		180

I INTRODUCTION

Colouring of the glasses is an ancient art but compared to this a rather new one in science. Coloration of glasses by metal or non-metal ions (i.e. Co^{2+} , Cu^{2+} , Fe^{2+} , Fe^{3+} , Cr^{3+} , Cr^{6+} , S_x^{2-}) was known to mankind some thousand of years ago in Egypt [1]. In this method of colouring, each batch of glass has to be melted separately and the colours produced are generally diffused and dull.

Another rather modern alternative for the production of coloured glasses is to coat them with a film containing 1 - 10 nano-meter size metal colloids (i.e. Cu, Ag, Au and Pb) [2]. Silver metal colloids are known to produce a yellow colour and gold and copper produce ruby colour. This method allows the generation of very intense colours by a film as thin as 100 nm and this does not necessitate melting a separate batch for each colour.

These intense colours produced by metal colloids are attributed to sharp plasmon resonance bands. It is known that the total absorbance (absorption and scattering) in metal colloids results from the movement of the electrons under the influence of the electric field vector of the incoming light, which leads to a dipole excitation across the particle sphere. The positive polarisation charge acts as a restoring force, which makes the electrons oscillate. Thus the electron density within a surface layer oscillates whereas the density in the interior of the particle remains constant, which is termed as plasmon resonance. It is known that the extinction band due to the copper-, silver- and gold- in visible region can be easily influenced by the concentration and the geometry of the colloidal particles [3-5]. From the theoretical results (Mie theory) and the experimental observations it comes out that colloidal size depends upon the half-width of extinction band, but hardly on the position of the peak maxima. That is the reason, for example, silver always gives the yellow colour. It is known that the area under the extinction band to the first approximation is independent of the colloid size and proportional to the colloid concentration [6].

It is also known [7] that the colour due to colloidal particles can also be changed by changing the dielectric constant of the particle, which in fact can be changed by alloying or mixing of the two metals with different dielectric constant. There have been some attempts to synthesise such intermediate colours by mixed colloids, though it has not been studied extensively.

Such nano-composite thin films containing 1-10 nm size metal particles dispersed in glass matrices have also drawn attention because of their second order non-linear effects those can find applications in developing high speed and low power optical devices for future communication systems. Such non-linearity is known to originate from local field and hot electron effect in the metal particles. The non-linear response time shorter than several pico-seconds and non-linear susceptibilities of the order of 10^{-12} esu have been reported [8]. This value of susceptibility is however not sufficient for realising a practical non-linear device.

This pursuit of materials with high non-linearity has lead to investigations in another related class of materials, i.e., nano-composites containing semiconductor nano-crystals in various matrices. The non-linearity of the compounds contained in this group is of the third order and it mainly originates from quantum confinement and band filling effects [9]. Although such materials have been reported to show non-linear susceptibility $\chi^{(3)}$ of the order of 10^{-9} - 10^{-8} esu [10], it still remains insufficient for the realisation of practical devices [11].

One of the implications of the exciton peaks is that these nano-composites show very sharp absorption edge [24]. If we examine this fact with the background that the commercially known filters show a rather broad and gradually changing absorption edge, semi-conductor nano-crystals doped glasses become important candidates for realising optical filters with a sharp cut-off. Further, filters, which would completely block the UV radiation in the visible light, would be of significant technological importance and it is known that the exciton absorption peaks of Cu-Halides nano-crystallites fall very close to this UV-VIS boundary [33].

Schott [12] and Corning [13] produce some such semiconductor nano-crystals containing filter glasses with a sharp absorption edge. In the fabrication process of such sharp cut filter glass, semiconductor materials (CdS and CdSe) are added to the batch materials in the form of CdO, CdS and elemental sulphur or selenium's. The batch is typically melted with in the range of 1300-1400 °C and then formed using conventional casting techniques. Upon subsequent heat treatment the dopants form nano-crystallites of $\text{CdS}_x\text{Se}_{1-x}$ with a typical diameter of $2r = 10$ nm inside the glasses [14].

Such a high temperature dedicated batch melting process makes these filters costly and thus limits their applicability. Chemical and physical vapour deposition (CVD and PVD) and ion implantation are some other methods for the incorporation of nano-crystallites in glass or onto the surface of glass, which also are cost and time intensive.

The investigation of sol-gel as a new and cheaper alternative for the coating of large area glass substrates has also proceeded at a rapid pace over the last few years and it has been realised that sol-gel can indeed be the method of choice for such large area decorative coatings. Therefore the present work was started with an objective of synthesising nano-composite glass like films containing semiconductor nano-crystals and mixed- and alloy- noble bimetallic colloids using sol-gel route. The synthesis of such coatings and the evaluation of their optical properties and structure have been studied by Jain et al. [15] and Yumoto et al. [16].

II OPTICAL NANO-COMPOSITES: THE STATE OF THE ART

The term 'Nano-composite' describes the materials in which hetero structures of the length scale 1–100 nm are dispersed in a solid matrix. Such materials are promising for various technological applications like mechanical, electronic, magnetic and optical [17]. Optical functionality of nano-composites arises because the elementary excitations like electrons are confined in all the directions in these quasi zero dimensional structures. These samples, thus in principle exhibit discrete energy level structure leading to sharp optical absorption lines. In addition such concentration of the oscillator strength makes them attractive for non-linear optics [18] and electro-optic applications [19].

Two such systems are of interest and are materials containing nano-crystals of compound semiconductor also termed as quantum dots, dispersed in glass matrices and those in which nano-crystalline phase consists of noble metal colloids. The former system is of interest for filters with sharp absorption edges whereas the latter system is being already commercially exploited for colouring of glasses, beside the application potential of both these systems for non-linear optical devices. Therefore, nano-composites containing Cu-halide quantum dots have been synthesised and characterised in the following chapters. As it has been discussed previously, the synthesis of bimetallic colloids presents the possibility of the generation of interesting colours. Bimetallic colloids from Ag-Cu and Ag-Au systems have also been synthesised in glass matrices and characterised for their optical properties and structure.

The conventional method for the synthesis of these materials has been melting followed by the phase precipitation of the nano-particles. The high temperature involved in the melting of the glasses restricts the applications potential of such materials to a narrow domain. Further, it is not possible to synthesise films by melting because of the very high viscosity (2×10^7 Poise for SiO₂ glass at 1600 °C [20]) of molten glass.

The sol-gel process is based on the hydrolysis and poly-condensation of the metal alkoxides and salts and has been investigated as a low temperature alternative of melting. The sol-gel process also facilitates the synthesis of coatings on large substrates. The science and technology of sol-gel is explained in an extensive book by

Brinker and Scherer [21]. Further, [22] and [23] are other important references those cover the fundamentals of sol-gel research and therefore sol-gel processing is not being discussed here. However, the state of the art of copper halide quantum dots and bimetallic noble metal colloids has been summarised in the following sections.

2.1 Synthesis of copper halide containing bulk glasses

A microcrystal in a dielectric matrix of a nano-composite may be treated as the three-dimensional potential well for electrons, holes, excitons etc. The depth of the well in such systems may be of the order of a few electron volts [24]. Since quasi particles have a limited space to move, their energy spectrum is quantized. It has been observed that the quantum size effect in such systems is revealed as a short wavelength shift of the spectra with the decrease of microcrystals size. The value of the quantum size shift is strongly dependent on the coulomb interaction between electron and holes. There are two limiting cases, first is when the microcrystal size 'a' is far less than the exciton radius 'a_{ex}' and the shift of the absorption edge is due to the quantization of the free carriers. The second is when the a_{ex} << a and the size quantization of excitons occur [25].

In strong confinement case where the microcrystal size is far less then the exciton radius a_{ex}, both electron and hole confinement were assumed to be dominant relative to the coulomb interaction [24]. This results in a splitting of both the valence and conduction band into a series of the sub bands. The position of the absorption lines due to interband transitions to quantum sub-levels of the conduction band as a function of the average size 'ā' of the microcrystals can be described by the following expression [25],

$$\hbar\omega_{ln} = E_g + 0.71 \frac{\hbar^2}{2m_e \bar{a}^2} \psi_{ln}^2 \quad (1)$$

Where m_e is the effective mass of the electrons, ψ_{ln} are the roots of the Bessel function [26] and the factor 0.71 appears due to the size dispersion of the microcrystals described by the Lifshitz and Slesov distribution [27].

In the second case for which a_{ex} << a, the coulomb interaction is retained and the exciton is confined. In this case discrete sub-bands of the excitons with lower energy

are formed. This situation has been studied experimentally by Ekimov et al. [31] for CuCl microcrystals.

Copper halides CuCl and CuBr crystallise under normal conditions in the zinc blende structure and constitute a member of group I-VII tetrahedral semiconductors. The 3d electrons of the copper hybridise very heavily with the p-like valence electrons of the halogen, and thus the number of valence electrons per CuCl unit becomes 18 instead of 8. The hybridisation of p- and d- orbitals can be understood by the following figure, which shows the energy levels of CuCl and CuBr, estimated by the method proposed by Seitz [28].

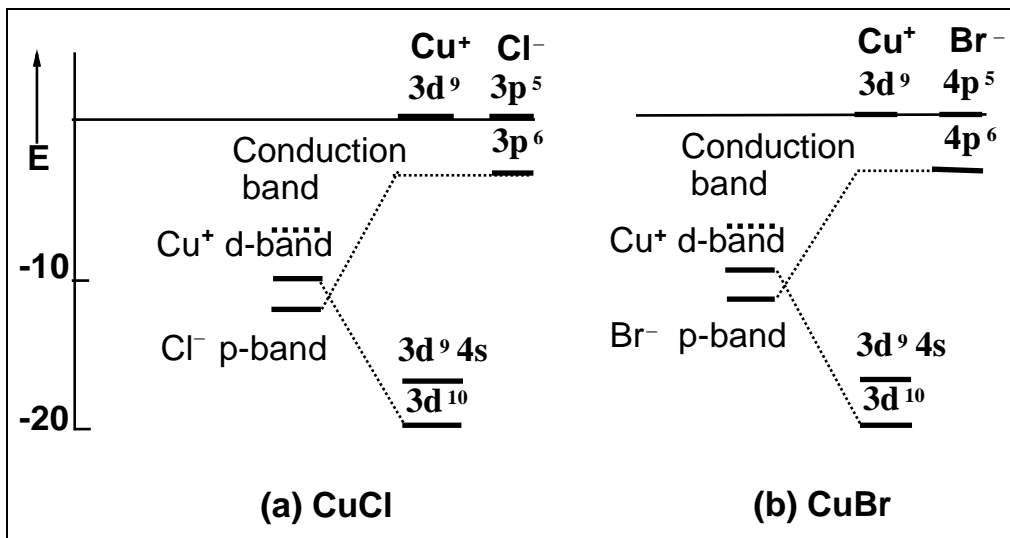


Figure 1: The energy level relations in cuprous halides (CuCl and CuBr) [28].

The figure suggests that the p-bands of anions and the d-bands of cations may be rather close to each other energetically in these compounds. This means that the d-orbital of cation and p-orbital of anion mix strongly at the valence band. This mixing of p- and d- orbitals is the origin of a number of interesting properties of these materials, such as the negative orbit splitting of uppermost valence band of CuCl [29].

Since, in the later case as discussed above discrete sub-bands of the excitons with lower energy are formed, CuCl crystallites show two lines in their absorption spectra as shown in Figure 2 below [42].

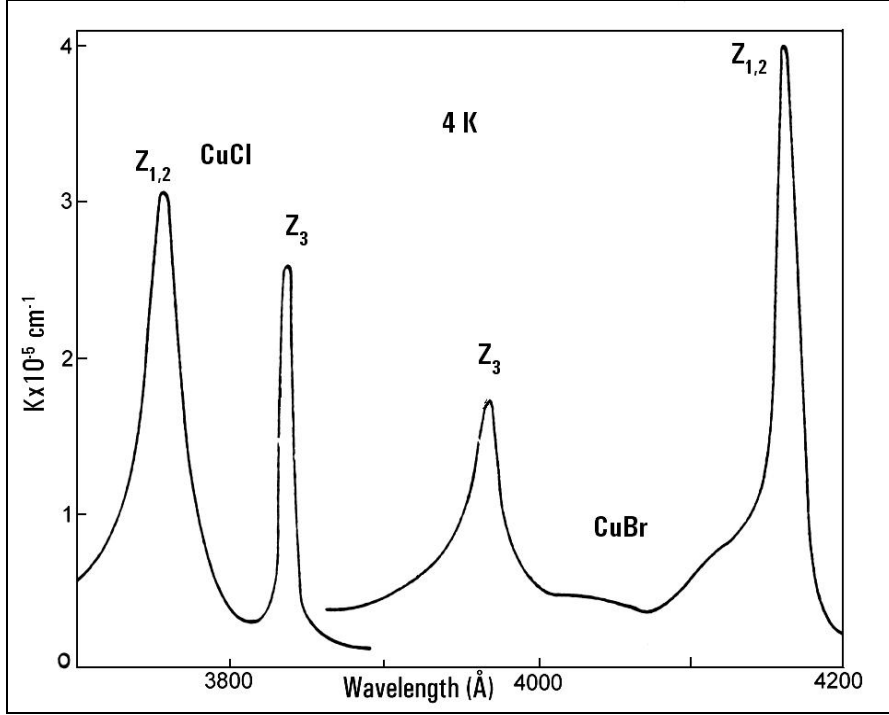


Figure 2: Exciton spectrum of CuCl and CuBr at 4 K [42].

Figure 2 shows the exciton spectrum of CuCl and CuBr at liquid helium temperature. Cardona suggested that the top of the valence band (Γ_{15}) is triply degenerate without spin orbit interaction in the zincblende structure. This degeneracy is reduced by spin-orbit splitting to a doubly degenerate state Γ_8 and a singlet Γ_6 . The doublet (Γ_8) gives the $Z_{1,2}$ peak and singlet (Γ_6) gives Z_3 peak [42].

The spectral position of the Z_3 line originating from the two-fold degenerate sub-band Γ_6 , as a function of the average particle size ' \bar{a} ' can be described by the following expression [30]

$$\hbar\omega_{Z_3} = E_g - E_{ex} + 0.67 \frac{\hbar^2}{2M_s \bar{a}^2} \pi^2 \quad (2)$$

The spectral position of the $Z_{1,2}$ line from four-fold degenerate valence sub-band Γ_8 is given by [30]

$$\hbar\omega_{Z_{1,2}} = E_g - E_{ex} + 0.67 \frac{\hbar^2}{2M_h \bar{a}^2} \left[\psi \left(\frac{M_l}{M_h} \right) \right]^2 \quad (3)$$

Because of these interesting observations, significant efforts have been done to synthesise materials containing cuprous halide micro-crystals in various matrices.

Ekimov et al. [31] have developed a technique for the growth of CuX (X= Cl, Br) semi-conducting micro-crystals in a glassy dielectric matrix. This technique permits to vary the size of the grown micro-crystals in a controlled manner from some tens to thousands of Angstroms. They have also studied the size dependence of the absorption spectra of the number of I-VII and II-VI compounds. With the decrease of the size of the micro-crystals, a considerable short wavelength shift of the exciton lines and the fundamental absorption edge was observed.

Goto et al. [32] have studied the emission, absorption, and reflection spectra of single crystals of cuprous halides. The single crystals were grown by purified CuCl and CuBr, sealed in an evacuated silica tube, 1.5 cm in diameter and 15 cm in length, under hydrogen gas pressure of 1/4 to 1/2 atmosphere. The ingot was first molten in the tube held horizontally in an electric furnace and solidified again by cooling it to room temperature. All these crystals were found to have a zincblende structure. They observed three types of emission spectra namely 1) Resonance emission due to the annihilation of lowest energy intrinsic exciton, 2) Narrow lines due to bound excitons at defects 3) Broad bands and overlapping equidistant narrow bands.

Ruller et al. [33] have synthesised and characterised aluminoborosilicate glass containing Cu(I)Cl microcrystals. The glass containing 1% CuCl was melted in a platinum crucible at 1400 °C, for 2-3 h. They were then annealed between 520-585 °C for three hours. After annealing samples were placed in a preheated furnace for various heat treatment times and temperatures. The average particle size for the samples heated at 585 °C for 4 h was found to be 3.4 nm, whereas for the samples heated at 900 °C for 5 min it was 5.8 nm. They studied the volume of the CuCl particles with the heat treatment time. If the growth is due to the diffusion, the average size of the crystal (R) should increase by $t^{1/3}$ [34].

$$R = 4/9 \alpha Dt^{1/3} \quad (4)$$

where α is surface tension, $D = D_0 \exp (-\Delta E/KT)$ is the diffusion coefficient, and t is the heat treatment time. Thus the average volume should increase linearly with time.

$$R^3 = 4/9 \alpha t \quad (5)$$

Thus based on a straight line between the volume and time they concluded that the crystal grow linearly as a function of time.

Kadono et al. [35] have studied the effect of the glass composition on the precipitation of CuCl crystallites for CuCl doped borosilicate and alumioborosilicate glasses. Alumina was introduced in order to avoid the phase separation of the glass matrices. Reagent grade raw materials SiO_2 , B_2O_3 , Na_2CO_3 and Al_2O_3 were used for the preparation of glasses. Batch mixtures of appropriate compositions with addition of Cu_2O and NaCl were melted in alumina crucible at 1400-1450 °C for 2 h. The melts were quenched between two graphite plates. The glasses were transparent and slightly yellowish owing to very small amount of Cu^{2+} ions. UV-VIS spectra of the borosilicate glass annealed at 580 °C showed an absorption peak at around 370 nm of CuCl excitons, whereas no absorption peak was observed for the aluminoborosilicate glasses annealed at various temperatures. On the basis of these observations they concluded that the phase separation of glass is necessary in order to grow the CuCl nanoparticles in bulk glasses.

CuX (X = Cl, Br) microcrystallite doped glasses were synthesised by Sugimoto et al. [36]. Glass having the composition $10\text{Na}_2\text{O} - 52.5\text{B}_2\text{O}_3 - 7.5\text{Al}_2\text{O}_3 - 30\text{SiO}_2 - \text{YCuX} - 0.5\text{YSnO}$ (molar ratio, Y = 0.5-1) were prepared by melting and heat treatment method. Third order optical non-linearities were measured by a degenerate four wave mixing with two beam configuration. CuCl and CuBr doped glasses exhibited third order optical non-linearities of 10^{-8} - 10^{-7} esu at 385 nm and 410 nm, which corresponded to CuCl and CuBr exciton absorption wavelength respectively. The UV-VIS absorption spectra of the CuCl microcrystallite doped glasses heat treated for 30 min at different temperatures and measured at 77 K showed that the peak shifted toward the lower energy with increase in temperature. Same behaviour was also observed for the glasses doped with CuBr microcrystals. The shift of Z_3 absorption peak of CuCl and CuBr from the bulk crystal ranges from 10 to 60 meV and 20 to 70 meV respectively. These results indicated that the translational motion of the excitons is indeed confined in the microcrystallites.

CuCl microcrystallite doped SiO_2 glass films have been prepared by Tsunetomo et al. [37] using RF sputtering method. Transmission electron microscopy (TEM) measurement showed that the microcrystallites had a spherical configuration. The average size of the microcrystallites was less than 5 nm, and was affected by the preparation conditions and post-deposition annealing time. They compared the observed peak positions with the peak positions of the bulk glasses and observed that

the peaks are shifting slightly to the shorter wavelength side and the peak width become broader.

In all the methods shown above copper halide containing bulk glasses were synthesised by melting and heat treatment, which requires a very high temperature. Further the concentration of copper used is also very limited. High temperature process limits the application of such glasses to a narrow range. Sol-gel method [39] has been explored as a low temperature alternative for the synthesis of such copper halide containing glasses. Sol-gel is an interesting method for the synthesis of coatings on commercial glasses. Some of the efforts to synthesise copper halide containing glasses by sol-gel route are summarised in the following section.

2.2.2 Copper halide containing glasses by sol-gel route

Nogami et al. [38] have applied the sol-gel process to prepare CuCl doped silica bulk glass with a significant quantum sized effect. Gel synthesised by the hydrolysis of a complex solution of $\text{Si}(\text{OC}_2\text{H}_5)_4$ and CuCl with an HCl catalyst was heated to 900 °C to form fine, cubic CuCl crystals. Above 700 °C absorption peaks observed at 370 and 380 nm were attributed to the excitation of the confined $Z_{1,2}$ and Z_3 excitons, respectively, in the CuCl microcrystals. They also studied the UV-VIS absorption spectra of CuCl containing glasses heat treated at 800 °C for different time periods. The energy shift also increased upward with decreasing heat treatment time, indicating crystal growth, and hence the formation of bigger particles on increasing the heat treatment time. Exciton shift to the higher energy side was observed with the decrease in the size of CuCl crystals. The resonant third-order non-linear susceptibility at 77 K was 1.1×10^{-8} esu.

They calculated particle size using an equation [31] relating the particle radius (R) and the lowest energy of the confined Z_3 exciton. Crystal size was found to range from 3 to 6 nm in diameters, and the particle diameter was found to increase from 3 nm to 6 nm with increasing heat treatment time from 0.5 h to 60 h. They compared the growth rate with the results of Ekimov et al. [31] who measured the faster growth rate of CuCl microcrystals in borosilicate glasses. This was attributed to the low viscosity of the borosilicate glasses and hence the faster growth rate.

Nogami et al. [39] have used the sol-gel method to prepare CuBr microcrystal doped glasses also. Glasses containing CuBr microcrystals were prepared by heat treating

the gels synthesised through hydrolysis of a solution of $\text{Si}(\text{OC}_2\text{H}_5)_4$, $\text{Al}(\text{OC}_2\text{H}_5)_3$ and CuBr , heated to $900\text{ }^\circ\text{C}$ in nitrogen atmosphere. Cubic CuBr microcrystals with the diameter ranging from 5 to 8 nm were formed. In the optical spectra of the samples heated above $700\text{ }^\circ\text{C}$, peaks were observed at 3.05 and 3.20 eV at 77 K, which were attributed to $Z_{1,2}$ and Z_3 excitons respectively. The shift of the peak positions to the higher energy side with the decrease in crystal size (quantum size effect) was also observed for the CuBr containing bulk glasses. The limitations of the methods mentioned above are, copper concentration is very low and the exciton peaks are visible at very low temperatures (77 K) only. Because these methods require too high temperatures, they can not be applied for the coating on float glasses.

Reisfeld et al. [40] have synthesised semiconductor quantum dots containing thin films by the sol-gel method. Tetramethoxysilane (TMOS) was used as a precursor for silica for the synthesis of CuCl containing films, and the films were dried only at $40\text{ }^\circ\text{C}$. Absorption spectra of films containing CuCl nanocrystallites, measured at room temperature and prepared with the initial concentration of $\text{Cu}_2\text{O} = 0.061, 0.091$ and 0.122 mole per mole TMOS showed two very weak peaks located at 376 and 384.5 nm in spite of having relatively large concentration of copper.

In order to synthesise CuBr doped films Reisfeld et al. [14] synthesised the sol with the molar ratio of TMOS, water and methanol = 1 : 6 : 11, and 2×10^{-4} M HCl aqueous solution was used for the hydrolysis. Na_2SO_3 , CuBr_2 and HBr were added after 1h hydrolysis. Their corresponding molar ratios were 0.014 / 0.0046 / 0.0015 per mole of TMOS. The average diameter of the copper bromide calculated from the X-ray diffraction using Scherrer's formula was found to be 48 to 52 nm. Addition of the montmorillonite to the precursor decreased the particle size down to 24 nm. UV-VIS spectra measured at room temperature showed very weak exciton peaks of CuBr . As the matrix is not very durable, this process is also unsuitable for making thin films, besides that the particles formed are too big to show a quantum size effect.

Cuprous halide microcrystals containing photochromic sol-gel glasses have been recently synthesised by Facht et al. [41] by the introduction of CuBr dissolved in CH_3CN into a sol-gel Al_2O_3 - SiO_2 glass. For the gel synthesis 33.09 ml $\text{Si}(\text{OC}_2\text{H}_5)_4$ were added dropwise into a mixture of 3.98 ml H_2O , 12.92 ml $\text{C}_2\text{H}_5\text{OH}$ and 0.033 ml HBr (48%) and stirred for 1 h. After that 3.42 g $\text{Al}(\text{OC}_2\text{H}_5)_3$ were added and the mixture was stirred for 20 h at $85\text{ }^\circ\text{C}$. The mixture was cooled down to room temperature and then

0.14 g CuBr (dissolved in 9.13 ml CH₃CN) were added. After a further stirring at room temperature for 3 h, a mixture of 0.26 g Cd(CH₃COO)₂·2H₂O dissolved in 13.06 ml H₂O and 0.11 ml HBr in 0.81 ml C₂H₅OH was then added dropwise to the sol. A stirring at room temperature for an additional 3 h completed the sol synthesis. The sol was covered for 15 days at room temperature and protected from the sunlight. After gelation the sample was dried at room temperature for 10 days. A heat treatment at 280 °C / 2 h and then 410 °C / 2 h in air or O₂ was necessary for the evaporation of solvent and the removal of organics. After that the light blue coloured sample (Cu²⁺) was heated to 700 °C under N₂ atmosphere for the reduction of Cu(II) to Cu(I). The temperature was maintained for 2 h. The light green colour indicated the successful reduction to Cu⁺. These reduced gel glasses showed a darkening by UV irradiation up to 24% and a fading at room temperature up to 13% within 10 min.

In all the methods shown above either the copper concentration used is very limited or the end product (CuX) is very less and the temperatures are far too high, or the matrix is not very durable. Due to the small concentration of CuX the exciton peaks appear as shoulder at room temperature and are clearly visible at very low temperatures (77 K or 4 K) only.

2.2.3 Thin films containing CuCl - CuBr mixed crystals

Cardona et al. [42] have first studied the optical properties (absorption and reflection spectra) of the thin films containing the mixture of copper halides, for energies between the energy gap 3.1 eV and 10 eV. The films containing copper halide alloys were prepared by evaporating a known mixture of the component. The peak positions of Z_{1,2} and Z₃ excitons were plotted against the Br⁻ concentration. It was observed that at x = 0.23 (where x = bromide concentration) both the curves cross each other. It was concluded that at this concentration the spin orbit splitting goes to zero, and after that the position of the multiplet was inverted. It was also observed that in CuCl the Z_{1,2} band locates on the high energy side of the Z₃ but in CuBr the relative positions of the two bands are opposite.

Kato et al. [43] have measured the absorption intensities of two exciton bands in CuCl-CuBr solutions. CuCl and CuBr powders were purified and ingots of solid solutions were prepared by melting the mixture of two materials with variable compositions. Thus prepared ingot was evaporated on a fused quartz plate kept at 120 °C in high vacuum

and the sample on a quartz plate was annealed to room temperature with a cooling rate of 50 °C / h and used for the optical measurements. The UV-VIS measurements were carried out at two different temperatures of 8 K and 77 K and the results of the relative densities of the two exciton bands were the same. The intensities of the two excitons $Z_{1,2}$ and Z_3 , were measured.

From the measured spectra of $\text{Cu}(\text{Br}_x\text{Cl}_{1-x})$ where $x = 1-0$, they observed that in CuCl the absorption area of the higher energy band, the $Z_{1,2}$ is greater than that of the Z_3 and with increasing the Br ion concentration in solid solution the difference in absorption becomes much larger. In CuBr on the other hand the area of the lower energy band, the $Z_{1,2}$ is larger than that of Z_3 band but with increasing Cl concentration the area of the Z_3 becomes larger than that of the $Z_{1,2}$. Namely with decreasing the separation between two band peaks the area of the higher energy band becomes greater than that of the lower energy band regardless to the fact that it is the $Z_{1,2}$ or Z_3 band.

Takahashi et al. [44] have measured the absorption and emission spectra of thin films of CuBr-CuCl solid solutions at 8 and 80 K prepared by the same method used above by Kato et al. [43]. The absorption bands shift continuously with the composition. The peak energies of the Z_3 and $Z_{1,2}$ absorption bands at 80 K were plotted as a function of the concentration of the Br^- ions, x . The variation of the absorption of the peaks-energy is in good agreement with that obtained by Cardona et al. [42]. The cross of the two curves (Z_3 and $Z_{1,2}$) occurs at $x = 0.23$. The band width of the Z_3 exciton band was also found to increase appreciably when the concentration, x , exceeded 0.23 and the band appears on the higher energy side of the $Z_{1,2}$ band. This fact was interpreted in terms of the shorter life time of the higher energy exciton (Z_3) owing to the scattering into the lower state of the $Z_{1,2}$ exciton [45]. When the Z_3 exciton is lower in energy than $Z_{1,2}$ exciton, there is no state for the Z_3 exciton to be scattered except within its own band, and the life time of the exciton is longer, thus the Z_3 band is sharper.

Emission spectra of the thin films of CuBr-CuCl solid solutions at 80 K were recorded by exciting the luminescence by light between 350 and 370 nm in wavelength. For the pure CuBr and the solution of $x = 0.72$ or 0.87 longer wavelength light was used. In the emission spectra only one emission band was observed. The energy of the band peak shifts continuously as a function of the Br^- ion concentration. Emission lines for CuCl

and CuBr were obtained at 389.9 and 420.4 nm respectively. The bandwidths of these emissions were between 6 Å and 20 Å.

Ruller et al. [46] have precipitated $\text{CuCl}_x\text{Br}_{1-x}$ microcrystals in borosilicate glasses. They have reported that the control of heat treatment permits the selective growth of quantum-dots over the range of 50-125 Å. They have used the photochromic glass purchased from 'corning glass works' that contained 1% $\text{CuCl}_x\text{Br}_{1-x}$. The glasses were melted in 1 kg batches for four hours at 1450 °C. The glass slabs were cut into 1 cm³ and heat treated at various temperatures and times. The absorption spectrum of the glass sample containing both chloride and bromide and heat treated at 585 °C for 4 h, recorded at room temperature, showed a peak at 383 nm and a shoulder at 394 nm. The spectrum of the same sample in a continuous flow crystal at 77 K on the other hand showed two clearly resolved peaks at 388 nm and 399 nm respectively.

Various attempts have been made to synthesise copper halide containing bulk glasses. But only a few attempts have been made to synthesise thin films containing CuX (X = Cl, Br) nanoparticles by the sol-gel route. Sol-gel route is a low temperature alternative that allows relatively higher concentration of copper precursor, ease of film formation and a relatively uniform particle size distribution in the films. But the low temperature and the H₂O content of the sol-gel shifts the $\text{Cu}^{2+} / \text{Cu}^+$ equilibrium to Cu^{2+} , thus making it difficult to prepare thin films containing mono-valent copper exclusively. As it is known from the literature that the exciton absorption peaks of copper halide nanocrystallites fall very close to this UV-VIS boundary. The present work is aimed towards the stabilisation of Cu^+ ions in solution resulting the formation of copper halides ($\text{CuCl}_x\text{Br}_{1-x}$, where x = 0-1) in thin films.

2.2 Bimetallic particles in solution and glasses

It has been mentioned in the introduction that noble metal colloids show intense colours because of characteristic absorbance band in the visible region of the absorbance spectra. The light absorption by colloidal metal particles is described by Mie's theory [47] and the absorption coefficient (in $\text{mol}^{-1} \cdot \text{L} \cdot \text{cm}^{-1}$) is calculated from the relation-

$$\alpha = \frac{18\pi}{\ln 10} \frac{10^5}{\lambda} \frac{M n_0^3}{\rho} \frac{\epsilon_2}{(\epsilon_1 + 2n_0^2)^2 + \epsilon_2^2} \quad (6)$$

where λ is the wavelength of light in nanometer, M and ρ are the molecular weight and density of the metal, n_0 is the refractive index of the solvent, and ϵ_1 and ϵ_2 are the real and imaginary parts of the dielectric constant of the metals.

When the size of the particles becomes smaller than the mean free path of the electrons, the absorption bands are broadened, this is taken care of by using size-corrected values of ϵ_2 [48]

$$\epsilon_2 = \epsilon_{2(\text{bulk})} + (\omega_p^2 / \omega^3) (\nu_F / R) \quad (7)$$

where ω is the light frequency, ω_p the plasmon frequency, ν_F the electron velocity at the fermi level, and R the particle radius.

The following Figure 3 shows the electronic energy level and optical transmission of silver schematically. Occupied and unoccupied levels in the 5sp band are shown with full and dashed lines respectively. Interband transitions as indicated by arrow 1, require the participation of a phonon; they do not significantly contribute to the absorption of light. 4d to 5sp interband transitions (arrow 2) starts at a photon energy of about 3.8 eV (or $\lambda = 320 \text{ nm}$) and contribute substantially to the absorption at higher energies.

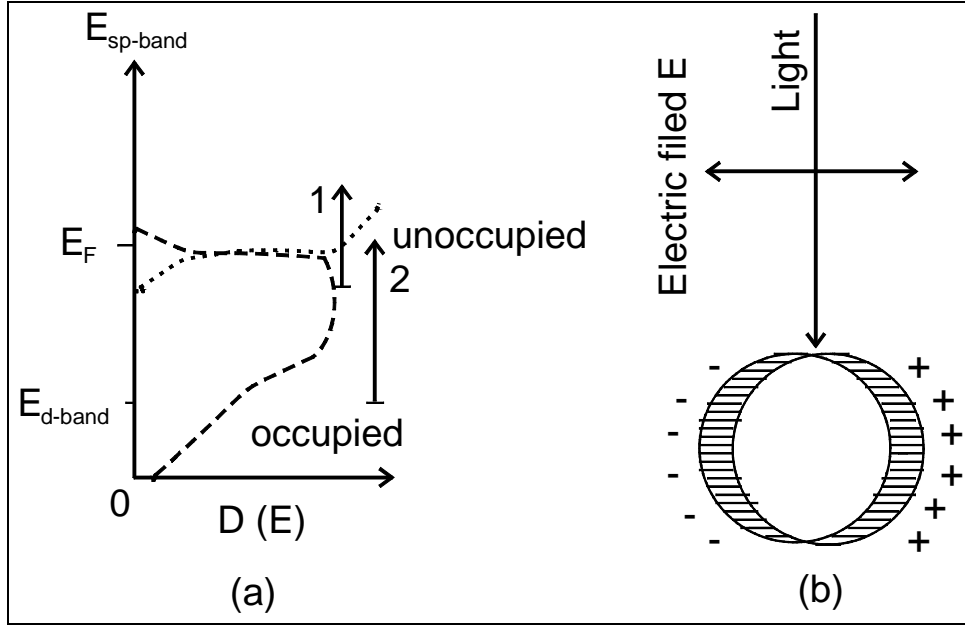


Figure 3 (a) Electronic energy levels and optical transitions in silver, E_F , Fermi energy, $D(E)$, density of states, (b) Polarisation of a spherical metal particle by the electric field vector of the incoming light [49].

However, an intense absorption band is observed for silver particles, which peaks at a lower photon energy of about 3.3 eV ($\lambda = 380$ nm) in aqueous solution. This absorption was resulted due to the collective excitation of all free electrons in the particles. The movement of the electrons under the influence of the electric field vector of the incoming light leads to a dipole excitation across the particle sphere, the positive polarisation charge acting as a restoring force, which makes the electron oscillate. Thus the electron density within a surface layer, the thickness of which is about equal to the screening length of a few angstroms, oscillates whereas the density in the interior of the particle remains constant. This phenomenon is known as the ‘*plasmon resonance*.’

Taking into the consideration the contribution of the plasmon oscillation to the absorption of a metal particle, the Mie equation of the absorption constant is then described by the relation [50]

$$K = 9\pi N V n_o^3 c \lambda^2 / \sigma [(\lambda_m^2 - \lambda^2)^2 + \lambda^2 \lambda_m^4 / \lambda_a^2] \quad (8)$$

where N is the particle concentration, V the volume per particle, and $\lambda_m^2 = \lambda_c^2 (\epsilon_0 + 2n_o^2)$ the wavelength of maximum absorption (e.g., high-frequency dielectric constant of the metal). The plasmon wavelength $\lambda_c^2 = (2\pi c)^2 m / 4\pi N_e e^2$ is a typical metal property. It is

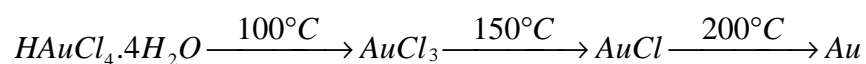
clear from the above expression that the plasmon wavelength (hence the colour) is also dependent to the dielectric function of the metal particles, which in fact can be changed by the alloying of the two different metals.

Because of these intense colours, bulk and thin films containing monometallic colloids have been studied. New methods to generate coatings on glass substrates have been developed and as a result such coloured glasses are commercially available now. Besides coloured coatings such noble metal colloids have also been explored for non-linear optical applications due to their opto-electronic potential. The following section summarises the important results reported in this area.

2.2.1 Synthesis of monometallic noble metal colloids in thin films

Sol-gel route is successfully used for gold-doped silica glasses by Matsuoka et al. [51, 52] and Kozuka et al. [53]. Former authors prepared Au microcrystal doped glass films with high optical non linearity by this route with dip-coating, using $\text{NaAuCl}_4 \cdot 2\text{H}_2\text{O}$ and tetraethoxy orthosilicate (TEOS) as starting materials. And the glass films with an Au/Si atomic ratio of 0.01 to 0.04 were successfully prepared.

Innocenzi et al. [54] have prepared 0.5-0.7 μm thick silica coatings doped with gold metal particles by heating gel films obtained from solutions of acid-catalysed MTES and TEOS mixture containing tetrachloroaurate tetrahydrate. Transparent films with deep blue, red and purple colours were obtained, and changes in size and shape of the gold particles with the MTES content were observed. According to Matsuoka et al. [51], gold ions are present as AuCl_4^- complexes in the gel film heated at 100 °C. These complexes dissolved in the pore liquids may be gradually decomposed to form gold metal particles at around 200 °C according to the following sequence [55].



By using the functionalised silanes as complexing agents [56 - 58], noble metals could be dispersed homogeneously in SiO_2 -xerogels [59, 56], in B_2O_3 - SiO_2 -xerogels [57] and in organic-inorganic and SiO_2 coatings [58, 60]. In these investigations it was proved that the organic groups of the used silanes act as reducing agent for silver and gold. These investigations showed the possibility to control the formation and growth of the colloids and the size of the metal particles in a wide range (5 to 30 nm).

This knowledge was exploited by Spanhel et al. [61] to synthesise metal nanocomposite containing gold nanoparticles with ORMOCER (Organically modified ceramics) matrices by a controlled precipitation process from HAuCl_4 solution. Silanes of the type $\text{NH}_2[(\text{CH}_2)\text{NH}]_x(\text{CH}_2)_3\text{Si}(\text{OR})_3$ (where $x = 1, 2$) were used as stabilising agents, and the formation and properties of ligand stabilised colloidal suspension was investigated. Different ligands influenced the absorption spectra showing surface plasma bands between 380 and 700 nm. With the DIAMO, photo reduction is required for the colloid formation, whereas with TRIAMO the colloid formation occurs spontaneously.

Mennig et al. [62] developed an organic-inorganic synthesis route for the synthesis of transparent SiO_2 coating containing Au colloids. They used four different types of functionalised silane as stabilising ligands for the Au. By varying the kind and concentration of the ligand in the sol the final colloid radii could be controlled in a range between 3 and 30 nm, after densification of the composite coatings on glass at 500 °C.

Mennig et al. [63] have also developed a preparation route for the synthesis of Au colloids in ormocer coatings based on methacryloxypropyl trimethoxysilene (MPTS). Where Au colloids are formed in a very quick low temperature process by UV and IR irradiation during the curing of the matrix.

De et al. [144] have prepared silver nanocrystal doped silica films by sol-gel route. The sol was prepared from 1 : 0.12 : 12 : 0.2 : 6 : 7 molar ratios of $\text{Si}(\text{OC}_2\text{H}_5)_4$: AgNO_3 : $\text{C}_3\text{H}_7\text{OH}$: $\text{C}_4\text{H}_9\text{OH}$. The glassy transparent films with high dopant concentration (Ag / Si atomic ratios = 0.12) were successfully prepared by dip-coating method. After drying in air at 60 °C for 30 min, samples were heat treated in air from 300-550 °C. Measurements on the films were made by UV-VIS and IR-spectroscopy, X-ray photoelectron spectroscopy, rutherford backscattering spectroscopy and transmission electron microscopy.

Nogani et al. [64] have synthesised Cu^{2+} containing SiO_2 and $\text{Al}_2\text{O}_3 \cdot 9\text{SiO}_2$ glasses by sol-gel route. The samples were heated under reducing atmosphere to precipitate small-sized Cu and Cu_2O crystals. Cu^{2+} ions incorporated in SiO_2 glass were reduced by heating in N_2 to precipitate Cu_2O and in H_2 to precipitate Cu microcrystals with diameter of about 5-15 nm.

Thin films containing monometallic particles of noble metals have been synthesised using sol-gel route. But the synthesis of thin films containing bimetallic colloids by sol-gel route has not been studied so far. However these types of films can be of immense interest for the scientific as well as industrial point of view. One interesting concept in the context of bimetallic particles could be their structure i.e., whether such bimetallic particles are formed by the corresponding solid solutions (*alloy colloids*) or they are mixtures of phase separated individual particles (*mixed colloids*). Such alloy and mixed particles can be distinguished on the basis of UV-VIS spectroscopy and EDX analysis of the individual particles.

2.2.2 Synthesis of Bimetallic Particles in Solution

Several methods have been used for the preparation of bimetallic particles in solution, e.g. chemical reduction [65-67] and UV photo-reduction [98, 68] of the mixed solution of two metal salts. Toshima et al. synthesised polymer protected bimetallic particles of Pd-Pt [69] and Pd-Au [70] in solution by the reduction of their ethanol water solutions and studied their catalytic activity.

Vasen et al. [71] have synthesised nanoparticles of Ag-Pd and Cu-Pd alloy colloids in aqueous solution with diameters ranging from 5-40 nm, by employing the heterogeneous reaction of dry methanol or ethanol with the mixtures of $\text{AgNO}_3 + \text{Pd}(\text{NO}_3)_2$ and $\text{Cu}(\text{NO}_3)_2 + \text{Pb}(\text{NO}_3)_2$ respectively. The nanoscale alloys were characterised by energy dispersive X-ray analysis (EDX), transmission electron microscopy (HR-TEM) and X-ray diffraction (XRD). All the alloy particles were found to possess 'fcc' structure.

Itakura et al. [72] have synthesised the bimetallic colloids of gold / silver and silver / copper by the UV irradiation of the mixture of their salts in presence of benzoin as a photo-initiator. An ethanolic solution of the mixtures $\text{AgClO}_4 + \text{Cu}(\text{ClO}_4)_2$ and $\text{HAuCl}_4 + \text{AgClO}_4$ in various molar ratios ($0.1 \text{ mm} / \text{dm}^3$) containing PVP ($0.1 \text{ mmol} / \text{dm}^3$) and benzoin ($0-1 \text{ mmol} / \text{dm}^3$) was de-aerated by bubbling with nitrogen for 2h. A 3 cm^3 portion of the solution was transferred to a rectangular quartz vessel in glove box under nitrogen. UV irradiation was carried out with a 200 W low-pressure mercury lamp. The average diameter of the Ag / Au composite particles increased from 5.1 to 17.0 nm with increasing molar ratio of the gold, and the average diameter for Ag / Cu particles was found to be 3-5 nm. They observed that on increasing the gold

concentration in Ag / Au alloy colloids, absorption peak gradually shifted from the silver to gold plasmon resonance peak. The observed optical spectra were found in good agreement with the calculated spectra for Ag / Au alloy colloids. In case of Ag / Cu the TEM observation showed the presence of phase separated composites which are made partly of silver and partly of copper. The very low metal (Ag, Au, Cu) concentration and the formation of particles in solution only are the limitations of this process.

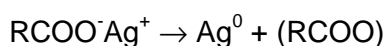
Toshima et al. [65] have prepared colloidal dispersions of polymer protected Cu / Pt and Cu / Pd alloy clusters by reduction of corresponding metal hydroxides with a cold alloying process. Cu / Pd Alloy colloids were synthesised by adding 20 ml dioxane solution of palladium (II) acetate to the 78 mg of $\text{CuSO}_4 \cdot 5\text{H}_2\text{O}$ dissolved in 150 ml of glycol at 80 °C in which 1 g of polyvinyl pyrrolidone was already added as a protective agent. The pH of the solution was adjusted to 10 by adding an aqueous solution of sodium hydroxide. This solution was refluxed at 198 °C for 3 h under a nitrogen flow, to give a colloidal dispersion of bimetallic clusters as a transparent dark brown homogeneous solution.

This method characterised by the formation of bimetallic hydroxide colloids before the reduction by so called polyol process overcomes the problems caused by difference in redox potential between both the metals and to reduce both the metal ions completely. This difference in the redox potentials is the main problem for designing a method to prepare stable bimetallic clusters composed of a noble metal and a light transition metal. The Cu / Pt colloids prepared by this method showed an average diameter of 19 Å for a molar ratio of 1 : 1 and an average diameter of 23 Å for a molar ratio of 3 : 1 with the alloy structure of CuPt and Cu_3Pt , respectively. So formed bimetallic Cu / Pd colloids were found to have a catalytic use in the selective hydration of acrylonitrile to acrylamide.

Wang et al. [73] have shown that the stable polymer protected bimetallic clusters can be obtained if one of the components of the bimetallic clusters located on the surface of the particles during the preparation, is strongly protected by the protective polymer even though the other component cannot be protected by the polymer due to the low co-ordination ability of the polymer on it.

Sato et al. [68] have also prepared Ag-Au composite colloids by the irradiation of aqueous solution of the mixture of gold salt (HAuCl_4) and silver salt (AgClO_4)

containing sodium alginate with 253.7 nm UV light. The particle diameter could be varied from 30-150 nm. Sodium alginate (a high molecular weight carboxylic acid) was found to be useful for the preparation of metal particles in thin films under mild conditions due to their ability to form metallic salts with various cations and its sensitivity to UV-VIS light, as well as the protective action of metal particles. The following mechanism was proposed for the synthesis of metal colloids in presence of sodium alginate.



Subsequent agglomeration processes of Ag^0 produce colloidal silver, $(\text{Ag}^0)_n$.

Morris et al. [74] have synthesised the bi-layered colloids of gold and silver. Starting with gold nuclei of 59 Å in diameter silver layers of 5 to 220 Å in thickness have been grown epitaxially. To grow silver on the gold nuclei silver oxide was reduced with hydroxylamine hydrochloride ($\text{NH}_2\text{OH}\cdot\text{HCl}$), which retards the formation of silver nuclei and favours the rapid growth of silver on the existing gold nuclei. The spectra of these hydrosols containing two layer particles were compared with the theoretical spectra calculated using theory of Aden and Kerker [75]. It was found experimentally that, as long as the thickness of the silver layer is smaller than 80 Å, two peaks were clearly seen in the absorption spectra. One of which was located at the wavelength slightly lower than the colloidal silver absorption peak and the other was located at the wavelength slightly lower than the colloidal gold absorption peak. As the thickness of the silver increases from 100 Å, only one peak due to silver was observed.

Extinction spectra of gold-coated silver clusters and silver coated gold clusters were compared with the extinction spectra of $\text{Ag}_x\text{Au}_{1-x}$ alloy particles embedded in glass by Sinzig et al. [7]. They observed that the conduction electron plasmon resonance is markedly different for both types of samples. In case of one particle coated with the other two peaks were obtained. This is due to the discontinuity of the background contribution to the dielectric constant at the interior interface in core shell clusters, which causes the single plasmon peak of the homogeneous materials to split into complex structure. Their results also indicated that in the Au-nucleus Ag-shell clusters, both the s-electrons from Ag and from Au cover the whole volume of the clusters. This appeared not to hold for the Ag-nucleus Au-shell clusters, pointing to a badly defined interface resulting from the difficulties of Au to grow on a Ag surface. In contrast the

alloy clusters exhibit a continuous shift of the plasmon peak with concentration of the Au to Ag position as expected from band structure model.

Gold was deposited onto colloidal silver (mean particle size 7.6 nm) in aqueous solution, by Mulvaney et al. [76] and the composite particles were studied by electron microscopy and spectrophotometry. The silver sols were prepared by γ -irradiation of de-aerated solution containing 50 or 100 μM AgClO_4 , 0.1 M 2-propanol, 0.01 M acetone, and 0.1 mM sodium polyphosphate, $(\text{NaPO}_3)_n$. The irradiation produced a silver sol with an absorption coefficient at the band maximum (380 nm) of $1.9 - 2.0 \times 10^4 \text{ M}^{-1}\text{cm}^{-1}$. De-aerated $\text{KAu}(\text{CN})$ solution was then added to the sol and the solution was re-irradiated.

Mulvaney [77] has calculated the absorption spectra of gold-silver alloy sols and gold-coated silver sols as shown below in Figure 4.

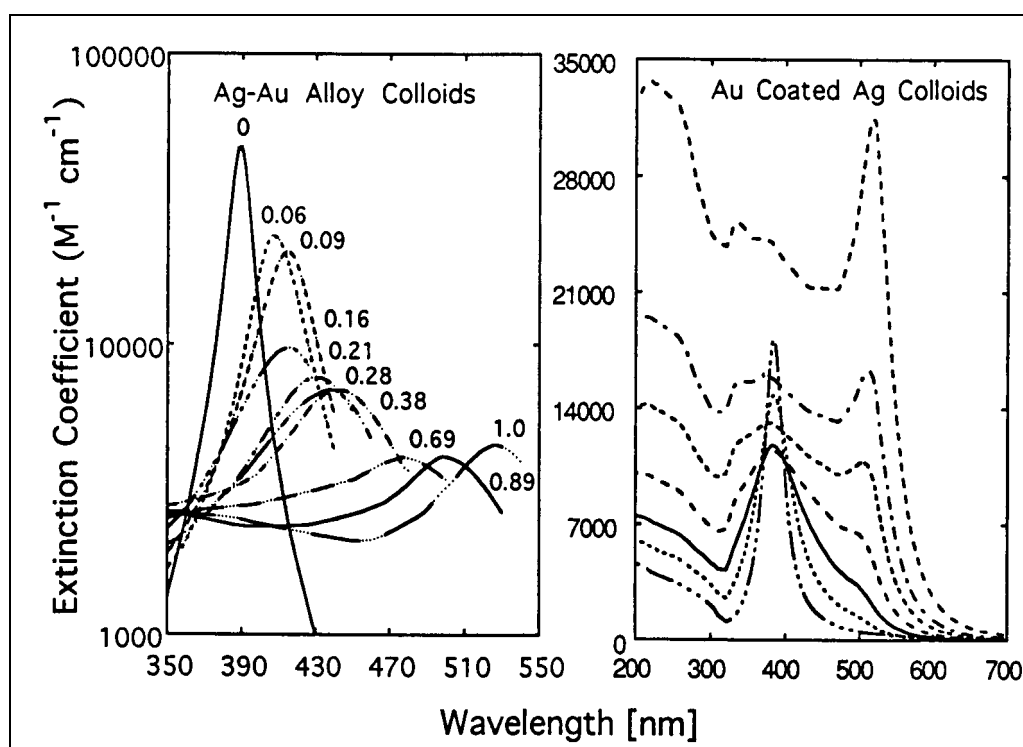


Figure 4: (left) Calculated spectra for 6 nm sized particles of Au/Ag alloys of various composition in water using Mie equation and the dielectric data from the references [78] and [79]. The numbers refer to the mole fraction of gold, (right) Calculated spectra of Au coated Ag- colloids in water for core radius = 3.0 nm, gold layer thickness used were 0, 0.32, 0.6, 1.0, 1.5, 2.0 and 3.0 nm [77].

It is obvious that whereas gold deposition on silver should result only in damping of the underlying silver surface plasmon band [49], alloy formation is accompanied by a continuous red shift in the band with increasing gold content. The origin of the red shift in the case of Au / Ag alloy colloids is quite interesting as the silver and gold have identical bulk plasma frequencies, so a peak shift due to a changing electron density is not expected. However the high frequency dielectric constants are quite different [156], primarily because the interband transitions in gold extend across most of the visible spectrum. The absorption band shift in this case is due to the perturbation of the d-band energy levels and not to changes in the free electron concentrations [77]. This results in a steady increase in the effective value of ϵ^∞ for the alloys and consequently, a red shift in the position of the absorption band. The fact that a linear shift is found between the peak position and the gold concentration by Papavassilou [80] as predicted using Ripken's [79] data, can be explained if the alloy dielectric function takes the form $\epsilon(\alpha) = (1-\alpha) \epsilon_{Ag} + \alpha \epsilon_{Au}$, where α is the mole fraction of Au in the particles [81].

Baddeley et al. [82] have synthesised ligand stabilised bimetallic colloids of Au / Pd starting from 18-20 nm Au colloids which were covered by Pd shells of different thicknesses. 16 ml of a 1% solution of HAuCl_4 and 80 ml of 1% tri-sodium citrate were added gradually to 1600 ml of vigorously stirred, boiling demineralised water. Boiling was continued for further 1 h yielding a ruby red gold sol. The sol was diluted to 8 l and 83 ml of a 0.037 M solution of H_2PdCl_4 was added over a period of 8 h simultaneously with 100 ml of a 1% solution of $\text{NH}_2\text{OH}\cdot\text{HCl}$. After 48 h stirring at room temperature, 2 g of $\text{p-H}_2\text{NC}_6\text{H}_4\text{SO}_3\text{Na}$ was added to stabilise the particles. HR-TEM observations indicated a narrow particle size distribution and revealed a well-defined Au (core) / Pd (shell) structure. Thermal treatment of these particles led to Au / Pd alloy formation. Lee et al. [83] have used the above prepared bimetallic particle with Au core and Pd shell, as an efficient catalyst for coupling and cyclization of acetylene, even at room temperature.

Mono-dispersed bimetallic palladium-copper nanoscale colloids were synthesised by Bradley et al. [84] by heating mixtures of palladium acetate and copper acetate hydrate in 2-ethoxyethanol to reflux (135 °C) in the presence of polyvinylpyrrolidone (MW = 40000) for 2 h. The resulting dark brown precipitate was filtered through 0.2 μm teflon filter and stored under nitrogen. Metal particles were characterised by TEM, selected

area diffraction and single particle EDX analysis. The particles in size ranging from 3 to 4 nm were obtained.

Esumi et al. [85] have prepared bimetallic colloids of Pd-Cu / Cu₂O by the thermal decomposition of their acetate compounds dissolved in methyl isobutyl ketone and bromobenzene. In methyl isobutyl ketone, the average diameter of Pd-Cu₂O colloids decreases from about 130 to 50 nm with an increase in molar fraction of palladium acetate, whereas in bromobenzene the size of Pd-Cu colloids increases from about 8 to 15 nm. The big difference in the particle size in two cases was explained by different nucleation rates. The nucleation rate in bromobenzene (having a higher boiling point than methyl isobutyl ketone) is much faster than that in methyl isobutyl ketone, resulting in a larger number of nuclei in the former and smaller particle sizes.

Pd - Pt bimetallic colloids were prepared by Esumi et al. [67] by the reduction of their corresponding salts extracted in organic solvents (cyclohexane, chloroform) with hydrazine or sodium borohydride. Trioctylphosphine oxide (TOPO) and distearyldimethylammonium chloride (DDAC) were used as extractants. Particle size was varied from 20-30 nm, and the reduction by hydrazine provided larger particles than by NaBH₄. It is likely as NaBH₄ being a stronger reducing agent than hydrazine would produce a large number of nuclei, resulting in a smaller mean particle size.

Mulvaney et al. [86] have synthesised bimetallic colloids of lead and gold by the reduction of lead ions on the surface of colloidal gold. 36 mg of KAuCl₄ was added to 285 ml of water, and the solution heated to boiling point (80 °C). 15 ml of 1% sodium citrate solution was added rapidly to the stirred gold solution. The solution was boiled for further 20 min to get the colloidal gold sol having the mean particle diameter of 18 nm. The maximum was obtained at 519 nm with an absorption coefficient of 3910 M⁻¹cm⁻¹. In order to coat the particle with a second metal, polyvinylsulfate was first added to the sol and then the second metal was added as perchlorate salt. When no stabiliser was added the sol coagulated upon the addition of the second metal ion. This is because the gold sol was stabilised by free citrate ions, which are readily neutralised by the heavy metal ions. The plasmon band of lead starts to assert itself after just two monolayers. More monolayers of lead atoms dampen the plasmon absorption of gold and cause a blue shift. It was proposed that the blue shift was not due to the change of the dielectric constant of the medium but was due to the double layer charging and the changes in the electron concentration in the surface layers due to the presence of the

absorbed lead atoms. Pb atom will act as electron donors in contact with gold metal, and the effective electron density of the surface layers will be increased by the formation of polar Pb-Au bond.

Liz-Marzan et al. [87] have prepared bimetallic dispersions by the simultaneous reduction of two metallic salts with borohydride, in the presence of imogolite rods (imogolite is an aluminosilicate with net composition $(\text{OH})_3\text{Al}_2\text{O}_3\text{SiOH}$ and consists of hollow tubes with an external diameter of about 2 nm and a length in the range of 400-1000 nm). Depending on the particular metals and on their relative concentrations, both the size distribution and the optical properties of the obtained dispersions changed noticeably.

Samples were prepared for all three possible combinations of Pt, Ag and Au, with the following molar ratios for every pair: 10 : 0, 8 : 2, 6 : 4, 4 : 6, 2 : 8, 0 : 10. In every preparation the total molar concentration of metal ions was 2×10^{-4} M, and excess reductant (10^{-3} M) was added. They observed that for monometallic dispersions, at constant metal concentration, an increase in the concentration of the reductant leads to the formation of smaller particles. This is probably due to a faster metal reduction rate when a larger amount of the reductant is present.

When they compared the particle sizes of different metals, they observed that the sequence is $\text{Ag} > \text{Au} > \text{Pt}$. This sequence was tried to correlate with the redox potentials. The standard redox potentials E° for the relevant redox couples at 1M are [88]



Which do not follow the sequence shown by the particle size. However this trend is a thermodynamic one, which does not include any kinetics. They assumed a kinetic control and gave a different argument to explain the sequence. For silver only a one-electron reduction is performed, which is kinetically much easier than the multi-electron reduction, in which several unstable valence states are passed through, thus slowing the rate down. For the bimetallic particles they observed that the simultaneous reduction of the two kinds of metallic salts leads to the formation of the composite

particle rather than the mixture of the two single particles. In case of Ag / Pt core shell structure was observed with silver as core. It was explained by the fact that the metal easier to reduce will nucleate first, and the formed nuclei will serve as a centre for heteronucleation of the second metal. According to this silver should always be a core metal.

Silvert et al. [89] have given a synthesis route of nanoscale Ag-Pd alloy colloids. Monodisperse suspensions of Ag-Pd (70 / 30 at. wt.%) particles have been prepared at 120 °C from the ethylene glycol solution of polyvinylpyrrolidone (PVP), silver and palladium nitrates. X-ray diffraction of this material confirms that the diffraction angle (2θ) for each scattering peak of this diffraction pattern coincides neither with those of pure silver nor with pure palladium metal, clearly indicating that the bimetallic Ag-Pd particles are true solutions and not co-precipitates of Ag and Pd. The amount of PVP added to the preparation is critical for preventing interparticle sintering, to control the average particle size of the polymer stabilised Ag-Pd alloy colloids. Bimetallic Ag-Pd colloidal dispersions with a narrow size distribution and an average particle size of 14 nm and 7 nm were synthesised after identifying the optimum polymer / precursor / solvent ratios.

Torigoe et al. [90] have prepared bi-metallic silver-palladium colloids by reduction of silver (I) bis (oxalato) palladate (II) with 253.7 nm UV light in the presence of poly (N-vinyl-2-pyrrolidone). The particles size was ranged from 3 to 11 nm in the 5×10^{-3} mol / lit PVP system. EDX profiles reveal that each particle is bimetallic Ag-Pd, although the composition was not uniform. Optical spectra of these colloids show a plasmon resonance band at 330-375 nm.

Torigoe et al. [91] have also described the synthesis of colloidal silver-platinum alloys. Silver-platinum alloys have been prepared by NaBH_4 reduction of silver(I) bis(oxalato)platinate(II) ($\text{Ag}_2[\text{Pt}(\text{C}_2\text{O}_4)_2]$) in ethylene glycol. The HR-TEM micrographs show that the metal particles thus prepared have homogeneous (111) lattice spacing of $2.31 \pm 0.02 \text{ \AA}$, which is an intermediate value between those of monometallic Ag and Pt colloid indicating that they are Ag-Pt alloys. The same trend is found in the XRD profiles. Optical spectra of the Ag-Pt alloy colloids show a plasma resonance band at 354 nm. The peak wavelength shifts in the range of 330-410 nm by varying the Ag/Pt ratio. The alloy formation has been studied by step by step reduction of $\text{Ag}_2[\text{Pt}(\text{C}_2\text{O}_4)_2]$.

It is suggested that the reduction of $[\text{Pt}(\text{C}_2\text{O}_4)_2]^{2-}$ takes place by catalytic action of the Ag particles to form the Ag-Pt alloy.

Aihara et al. [92] have prepared bimetallic colloids of gold and silver in laponite suspension by reducing the mixture with the help of sodium borohydrate. A 2 cm³ aqueous solution of mixture of metal salts (AgNO₃ and HAuCl₄) was added into a 17 cm³ aqueous suspension of laponite (0-15 g / lit) with stirring. Then to reduce metal ions in the suspension, 1 cm³ of freshly prepared aqueous solution of sodium borohydrate (10 mmol dm⁻³) was added to the suspension with stirring at room temperature. The final concentrations of Laponite, metal salts and sodium borohydride were 0 -12.7 g / lit, 1.0×10^{-4} mol / lit and 0.5×10^{-3} mol / lit respectively. Appearance of only one UV - VIS absorption peak shifting from the 401 (pure silver) to 525 nm (pure gold) with increasing ratio of gold was attributed to the formation of gold / silver alloy colloids.

Yonezawa et al. [93] have prepared three types of polymer protected bimetallic clusters of noble metals (Au, Pt and Pd) by simultaneous alcohol reduction. These particles were found to have totally core shell structure, on the basis of X-ray diffraction and quantitative X-ray photoelectron spectroscopic measurements. Palladium (II) chloride (PdCl₂, 5.9 mg, 3.3×10^{-5} mol) was added to ethanol (25 cm³) and stirred overnight resulting a clear yellow solution. Hexachloroplatinic(IV) acid (H₂PtCl₆.6H₂O) and tetrachloroauric(III) acid (HAuCl₄.3H₂O) were dissolved in water. In case of Pd-containing bimetallic clusters, i.e. Pd / Pt and Au / Pd, two metal ion solutions were mixed with water and ethanol added to form 50 cm³ of water-ethanol (1 : 1 v/v) solutions having a total metal concentration of 6.6×10^{-4} mol/lit. PVP, (40-41 mol / mol of total amount of metal ions), was added to each mixed solution as a protective agent. The mixture in a 100 cm³ flask was heat treated at 90-95 °C to reflux the mixed solution for 1-2 h depending on the elements. A clear homogeneous and stable dispersion of polymer protected bimetallic clusters was obtained.

They have explained the role of the protective polymer (PVP) in the formation of nanoscopic bimetallic clusters. The protective polymers can co-ordinate to noble metal ions before reduction [94] and then make a polymer metal ion complex. The metal ions can be reduced under mild conditions so that the resulting colloidal metal clusters are smaller and have narrower size distribution than those prepared without protective polymers. In the case of bimetallic clusters, the protective polymers can play another

important role to control the structure, in addition to the formation of the polymer-metal ion complex for smooth and mild reduction. The proposed mechanism is schematically shown below in Figure 5.

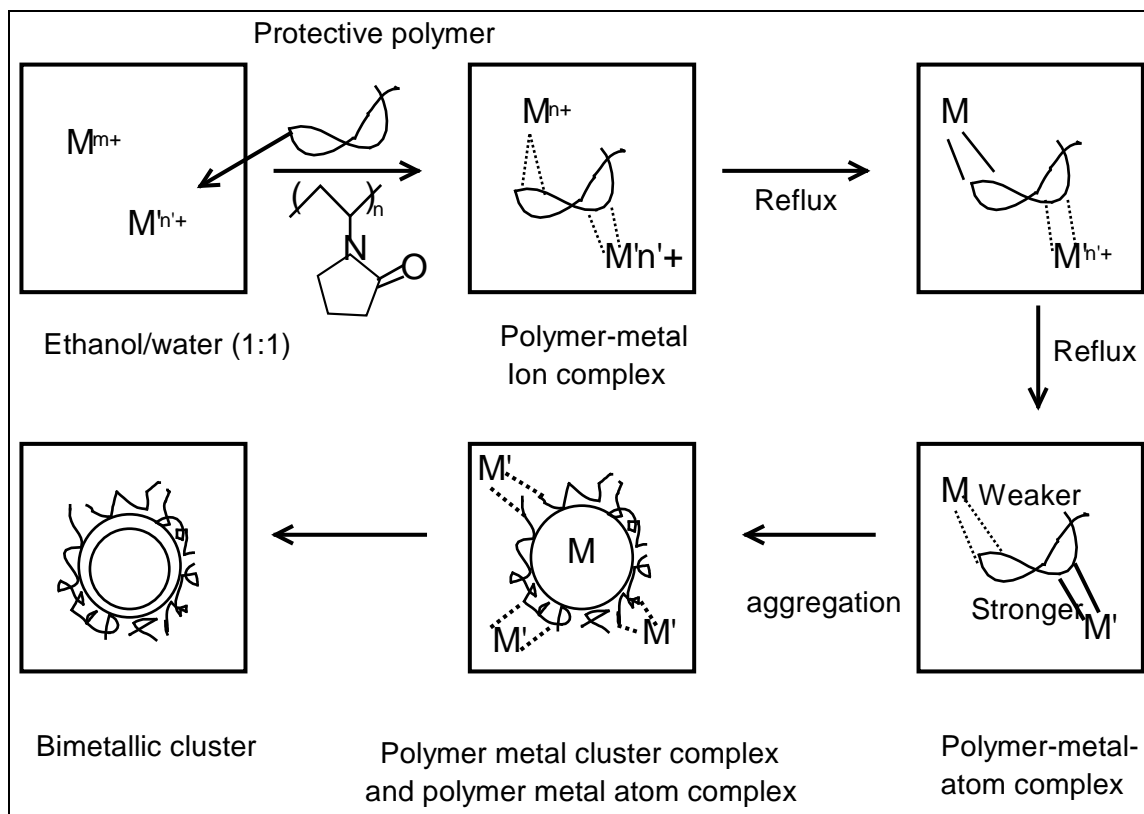


Figure 5: Proposed formation mechanism of polymer protected noble bimetallic clusters prepared by alcohol reduction in the presence of PVP [93].

From Figure 5 it is clear that the interaction between a zero-valent metal atom and the protective polymers is also of great importance. After the formation of 'polymer-metal ion complex' the metal ion having the higher redox potential is reduced first, after that the other metal ion (electro mediator) is reduced. Then the formerly reduced zero-valent metal atoms aggregate to form microclusters. Microcrystals are protected by a protective polymer, which is also co-ordinated to the secondly reduced metal atoms. This coexistence of 'polymer-metal cluster complexes' and 'polymer-metal atom complexes' causes the deposition of the secondly reduced metal atoms on the firstly reduced metal (micro) clusters, which gives the special 'core-shell' structure of the bimetallic clusters. This study shows that the polymers, which act as stabilising agent for the metal particles, have also an important role in the formation of bimetallic particles. But this method so far is restricted for the formation of bimetallic particles in solution only.

Above discussion shows that many reports have been published in the area of synthesis of bimetallic particles in solution. The exploration of the structure and properties of bimetallic particles is very interesting from scientific aspect. But for applications these particles should be incorporated into some matrix. Relatively little work has been done in the area of thin films containing bimetallic particles. The work, which has been done, is concentrated on the thin films prepared by ion implantation or by chemical vapour deposition methods. Following section summarises some important results reported in this area.

2.2.3 Bimetallic particles in thin films

Marguder et al. [95] have synthesised Ag-Cu bimetallic particles in nanometer dimension in silica. Ag and Cu were sequentially implanted with Ag to Cu ratios of 3 : 1, 1 : 1 and 1 : 3 and total nominal dose was 12×10^{16} ions/cm². The Ag ions were implanted first at 305 keV with substrate temperature of 270 K and a current density of 1.3 μ A/cm². Afterwards the Cu ions were implanted at 160 keV with substrate temperatures of 270 K. Energy dispersive X-ray spectra from individual particles indicate that the particles consisted of Cu rich or Ag rich alloy particles.

Timothy et al. [96] have studied the surface plasmon of thin silver / gold bimetallic films deposited by the vapour deposition method. The metal layers were thermally evaporated and sequentially deposited onto clean glass substrates. They observed that the alloy formation took place at the interface between the two metals. The optical properties of the Ag-Au alloy formed at the Ag / Au interface will certainly be different then those of either of the pure metal films. They found that the energy of the resonance absorption was nearly independent of the alloy composition.

Baba et al. [97] have synthesised silver-gold compound metal island films, and have studied the change in their resonance wavelength with the change in the mixture ratio of gold and silver. A very thin Ag island film was fabricated on a glass substrate by chemical vapour deposition. Au was deposited directly onto the Ag island film in the same manner, and the films were heated in a furnace at 300 °C for 10 min to make a complete alloy of Ag and Au. The shift of the resonance wavelength induced by the adjustment of the mixture ratio was attributed to two important factors: 1) The change of the island shape and 2) The change of the dielectric constant of the silver-gold alloy. For the silver rich films the island shape was observed to be near spherical or prolate

ellipsoidal. On the other hand, for the gold rich films, the island shape became more oblate. They have derived an equation relating the maximum absorption wavelength of Au / Ag alloy colloids with the molar fraction of gold and silver. This equation can be given as:

$$\frac{1}{\lambda_{bimetallic}} = \left[\left(\frac{X_{Au}}{\lambda_{Ag}^2} \right) + \left(\frac{1 - X_{Au}}{\lambda_{Au}^2} \right) \right]^{1/2} \quad (9)$$

where λ_{Au} and λ_{Ag} are maximum wavelength of the gold and silver particles respectively, and x_{Au} is the molar fraction of gold.

Teo et al. [98] have prepared metallic colloidal $Au_{1-x}Ag_x$ alloy aqueous solution of 20 - 40 nm and obtained their absorption spectra. It was found that the frequency of the absorption maxima is highly composition dependent. It varied monotonically from 520 nm in Au particle to 400 nm in Ag particles. The appearance of only one peak instead of the two distinct maximas at 520 and 400 nm for the bimetallic $Au_{1-x}Ag_x$ colloidal solution argues strongly against segregated Ag and Au particles.

Rivory et al. [99] have studied the optical properties of the Ag-Cu solid solutions over the whole composition range between 0.5 and 6 eV. Films were prepared by quenching the vapour of Ag and Cu on cold amorphous substrates. They analysed the imaginary part of the dielectric constant ϵ_2 and plotted it against the energy for Ag-Cu alloys with different Cu concentration for pure Ag and pure Cu. They observed that for the Ag-Cu alloys there is no continuous modification of the spectrum and one must consider separately the Cu-rich alloys, for which ϵ_2 is roughly Cu like. For Cu rich alloys, the ϵ_2 spectrum stays very similar to that for pure Cu spectrum (up to $c_{Cu} = 0.55$). For small Ag concentrations, the absorption edge is very steep and located at the same energy as in pure Cu. When c_{Ag} increases it is broadened but not shifted (broadening effects may simply be due to disorder in these microcrystalline samples).

For Ag-rich alloys on the other hand, the ϵ_2 spectrum showed two distinct parts, a high energy portion which is very similar to the interband absorption in pure Ag, and a low energy part which must represent the Cu impurity contribution. The absorption edge looks very much like that in pure Ag, except the broadening effect. The absorption due to the presence of impurity takes place by two processes, 1) resonant scattering of

conduction electron by the impurity d-state and 2) excitation of the impurity d-electrons to empty conduction states.

Nilsson et al. [100] have studied the plasma oscillations in Ag, Ag-Au, Ag-Cd and Ag-In by optical transmittance measurements using p-polarised light at oblique incidence. The specimens were prepared by vacuum evaporation (10^{-6} torr) onto quartz disks. The Ag-Cu samples were annealed for 3 h at 300 °C in the vacuum evaporator to remove concentration gradients. To obtain optimal transmittance, the films were made 35 - 45 nm thick. The plasma resonance was observed as an increased absorption at the plasma frequency. The resonance disappears at about 40 atom% Au and at as little as about 3 atom% Cd or In. The energy of the resonance was found to be almost constant with varying impurity content. For the Ag-Au system optical plasmon resonance results are in contrast with results obtained from electron energy loss experiments and from optical data. It was argued that in some cases optical plasma resonance absorption measurements are a more correct measure of the plasma frequency than the other experimental methods.

Gonella et al. [101] have used the sol-gel route to synthesise bimetallic Ag-Cu colloids. The coatings were prepared from a mixture of AgNO_3 and $\text{Cu}(\text{NO}_3)_2$ doped silica sols by the dip-coating technique. Cu to Ag molar ratios of 1 and 3 were maintained in the films, keeping the (Ag + Cu) to SiO_2 molar ratio constant at 0.175 in both cases. Coatings were heat treated in a 5% H_2 - 95% N_2 gas atmosphere at 700 °C to get spherical metal nanoclusters. In case of the Ag : Cu molar ratio of 1 the surface plasma resonance peaks for Ag and Cu were located at 393 and 568 nm whereas in case of Cu : Ag molar ratio of 3 the peaks were observed at 386 nm for Ag and 556 nm for Cu.

Significant work has been done for the synthesis of bimetallic colloids in solution. But the sol-gel route has not been explored much for the synthesis of thin glass films doped with bimetallic particles. These type of thin films doped with bimetallic particles can have their application as coloured coatings. Besides their applications as producing some interesting colours, non-linear optical effect of noble metal colloids in solutions, polymer matrices and glasses have attracted considerable attention due to their potential applications in opto-electronics. Hence in the present work sol-gel route was adopted to synthesise thin films containing bimetallic colloids of noble metals (Ag / Au and Ag / Cu) and their optical properties were measured.

2.3 Objective of the present work

The first objective of the present work was to stabilize the copper as Cu^+ state in solution. Once this has been done it was chosen to explore whether or not, Cu^+ state can be retained in thin films also. If the answer is affirmative, next aim was to explore whether the sol-gel route can be applied for the preparation of crack free and transparent glass like coatings on glass substrates. Once the glass like coatings containing CuCl nanoparticles have been achieved, the next aim was to see if it is feasible or not to substitute chloride by bromide ions to synthesise $\text{CuCl}_x\text{Br}_{1-x}$ (hence to shift the peak from 370 to 400 nm).

The other objective of the present work was to synthesise bimetallic colloids of noble metals. Once the particles are formed in thin films to study their microstructure, if they are alloy or phase separated mixed colloids, and to study the change in their optical properties with the change in their structure.

The objective of the present work can be summarised in the following points.

1. To stabilise ions in Cu^+ state and to synthesise nanocomposite thin films containing semiconducting nanocrystals of CuCl and CuBr using sol-gel route.
2. To study the stepwise substitution of Cl by Br to generate nanocomposites from the system $\text{CuCl}_x\text{Br}_{1-x}$ ($x = 0-1$) and to study the effect of such substitution on the optical and structural properties of the films.
3. To synthesise nano-composite thin films containing bimetallic noble metal colloids of Ag / Au and Ag / Cu .
4. To develop controlled synthesis routes for the synthesis of alloy and mixed colloids and to study their optical properties and structure.

III EXPERIMENTAL

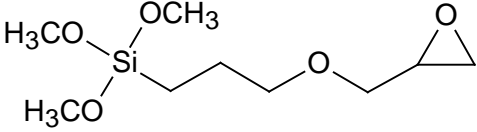
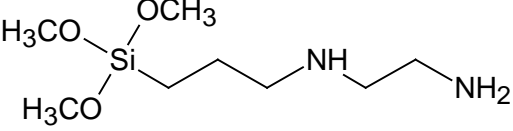
3.1 Material Used

The chemicals used for the synthesis of the sols are listed in Table 1, whereas the structures of the silanes are shown in Table 2.

Table 1: Chemicals used for the synthesis and their suppliers.

Chemical	Supplier
Tetrachloroaurate trihydrate	Chempur
Silver nitrate	Fluka
Copper (II) nitrate 2.5 hydrate	ABCR
Tetraethoxysilane 98%	Aldrich
3-Gycidoxypopyltrimothixysilane 98.5%	ABCR
Copper Powder (Particle size < 63 μm)	Aldrich
Hydrochloric acid 37%	Fluka
Hydrobromic acid 40%	Aldrich
Hydroiodic acid	Fluka
Copper (I) oxide	Aldrich
Polyvinylpyrrolidone K15	Fluka
Sodium citrate dihydrate	Merck
Ethanol	Fluka
Methanol 99.8%	Fluka
Lead (II) acetate Trihydrate	Fluka
Acetonitrile 99.9%	Aldrich
N-(-2-Aminoethyl-3-amino-propyl) trimethoxy silane	ABCR
Hydroxylamine hydrochloride	Fluka

Table 2: Functionalised silanes, used for the sol synthesis and their structure.

Name	Structural formula
Tetraethoxysilane (TEOS)	$\begin{array}{c} \text{OC}_2\text{H}_5 \\ \\ \text{H}_5\text{C}_2\text{O}-\text{Si}-\text{OC}_2\text{H}_5 \\ \\ \text{OC}_2\text{H}_5 \end{array}$
3-Glycidoxypropyltrimethoxy-silane (GPTS)	
N-(2-Aminoethyl-3-amino-propyl) trimethoxysilane (DIAMO)	

3.2 Synthesis of the sols from GPTS and TEOS

To synthesise GPTS / TEOS sols with a GPTS : TEOS molar ratio of 4 : 1, a mixture of 120 ml Ethanol, 160 ml GPTS and 40 ml TEOS was taken in a 500 ml round bottom flask connected with a water condenser and heating arrangement. After heating at 80 °C for 0.5 h, 28.5 ml of 0.1 molar HNO₃ solution was added dropwise to it within 3-4 min. This mixture was reacted for 24 h under the same conditions at 80 °C, and finally 120 ml more ethanol was added in it. After reacting it for 0.5 h at 80 °C, the resulting sol was cooled to room temperature. The sol synthesised this way was very stable at room temperature and could be stored for more than one year without gelation. Sol synthesis has been illustrated in following flow diagram. GPTS / TEOS sols with GPTS : TEOS molar ratios of 2 : 1, 1 : 1, 1 : 2 and 1 : 4 were also synthesised similarly.

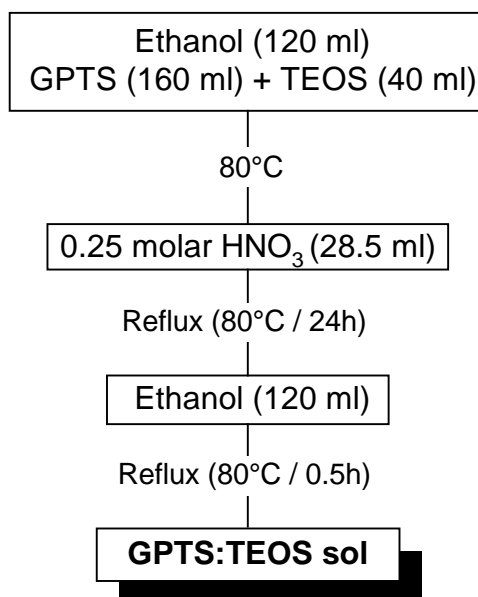


Figure 6: Flow diagram showing the synthesis of GPTS / TEOS sols.

3.3 Synthesis of nanocomposite thin films containing CuX (X = Cl, Br) nanoparticles

3.3.1 Synthesis of thin films containing CuCl nanoparticles

3.3.1.1 Synthesis of copper free reference sol

To synthesise copper free reference coating sols 7.5 ml of acetonitrile was added in 17.5 ml of pre-hydrolysed GPTS / TEOS sol (molar ratio of GPTS : TEOS = 1 : 1, synthesis section 3.2). After 15 min of stirring at 25 °C, 3.0 ml of hydrochloric acid (Fluka 37%) was added to it dropwise. Resulting mixture was further stirred at 25 °C for 48 h. Pre-washed (with Helmanex solution) sodalime and fused silica glass substrates were dip coated with the drawing speed of 4-6 mm/s. Samples were dried at 60 °C for 15 min in a drying oven and curing was carried out either in an oven at 150-250 °C for 1 h or in a UV-IR beltron machine (1200 W and 150 °C) for 4 min.

3.3.1.2 Synthesis of sol containing copper and chloride

To synthesise a sol containing copper and chloride, 0.60 g cuprous oxide (Cu_2O) was suspended in 7.5 ml of acetonitrile and was treated in ultrasonic bath for 5 min. In another glass container 17.5 ml of prehydrolysed GPTS / TEOS sol (molar ratio of GPTS : TEOS = 1 : 4 to 4 : 1) was taken. The cuprous oxide suspension was added

drop-wise in the GPTS / TEOS sol and stirred at 25 °C for 30 min. Finally 3.0 ml of hydrochloric acid (Fluka 37%) was added to it dropwise and stirred for 48 h.

3.3.1.3 Synthesis of thin films containing copper chloride nanoparticles

The resulting sol prepared as above was filtered with 0.8 µm filter before using for the sample preparation. Pre-washed (with Helmanex solution) fused silica and sodalime glass substrates with the dimensions 75 mm x 25 mm x 1 mm were dip-coated with the dipping speed of 4-6 mm/s. Samples were dried at 60 °C in an oven for 15 min, and curing was carried out either in an oven at 150-250 °C for 1 h, or in an UV-IR beltron machine operating with 1200 W, 150 °C for 4 min. Flow diagram representing the synthesis of thin films containing CuCl nanoparticles is shown in Figure 7.

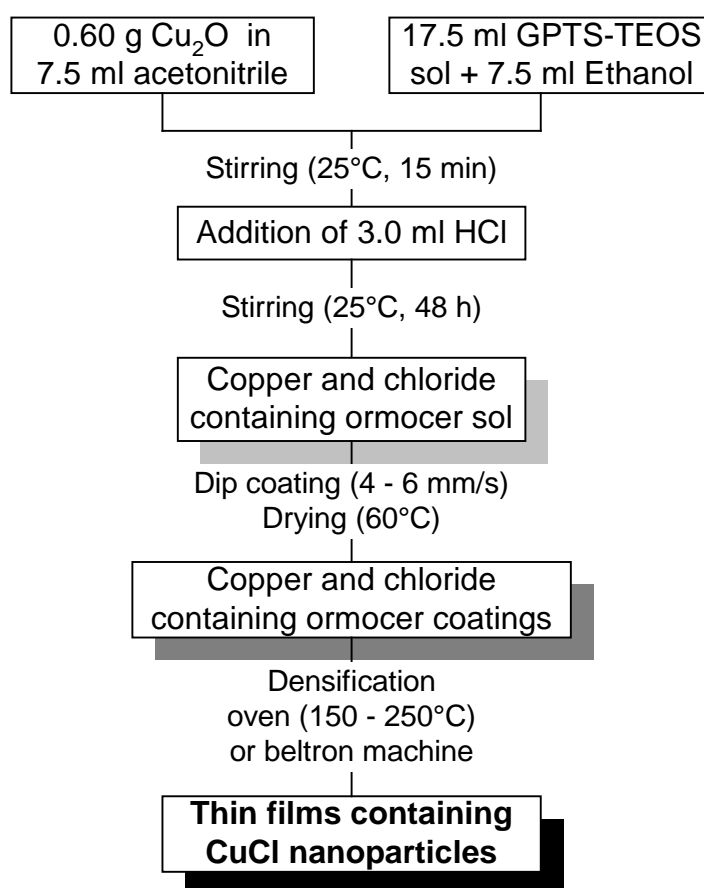


Figure 7: Flow diagram representing the synthesis of thin films containing copper (I) chloride nanoparticles.

3.3.2 Synthesis of thin films containing CuBr nanoparticles

3.3.2.1 *Synthesis of sol containing copper and bromide*

To synthesise a sol containing copper and bromide, 0.30 g of cuprous oxide was suspended in 7.5 ml of acetonitrile and was treated in an ultrasonic bath for 15 min. This suspension was added dropwise in 17.5 ml of GPTS / TEOS (molar ratios = 4 : 1 to 1 : 4) containing 7.5 ml of ethanol. After stirring for 15 min at 25 °C, 3.2 ml of hydrobromic acid (40%) was added to it dropwise to get a clear and transparent sol. The resulting sol was further stirred at 25 °C for 48 h.

3.3.2.2 *Synthesis of nanocomposite thin films containing copper bromide*

Above prepared sol was filtered with 0.8 µm filter before using for sample preparation. Cleaned sodalime and fused silica glass substrates were dip coated at room temperature with a lifting speed of 4-6 mm/s. After coating, the samples were dried in an oven at 60 °C for 15 min, and curing was carried out in air, either in an oven at 150-250 °C for 1 h or in a UV-IR beltron machine operating at 1200 W UV lamp and 150 °C for 4 min. Synthesis of thin films containing copper bromide nanoparticles is shown in Figure 8.

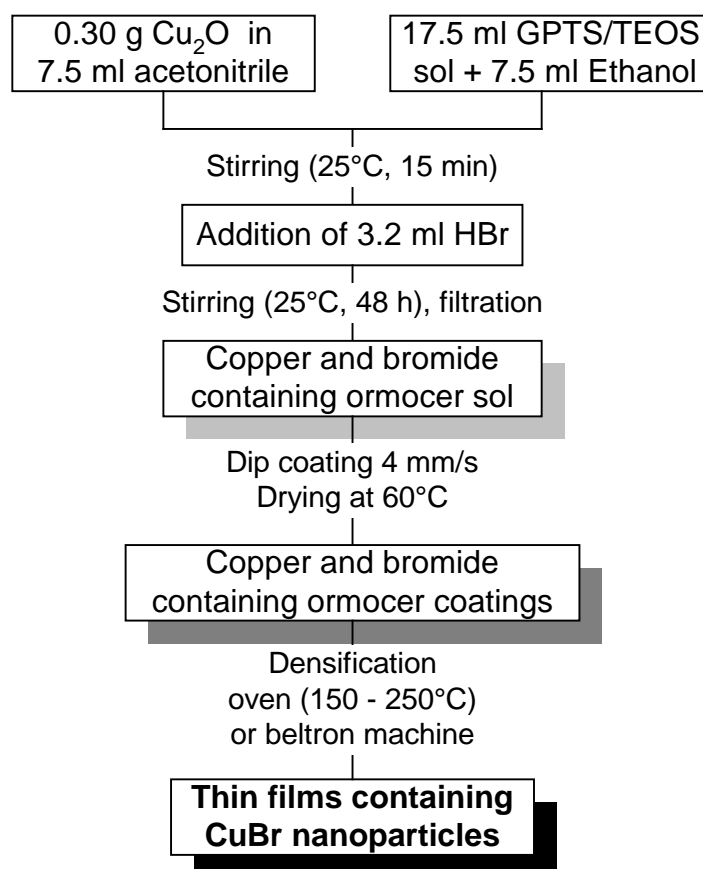


Figure 8: Flow diagram representing the synthesis of thin films containing copper (I) bromide nanoparticles.

3.3.3 Synthesis of nanocomposite thin films containing $\text{CuCl}_x\text{Br}_{1-x}$ ($x = 1-0$) nanoparticles

To synthesise thin films containing $\text{CuCl}_x\text{Br}_{1-x}$ ($x = 1-0$) nanoparticles, 0.60 g of cuprous oxide was suspended in 7.5 ml of acetonitrile, mixed in an ultrasonic bath for 15 min and added to 17.5 ml of GPTS / TEOS sol. After stirring at 25 °C for 15 min, 3.0 ml of hydrochloric acid (37%) was added dropwise to it to get clear and transparent sol. The resulting sol was stirred for 48 h at 25 °C and 0.15 ml hydrobromic acid (40%) was added. Sodalime and fused silica glass substrates were dip coated with the withdrawal speed of 4 mm/s. 0.15 ml hydrobromic acid was added to it again and coatings were synthesised. This process was repeated several times. Samples were dried in an oven at 60 °C for 15 min and curing of the coatings was carried out in air either by passing through the UV-IR beltron machine or in an oven at 150-250 °C for 30 min. The flow diagram representing the synthesis of thin films containing $\text{CuCl}_x\text{Br}_{1-x}$ ($x = 1-0$) nanoparticles is shown in Figure 9.

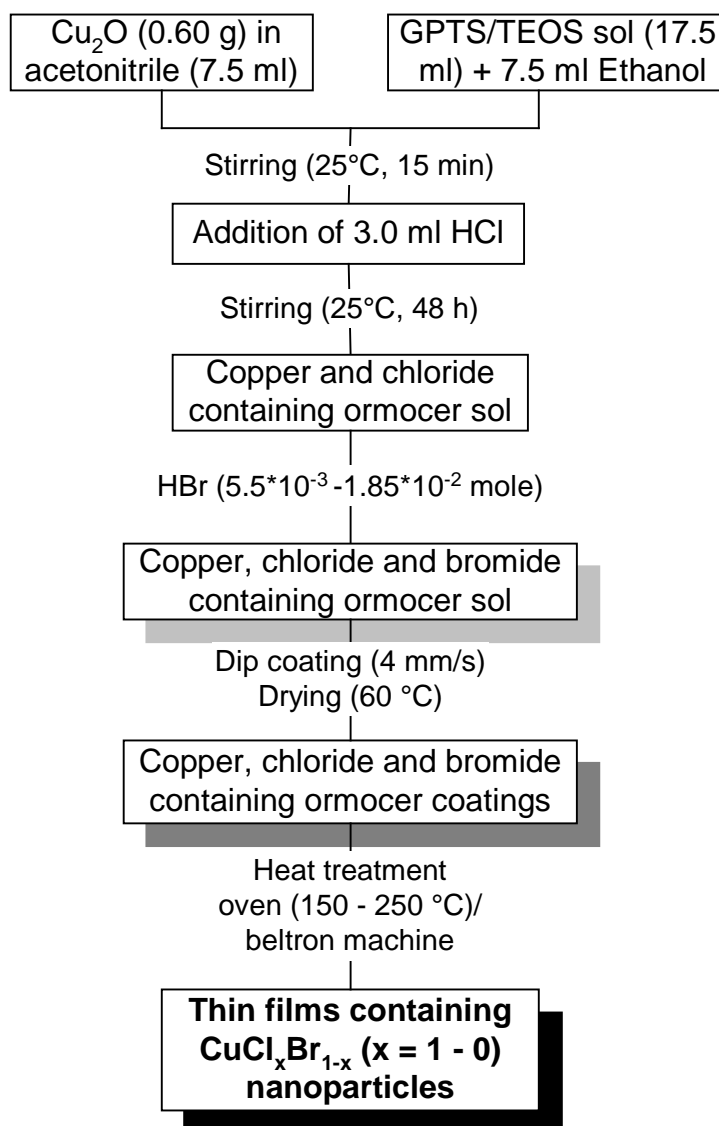


Figure 9: Flow diagram representing the synthesis of thin films containing copper chloride bromide ($\text{CuCl}_x\text{Br}_{1-x}$, $x = 0-1$) nanoparticles.

3.4 Synthesis of nanocomposite thin films containing bimetallic colloids of Ag / Au and Ag / Cu

3.4.1 Alloy- and mixed- colloids from Ag / Au system

3.4.1.1 Synthesis of Ag / Au Alloy colloids in thin films

To prepare thin films containing Ag / Au alloy colloids two different mixtures were synthesised. First colloidal gold particles were synthesised in an aqueous solution, whereas silver containing SiO_2 / PbO-SiO_2 sols were synthesised as the second mixture. Synthesis of both the sols is given below.

3.4.1.1.1 Synthesis of colloidal gold sol in aqueous solution

To synthesise colloidal sol of gold, 1.0 g of polyvinylpyrrolidone K15 (PVP) was dissolved in 10.5 ml of water in which 0.34 g of hydrogen tetrachloroaurate ($\text{HAuCl}_4 \cdot 3\text{H}_2\text{O}$) was dissolved. This solution was heated at 80 °C for 5 min, followed by the dropwise addition of aqueous solution of sodium citrate dihydrate (0.88 g of sodium citrate dihydrate in 2 ml of water) under vigorous stirring. This solution was heated at 80 °C for 10 min and was further stirred at room temperature for 30 min.

3.4.1.1.2 Synthesis of SiO_2 sol containing silver

To synthesise silver containing SiO_2 sol, 0.400 g AgNO_3 was dissolved in 14 ml of methanol, in which 1.04 ml of DIAMO ($\text{Ag} : \text{DIAMO} = 1 : 2$) was added dropwise. After stirring for 10 min at 25 °C, 25 ml of GPTS / TEOS sol (molar ration of GPTS : TEOS = 4 : 1, synthesis is given in *section 3.2*) was added in it. This solution was left for stirring at room temperature for 4 h.

3.4.1.1.3 Synthesis of PbO-SiO_2 sol containing silver

To synthesise PbO-SiO_2 sol containing silver, 0.400 g AgNO_3 was dissolved in 9 ml of methanol, in which 1.04 ml of DIAMO ($\text{Ag} : \text{DIAMO} = 1 : 2$) was added dropwise. After stirring for 10 min 25 ml of GPTS / TEOS sol was added in it and stirred for 30 min. In another container 0.5 g of $\text{Pb}(\text{CH}_3\text{COO})_2$ was dissolved in 5.0 ml methanol and 0.5 ml DIAMO was added as a complexing agent. This lead containing methanolic solution was added dropwise in silver containing sol. The resulting solution was stirred at 25 °C for 4 h.

To synthesise Ag / Au alloy colloids with the molar ratio of $\text{Ag} : \text{Au} = 2 : 1$, 2.5 ml of gold sol (prepared as above in *section 3.4.1.1.1*) was taken in a glass container, in which 0.11 gm of hydroxylamine hydrochloride (HAH) dissolved in 2 ml of methanol was added dropwise. When the addition of HAH was complete, 6.8 ml of silver containing SiO_2 / PbO-SiO_2 sol (synthesised as above in *section 3.4.1.1.2* and *3.4.1.1.3*) was added to it dropwise under stirring at 25 °C. After stirring for 4 h at 25 °C, sodalime glass substrates were dip coated with the lifting speed of 4 mm/s, dried at 80 °C for 30 min. These dried samples were heat treated under reducing atmosphere ($\text{N}_2 / \text{H}_2 = 92 / 8$, 80 l / h) with the heating rate of 100 K / h at temperatures

ranging from 150-550 °C. Synthesis of Ag / Au alloy colloids (molar ratio of Ag : Au = 2 : 1) is shown below in Figure 10.

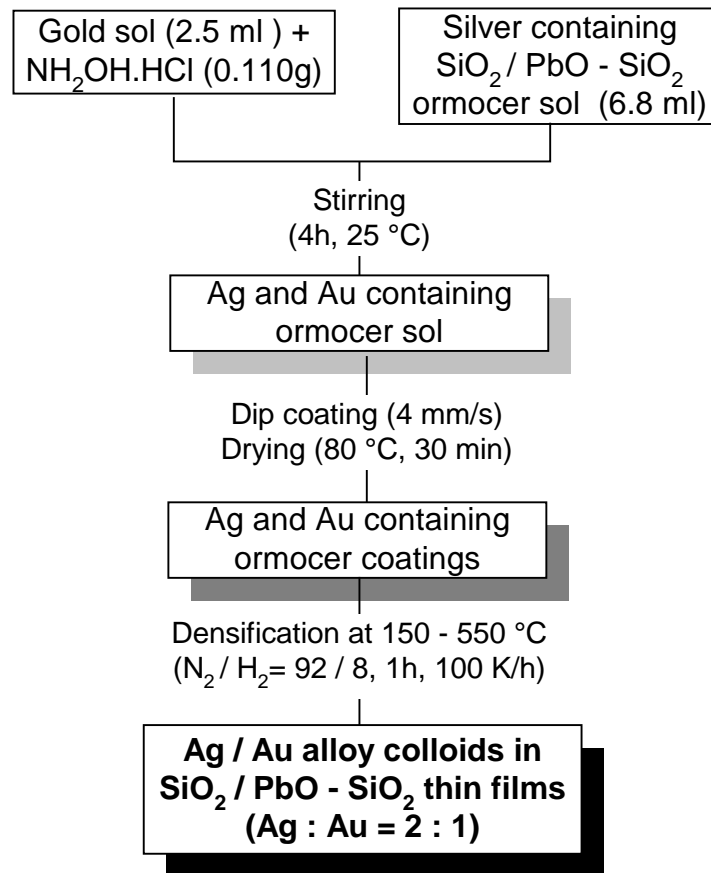


Figure 10: Flow diagram representing the synthesis of thin films containing Ag / Au (Ag : Au = 2 : 1) alloy colloids.

The amount of colloidal gold sol, silver containing sol and NH₂OH.HCl required to get Ag / Au molar ratios corresponding to 1 : 0, 4 : 1, 2 : 1, 1 : 1, 1 : 2 and 0 : 1 are given below in Table 3.

Table 3: Quantitative composition of the sol used for the synthesis of glass like coatings containing Ag / Au alloy colloids for different molar ratios of silver and gold.

Ag : Au Molar ratio	AgNO ₃ / g	HAuCl ₄ .3H ₂ O ml	NH ₂ OH HCl / g	GPTS / TEOS Sol / ml
1 : 0	17.0	0	0.138	9.4
4 : 1	13.6	2.5	0.110	11.5
2 : 1	6.8	2.5	0.055	15.7
1 : 1	3.4	2.5	0.027	17.8
2 : 1	1.7	2.5	0.014	19.0
0 : 1	0	2.5	0.0	20.0

In order to synthesise Ag / Au alloy colloids in PbO-SiO₂ thin films, different amounts of lead acetate were dissolved in 5 ml of methanol and the DIAMO was added in it. This lead containing solution was added in the silver containing sol prior to mixing with the colloidal gold sol. The amount of lead acetate and DIAMO corresponding to different molar ratios of Ag and Au are given below in. The rest process is the same as described above for the synthesis of SiO₂ thin films containing Ag / Au alloy colloids.

Table 4: Required amount of lead acetate and DIAMO for the synthesis of PbO-SiO₂ thin films containing different molar ratios of Ag and Au.

Ag : Au	1 : 0	4 : 1	2 : 1	1 : 1	1 : 2	0 : 1
Pb(Ac) ₂ / g	0.498	0.540	0.625	0.668	0.689	0.710
DIAMO / ml	0.340	0.369	0.427	0.456	0.470	0.485

3.4.1.2 Synthesis of Ag / Au mixed colloids in thin films

Synthesis of Ag / Au mixed colloids having a Ag : Au molar ratio of 1 : 1 was carried out by dissolving 0.174 g of hydrogen tetrachloroaurate (HAuCl₄.3H₂O) in 5.6 ml ethanol and 0.340 ml of DIAMO (Au : DIAMO = 1 : 3) was added to it dropwise. After 15 min of stirring 4.8 ml of GPTS / TEOS sol was added to it. In another glass container, a silver containing sol was synthesised parallelly by dissolving 0.086 g of AgNO₃ in 4.0 ml methanol in which 0.113 ml of DIAMO (Ag : DIAMO = 1 : 1) was added dropwise. After 15 min of stirring 6.8 ml of GPTS / TEOS sol was added in it. Both silver and gold containing sols were left for stirring at 25 °C for 4 h.

Similarly sols were synthesised for Au : DIAMO and Ag : DIAMO ratios corresponding to 1 : 3 and 1 : 1 respectively. Table 5 and Table 6 show the composition of the sols.

Table 5: Quantitative data for the synthesis of silver containing sol.

	AgNO₃ (g)	Methanol (ml)	DIAMO (ml)	GPTS / TEOS sol (ml)
A	0.138	6.6	0.182	8.8
B	0.113	6.0	0.150	7.5
C	0.086	4.0	0.113	6.0
D	0.058	2.6	0.074	4.2

Table 6: Quantitative data for the synthesis of gold containing sol.

	HAuCl₄.3H₂O (g)	Ethanol (ml)	DIAMO (ml)	GPTS / TEOS sol (ml)
A ₁	0.069	3.0	0.135	2.0
B ₁	0.120	3.5	0.235	3.3
C ₁	0.174	5.6	0.340	4,8
D ₁	0.237	7.0	0.470	6.6

Gold and silver containing sols prepared as above and shown in Table 5 and Table 6 were mixed together in order to obtain the required proportion of gold and silver. Sol (A) was mixed with sol (A₁), sol (B) was mixed with sol (B₁), sol (C) was mixed with sol (C₁) and sol (D) was mixed with sol (D₁) to get the Ag : Au ratios corresponding to (4 : 1), (2 : 1) (1 : 1) and (1 : 2) respectively. Mixing was carried out by adding Ag containing sol dropwise in Au containing sol. The total concentration of gold + silver was kept constant for all the ratios of gold and silver and is 1.02×10^{-3} mol.

After stirring, these sols were used for the coating of glass substrates using the dip coating method. Samples were prepared with the lifting speed of 4 mm/s, dried at 80 °C in an oven for 30 min. After drying, these samples were heat treated in air at the temperatures ranging from 150-550 °C. Flow diagram representing the synthesis of thin films containing Ag / Au mixed colloids (molar ratio of Ag : Au = 2 : 1) is shown below in Figure 11.

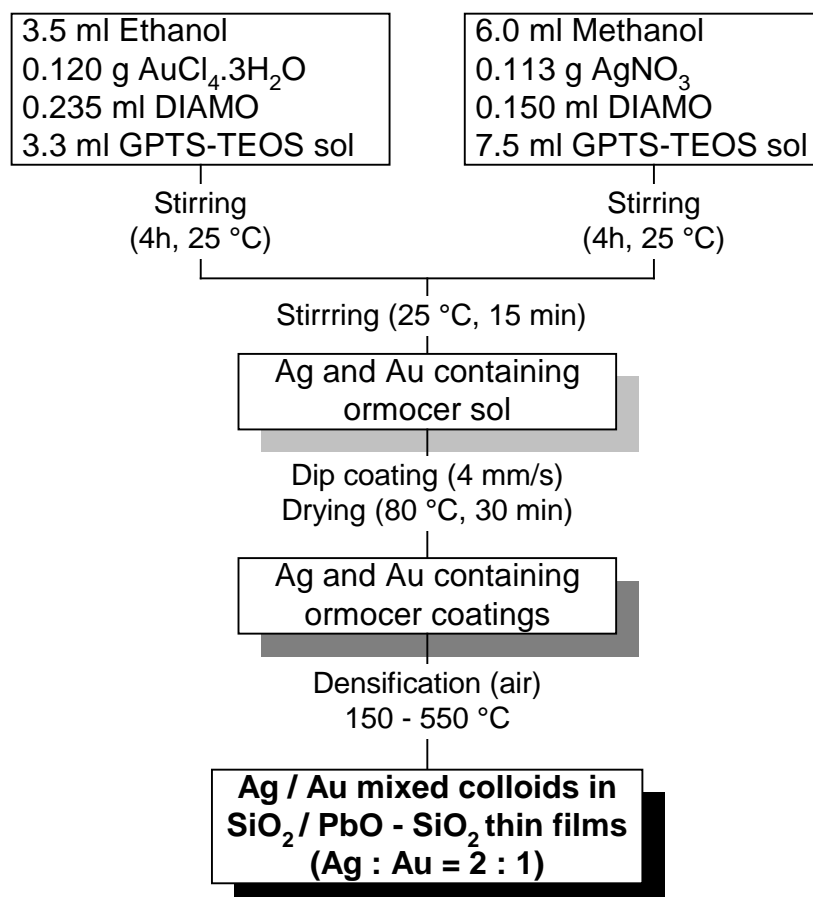


Figure 11: Flow diagram representing the synthesis of SiO₂ thin films containing Ag / Au (molar ratios of Ag : Au = 2 : 1) mixed colloids.

In order to synthesise PbO-SiO₂ thin films containing Ag / Au mixed colloids, lead was added to the sols as water free lead acetate [Pb(CH₃COO)₂]. 0.578 g lead acetate was dissolved in 3 ml of methanol and 0.395 ml DIAMO (Pb : DIAMO = 1 : 1) was added as a complexing agent. After stirring for 15 min, it was added to the silver containing sol, and stirred for further 4 h before mixing with the gold containing sol. For all the molar ratios of Ag and Au, the amount of lead acetate was kept constant and was equal to Si : Pb = 12 : 1. The rest of the process is the same as described above for the synthesis of SiO₂ thin films containing Ag / Au mixed colloids.

3.4.2 Alloy and mixed- colloids from Ag / Cu system

3.4.2.1 Synthesis of Ag / Cu alloy colloids in thin films

To synthesise thin films containing Ag / Cu alloy colloids, first a colloidal silver containing sol was synthesised. The synthesis was carried out by dissolving 1.0 g of polyvinylpyrrolidone (PVP) K15 (molecular weight = 10000) in 17 ml of methanol.

0.60 g of silver nitrate was then dissolved in it followed by the addition of 1.57 ml DIAMO (Ag : DIAMO = 1 : 2). The resulting sol was stirred for 15 min at 25 °C and 37.5 ml of GPTS / TEOS sol was added to it. After 4 h of stirring at 25 °C, 0.49 g of hydroxylamine hydrochloride (NH₂OH.HCl) dissolved in 4.0 ml of methanol was added to it dropwise with the continuous stirring. Resulting silver sol was used for the synthesis of the coatings.

To synthesise thin films containing Ag / Cu alloy colloids with the molar ratio of Ag : Cu = 2 : 1, 11.3 ml of colloidal silver sol prepared as above was taken in a glass container, in which copper containing sol was added dropwise. The copper containing sol was synthesised by dissolving 0.063 g of copper nitrate (Cu(NO₃)₂·2.5H₂O) in 5 ml methanol and complexing with 0.073 ml DIAMO (Cu : DIAMO = 1 : 1). Resulting sol was stirred at 25 °C for 1 h. Glass substrates were dip coated and heat treated under reducing atmosphere (N₂ / H₂ = 92 / 8, 80 l/h) with the heating rate of 100 K/h at temperatures ranging from 150-550 °C to get thin films containing Ag / Cu alloy colloids. Synthesis of Ag / Cu alloy colloids for the molar ratio of Ag : Cu = 2 : 1, is shown below in Figure 12.

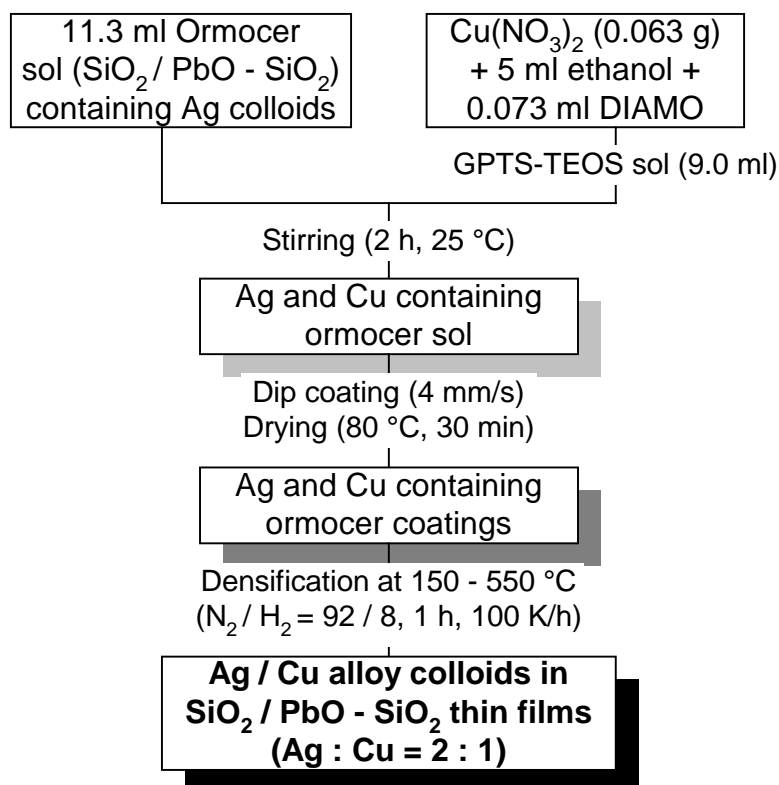


Figure 12: Flow diagram representing the synthesis of thin films containing colloidal Ag / Cu (molar ration of Ag : Au = 2 : 1) alloy nanoparticles.

The compositions of the sols containing different molar ratios of Ag and Cu are shown below in Table 7. In all cases, the total concentration of silver + copper was kept constant at 1.0×10^{-3} mol.

Table 7: The composition of the sol used for the synthesis of thin films containing Ag / Cu alloy colloids containing varying amount of silver and copper.

Molar ratio Ag : Cu	AgNO ₃ sol ml	Cu(NO ₃) ₂ x 2.5 H ₂ O g	DIAMO for copper	GPTS / TEOS- Sol / ml
1 : 0	17.0	0	0	9.4
4 : 1	13.6	0.038	0.044	11.5
2 : 1	11.3	0.063	0,073	13.0
1 : 1	8.5	0.094	0.109	14.7
1 : 2	5.6	0.126	0.146	16.5
0 : 1	0	0.187	0.219	20.0

3.4.2.2 Preparation of Ag / Cu mixed colloids in thin films

Thin films containing Ag and Cu mixed colloids were prepared by mixing of the silver containing sol with the copper containing sol. To synthesise Ag / Cu mixed colloids with a molar ratio of Ag : Cu = 1 : 1, 0.085 g of silver nitrate (AgNO₃) was dissolved in 2.8 ml methanol and 0.222 ml of DIAMO (Ag : DIAMO = 1 : 2) was added as a complexing agent. After stirring at 25 °C for 15 min 5.6 ml of GPTS / TEOS (molar ratio 4 : 1) sol was added in it. In another glass container 0.095 g of copper nitrate Cu(NO₃)₂.2.5H₂O was dissolved in 3.75 ml ethanol followed by dropwise addition of 0.111 ml of DIAMO (Ag : DIAMO = 1 : 1). After stirring for 15 min at 25 °C, 12.4 ml of GPTS / TEOS sol was added in it.

Both silver and copper containing sols were stirred at 25 °C for 4h and then the copper containing sol was mixed with silver containing sol. After further stirring for 15 min, glass substrates were dip coated with the dipping speed of 4 mm/s and dried in an oven at 25 °C for 30 min. The heat treatment of the samples was carried out under reducing atmosphere (N₂ / H₂ = 92 / 8, 80 l/h) with the heating rate of 100 K/h at the temperatures ranging from 150-550 °C. Synthesis of thin films containing Ag / Cu (Ag : Cu = 2 : 1) mixed colloids is shown below in Figure 13.

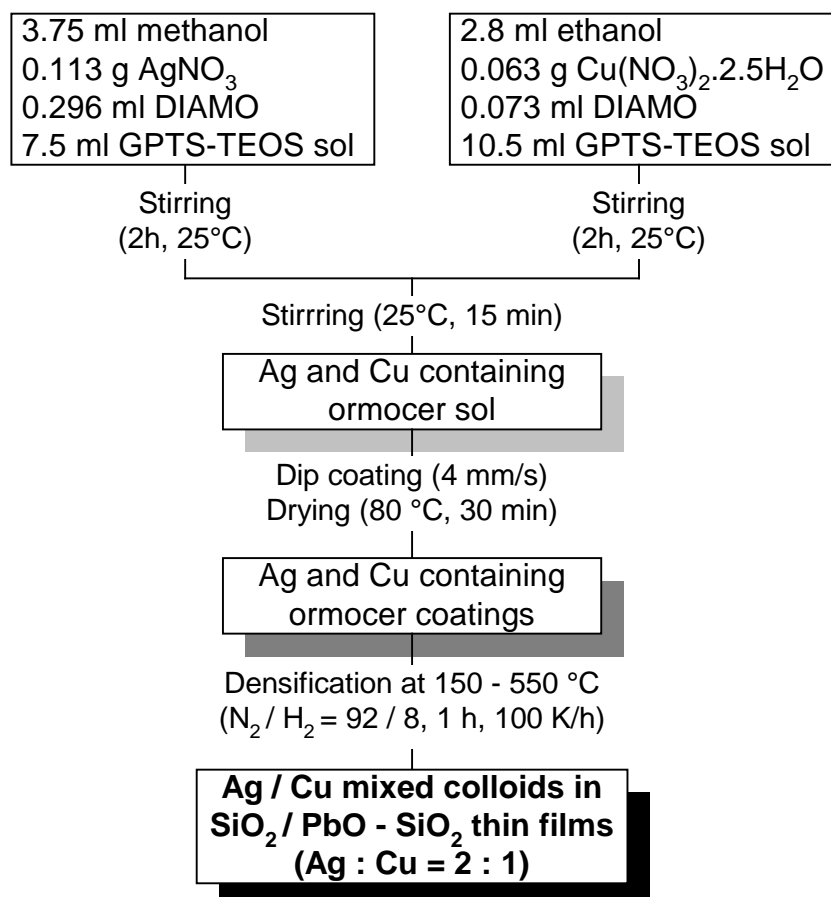


Figure 13: Flow diagram representing the synthesis of thin films containing Ag / Cu (Ag : Cu = 2 : 1) mixed colloids.

The compositions of the silver and copper containing sols used for the synthesis of different molar ratio of Ag and Cu has been given below in Table 8 and Table 9.

Table 8: The compositions for the synthesis of silver containing sol.

	AgNO ₃ (g)	Methanol (ml)	DIAMO (ml)	(GPTS / TEOS) sol (ml)
A	0.136	5.60	0.356	9.0
B	0.113	3.75	0.296	7.5
C	0.085	2.80	0.222	5.6
D	0.057	1.90	0.148	3.8

Table 9: The compositions for the synthesis of copper containing sol.

	Cu(NO₃)₂·(H₂O)_{2.5} (g)	Ethanol (ml)	DIAMO (ml)	(GPTS / TEOS) sol (ml)
A ₁	0.038	1.90	0.044	9.0
B ₁	0.063	2.80	0.073	10.5
C ₁	0.095	3.75	0.111	12.4
D ₁	0.126	5.6	0.145	14.2

Sol A was mixed with A₁, B was mixed with B₁, C was mixed with C₁ and D was mixed with D₁ in order to get the Ag : Cu molar ratios corresponding to 4 : 1, 2 : 1, 1 : 1, and 1 : 2 respectively.

IV CHARACTERISATION METHODS

4.1 Apparatus Used

The thin films were characterised by using UV-VIS-spectroscopy, normal and high resolution electron microscopy (TEM & HR-TEM) and with X ray diffraction (XRD) methods. Thickness of the films was measured with profilometer and ellipsometer. DTA-TG measurements of the gel powders were carried out up to 1000 °C.

Table 10: Apparatus as used for the different characterisation methods.

Apparatus	Manufacturer	Type
UV-VIS Spectrometer	Bruins	Omega 20, Omega 30
UV-VIS Spectrometer	Varien Cary	5 E
ESCA-Spectrometer	Perkin Elmer	PHI 5500
Diffractionmeter	Siemens	Kristalloflex
High Resolution Electron-microscope	JEOL	200 CX
Transmission Electron-microscope	Phillips	CM 200
Kalorimeter and Thermogravimetry	Seiko Instruments	TG/DTA 320
Profilometer	SAS Technology	Nanosurf 488
Ellipsometer	SOPRA	ES4G

4.2 UV-VIS Spectroscopy

The UV-VIS absorption spectra of the thin films were measured with the help of double beam spectrophotometer (Bruins, Type Omega 30 and Omega 20) for wavelengths between 200 to 1000 nm. A slit of 1 mm was chosen, the measurements were made in the 0.5 nm steps and 5 scans were accumulated. For the measurements of UV-VIS spectra of solutions, silica cuvettes with the thickness of 2 mm were used whereas all the other measurement parameters were kept same as used for the measurements of the thin films. The absorption spectra were converted in extinction spectra.

The extinction spectra for particle having same refractive index were calculated as a function of their radii with the help of a computer program using Mie-theory [3]. From

these calculations the volume concentration of the colloids in thin films or in solutions was defined in the same way as has been shown in the previous studies [102].

For carrying out low temperature UV-VIS measurements, VARIAN CARY 5E spectrophotometer was used. Extinction spectra of thin films were measured at liquid nitrogen temperature ($T= 84$ K) and at the pressure of 5×10^{-4} m bar. The UV-VIS spectra were recorded in the wavelengths ranging from 300 to 1000 nm. The slit was kept constant at 1.0 mm, the measurements were carried out in an interval of 0.5 nm and 5 scans were recorded.

4.3 X-Ray Diffraction Studies

The X-ray diffraction patterns of the films were recorded by a thin film-diffractometer (Siemens Type D 500). For focussing the x ray's a copper fine focussing arrangement with a 0.3° aperture width was used. The glass samples were put on the sample holder, and the incident angle for the X-ray was chosen as 2° . All the X-ray diffraction measurements were conducted using $\text{CuK}\alpha$ radiation and a graphite monochromator. The diffracted X-rays were collected by scanning between $2\theta = 20$ to 60° in 0.04° steps and counting for 100 s.

The average crystal diameter d_k was calculated from the Scherrer's equation. If corrected half width β , angle 2θ corresponding to the most intense reflex peak and the wavelength λ of the X- rays used are known one can evaluate the crystallite size by the use of well known Scherrer equation [103] given below. To determine the corrected half with the observed X- ray reflex was fitted with the Cauchy profile and the half width was estimated with this fitted curve.

$$d_k = \frac{K \cdot \lambda}{\beta \cdot \cos\theta} \quad (10)$$

K	Scherrer-constant
λ	Wavelength of the used X- ray's
β	Corrected Halfwidth
θ	Bragg diffraction angle
d_k	Average crystal diameter

The Scherrer's constant K is dependent on the geometry of the crystal and has a value in between 0.85 and 0.95, provided the value of β is given as the half width of the peak.

4.4 Transmission Electron Microscopy

In order to determine the particles size electron microscopic investigations were carried out using a transmission electron microscope (TEM, JEOL, Type 200 CX) and with a high resolution transmission electron microscope (Philips, Type CM 200 FEG) at the energy of 200 KeV. Diffraction and scattering absorption contrasts, structure imaging and the selective area diffraction patterns were recorded [104]. Two methods for the sample preparation were used. In the first method, the samples were prepared by scratching the splinters from the nanoparticles containing coatings. This scratched material was deposited onto carbon coated copper grid and was investigated using HR-TEM. Whereas a cross sectional preparation was used for the sample preparation in the other method. Thinning of the samples was carried out with argon ion thinning method. To determine the composition of the particles formed, electron dispersive X-ray analysis (EDX) was carried out by focussing the electron beam on the particles.

4.5 Differential Thermal Analysis and Thermogravimetry

To see the thermogravimetric and thermal effect on zero-gel powder, gel pieces were dried at the temperature of 100 °C. Differential Thermal Analysis (DTA) and Thermogravimetric Analysis (TGA) were carried out using a combined apparatus (From Seiko Instruments). 40-50 mg of the gel powders were taken in alumina (Al_2O_3) crucibles and heated from 100 to 1000 °C under synthetic air (80% N_2 / 20% O_2) and under reducing atmosphere (92% N_2 / 8% H_2) with a flow rate of 10 ml/s. The heating rate was kept 600 K/h. Pre-fired Al_2O_3 powder was used as reference.

4.6 Spectroscopic Ellipsometry

The measurements were carried out with SOPRA apparatus and Type ES4G. A high pressure Xenon lamp was used as a light source combined with a grating prism double monochromator and a photomultiplier as a detector. The measurements were carried out between the wavelengths ranging from 200 to 900 nm with a measurement interval of 5 nm. The error in the accuracy for the film thickness $< 0.5 \mu\text{m}$ is about 10-20 % and for the thickness $> 0.5 \mu\text{m}$ is about 10%. Whereas, error in the dispersion in the

wavelengths between 450-800 nm is about 1%. The error in the dispersion increases considerably in the wavelengths < 450 nm. The results were interpreted with the help of system software by fitting the Cauchy or Sellmeyer parameters on the measured curve.

4.7 Profilometry

The coating thickness measurements were done with the help of a profilometer (SAS technologies, type Nanosurf 488). The error in the accuracy of the film thickness < 1 μm is about 10-20% and for the thickness < 3 μm is about 10%.

V RESULTS AND DISCUSSIONS

5.1 Synthesis and characterisation of thin films containing CuX (X = Cl, Br) nanoparticles

5.1.1 CuCl nanoparticles

To synthesise thin films containing copper chloride nanoparticles, the matrix sol used was prepared from a precursor solution with the molar ratios 3-glycidoxypropyl-trimethoxysilane (GPTS) : tetraethoxysilane (TEOS) : water : alcohol = 1 : 1 : 2 : 9. The molar ratios of GPTS : TEOS were varied from 4 : 1 to 1 : 4. The GPTS : TEOS system was chosen, since it is known from the literature [143] that its short chain organic groups can be burnt off without any cracking of coatings. The synthesis details are given in chapter III, page 35.

Most of the copper (I) compounds are insoluble in any other medium except strong acids or bases. Hence, the chlorination of copper ions was done by incorporating HCl to the sol containing copper precursor. The addition of halide ions greatly increases the solubility of the cuprous salts due to the formation of halocuprate(I) anions [105] of the type CuX_2^- and CuX_3^{2-} resulting to a green coloured and transparent solution. The green colour is attributed to the presence of Cu^+ and Cu^{2+} both. Therefore, the suspension of cuprous oxide in acetonitrile was mixed with the matrix sol and the chloride ions were added to it to get a clear and transparent solution. Since the stability of the cuprous ion relative to that of cupric ion may be affected by the solvent acetonitrile, in which Cu^+ is more stable than Cu^{2+} [106], acetonitrile was chosen as a solvent.

In order to dissolve the Cu_2O completely, this being an ionic reaction more than stoichiometric amount of HCl has to be added. As it will be shown in the latter section that CuCl is unstable in the presence of moisture and air, therefore to decrease the amount of HCl, and hence the water, another method was used for the synthesis of thin films containing CuCl nanoparticles. In this method an acidic solution of CuCl_2 (pH = 0.5) was reduced in presence of metallic copper powder (particle size < 63 μm).

Colourless transparent coatings with thicknesses from 0.7 to 1.0 μm were obtained by a single deposition process after heat treatment at 200 °C in an oven for 30 min or in a

UV-IR beltron machine connected with a low pressure Hg-Xe lamp (1200 W) and thermal irradiation (150 °C).

5.1.1.1 UV-VIS spectroscopic characterisation

To investigate the optical properties of thin films containing CuCl nanoparticles, UV-VIS absorption spectra of the thin films coated on the glass slides were recorded, together with a reference coating from the matrix sol. Spectra measured at room temperature are shown below in Figure 14. GPTS : TEOS ratio of 1 : 1 was chosen for these studies.

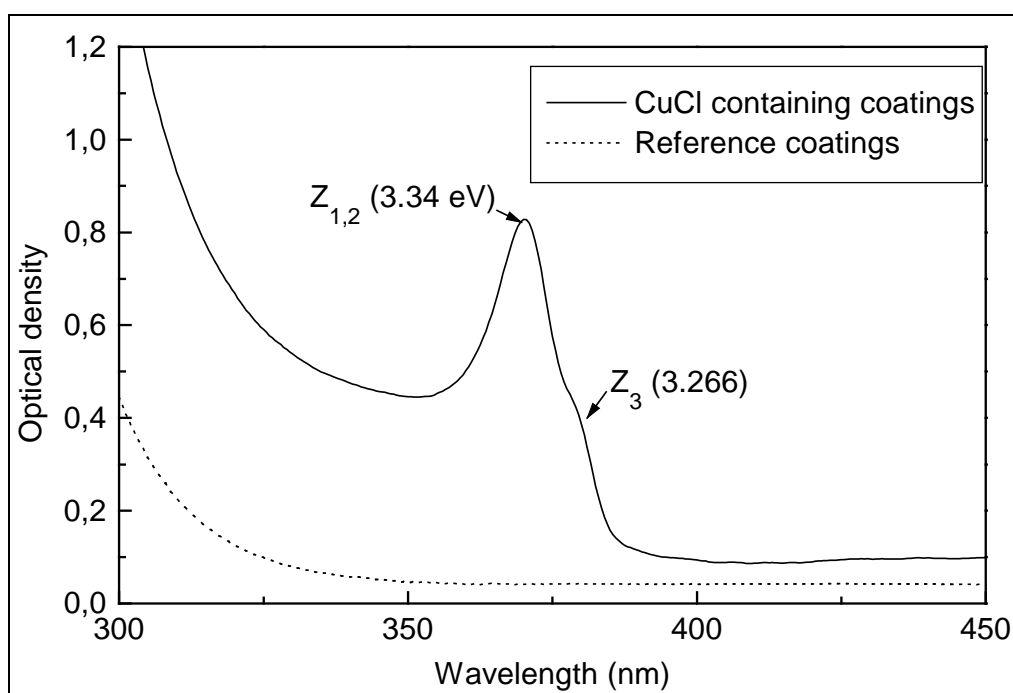


Figure 14: UV-VIS spectra of the thin films containing CuCl nanoparticles heat treated in a UV-IR beltron machine at 150 °C / 4 min, 1200 W, reference : air (experimental conditions are in ch. III, p. 35).

The above spectrum closely resembles with that reported in the literature [37, 38]. The peaks at 371 and 381 nm can be attributed to copper chloride nanoparticles. These are termed as Z_3 and $Z_{1,2}$ resulting from the excitation associated with two spin orbital valence sub-bands. The Z_3 line originates from two-fold degenerate subband Γ_6 , and the $Z_{1,2}$ line originates from four fold degenerate valence subband Γ_8 [42].

5.1.1.2 The effect of GPTS / TEOS ratio on the formation of CuCl nanoparticles

In order to study the effect of sol composition on the formation of CuCl and CuBr nanoparticles, five sols with different GPTS / TEOS ratios were synthesised and the resulting coatings were studied with UV-VIS spectroscopy. The resulting spectra for the films containing CuCl nanoparticles have been shown in Figure 15.

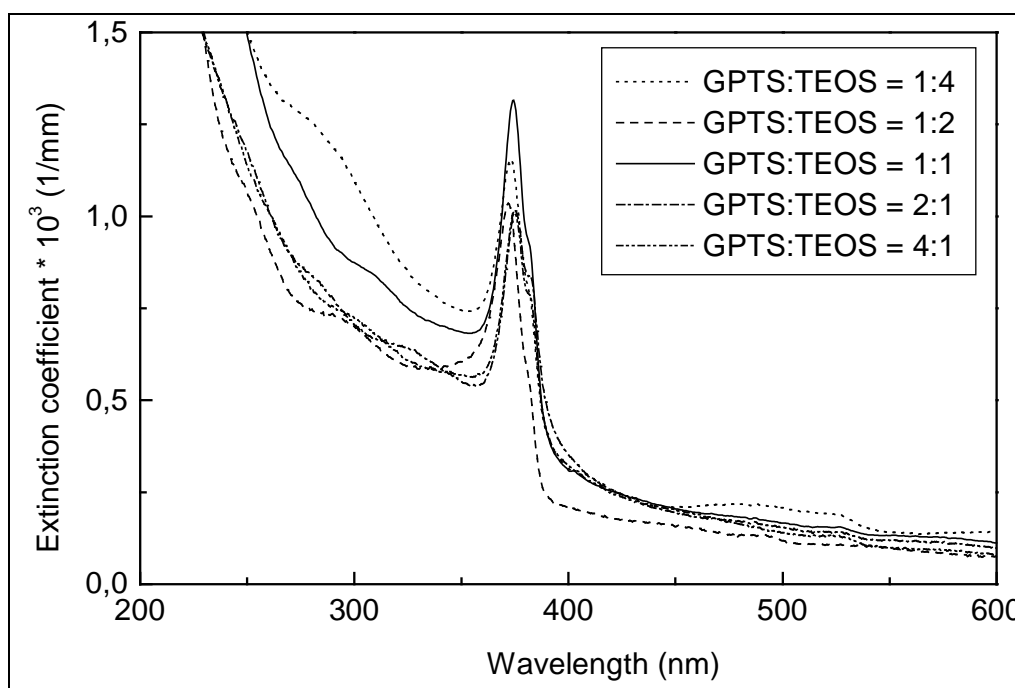


Figure 15: Extinction spectra of CuCl nano-composite films synthesised using different GPTS / TEOS ratios, films densified at 150 °C / 4 min in UV-IR beltron machine (experimental conditions in ch. III, p. 34).

It is clear from Figure 15 that the most intense copper chloride peak was observed for the sol having GPTS / TEOS ratio of 1 : 1. This difference possibly can be attributed to the combined effect of the flexibility and the texture of the matrix, which is expected to influence the growth of the particles. From the above spectra it is clear that a small shift of the peak position (from 370.5 nm for GPTS : TEOS = 1 : 4, to 373.5 nm for GPTS : TEOS = 4 : 1) towards the higher wavelength (lower energy) is observed with increasing GPTS ratio, which is well justified as the increase of molar ratio of TEOS in matrix sol will result in more dense coatings which will hinder the growth of particles, resulting the formation of relatively small particles in the matrix sol. For the further investigations, a fixed ratio of GPTS : TEOS = 1 : 1 was chosen, because it leads to the maximum yield of CuCl nanoparticles.

5.1.1.3 The evolution of CuCl nanoparticles as a function of heat treatment

In order to understand the mechanism of the formation of copper chloride nanoparticles in thin films, the UV-VIS spectra of the samples were measured at various intervals of the curing procedure. Figure 16 shows the UV-VIS spectra of the CuCl containing thin films after drying at 60 °C in air for 30 min and for different time periods of treatment in the UV-IR irradiation (beltron machine, see in ch. III, p. 36).

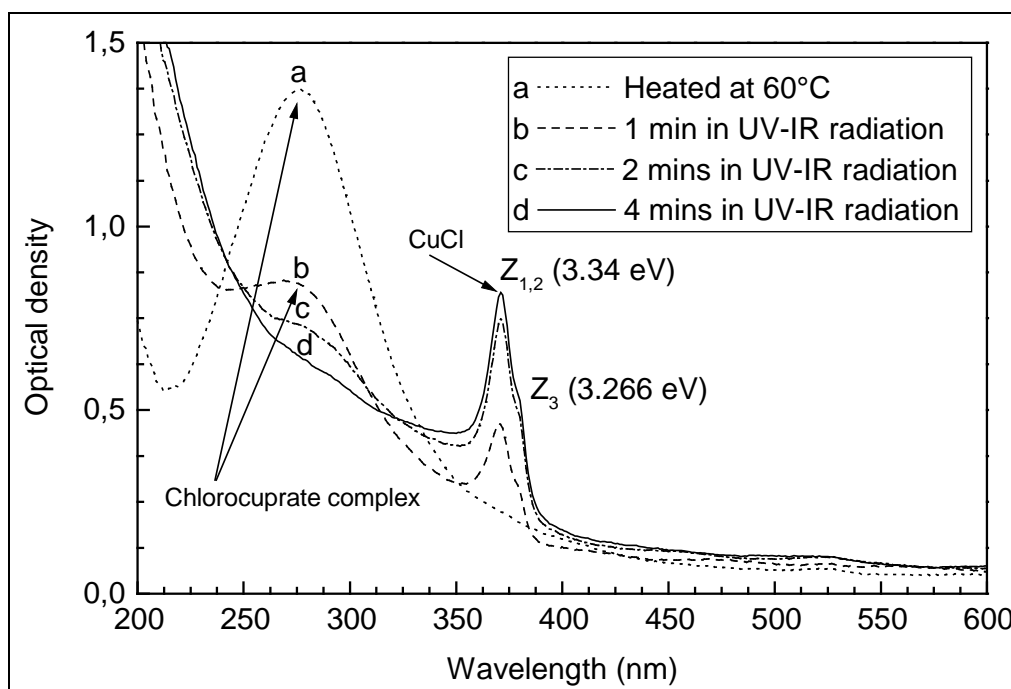


Figure 16: Stepwise generation of CuCl nanocrystals under different heat treatment conditions, (a) 30 min 60 °C in an oven (b) 1 min UV-IR (1200 W, 150 °C) (c) 2 min UV-IR (d) 4 min UV-IR. (GPTS : TEOS ratio = 1 : 1, experimental conditions in ch. III, p. 35).

The sample dried at 60 °C shows only one broad peak at 280 nm (Figure 16a), which can be attributed to the chlorocuprate anions [112]. After curing for 1 min with UV-IR radiation a new peak is obtained at around 371 nm, resulting in the decrease of the intensity of the peak at 280 nm (Figure 16b). The curing of the same sample for 4 min in a beltron machine gave an intense characteristic peak of cuprous chloride at 371 nm, resulting complete disappearance of the peak at 280 nm (Figure 16d). No further change in absorption spectra was observed on curing the samples for longer time (6 to 10 min). Whereas heating of the sample at 150 °C for 20 min in an oven resulted in two peaks at 280 nm and 345 nm. An intense characteristic peak of cuprous chloride

at 371 nm and complete disappearance of the peak at 280 nm was observed on heating at 150 °C for 60 min (Figure A 1 in appendix).

The growth of the CuCl particles is diffusion controlled, therefore the much higher growth rate in Beltron (4 min) could be attributed to higher temperature compared to the furnace where it takes 60 min. Another possibility can be, as the chlorocuprate complex is strongly absorbing in UV range it decomposes easily by UV irradiation but not as easily by thermal treatment.

It has been discussed in 'state of the art', that Ekimov et al. [107] reported an equation relating the particle radius (R) and the lowest energy (E) of the confined Z_3 exciton in UV-VIS spectra (please refer *section 2.1*, equation 2). Where $E_g - E_{ex}$ is the Z_3 exciton energy for the bulk crystal (3.218 eV for CuCl at 77 K) \hbar is Plank's constant divided by 2π and M_s is the translational mass ($= 1.9 m_0$ where m_0 is the free electron mass).

In order to apply this equation for calculating the particle size by the position of Z_3 exciton energy, the UV-VIS spectrum of thin films containing CuCl nanoparticles was recorded at liquid nitrogen temperature (88 K). Figure 17 shows the UV-VIS absorption spectrum of thin films containing CuCl nanoparticles at 88 K.

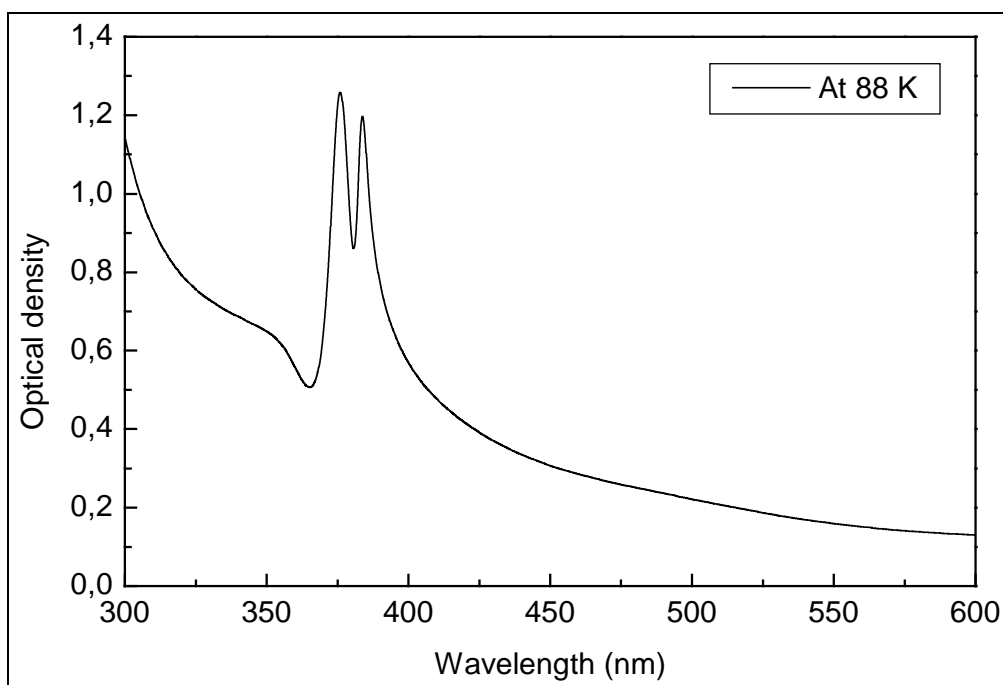


Figure 17: UV-VIS absorption spectra of thin films containing CuCl nanocrystallites at room temperature and at 88 K (experimental conditions in ch. III, p. 35).

Subsequently, the particle radius (r) was determined using the observed positions of Z_3 peaks from the above spectra using equation (2) [section 2.1]. The particle radius was found to be 5 nm for CuCl, which is of the same order as determined from HR-TEM, reported in the section 5.1.3.

5.1.1.4 X-ray diffraction characterisation

In order to confirm the crystalline behaviour of the nanoparticles and the phase in which these particles exist in the films, X-ray diffraction measurements were carried out using $\text{CuK}\alpha$ in 2θ range $20 - 60^\circ$ in the steps of 0.04 steps and counting for 100 s. The X ray diffraction patterns of the thin film containing CuCl nanoparticles and the relative peak intensities (experimental and literature reported) are shown below in Figure 18.

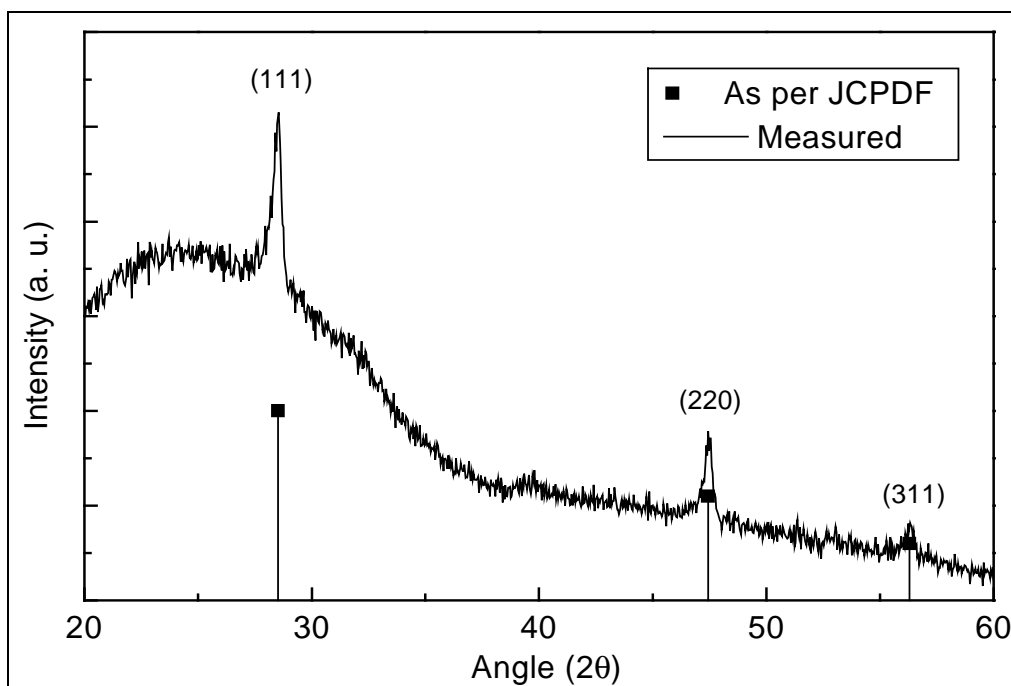


Figure 18: X ray diffraction patterns of thin films containing CuCl nanocrystals, literature reported intensities are also shown (experimental conditions in ch. III, p. 35).

XRD patterns observed are in very good agreement with the literature values and three characteristic peaks are of copper chloride [108]. The most intense peak corresponding to (111) plane is centred at 28.55° , while two other less intense peaks corresponding to (220) and (311) planes are centred at 47.47° and 56.33° respectively.

A comparison in reported and experimental X-ray diffraction peak positions and their intensities is shown below in Table 11.

Table 11: A comparison of literature reported [18] and experimentally observed X-ray diffraction peak positions and intensities for nantokite CuCl.

Plane (<i>hkl</i>)	Literature data for CuCl		Experimental data for CuCl	
	2θ	Intensity	2θ	Intensity
111	28.52	100	28.55	100
220	47.43	55	47.47	52
311	56.29	30	56.33	27

The observed X-ray diffraction pattern indicates that the copper chloride is present as nantokite (powder diffraction file no. 6-344) phase in thin films.

5.1.1.4. Study of evolution of CuCl nanoparticles using X-ray diffraction analysis

The stepwise generation of copper (I) chloride nanoparticles with the change in heat treatment conditions was also followed using X ray diffraction pattern. The measured X-ray diffraction patterns are shown below in Figure 19.

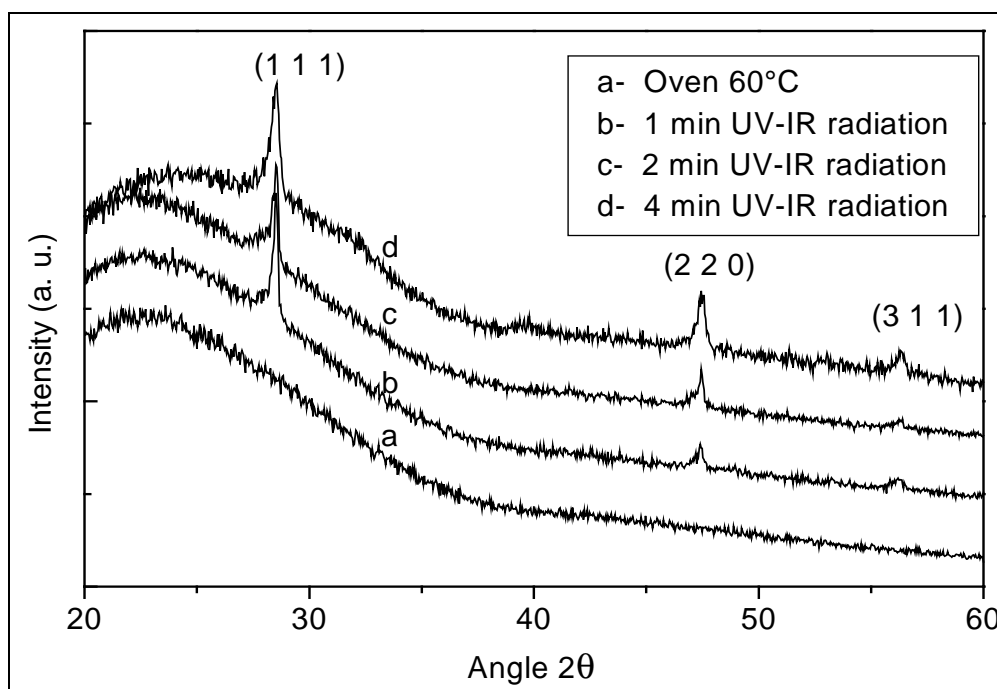


Figure 19: X ray diffraction pattern as a function of heat treatment conditions, (a) dried in an oven at 60 °C, and UV-IR machine (1200 W) for (b) 1 min (c) 2 min and (d) 4 min (experimental conditions in ch. III, p. 35).

In this figure, it is clearly to be seen that for the sample heated at 60 °C in an oven no X-ray diffraction peak was observed (Figure 19a), indicating the absence of CuCl in thin film after heating the sample at 60 °C for 15 min. The same behaviour was also shown by UV-VIS spectra. The sample treated in UV-IR irradiation (1200 W / 150 °C) for 1 min, shows all the three diffraction peaks corresponding to (111), (210) and (311) planes of nantokite CuCl (Figure 19b). Treating the sample for 3 and 4 min in a beltron machine shows only an increase in the intensities of all the three diffraction peaks (Figure 19c and d).

From the angle corresponding to the maximum diffraction (111 peak here) and the halfwidth of the diffraction peak, the average size of the nanoparticles was calculated using Scherrer's equation. Half width of the peak was measured to be 0.935° , and 2θ was measured equal to 27.208° . Using these parameters a particle radius 'r' of 5.5 nm was determined.

The following Table 12 shows the size of CuCl nanoparticles calculated using Scherrer's equation, UV-VIS spectra and HR-TEM analysis.

Table 12: The size of CuCl nanocrystals using Scherrer's equation, UV-VIS spectra and HR-TEM analysis.

Scherrer's formula 'r'	UV-VIS spectra [1071 'r'	HR-TEM 'r'
5.5 nm	5 nm	6 nm

Particle size determined by three different methods compares well. A lattice constant of 5.41 \AA was determined using XRD pattern. This value compares very well with the literature value of CuCl [121].

It was observed that after storage of the samples in air a decrease in the intensity of the characteristic copper halide UV-VIS absorption peak was observed, which vanishes completely after certain time period. Therefore, the stability of CuCl in thin films was studied in different atmospheres. The change in the area of CuCl absorption peak as a function of time is shown below in Figure 20, for the samples stored in air, in desiccator (exclusion of moisture) and in vacuum.

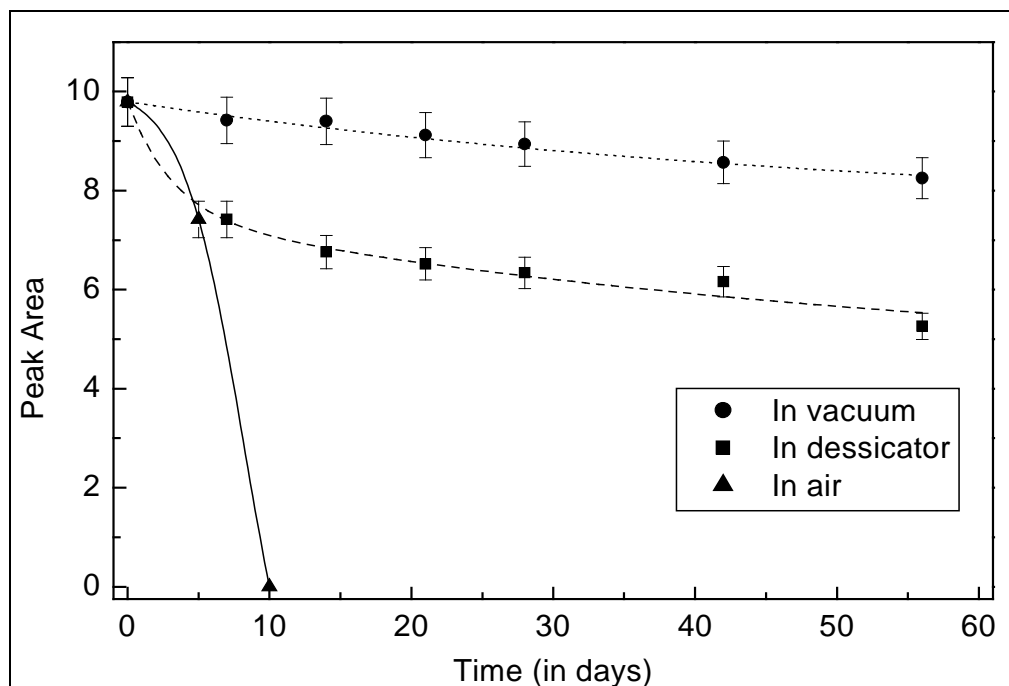


Figure 20: The change in UV-VIS absorption peak area of CuCl in different atmospheres, as a function of time (in days).

It can be seen from the above figure that the CuCl was found to be least stable in air and most stable in vacuum. Whereas the peak vanishes completely in air within 10 days, on standing the samples in a desiccator (exclusion of moisture) on the other hand, relatively small decrease in the intensity of absorption peak was observed even after 56 days also. A decrease in the peak intensity can be observed in vacuum as well, though it is very small. As exclusion of moisture drastically increases the stability of CuCl, it can be said that that the CuCl is very sensitive for the moisture.

The possible explanation for this behaviour is a very unstable nature of copper (I) chloride. In presence of moisture and air the Cu(I)Cl is known to be oxidised and hydrolysed to a green product that approaches to copper (II) oxychloride $\text{CuCl}_2 \cdot 3\text{Cu}(\text{OH})_3$ [109]. In order to confirm the transformation of Cu (I) into Cu (II) X-ray diffraction pattern of the thin films standing in air at 25 °C for 3 weeks at 25 °C was measured. The XRD patterns of thin films as prepared and those standing at 25 °C for 3 weeks are shown below in Figure 21.

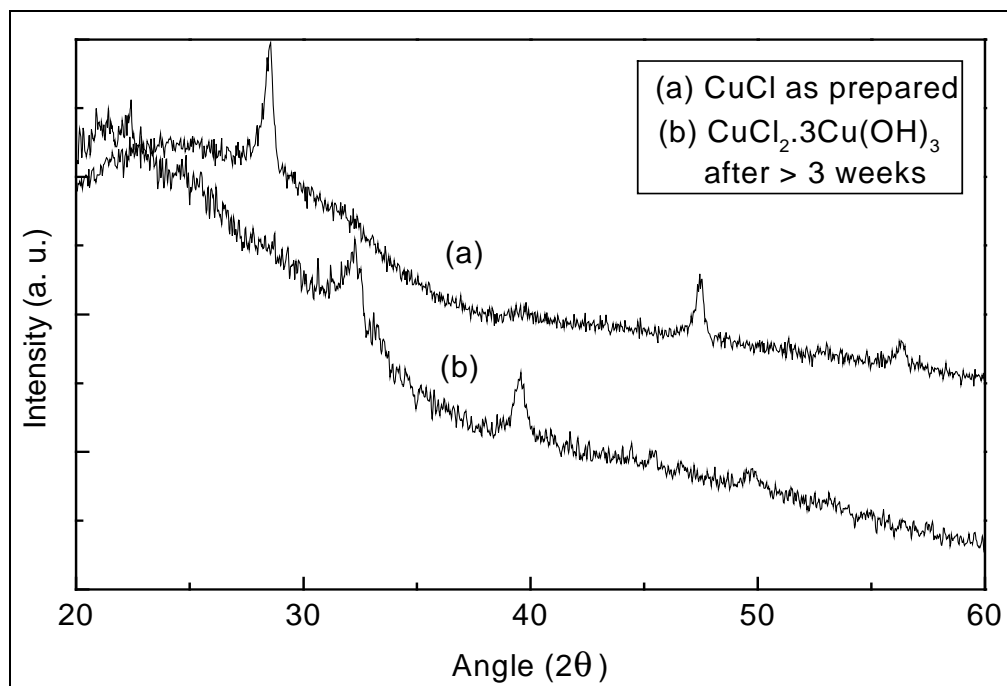


Figure 21: X- ray diffraction patterns of thin films containing CuCl nanocrystals, (a) as prepared (b) after standing in air at 25° C for three weeks.

A remarkable change in XRD patterns can be observed from Figure 21. The samples standing at 25 °C in air for 3 weeks showed three XRD reflexes corresponding to copper (II) oxychloride [110]. Therefore XRD measurements also support the conversion of Cu (I) into Cu (II).

5.1.1.5 Effect of post heat treatment on the samples containing CuCl nanoparticles

During the heat treatment of thin films containing CuCl at higher temperatures (>200 °C), it was observed that the intensity of CuCl exciton peaks decreases and disappears completely after a certain time. To understand the mechanism, CuCl containing sample was treated at 250 °C in an oven for different time periods and the UV-VIS spectra were measured. The UV-VIS spectra are shown below in Figure 22.

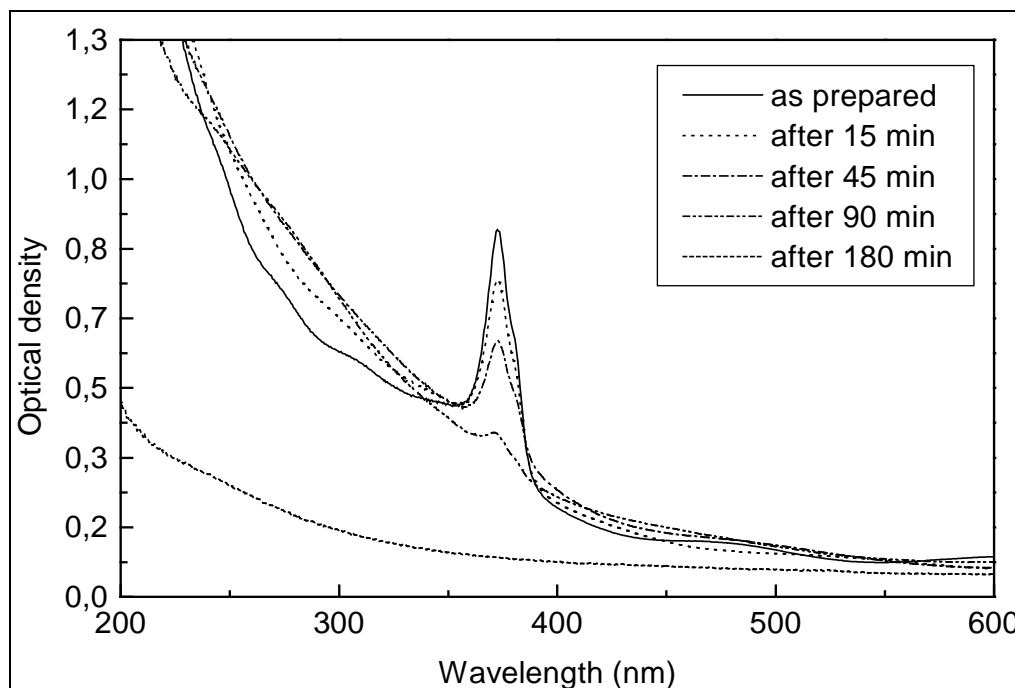


Figure 22: UV-VIS absorption spectra of thin films containing CuCl nanocrystals on heating at 250 °C in air for different time periods (a) as prepared, after (b) 15 min, (c) 45 min, (d) 90 min and (e) 180 min.

It is clear from the above figure that on heating the sample at 250 °C in air for 15 min there is a small decrease in the intensity of UV-VIS absorption peak. Whereas a remarkable decrease in the intensity can be seen after 45 min. After 3 h of heat treatment at 250 °C in air results a complete disappearance of the characteristic absorption peak due to CuCl. Indicating that there is no CuCl left in the films after 3 h. Simultaneously a strong absorbance in the UV range (200-300 nm) was observed that may be attributed to the decomposed organics in the coatings. It initially increases till 45 min of heating and remarkably decreases after 3 h of heating.

As it is known that Cu^+ is very unstable in presence of moisture, and from the above experiments it has been proved that it oxidises to Cu^{2+} . To understand the mechanism of this transformation, two possibilities may be considered. 1) either cuprous chloride has been changed into cupric compound with the formation of $\text{CuCl}_2 \cdot 3\text{H}_2\text{O}$ or 2) CuCl has been decomposed into Cu^+ and Cl^- , resulting in the disappearance of chlorine. If there is $\text{CuCl}_2 \cdot 3\text{H}_2\text{O}$ in the films it should show crystalline behaviour. But X-ray diffraction measurement of the sample heated at 250 °C for 3 h shows a noncrystalline behaviour (figure A 5 in appendix). This indicates that the decomposition of CuCl into $\text{Cu}^+ / \text{Cu}^{2+}$ and Cl^- . If copper is still present in the films as ionic copper, it should form copper colloids under reducing atmosphere. Therefore samples standing in air for 3

Thin films containing copper halide nanoparticles

weeks were heat-treated under reducing atmosphere ($N_2 / H_2 = 92 / 8$, 80 l/h) at 450 °C for 1 h with the heating rate of 100 K/h. The formation of copper colloids was followed by UV-VIS absorption spectroscopy. The UV-VIS absorption spectra of thin films heated under reducing atmosphere is shown in Figure A 3 in appendix. As this figure shows only one absorption peak at 587 nm, indicating the formation of copper colloids in thin films. This result supports the presence of copper as ionic form in the films.

5.1.2 Thin films containing CuBr nanocrystallites

5.1.2.1 UV-VIS characterisation

To investigate the optical properties of thin films containing copper bromide nanoparticles, UV-VIS absorption spectra of the thin films coated on the glass slides were recorded with a spectrometer (Bruins Instrument). The UV-VIS spectra of thin films containing nanocrystalline CuBr particles and a reference coating from the matrix sol, measured at room temperature are shown below in Figure 23.

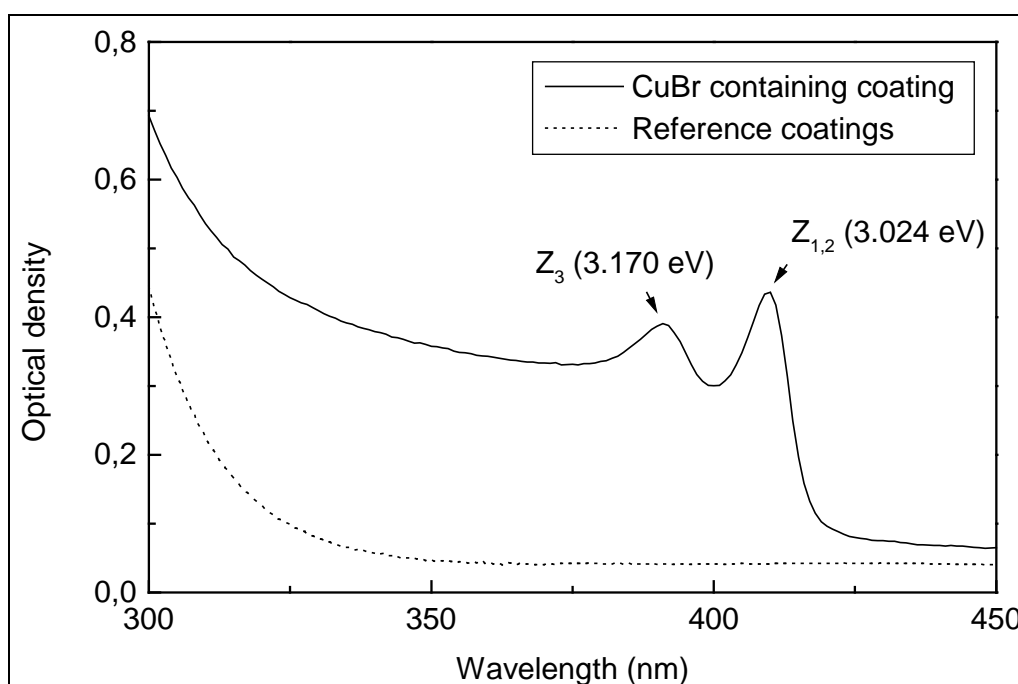


Figure 23: UV-VIS spectra of the thin films containing CuBr nanoparticles heat treated in a UV-IR beltron machine at 150 °C / 4 min, 1200 W, reference : air (for experimental conditions see ch. III, p. 37).

The above spectrum closely resembles with that reported in literature [39] and the peaks at 391 and 410 nm can be attributed to copper bromide nanoparticles.

5.1.2.1.1 Study of the evolution of CuBr nanoparticles in thin films using UV-VIS spectroscopy

In order to follow the generation of CuBr nanoparticles during UV-IR treatment, the UV-VIS spectra of the samples were recorded after 1, 2, 3, 4 min of UV - IR treatment. Figure 24 shows the UV-VIS spectra of the films treated at different intervals.

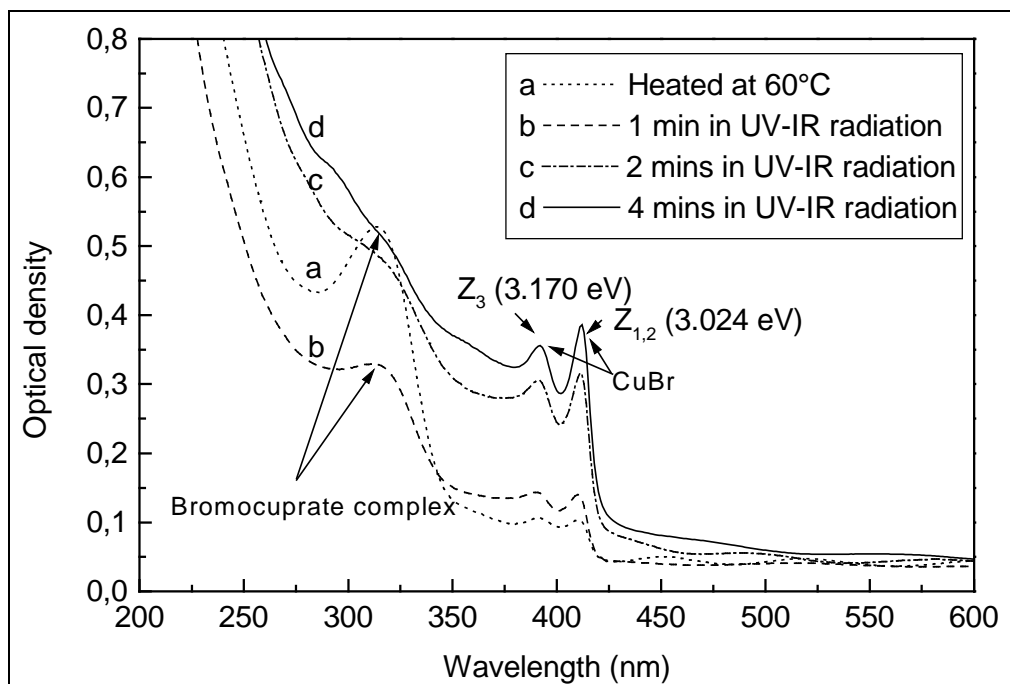


Figure 24: UV-VIS spectra of thin films containing CuBr nanocrystals as a function of heat treatment conditions, (a) 60 °C / 15 min in an oven and in UV-IR machine (1200 W) / 150 °C for (b) 1 min, (c) 2 min and (d) 4 min (experimental conditions are in ch. III, p. 37).

The sample dried at 60 °C shows a broad peak at 310 nm corresponding to bromocuprate complexes [112] and two very weak peaks at 390 and 410 nm, characteristic of CuBr (Figure 24 a). On passing the samples through the UV-IR irradiation, the intensity of the peak at 310 decreases and the intensity of cuprous bromide at 390 and 410 nm increases. The intensity of absorption peak becomes constant after 4 min of UV-IR treatment. Unlike copper chloride (refer Figure 16) CuBr exciton peaks can be seen even for the samples heat treated in an oven at 60 °C, whereas in case of copper chloride CuCl peak appeared only after passing the samples through UV-IR beltron machine. As it is known from the literature [111], that the dissociation constant (pK) for the $[\text{CuBr}_2]^-$ complex, which gives following dissociation products is -3.3 to -2.3.



Therefore the soluble bromocuprate complex unlike chlorocuprate complex dissociates in copper bromide even at 60 °C, resulting in a CuBr absorption peak in UV-VIS absorption spectra (Figure 24 curve a).

From these observations it can be concluded, that the addition of halide ions to the suspension containing Cu_2O results in some acid soluble halocuprate complex ions. The addition of HBr results in dibromocuprate(I) and tribromocuprate(I) anions) showing an absorption at 310 nm for halobromate anions (Figure 24a) [112]. During the UV-IR treatment, these acid soluble halocuprate complexes were decomposed to form cubic CuBr nanocrystals in the SiO_2 -films.

In order to determine the particle size of the CuBr nanoparticles using the equation given by Ekimov et al. [30], UV-VIS spectrum of the thin films containing cuprous bromide was recorded at liquid nitrogen temperature (88 K). This spectrum is shown below in Figure 25.

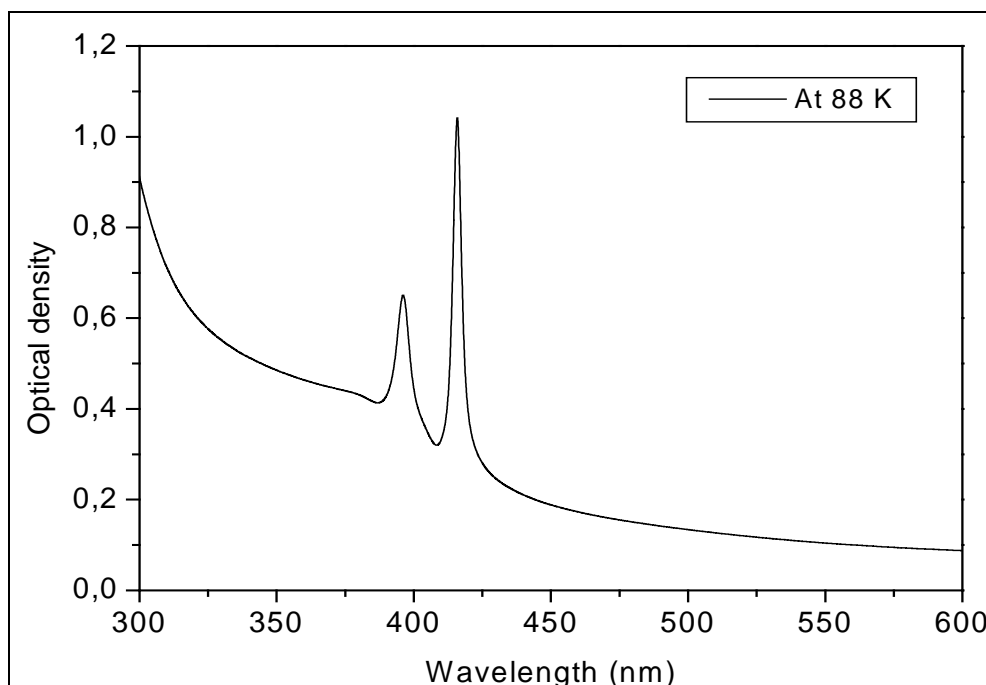


Figure 25: UV-VIS absorption spectra of thin films containing CuBr nanocrystallites at 298 K and at 88 K (experimental conditions in ch. III, p. 37).

The particle radius using observed peak position in Ekimov equation was determined to be 6.0 nm. The Z_3 exciton energy for CuBr bulk crystals was taken to 3.125 eV at 77 K.

5.1.2.1.2 Temperature dependence of $Z_{1,2}$ and Z_3 exciton peaks of CuBr nanoparticles in thin films

In case of CuCl, the splitting of $Z_{1,2}$ and Z_3 excitons, originating from Γ_8 and Γ_6 of the spin orbit split valence band maximum has been found to be dependent of the temperature by Kaifu et al. [113]. This has not been reported for CuBr and therefore the temperature dependence of $Z_{1,2}$ and Z_3 excitons in CuBr was studied. The absorption spectra of CuBr nanoparticles as a function of temperature are shown in Figure 26, whereas the positions of $Z_{1,2}$ and Z_3 exciton peaks as a function of temperature and the half width of $Z_{1,2}$ absorption peak as function of square of the temperature are given below in Figure 27. The absorption spectra were recorded in the spectral range from 300-1000 nm (i.e. 4.13-1.24 eV) at four different temperatures. However the spectra have been shown here only in the range from 2.5-3.5 eV.

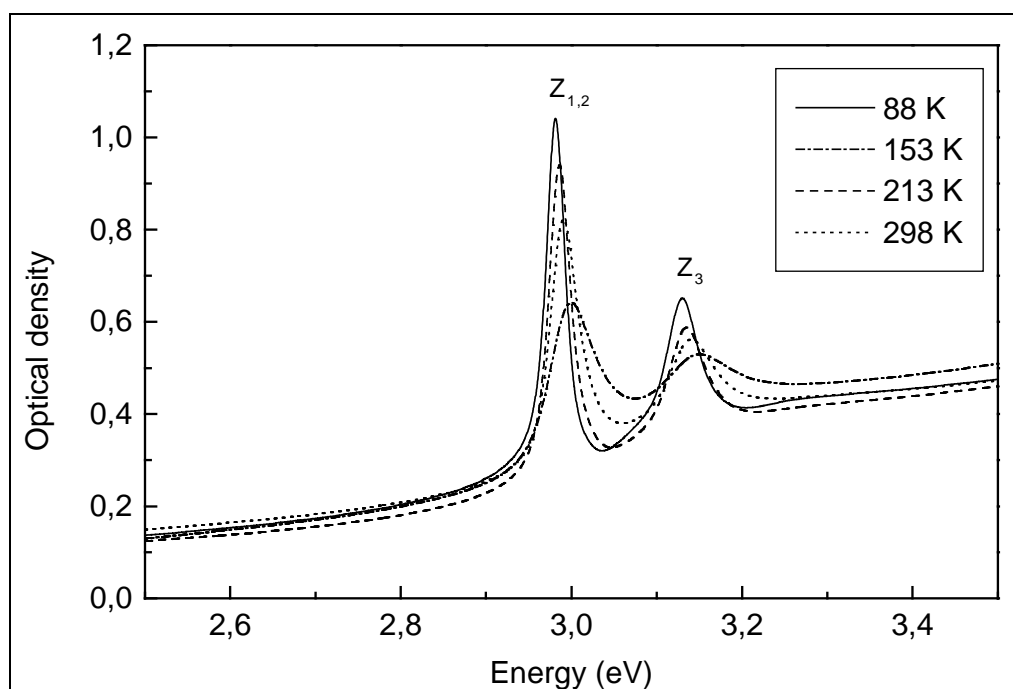
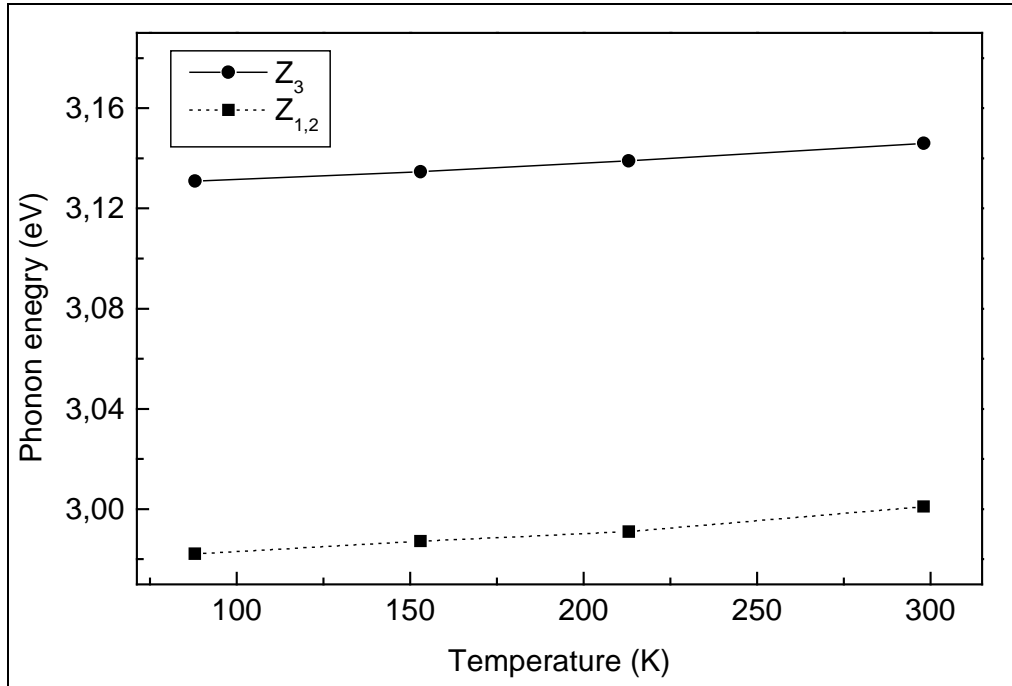
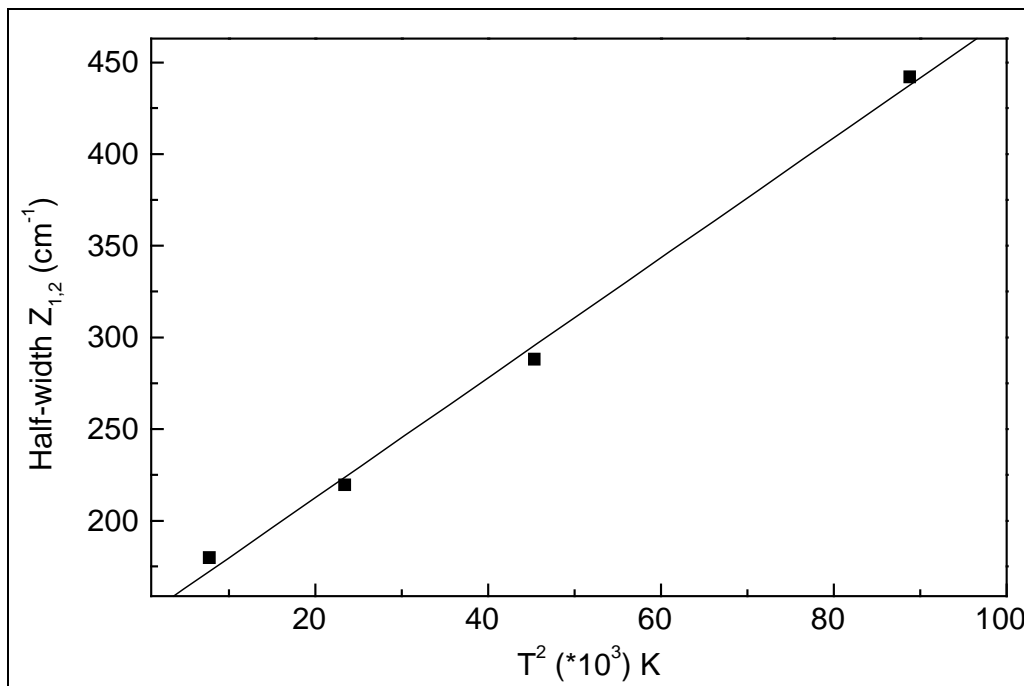


Figure 26: Change in exciton peaks of thin films containing CuBr nanocrystals as a function of temperature.



(a)



(b)

Figure 27: (a) Z_3 and $Z_{1,2}$ absorption peak position as a function of temperature (b) Halfwidth of $Z_{1,2}$ exciton peak as a function of square of the temperature.

The position of the absorption maxima for Z_3 and $Z_{1,2}$ are plotted in Figure 27 (a) as a function of temperature. These figures indicate that the splitting of the $Z_{1,2}$ and Z_3

excitons remains practically constant with the temperature. The same observations were made by Garro et al. [114] in case of the CuCl nanoparticles.

The dependence of the excitons of CuCl on temperature has been explained by Garro et al. [114] by postulating that the vibration of the Cu ions leads to an increase in the gap while the opposite is true for the halogen ions. They considered that the copper vibrates predominantly at low frequencies, while Cl vibrates mainly at high frequencies, because of its smaller mass. Hence the Cu-vibrations cause a linear variation of the gap at rather low temperature. Hence the analogous temperature dependent observed in case of CuBr can also be interpreted in the similar way.

The half width of the $Z_{1,2}$ exciton peak is plotted in Figure 27 (b) as a function of T^2 . It can be seen that the data points lie in a straight line. All the plots are limited to the temperatures below 298 K, because at higher temperatures the determination of the width is uncertain. Here only the $Z_{1,2}$ line is considered, because Z_3 is superimposed on higher order exciton or satellite lines [115], and therefore its half width varies in a more complicated way. To determine the half width of the $Z_{1,2}$ peak, the spectrum was deconvoluted, and the curve fitted on the lower energy peak (i.e. $Z_{1,2}$ peak) was taken for half width calculations.

The broadening of the peak with temperature has been explained by Toyazawa's theory [116], who found that the half width in terms of the energy units can be expressed $W = g^2(kT)^2 / 8\pi^2 m^*u^2$, where K is the Boltzmanns constant, m^* is the reduced effective mass of the exciton, u is the longitudinal sound velocity and g is the dimensionless coupling constant. This equation implies that the halfwidth of the excitons is proportional to (temperature)².

5.1.2.2. X-ray diffraction characterisation

In order to see if the CuBr nanoparticles are crystalline or not and to determine the phase of these nanoparticles, X-ray diffraction patterns were recorded. The X-ray diffraction patterns of the thin film containing CuBr nanoparticles and the relative peak intensities (experimental and literature reported) are shown below in Figure 28.

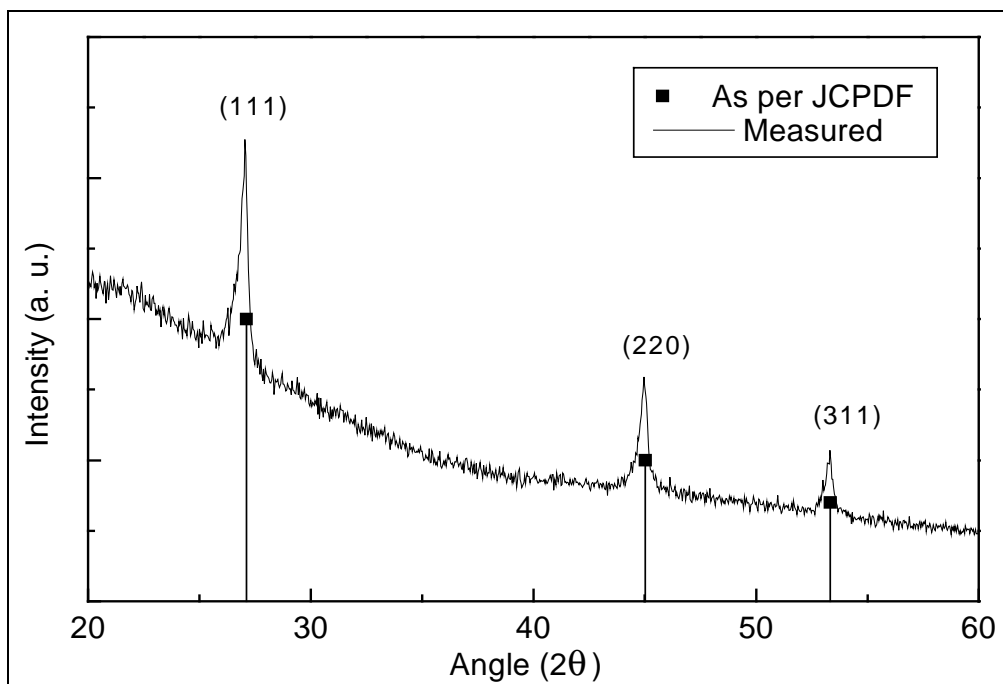


Figure 28: XRD patterns of thin film containing CuBr nanocrystals and the literature reported intensities (powder diffraction file no. 6-292) for gamma phase (for experimental conditions see ch. III, p. 37).

XRD patterns observed are in good agreement with the literature values for CuBr and the observed peaks can be attributed to the copper bromide gamma phase [117]. The most intense peak corresponding to the (111) plane is centred at 27.26° , while two other less intensity peaks corresponding to (220) and (311) planes are centred at 45.07 and 53.54° respectively. A comparison between the experimental and literature reported X-ray diffraction peak positions and intensities is shown below in Table 13.

Table 13: A comparison of experimentally observed and literature reported [18] X-ray diffraction patterns for CuBr.

Plane (<i>hkl</i>)	Experimental data for CuBr		Literature data for CuBr	
	2θ	Intensity	2θ	Intensity
111	27.26	100	27.12	100
220	45.07	51	45.02	50
311	53.54	32	53.34	35

Therefore it can be said that the observed X-ray diffraction pattern was found in very good agreement with the gamma - CuBr patterns, indicating that the copper bromide is present as gamma phase in thin films.

5.1.2.2.1 Study of the evolution of CuBr nanoparticles using X-ray diffraction analysis

The stepwise generation of copper (I) bromide nanoparticles with the change in heat treatment conditions was also followed by recording the X-ray diffraction patterns after every step of heat treatment. The recorded X-ray diffraction patterns are shown below in Figure 29.

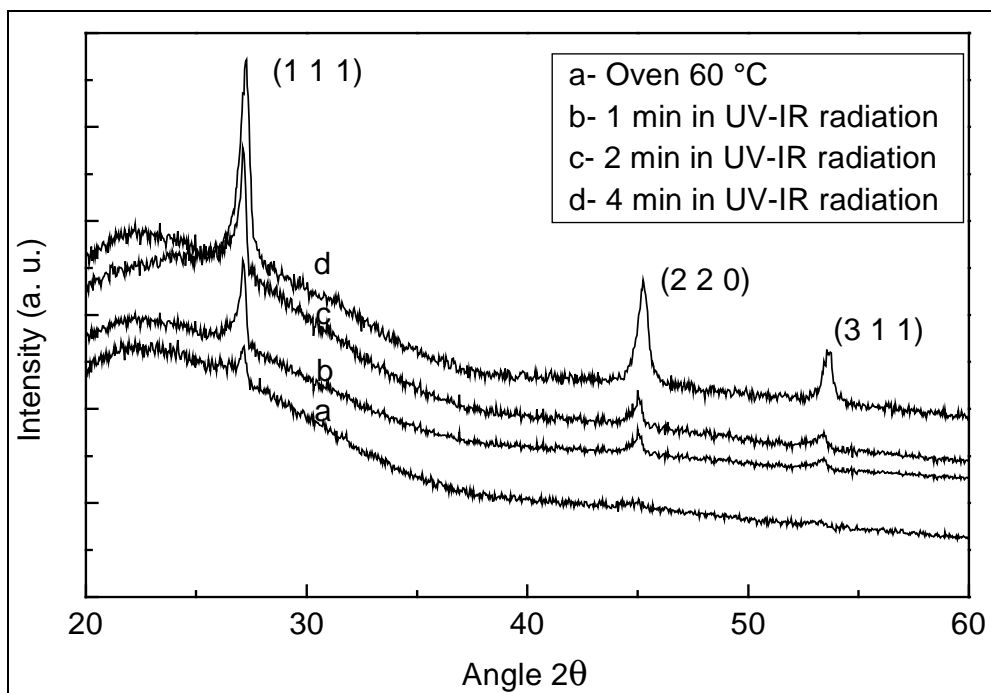


Figure 29: X ray diffraction patterns of thin films containing CuBr nanocrystals with the change in heat treatment conditions, (a) in an oven at 60 °C / 15 min, and UV-IR machine (1200 W) for (b) 1 min, (c) 2 min and (d) 4 min.

It is clearly to be seen from the above figure that for the sample heated at 60 °C in an oven one diffraction peak corresponding to the (111) plane is observed (Figure 29 a), whereas no diffraction peaks were observed corresponding to (211) and (311) planes. It shows that a small amount of copper has already been converted to CuBr after heating the sample at 60 °C for 15 min. This behaviour has already been observed by UV-VIS spectra. For the sample treated for 1 min in UV-IR irradiation, all three diffraction peaks corresponding to gamma CuBr are clearly visible (Figure 29 b). Peak intensities increase with increasing the UV-IR treatment time and maximum peak intensities were observed for the samples treated for 4 min in a UV-IR irradiation.

The particle size of CuBr nanoparticles was also determined using Scherrer's equation. The maximum intensity at $2\theta = 29.198^\circ$ was chosen for the calculation. Half width of the peak was measured using a computer programme and the observed x ray reflex was fitted with the Cauchy profile and the half-width was estimated to be 0.88 degree.

Using these values the particle radius 'r' was calculated to be 6 nm. For a comparison particle sizes measured using three different methods have been listed in following Table 14.

Table 14: Radius 'r' of CuBr nanocrystals as measured using Scherrer's equation, UV-VIS spectra [107] and HR-TEM analysis.

Scherrer's equation 'r'	UV-VIS spectra [107] 'r'	HR-TEM 'r'
6 nm	6 nm	7 nm

The particle sizes measured using three different methods are in good agreement with each other. The lattice constant calculated by using the X-ray diffraction pattern was equal to 5.68 Å, which also is in good agreement with the literature reported value for CuBr [121].

5.1.2.3 Effect of post heat treatment on the films containing CuBr nanoparticles

During the heat treatment of thin films containing CuBr at higher temperatures (>200 °C), it was observed that the intensity of CuBr exciton peaks decreases slowly and it disappears completely after a certain time period. To understand the mechanism of this decay, a CuBr containing sample was treated at 250 °C in an oven for different time periods and the UV-VIS spectra were recorded. The UV-VIS spectra are shown below in Figure 30.

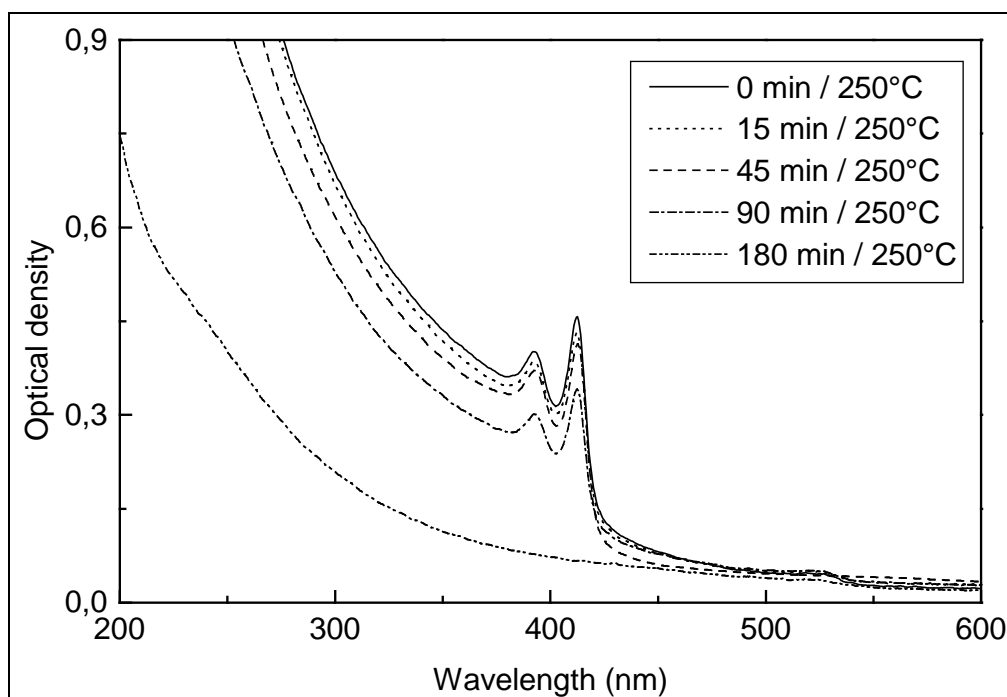


Figure 30: The UV-VIS absorption spectra of thin films containing CuBr nanocrystals heat treated at 250 °C for (a) 0 min, (b) 15 min, (c) 45 min, (d) 90 min and (e) 180 min.

It is clear from the above figure that on heating the sample in air at 250 °C for 15 min there is a small decrease in the intensity of UV-VIS absorption peak. Whereas a remarkable decrease in the intensity was observed after 45 min. 3 h of heat treatment in air at 250 °C results a complete disappearance of the characteristic absorption peak due to CuBr. It indicates that there is no CuBr left in the film after 3 h of heat treatment at 250 °C.

X-ray diffraction measurements were carried out for the film heated at 250 °C for 3 h. No diffraction peak was observed, indicating noncrystalline behaviour. One of the possibilities can be the decomposition of CuBr into $\text{Cu}^+ / \text{Cu}^{2+}$ and Br^- . If copper is still present in the films as ionic copper, it should form copper colloids under reducing atmosphere. So the samples were heat treated under reducing atmosphere ($\text{N}_2 / \text{H}_2 = 92 / 8, 80 \text{ l/h}$) at 500 °C for 1 h with the heating rate of 100 K/h. The formation of copper colloids was followed by UV-VIS absorption spectroscopy. The UV-VIS absorption spectra of thin films heated under reducing atmosphere showed only one absorption peak at 587 nm (appendix Figure A 4) indicating the formation of copper colloids in thin films. This result supports the presence of copper as ionic form in the films.

5.1.3 HR-TEM characterisation

In order to determine the size and structure of the CuX ($x = \text{Cl}, \text{Br}$) nanoparticles, high resolution electron microscopy (HR-TEM) was carried out. The HR-TEM pictures of the thin films containing uniformly dispersed CuCl and CuBr nanoparticles are shown in Figure 31 and Figure 33, respectively.

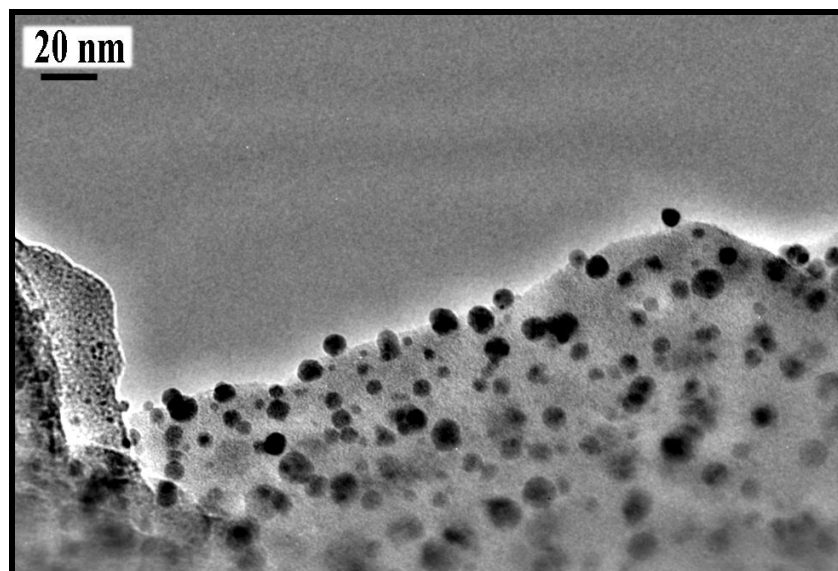
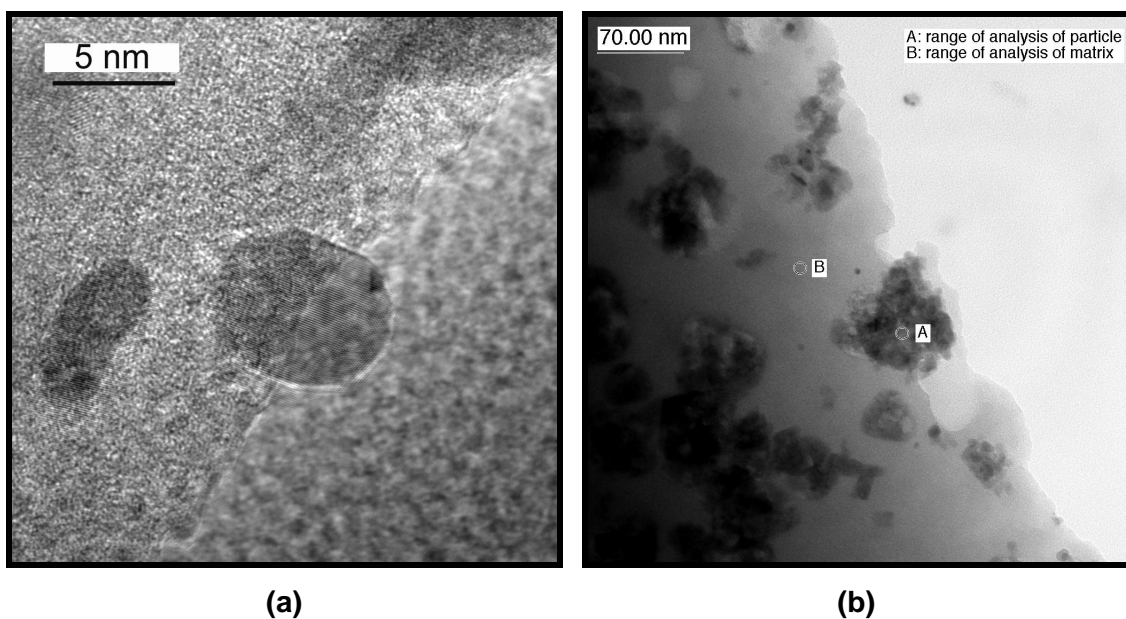


Figure 31: HR-TEM image of thin films containing CuCl nanoparticles.

The CuCl particles present within the wedge shaped region of the splinter show a diameter ranging from 4 to 16 nm (average diameter = 12 nm). A single particle having a diameter of 10 nm embedded in glass matrix is shown at higher magnification in Figure 32 (a).



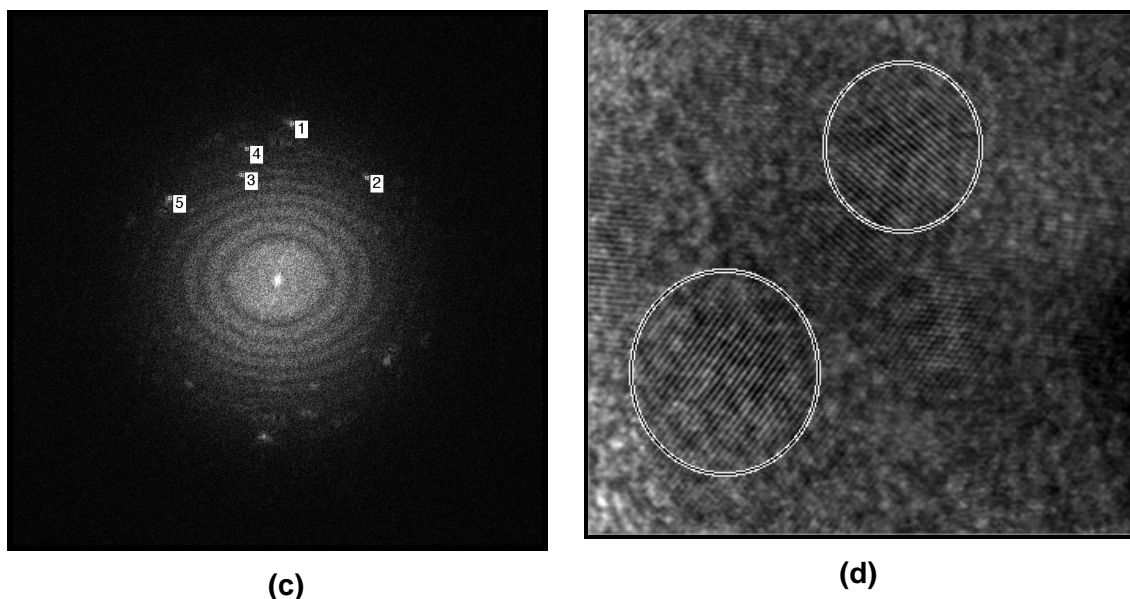


Figure 32: (a) Higher magnification HR-TEM image of single CuCl particle (b) HR-TEM image of some agglomerated particles, (c) Electron diffraction pattern of a small region selected from the agglomerates, (d) Probable nanocrystals, the spots in electron diffraction pattern are formed from.

For the samples having a GPTS / TEOS ratio of 1 : 1, the particles are well separated and uniformly dispersed, whereas for the GPTS / TEOS ratio of 4 : 1, formation of some agglomerates are also observed during the investigation. Figure 32(b) shows a HR-TEM picture of selected region containing some agglomerates. In order to see what these agglomerates are formed of, their electron diffraction pattern was recorded and the lattice spacing was calculated. Figure 32(c) shows the electron diffraction pattern and Figure 32(d) shows the crystal structure of agglomerated particles.

The analyses of the reflexes of the electron diffraction pattern yield the following distances.

$$2.02 \text{ \AA} = (111) \text{ reflex of Cu, } d = 2.09 \text{ \AA}$$

$$2.34 \text{ \AA}, 2.36 \text{ \AA}, 2.35 \text{ \AA} = (200) \text{ reflex of CuCl, } d = 2.47 \text{ \AA}$$

$$2.87 \text{ \AA} = (111) \text{ reflex of CuCl, } d = 2.85 \text{ \AA}$$

A lattice plane measurement of these particles indicates that the films consist still of nanokite phase of copper chloride. Observation of these lattice spacing suggests that the big clusters resulted from the agglomeration of small CuCl particles. In Figure 32(d) probable nanocrystals are imaged using probable CuCl spots of the diffractogram and applying the Fourier fittings. The investigated particles, which are marked by circles possess diameters in the order of 10 nm (6-11 nm). The high-

resolution micrograph of the sample heated at 200 °C for 2 h indicates the formation of clusters 70-80 nm in size, which can again be explained by the agglomeration of small CuCl nanoparticles on standing the sample at 200 °C for 2 h

Apart from the CuCl, lattice spacing measurements show the spacing corresponding to Cu reflex, confirming the presence of copper also in the agglomerates. But as the UV-VIS spectra do not show any absorption peak corresponding to the copper plasmon peak, it is very probable that the formation of copper is induced by the incidence of the electron beam on the CuCl particles.

The HR-TEM image of thin films containing CuBr nanocrystals is shown below in Figure 33.

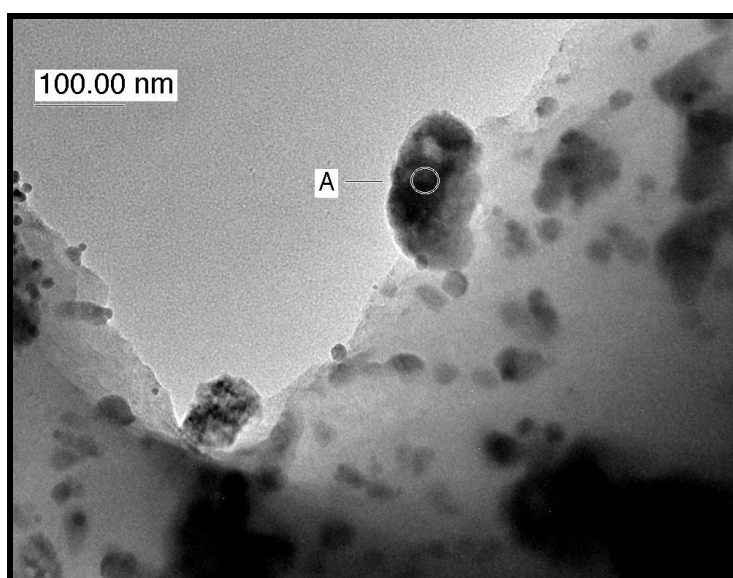


Figure 33: HR-TEM image of thin films containing CuBr nanoparticles.

This figure shows that in case of CuBr, nanoparticles are not uniform and some agglomerates are also formed. Particles with diameters ranging from 2-28 nm (average diameter = 14 nm) are formed.

5.1.4 Thin films containing $\text{CuCl}_x\text{Br}_{1-x}$ ($x = 0-1$) nanoparticles

5.1.4.1 Stepwise substitution of chloride by bromide ions

It has been shown in the previous sections that CuCl has an UV absorption peak at 371 nm, and CuBr has an UV absorption peak at 411 nm. So the synthesis of $\text{CuCl}_x\text{Br}_{1-x}$ ($x = 0-1$) can be helpful to tailor the absorption peak in between these wavelengths, which can be useful for the filtering of UV. Hence the synthesis of thin films containing $\text{CuCl}_x\text{Br}_{1-x}$ ($x = 0-1$) particles is carried out in the following section.

In order to synthesise thin films containing $\text{CuCl}_x\text{Br}_{1-x}$ nanoparticles, chloride ions were substituted by bromide ions. Different amount of HBr was added to the sol containing copper oxide dissolved in HCl for this (experimental conditions in ch. III, p. 39).

5.1.4.2 UV-VIS spectroscopic study of the sequential substitution of Cl by Br

In order to study the sequential substitution of chloride by bromide ions UV-VIS spectroscopic analysis was carried out. The UV-VIS spectra of the samples treated with UV-IR radiation for 4 min, recorded at room temperature after the stepwise addition of hydrobromic acid are shown below in Figure 34.

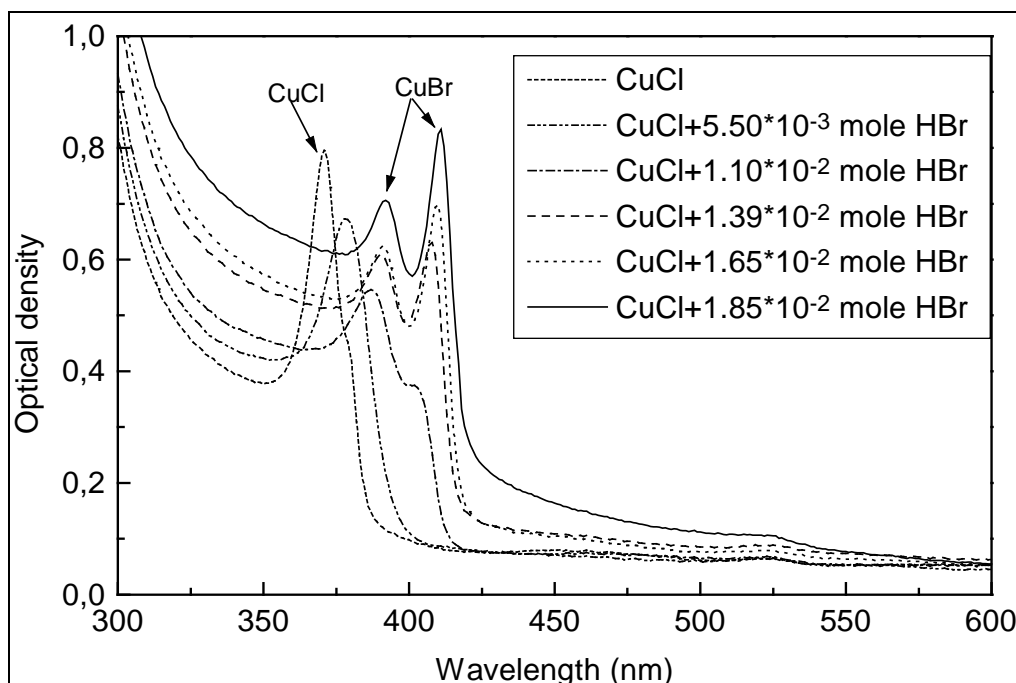


Figure 34: The UV-VIS absorption spectra of the sample prepared by the stepwise addition of HBr to the CuCl containing sol, (films were densified at 150 °C in UV-IR beltron machine, 1200 W / 4 min, experimental details are in ch. III, p. 39).

From the above spectra it is clear that the addition of 5.5×10^{-3} mole HBr shifts the absorption peak slightly towards higher wavelengths but it remains as a single absorption peak, whereas the addition of 1.1×10^{-2} mole of HBr shifts the peak towards still higher wavelengths and the single absorption peak splits into two sharp peaks. This absorption spectrum is in good agreement with the $\text{CuCl}_x\text{Br}_{1-x}$ doped bulk glasses as reported by Ruler et al. [33]. The addition of 1.85×10^{-2} mole of HBr changes the absorption spectra significantly and such sample showed two sharp peaks at 390 and 410 nm, as seen previously in case of thin films containing CuBr nanocrystals. Thus complete replacement of chloride by bromide ions seems to be taking place in this sample.

In all the spectra shown above, a very weak peak at around 525 nm is also visible. This peak may be assigned to the ${}^2B_{1g} \rightarrow {}^2A_{1g}$ transition of copper (II) ions in a square-planar co-ordination [118].

This behaviour can be explained by the fact that the bromide being less electronegative would easily replace the chloride in the solution. Since the stability sequence of halide complexes of Cu^+ is known to be $\text{I} > \text{Br} > \text{Cl} > \text{F}$ [119], CuBr is expected to be more stable than CuCl. From this experiment it can be concluded that 1.85×10^{-2} mole of HBr per 4.2×10^{-3} mole of Cu_2O dissolved in 8.2×10^{-2} mole HCl replaces chloride completely to give CuBr containing thin film. Therefore the mole fractions of bromine in films were calculated by assuming that the addition of a fraction of this amount of HBr results in the formation of the corresponding fraction of CuBr.

5.1.4.3 Comparison of the absorption spectra of CuCl and CuBr

The UV-VIS absorption spectra of thin films containing only CuCl, only CuBr and the reference coatings from the reference sol are shown in the Figure 35 for a comparison.

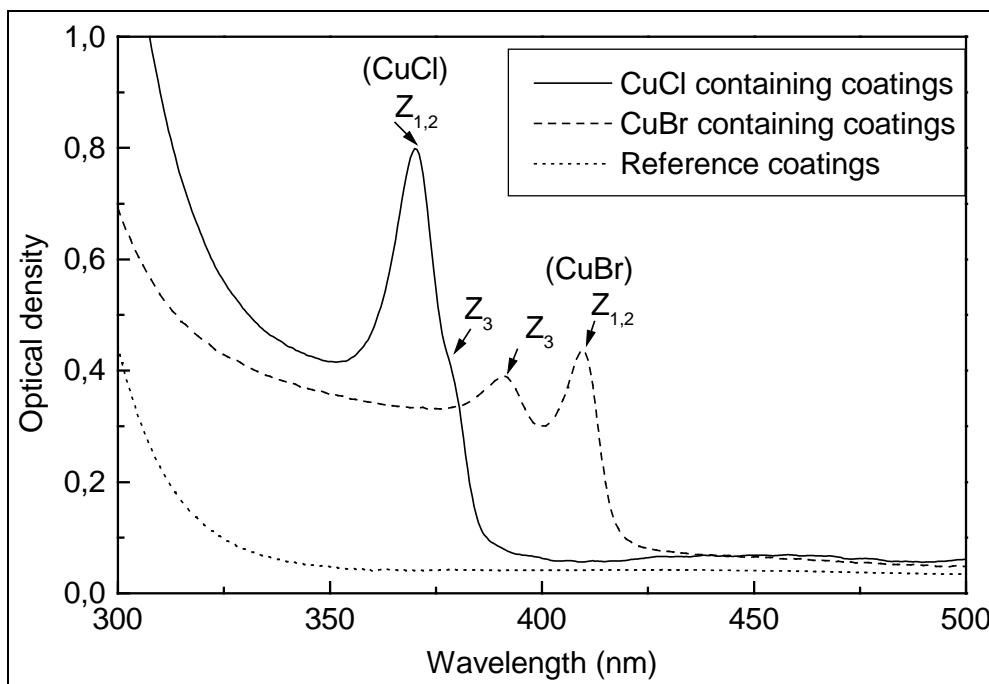


Figure 35: A comparison of the exciton absorption of CuCl and CuBr nanocrystals at room temperature (reference: air).

It is clear from the figure that in CuCl, $Z_{1,2}$ and Z_3 bands appear as high and low energy bands respectively. On the other hand in CuBr their positions are inverted (i.e. $Z_{1,2}$ and Z_3 bands correspond to the low and high energy bands respectively).

To understand this reverse behaviour of CuCl and CuBr, Cardona [42] suggested that the top of the valence band (Γ_{15}) is triply degenerated without spin orbit splitting in the zincblende structure. This degeneracy is reduced by spin orbit splitting to a doubly degenerated (Γ_8) and a singlet (Γ_6) states. The Γ_8 doublet state gives a $Z_{1,2}$ peak whereas the Γ_6 state gives the Z_3 peak. Since the strongest line should be the doublet line because of the larger number of states available for transition from the doubly degenerate valence band, they concluded that the spin orbit splitting is negative in case of CuCl i.e. the triplet in CuCl is inverted. The energies of the $Z_{1,2}$ and Z_3 absorption peaks of $\text{CuCl}_x\text{Br}_{1-x}$ ($x = 0-1$) at 25 °C are shown as a function of bromide ion concentration ($1 - x$) below in Table 15.

Table 15: The $Z_{1,2}$ and Z_3 peak positions of $\text{CuCl}_x\text{Br}_{1-x}$ at 25 °C as a function of $1 - x$ (bromide ion concentration).

$(1 - x)$ in $\text{CuCl}_x\text{Br}_{1-x}$	$Z_{1,2}$ Peak (in eV)	Z_3 Peak (in eV)
0	3,34	3,27
0.3	3,22	--
0.6	3,08	3,20
0.7	3,04	3,18
0.9	3,03	3,17
1.0	3,02	3,16

The above $Z_{1,2}$ and Z_3 absorption peak positions of the thin films containing $\text{CuCl}_x\text{Br}_{1-x}$ ($x = 1-0$) as the function of the bromide ion concentration ($1 - x$) at 25 °C are plotted in Figure 36.

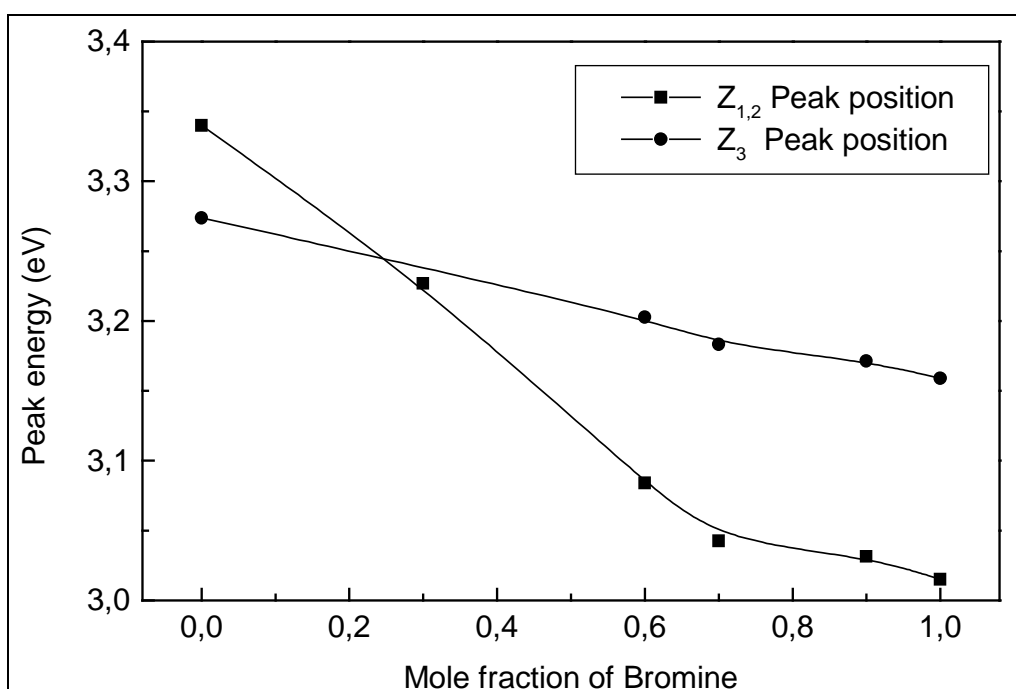


Figure 36: Energies of the $Z_{1,2}$ and Z_3 absorption peaks in $\text{CuCl}_x\text{Br}_{1-x}$ as a function of bromide concentration ($1 - x$) at 25 °C.

The variation of the absorption peak energy is in good agreement with that obtained by Cardona [42]. From this figure it is clear that the two curves (a) and (b) cross each other at $x = 0.24$, this indicates that there is no spin orbit splitting corresponding to this concentration. The band width of the Z_3 exciton band increases appreciably as the concentration ($1 - x$) exceeds the 0.24, and the band appears on the high energy side

of the $Z_{1,2}$ exciton. This fact is interpreted in terms of the shorter life time of the higher energy Z_3 exciton owing to the scattering into the lower state of the $Z_{1,2}$ exciton [120]. When the Z_3 exciton is lower in energy than that of the $Z_{1,2}$ exciton, there is no state for the Z_3 exciton to be scattered to except within its own band, and the life time of the excitons is longer. Thus the Z_3 exciton band is sharper. At $x = 0.24$ to where the relative position of the two bands are inverted but the separation between them is not too large, the $Z_{1,2}$ band is much weaker than the Z_3 band. The intensity of the $Z_{1,2}$ band increase gradually as $(1 - x)$ increase, from 0.24 and the separation between Z_3 and the $Z_{1,2}$ bands increases.

5.1.4.4 Study of sequential substitution of Cl^- by Br^- using XRD analysis

The sequential substitution of Cl^- by Br^- was also followed by XRD analysis. Figure 37 shows the XRD patterns of the films containing varying amount of bromide and chloride.

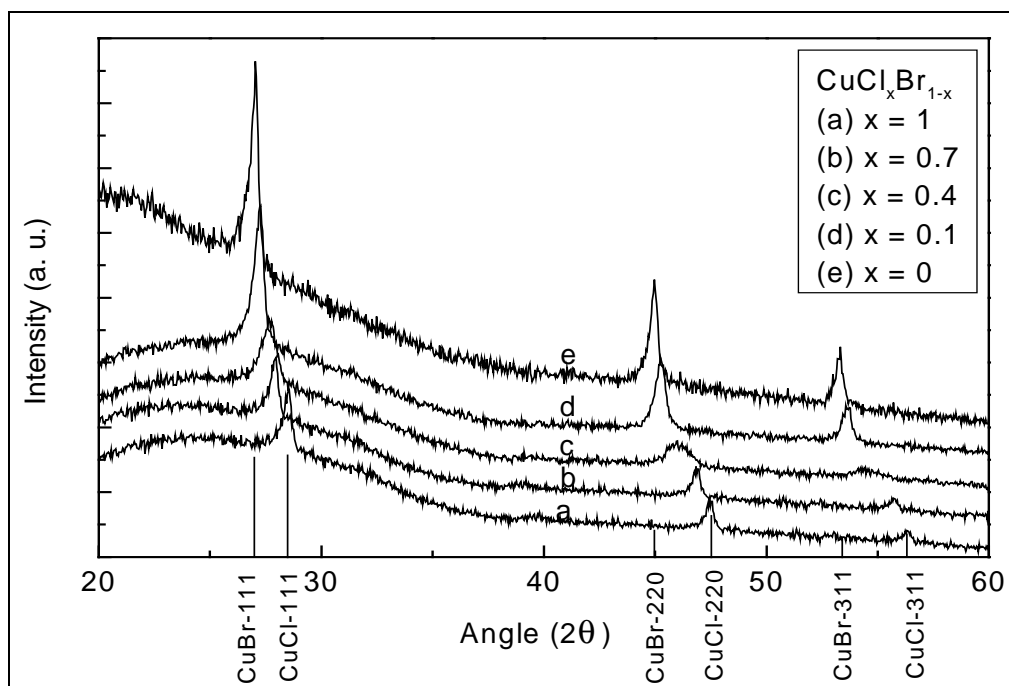


Figure 37: X- ray diffraction patterns of thin films containing $CuCl_xBr_{1-x}$, (a) $x = 1$, (b) $x = 0.7$, (c) $x = 0.4$, (d) $x = 0.1$ and (e) $x = 0$ (experimental conditions are in ch. III, p. 39).

When there is no HBr in the solution all the three diffraction peaks of CuCl (Figure 37a) were obtained. The addition of 5.50×10^{-3} to 1.66×10^{-2} mole HBr per 4.2×10^{-3} mole of Cu_2O dissolved in 8.2×10^{-2} mole HCl gradually shifts the peaks toward the

lower 2θ 's. Addition of 1.85×10^{-2} mole HBr finally leads to all the three characteristic peaks (Figure 37 e) of CuBr.

In order to see, if Br ions are sequentially substituting Cl ions or they are occupying the interstitial voids for the intermediate compositions, Lattice parameters of the compounds $\text{CuCl}_x\text{Br}_{1-x}$ ($x = 0-1$) were determined from the XRD spectra using the following relation

$$\frac{1}{d^2} = \frac{h^2 + k^2 + l^2}{a^2} \quad \text{where,} \quad \begin{array}{l} h, k, l \text{ Miller indices} \\ d \text{ Inter planer spacing} \\ a \text{ lattice constant} \end{array}$$

Precise lattice constants were determined by taking an average of the lattice constant based on three peaks (111), (220) and (311). The variation of lattice constant as a function of bromide ion concentration is shown below in Figure 38.

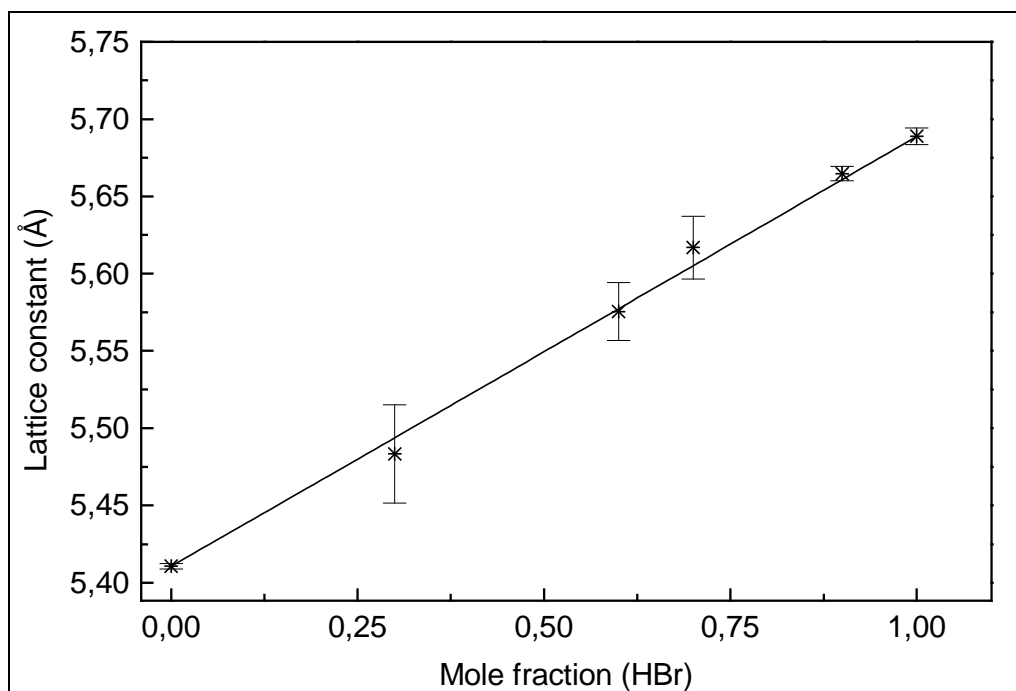


Figure 38: Variation of lattice constant with the substitution of chloride by bromide ions.

For the samples without HBr, the lattice constant of 5.42 \AA was determined which is in agreement to the literature-cited value for CuCl [121]. Addition of HBr gradually increases the lattice constant and finally gives the value of 5.68 \AA , which is in good agreement with the literature reported value for CuBr [121] for 1.85×10^{-2} mole of HBr.

The data points lie in a straight line, which indicates that the chloride ions are 'substituted' by the bromide ions in the complete composition range thus confirming the Vegard's law [122] behaviour.

5.1.5 Summary and Conclusion

Sol-gel process has successfully been used for the synthesis of nanocomposite thin films containing CuCl, CuBr and $\text{CuCl}_x\text{Br}_{1-x}$ ($x < 1$ and > 0) nanocrystal. Copper could be stabilised as Cu^+ as acid soluble halocuprate complex in solution, in the presence of acetonitrile. These complexes decompose during heat treatment and form copper halide nanoparticles. The formation of acid soluble halocuprate complexes like CuX_2^- and CuX_3^{2-} ($x = \text{Cl}, \text{Br}$) and their decomposition during the heat treatment to CuCl and CuBr was confirmed by the UV-VIS spectroscopy. UV-VIS spectroscopy showed high intensity $Z_{1,2}$ and Z_3 exciton peaks thus confirming the formation of Cu halide nanocrystals. For thin films containing CuBr, shift of $Z_{1,2}$ and Z_3 excitons towards the higher energies with increasing the temperature was observed.

The nanocomposite thin films containing CuCl, CuBr and $\text{CuCl}_x\text{Br}_{1-x}$ were characterised with the help of X-ray diffraction measurements. For nanocomposites containing copper chloride heat treated at 150 °C in a UV-IR beltron machine (at 1200 W), particles with average diameter of 11 nm were formed, and their lattice constant was determined to be 5.42 Å. For copper bromide the particles with the average diameter of 14 nm were formed under the same conditions and the lattice constant was determined to be 5.68 Å. Cubic, gamma- and nantokite- phases were observed for (CuBr) and (CuCl) nanoparticles respectively.

Stepwise substitution of chloride ions by bromide ions was carried out successfully. For the samples having no bromide, UV-VIS absorption spectra showed a sharp absorption edge at 371 nm. Addition of HBr shifted the peak towards the higher wavelength and characteristic peaks corresponding to $\text{CuCl}_x\text{Br}_{1-x}$ were observed. Addition of 1.39×10^{-2} mole of HBr finally produced the peaks corresponding to CuBr indicating the complete substitution of chloride by bromide ions.

These experiments confirmed that the position of the absorption edge can favourably be shifted by the substitution of chloride ions by bromide ions. Thus the absorption edge was successfully shifted from 371 nm (for pure CuCl) to 411 nm (for pure CuBr). Further research has to be conducted in order to find an impervious matrix, which

Thin films containing copper halide nanoparticles

prohibits the reduction of cuprous to cupric ions, thus opening the fields of applications like UV-VIS filters with sharp edge and non-linear optics.

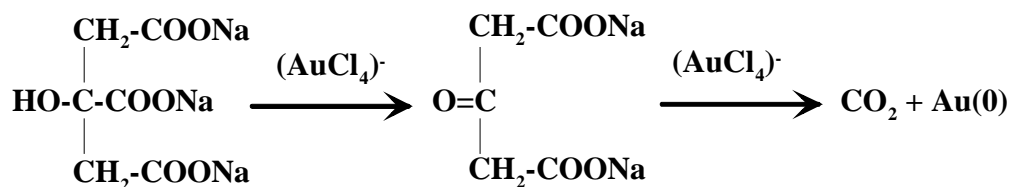
5.2 Synthesis and characterisation of nanocomposite thin films containing bimetallic colloids of Ag / Au and Ag / Cu

5.2.1 Ag / Au system: Thin films containing alloy- and mixed-colloids

5.2.1.1 Alloy colloids

As it has been discussed in the introduction, thin films doped with monometallic colloids have been studied by various authors, but the preparation of nanocomposite coatings containing bimetallic particles composed of both gold and silver has not received much attention. It is known from the calculated absorption spectra of gold-silver alloys [72] that the plasmon band remains as a single peak and shifts continuously from 410 to 530 nm with increasing molar ratio of gold. Therefore, thin films containing Ag / Au alloy colloids have been synthesised in order to get colours intermediate to those obtained by pure gold colloids and pure silver colloids and their optical properties in the visible region have been studied.

For this a new route to synthesise thin films containing noble metal alloy colloids by sol-gel technique had to be developed. It is known from the work of Morris et al. [74] that in solution silver coated gold colloids can be synthesised by reducing silver onto the pre formed gold particles with the help of hydroxylamine hydrochloride. Using this concept, gold colloids were synthesised first in aqueous solution. Polyvinylpyrrolidone was chosen as a stabiliser for gold, due to its solubility in water. An aqueous solution containing colloidal gold was synthesised by reducing Au^{+3} with sodium citrate dihydrate. The yellow colour of AuCl_4^- anions disappeared immediately after the addition of sodium citrate, and after about 3 min the solution slowly became violet and then deepened to a wine red colour. If no stabiliser was added the addition of reducing agent leads to a brown precipitate. It is assumed that this was due to the agglomeration of the colloidal particles. As it is known that to obtain mono-disperse monometallic particles, some protective agents such as polyvinylpyrrolidone [123, 124] have often been required to stop coagulation and protect the agglomeration of particles in solution. Turkevich et al. [125] proposed the following mechanism for metal salt reduction by citrate in solution.



Silver was added dropwise to the gold sol in the presence of hydroxylamine-hydrochloride (HAH) to reduce the Ag^+ onto the surface of gold (details of the synthesis can be seen in ch. III, p. 40).

The formation of gold colloids was confirmed by the UV-VIS spectroscopy (it will be shown later). The amount of sodium citrate dihydrate for the reduction of ionic gold into colloidal gold was optimised for a 100% colloid turnover. The addition of polyvinylpyrrolidone is necessary in order to stabilise the gold colloids in solution, if no polymer was added the addition of aqueous solution of sodium citrate dihydrate in the aqueous solution of tetrachloroaurate always led to a precipitate. The ratio of gold and PVP was kept the same as reported in literature [70]

Complexing of silver with DIAMO was necessary as the addition of silver into the gold sol containing HAH always led to the AgCl precipitate. PbO was incorporated in the silica matrix in order to get the dense coatings resulting a decrease in the rate of reduction of silver into silver oxide on standing in air (it will be shown in the later section). Lead acetate was chosen as a precursor for lead due to its good solubility in alcohol.

5.2.1.1.1 Synthesis of colloidal gold particles in solution

The absorption spectra of the colloidal gold containing sols showed a maximum at 526 nm for gold colloids, and TEM analysis confirmed the formation of gold colloids of radii 8-10 nm in solution (Figure A 6 in appendix). But now the question arises, that how much ionic gold has been converted to the colloidal gold. In order to determine the percentage of colloidal gold in solution following calculations were performed.

5.2.1.1.2 Calculation of colloidal turnover of Au colloids in aqueous solution

It is known that the area under the absorption band is directly proportional to the volume concentration of the colloids [126]. Therefore, it is possible to calculate the colloidal turnover from the measured absorption spectra. For this calculation the proportionality factor 'f' between the peak area and colloid volume concentration must

be determined. The proportionality factor is given by $f = C/A$, (C = concentration of metal colloids, and A = area of the extinction band).

In order to calculate the 'f', various extinction spectra were calculated for the particles with different radii at a constant volume concentration (10^{-6}) and a constant refractive index (1.33) for the solution using a computer programme used by Quinten [127], based on Mie-theory [134]. Absorption maxima were determined and the spectrum was integrated to the long wavelength side (from wave maxima to 1000 nm). The proportionality factor for the particles of different radii is shown below in Table 16.

Table 16: The proportionality factor for the particles of different sizes, Avg. is the average of the proportionality factor of the particles with radii 3, 5, 8 & 10 nm. $C_{\text{composition}}$ is the colloidal volume concentration calculated assuming that all the gold has been converted to colloidal Au, ρ_s and ρ_{Au} are the densities of the solution and gold respectively.

Particle size	Proportionality factor 'f'
Avg.	2.58×10^{-7}
20 nm	2.32×10^{-7}
30 nm	1.68×10^{-7}
40 nm	1.31×10^{-7}
ρ_s	1.0 gm / cm ³
ρ_{Au}	19.3 gm / cm ³
$C_{\text{composition}}$	4.06×10^{-4}

The calculations indicated that the proportionality factor 'f' for the particles ranging in radii from 1 to 10 nm, was nearly independent of the colloid radius.

Now the experimentally observed absorption spectra were converted into the extinction spectra using following equation (1).

$$k = \ln 10 \cdot \frac{OD}{d} \quad (11)$$

k Extinction coefficient (1/mm)

OD Optical density

d Film thickness (mm) both side (for the films) and thickness of the cuvette (for the solution).

Then the extinction coefficient at 1000 nm was taken as baseline and the extinction spectra were also integrated from peak maxima to the 1000 nm. Finally the volume

concentration of the colloids C_{measured} was calculated by multiplying the peak area of the measured curve with the proportionality factor 'f'. The colloidal turnover was calculated using the following equation-

$$\text{Colloid turnover} = \frac{C_{\text{measured}}}{C_{\text{composition}}} \quad (12)$$

Where the $C_{\text{composition}}$ is the original colloid volume concentration of metal salt used for the colloid formation and was calculated assuming that all the metal ions have been converted into colloids.

The measured UV-VIS spectrum (extinction) for the aqueous sol containing gold colloids is shown below in Figure 39.

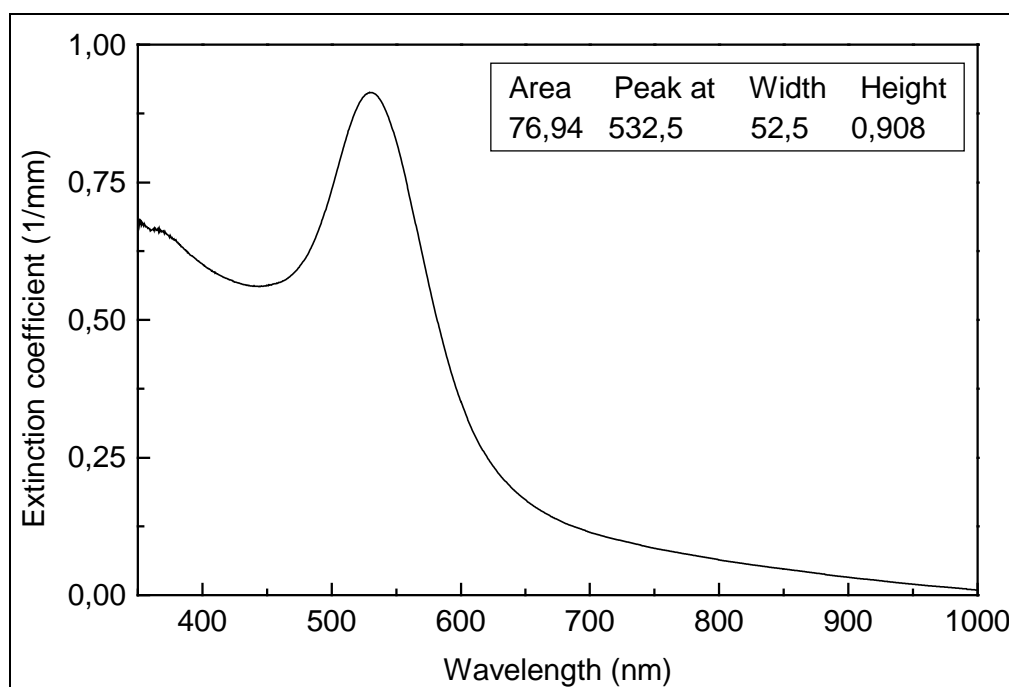


Figure 39: UV-VIS extinction spectra of the aqueous solution containing the colloidal gold sol. The sol was diluted 20 times with distilled water, a 2 mm quartz cuvette was used for the measurements; reference: air.

From the above curve the area of the curve was determined to be equal to 79.84, but since the sol is diluted 20 times with water, the actual area will be $20 \times 77.20 = 1544$. Hence the C_{measured} will be $1544 \times 2.58 \times 10^{-7}$. Using the above equation (2) the colloidal turnover for the gold particles in aqueous solution was equal to 98%, indicating that almost all the ionic gold has been converted to colloidal gold.

Kenneth et al. [128] have shown that the hydroxylamine functions as a seed for the growth of Au nanoparticles in solution. Morris et al. [137] have grown silver on the gold nuclei using hydroxylamine hydrochloride which retards the formation of silver nuclei and favours the growth of silver nuclei on existing gold nuclei. Therefore, colloidal gold nanoparticles synthesised as above were used for the synthesis of alloy colloids and it was expected that the addition of hydroxylamine followed by silver ions would facilitate the growth of the silver shell on the existing gold nuclei. During the heat treatment at higher temperatures, diffusion of silver particles inside the gold will take place and the alloy colloids will be formed. This is shown schematically in the following Figure 40.

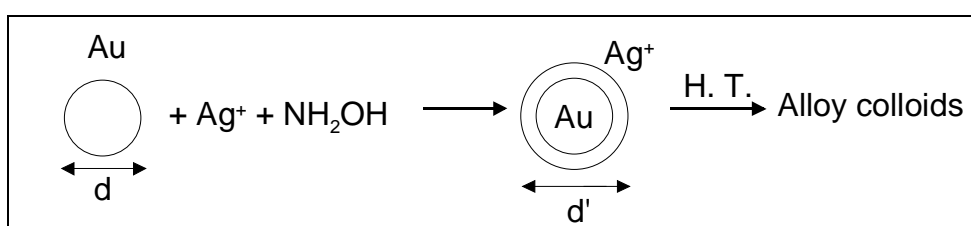


Figure 40: Schematic representation of the formation of Ag / Au alloy colloids.

SiO₂ thin films (for synthesis see chapter III, page 40) containing Ag / Au alloy colloids were characterised by various characterisation methods.

5.2.1.1.3 UV-VIS spectroscopic study

The UV-VIS spectra of SiO₂ thin films containing Ag / Au alloy colloids as a function of their molar ratios at a constant densification temperature of 350 °C are given below in Figure 41. Whereas the other absorption spectra of thin films densified at the temperatures ranging from 50 to 550 °C are given in appendix (Figure A 21 to A 25).

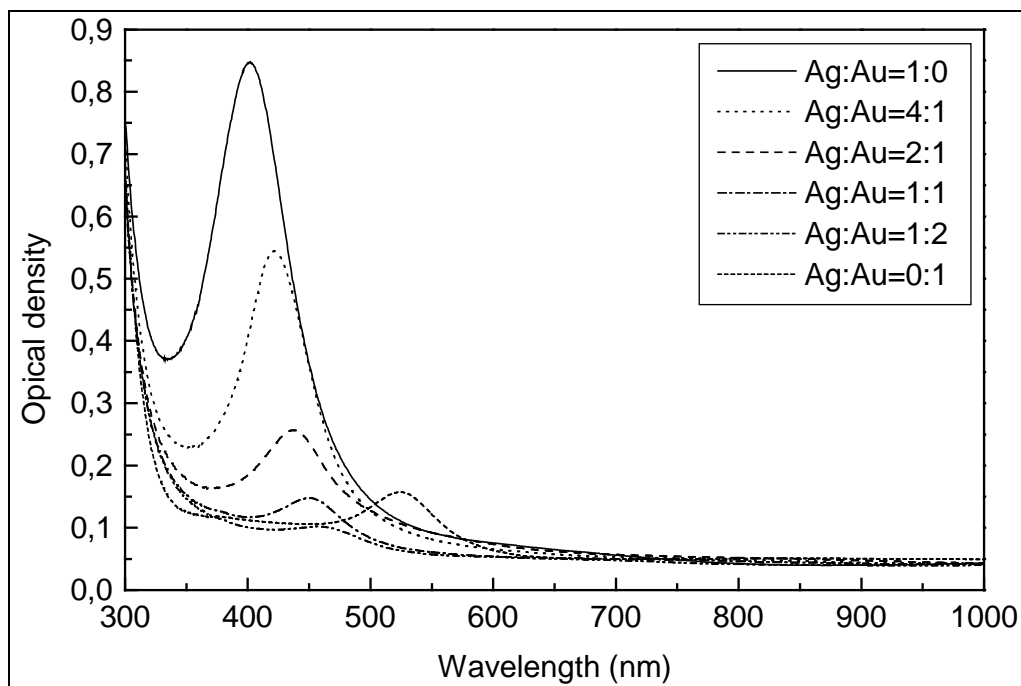


Figure 41: UV-VIS absorption spectra of SiO_2 thin films containing Ag / Au alloy colloids as a function of their molar ratios heat treated at 350°C under reducing atmosphere ($\text{N}_2 / \text{H}_2 = 92 / 8$, 80 l/h); reference: air, (experimental details are in ch. III, p. 40).

It is clear from the above figure that plasmon peak always remains as a single peak and continuously shifts from 401 nm (for pure silver) to 522 nm (for pure gold) on increasing the molar fraction of gold. In a solution containing gold and silver ions the possible two states are 1). alloy particles and 2). particles with core-shell structure. But the theoretical spectra calculated by Itakura et al. [72] for the core-shell type structure of Ag / Au, by using the equation given by Bohren and Hoffman [129] show that the single plasmon peak splits as two peaks, one of which is located at the shorter wavelength than that of silver nanoparticles and the other is located at the wavelength slightly shorter than that of gold nanoparticles with increasing molar fraction of silver. Whereas for the alloy colloids of gold and silver, the plasmon peak always remains a single peak. Therefore the colloids formed under the present work are alloy colloids.

However on standing these samples in air for a long time a decrease in the intensity of the absorption peak was observed. UV-VIS spectra of the above samples after standing in air for 6 months are shown below in Figure 42.

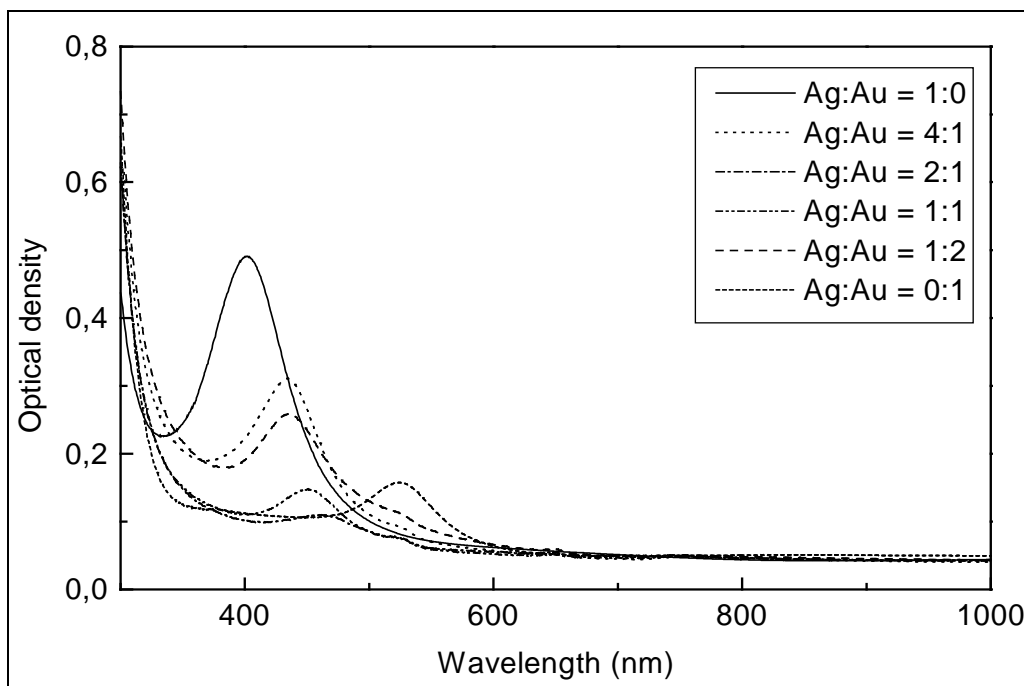


Figure 42: Change in UV-VIS spectra of SiO_2 thin films containing Ag / Au alloy colloids with different molar ratios of Ag and Au, after standing in air for 6 months.

On comparing Figure 41 and Figure 42 it is clear that the peak intensity of the samples decreases with time in air. This decrease in the intensity can be attributed to the oxidation of silver to silver-oxide on standing in air for a long time. The decrease in the peak intensities for the samples containing higher molar percentage of silver is large. Whereas, for the sample containing pure gold no decrease in the intensity was observed. This is because the reduction potential for gold is higher than that of silver, hence gold will have lower tendency to oxidise in gold oxide than the silver to silver oxide. Besides that on standing the samples in air, a new absorption peak at 520 nm (characteristic plasmon peak of colloidal gold) was also generated. Which indicates that the reduced silver comes out from the alloy particles, leaving behind some free particles of colloidal gold.

PbO is known to reduce the transformation temperature and to increase the thermal expansion coefficient of the glass when incorporated into SiO_2 [130] based glasses. The synthesis of PbO-SiO_2 thin films by the sol-gel route has been carried out by Strawbridge [131], James [132] and Kalleder [133]. M. Schmitt [143] has also made systematic investigations towards the synthesis of PbO-SiO_2 thin films containing silver and gold by the sol-gel route, in order to form dense coatings which could partially stop the penetration of oxygen from the atmosphere and hence the oxidation of metal

colloids. So the Ag / Au alloy colloids were synthesised in PbO-SiO₂ thin films in the present work also to avoid the oxidation of silver. The UV-VIS spectra of PbO-SiO₂ thin films containing Ag / Au alloy colloids as a function of their molar ratios, heat treated at 350 °C are shown below in Figure 43, whereas the UV-VIS spectra of films heat treated at different temperatures ranging from 50 °C to 550 °C are shown in the appendix (from Figure A 13 to A 17).

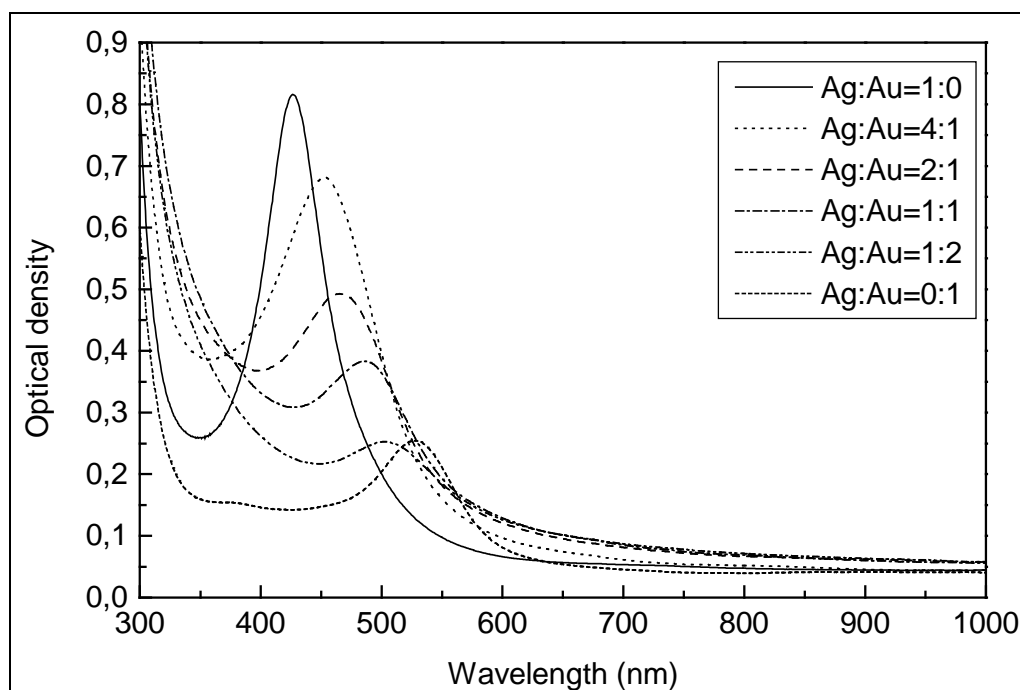


Figure 43: The UV-VIS absorption spectra of PbO-SiO₂ thin films containing Ag / Au alloy colloids as a function of their molar ratios heat treated (350 °C / 1 h) under reducing atmosphere (N₂ / H₂ = 92 / 8, 80 l/h, reference: air).

It can be observed from the measured spectra of SiO₂ and PbO-SiO₂ thin films containing Ag / Au alloy colloids that the general trend of appearance of a single UV-VIS peak and a continuous shifts from 401 to 522 nm with increasing molar ratios of gold is the same in both cases. But in case of PbO-SiO₂ coatings the absorption peaks are centred at higher wavelength than in the case of SiO₂ coatings. This shift can be attributed to the increase in refractive index of PbS-SiO₂ coatings.

The thickness of the PbO-SiO₂ and SiO₂ thin films was measured using a profilometer. For the SiO₂ films, heat treated at 350 °C, the thickness was measured equal to 0.7 µm, which decreases to 0.5 µm after heating to 450 °C and finally to 0.3 µm after heat treating at 550 °C. Whereas for the PbO-SiO₂ films the thickness was measured

to 1.1 μm for the sample heat treated at 350 $^{\circ}\text{C}$, which decreases to 0.7 μm at 450 $^{\circ}\text{C}$ and finally to 0.55 μm at 550 $^{\circ}\text{C}$.

5.2.1.1.4 Calculation of theoretical spectra of Ag / Au alloy colloids

To get a better understanding of the absorption spectra of the colloidal Ag / Au alloy particles, a computer simulation of the composition dependence of plasmon frequency was performed. As it is known from the Mie's theory [134], the frequency of the absorption peak is proportional to $\varepsilon_2 / [(\varepsilon_1 + 2\varepsilon_0)^2 + \varepsilon_2^2]$ (13)

where ε_1 and ε_2 are the real and the imaginary parts of the dielectric constant and ε_0 is the dielectric constant of the medium. For calculating the absorption spectra of alloy colloids we take ε_1 and ε_2 to be the composition weighted averages [135] of the bulk dielectric constants of Au and Ag

$$\varepsilon_i = (1-x) \varepsilon_i^{\text{Au}} + x \varepsilon_i^{\text{Ag}} \text{ for } i = 1, 2 \quad (14)$$

Theoretical spectra obtained by this way for the alloy particles are shown in Figure 44.

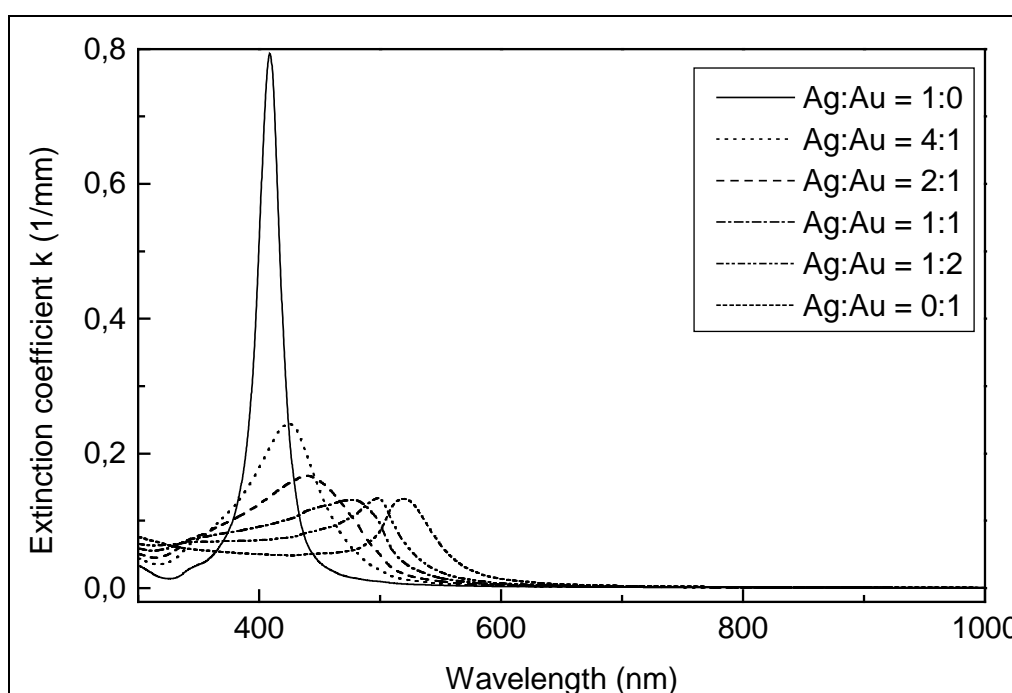


Figure 44: Theoretical extinction spectra for gold / silver alloy colloids calculated by Mie theory using a computer simulation programme for the varying molar ratios of gold and silver. (Particle radius = 10 nm, refractive index of the matrix = 1.46 and total volume concentration of gold and silver is 10^{-6}).

It can be seen from the Figure 43, that the plasmon peak remains as a single peak and continuously shifts from 410 to 530 nm with increasing molar fraction of gold. Comparing the observed (Figure 43) and theoretical (Figure 44) spectra it is clear that the observed spectra are in good agreement with the theoretical spectra of gold / silver alloy particles. Further the shifting of the peak with increasing molar ratio of gold in the theoretical spectra also is in good agreement with the observed spectra. The peak positions are however not the same in both the cases. It is assumed that this difference is largely due to, 1). The use of the bulk dielectric constant for these nanosized colloidal particles is inappropriate, 2). Neglecting the effect caused by the smallness of the particle size compared with the electron mean free path [126].

The origin of the red shift in the case of Ag / Au alloy colloids is interesting. As silver and gold have identical bulk plasmon frequencies [77], such a peak shift due to changing electron density is not expected. However, the high frequency dielectric constants are quite different, primarily because the interband transition in gold extends across most of the visible spectrum. So the absorption band shift in this case is due to the perturbation of d-band energy levels and not to changes in free electron concentration [136]. This results in a steady increase in the effective value of ϵ for the alloys and consequently, a red shift in the position of the absorption band.

5.2.1.1.5 Change in absorption peak positions as a function of temperature

The evolution of the silver / gold alloy peak as a function of densification temperature for a constant molar ratio of Ag : Au = (2 : 1) is shown below in Figure 45, whereas the spectra as a function of temperature for the other molar ratios of Ag and Au are given in the appendix (Figure A 18 to A 20 for PbO-SiO₂ thin films and Figure A 26 to A 29 for SiO₂ thin films).

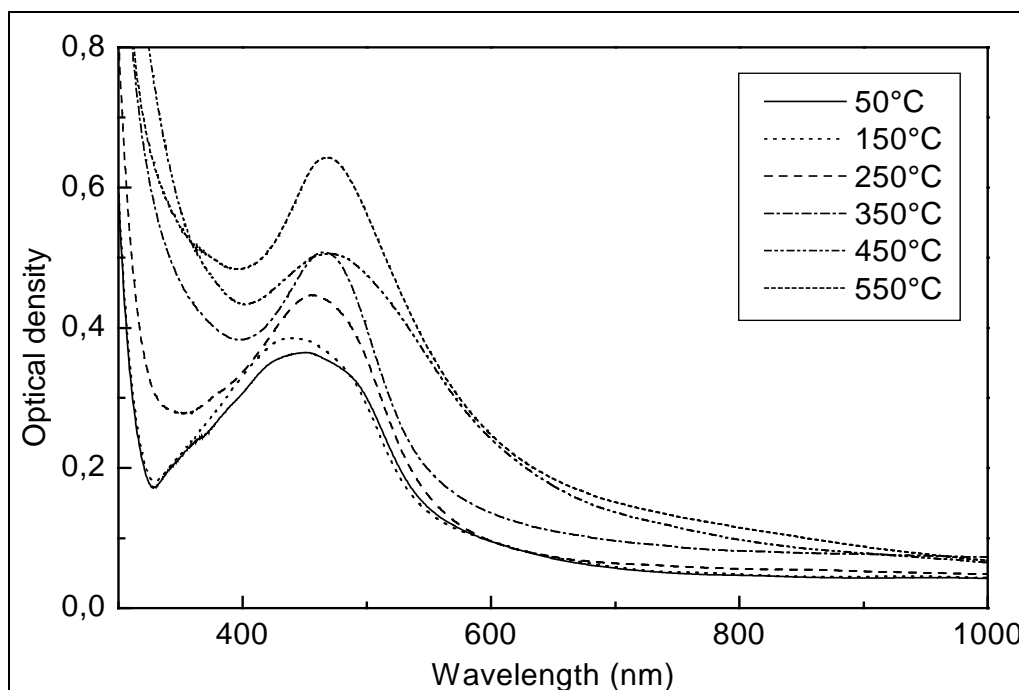


Figure 45: The absorption spectra for PbO-SiO₂ thin films containing Ag / Au alloy colloids with the increase in densification temperature (molar ratio of Ag : Au = 2 : 1, N₂ / H₂ = 92 / 8, reference: air (experimental details in ch. III, p. 40).

The above figure shows that at 50 °C there is a very broad band, which is composed of two peaks, situated at 490 nm and 430 nm. On heating the sample at 150 °C the nature of the absorption peak remains same but there is a slight increase in the intensity of the peak at 430 nm. The sample heat treated at 250 °C, shows only one peak centred at 455 nm, which remains as a single peak during the heat treatment at the higher temperatures up to 550 °C.

Morris et al. [137] have measured the absorption spectra of silver coated gold particles (gold as a core and silver as the shell) in aqueous solution and have calculated the theoretical spectra using Adan and Kerker theory [75] for the different shell thicknesses. Starting with gold nuclei of 59 nm concentric layers of the silver ranging from 5 to 220 nm have been deposited. They observed that as long as the silver shell thickness is less than 80 nm two peaks were obtained one due to gold shifted slightly towards the lower wavelength and other due to silver, which also shifted towards the lower wavelength. Whereas increasing the shell thickness to 100 nm gave only one peak corresponding to silver. Hence the absorption spectra obtained for the samples heated at 50 °C and 150 °C may be attributed to the core-shell structure.

The UV-VIS absorption spectra of thin films as a function of increasing molar ratio of silver, hence the thickness of the shell at a constant densification temperature of 150 °C can be seen in appendix Figure A 14. It is seen that for the molar ratio of Ag : Au = 1 : 2 both the peaks due to silver and gold (centred at 403 nm and 500 nm) are visible. For the molar ratio of Ag : Au = 1 : 1 also two peaks are visible. Whereas for the molar ratios of Ag : Au = 2 : 1 and 4 : 1, only one peak due to silver is visible which is centred at 430 nm, and that of gold is completely masked. These observed spectra are in good agreement to the work done by Morris et al. except than the silver peak positions observed in the present study is higher than observed by them. This can be due to the increase in refractive index of the medium in the present case. Besides that an absorption spectra corresponding to the simple physical addition of gold and silver mixed colloids was never obtained, it can be said that the particle in thin films are not phase separated particles of Ag and Au. Unfortunately, as the lattice spacings for gold and silver are almost the same, TEM observations also could not give more information about the structure of the bimetallic particles.

From the absorption spectra of the thin films containing different Ag / Au molar ratios it is clear that at the temperatures between 250-350 °C the two peaks due to gold and silver merge to one. This is the temperature range where the decomposition of polyvinylpyrrolidone and DIAMO takes place. It can be said that the silver and DIAMO complex makes some bonding with the polymer, which is absorbed onto the surface of the gold. Decomposition of polyvinylpyrrolidone and DIAMO leads to the formation of gold covered with silver particles which on heating at higher temperatures results in the diffusion of silver into gold and finally to the alloy colloids.

However, for the samples heat treated above 250 °C some absorption was also observed in the region of 550-700 nm. In order to understand the exact reason of this absorption, some reference coatings without colloids were also prepared and heat treated at the temperatures ranging from 350-550 °C under reducing atmosphere. The absorption spectra can be seen in appendix Figure A 32. It is clearly visible from these spectra that the reference coatings also show some absorption in the wavelengths ranging from 400-700 nm, which increases remarkably at 550 °C. This absorption can be attributed to the organics, which could not decompose completely under the reducing atmosphere.

Baba et al. [138] have given a theoretical equation for Ag / Au alloy particles that relates the absorption wave maxima of colloids with their molar fractions, in the following form, without using the dielectric constant of the individual particles.

$$1/\lambda_{\text{bimetallic}} = [(x_{\text{Au}} / \lambda_{\text{Au}}^2) + (1-x_{\text{Au}}) / \lambda_{\text{Ag}}^2]^{1/2} \quad (15)$$

Where λ_{Au} and x_{Au} are the maximum wavelength and the molar fractions for gold and λ_{Ag} and x_{Ag} are the maximum wavelength and the molar fractions for silver particles respectively. Wavelengths corresponding to maximum UV-VIS absorption from observed spectra and calculated wavelength for alloy colloids using above equation (3) are plotted against the molar fraction of gold. Figure 46 and Figure 47 show the observed and calculated peak positions for alloy colloids in SiO_2 and PbO-SiO_2 matrices respectively.

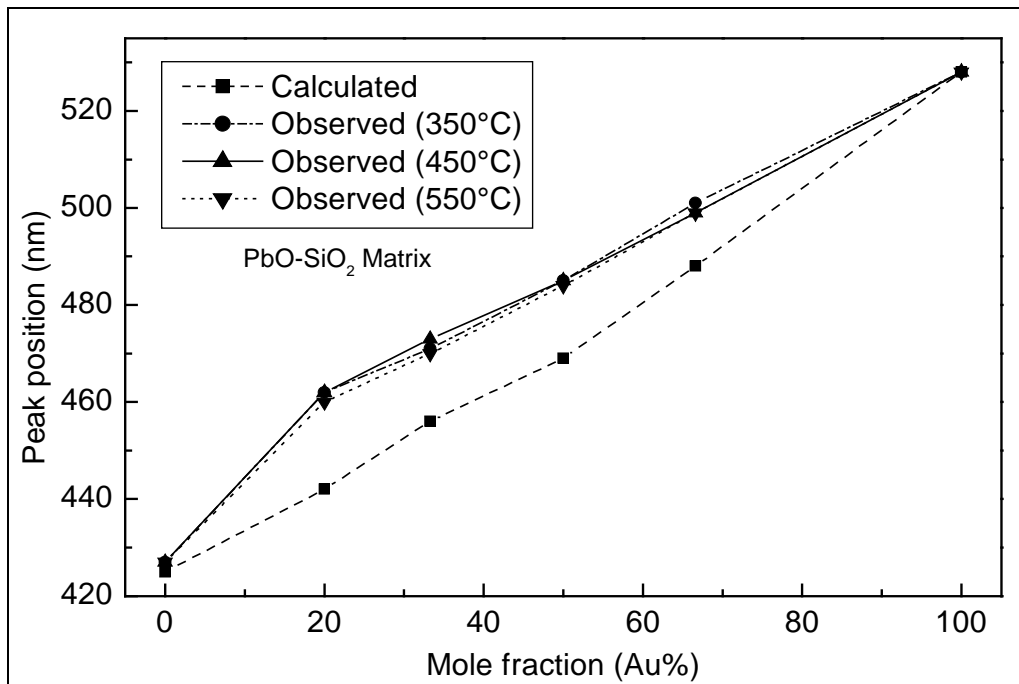


Figure 46: Measured and calculated peak positions (using a theoretical equation used by Baba et al. [138]) for different mole fraction of Au (SiO_2 matrix).

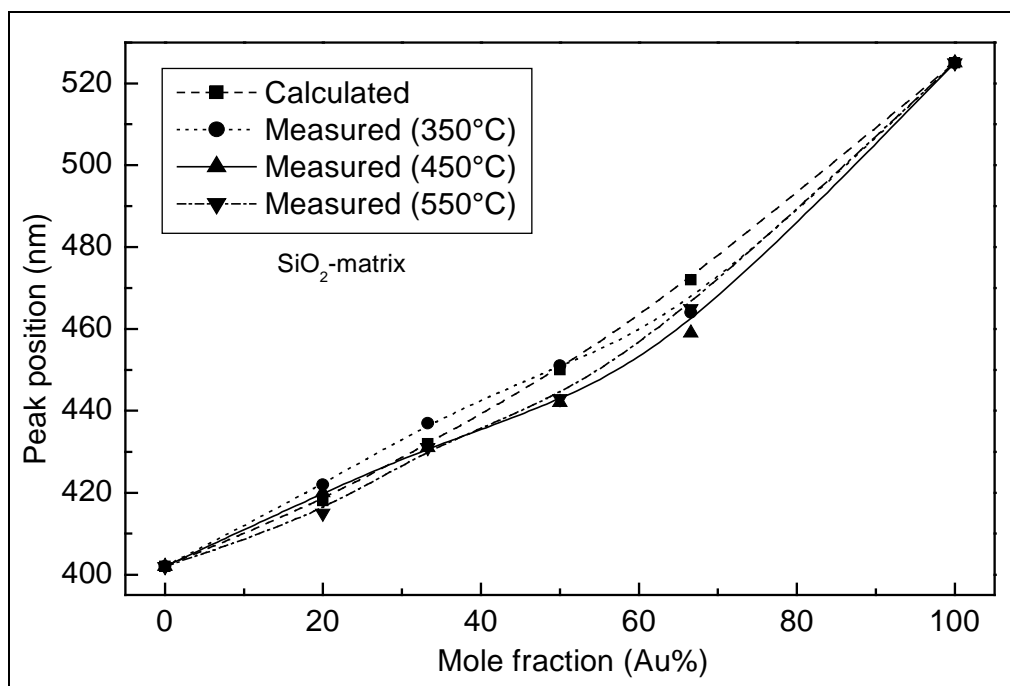


Figure 47: Measured and calculated peak positions (using a theoretical equation used by Baba et al. [138]) for different mole fraction of Au (PbO-SiO₂ matrix).

From Figure 46 it is clear that the heating of samples at higher temperature shifts the peak slightly towards lower wavelengths, i.e. for Ag : Au = 2 : 1, the absorption peak shifts from $\lambda_{\max} = 437$ to $\lambda_{\max} = 431$ on increasing the heat treatment temperature from 350 to 550 °C. This shift in the peak maxima can be explained by the fact that on heating at higher temperatures more and more silver particles are diffusing inside the alloy particles, hence shifting the peak position towards the silver maximum was observed. The observed values for the peak maxima are in good agreement to the calculated ones. Figure 47 also shows the same type of behaviour on heating the samples at higher temperatures. Whereas for the PbO-SiO₂ matrix the deviation of the observed peak position from the calculated one is higher than that for the SiO₂ glass. This increase in peak positions for the lead containing thin films can be attributed to the increase in refractive index by the addition of PbO. Refractive index of the SiO₂ and PbO-SiO₂ thin films was measured to be 1.46 and 1.50 respectively, using ellipsometer.

The calculated peak positions (using Mie's theory and a theoretical equation given by Baba et al.) and the experimentally observed peak positions for Ag / Au alloy colloids in SiO₂ and PbO-SiO₂ thin films are given below in Table 17 and Table 18.

Table 17: Peak positions of calculated curves (using Mie-theory), those using theoretical equation given by Baba et al. [138] and experimentally observed peak positions of PbO-SiO₂ thin films containing Ag / Au alloy colloids.

Au (mole%)	Experimentally observed λ_{\max} (nm)			Peak position after Mie-theory		Baba et al.
	350 °C	450 °C	550 °C	r = 10 nm	r = 20 nm	
0	427	427	427	414	429	427
20	462	462	460	431	445	442
33.33	471	473	470	448	466	454
50	485	485	484	483	493	470
66.6	501	499	499	500	505	587
100	528	528	528	525	533	528

Table 18: Peak positions of calculated curves (using Mie-theory), those using a theoretical equation given by Baba et al. [138] and peak positions of SiO₂ thin films containing Ag / Au alloy colloids.

Au (mole%)	Experimentally observed λ_{\max} (nm)			Peak position after Mie-theory		Baba et al.
	350 °C	450 °C	550 °C	r = 10 nm	r = 20 nm	
0	402	402	402	405	410	401
20	422	420	415	425	440	418
33.33	437	431	430	440	455	432
50	451	442	443	480	485	450
66.6	464	460	460	499	500	472
100	525	525	525	520	530	525

As the samples were heat treated under reducing atmosphere, it was not possible to calculate the colloidal turnover for the gold / silver alloy colloids due to the presence of organics which could not be decomposed completely under reducing atmosphere. So the colloidal volume concentration for the samples heated at different temperature was calculated from the measured absorption spectra. The colloidal volume concentration increases from 5.99×10^{-3} to 6.10×10^{-3} for the glass samples heat treated at $350\text{ }^{\circ}\text{C}$ and $550\text{ }^{\circ}\text{C}$ under reducing atmosphere in PbO-SiO_2 glass films. These results also support the above finding, that with increasing temperature more and more silver diffuses inside the gold particles.

In order to completely remove the organic components, glass samples containing both gold and silver were first heat treated in air at $400\text{ }^{\circ}\text{C}$ at the heating rate of 100 K/h and kept there for 1 h. Samples were taken out and allowed to cool. After that these samples were heat treated at $450\text{ }^{\circ}\text{C}$ with a heating rate of 100 K/h under reducing atmosphere ($\text{N}_2 / \text{H}_2 = 92 / 8$, flow rate 80 l/h). The UV-VIS absorption spectra of these samples were measured and the observed spectra are shown in Figure 48.

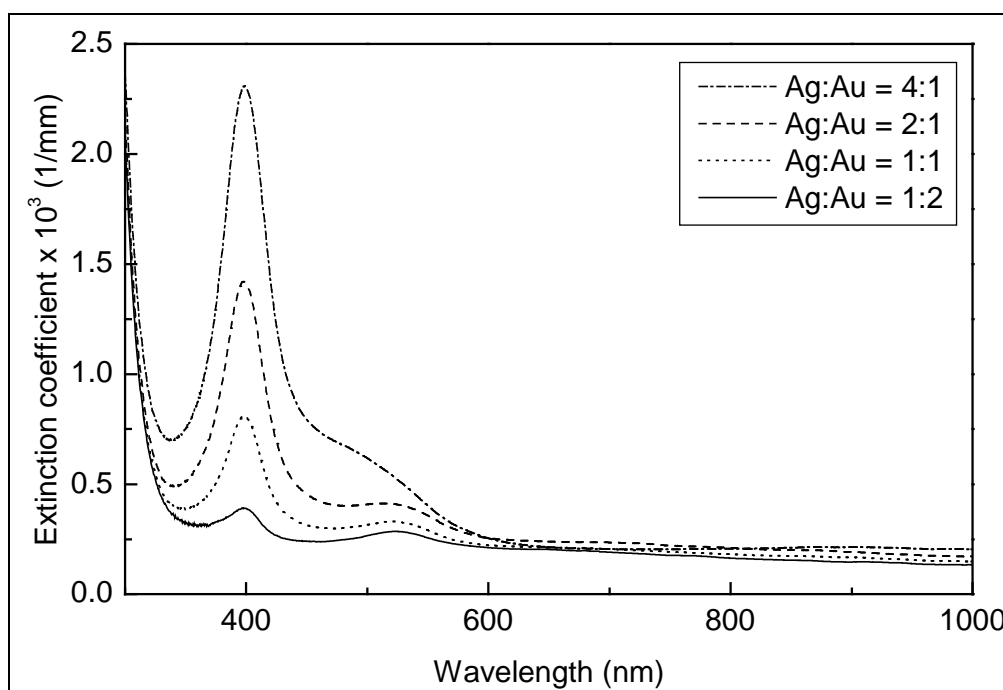


Figure 48: UV-VIS spectra of thin films containing Ag / Au mixed colloids, heated in air at $400\text{ }^{\circ}\text{C}$ before heating under reducing atmosphere at $450\text{ }^{\circ}\text{C}$; reference: air.

From the observed spectra of the thin films containing gold and silver in different molar ratios it is clearly seen that two absorption peaks are obtained. One is centred at

400 nm (the plasmon peak of silver) while the other is centred at 522 nm (plasmon peak for gold). The UV-VIS spectra are contradictory to the UV-VIS spectra of thin films containing alloy colloids, where only one peak was observed. These results indicate that the heating of samples in air at 400 °C prior to heating at 450 °C under reducing atmosphere generates phase separated mixed colloids of silver and gold, instead of alloy colloids. This behaviour can be explained by the fact that once the film is heated at 400 °C in air silver is oxidised. Schmitt [143] has investigated that the silver ions get exchanged with sodium ions of glass during heat treatment in air. Appearance of both the peaks of gold and silver in UV-VIS spectra indicates that the silver, which was oxidised during heat treatment under air, has reduced into silver colloids once again during heat treatment under reducing atmosphere.

Now the question arises what happens, if the glass, in which silver ions have been exchanged with the sodium ions, is heat treated under reducing atmosphere. One of the possibilities is the formation of colloidal silver particles inside the glass itself. To study this behaviour, gold and silver colloids containing thin films were prepared by heating the samples in air at 400 °C. The UV-VIS spectra of these samples are shown Figure A 30 in appendix. These spectra show an intense peak at 523 nm due to gold, and a very weak peak at around 400 nm due to silver. Indicating that only a small proportion of silver is present as silver colloids in thin films. Now these films were etched with 5% solution of HF (hydrofluoric acid) for removing the coatings. After etching, these samples were heat treated at 450 °C under reducing atmosphere ($N_2 / H_2 = 92 / 8$, 80 l/h) for 1 h. The UV-VIS spectra of these samples are shown below in Figure 49.

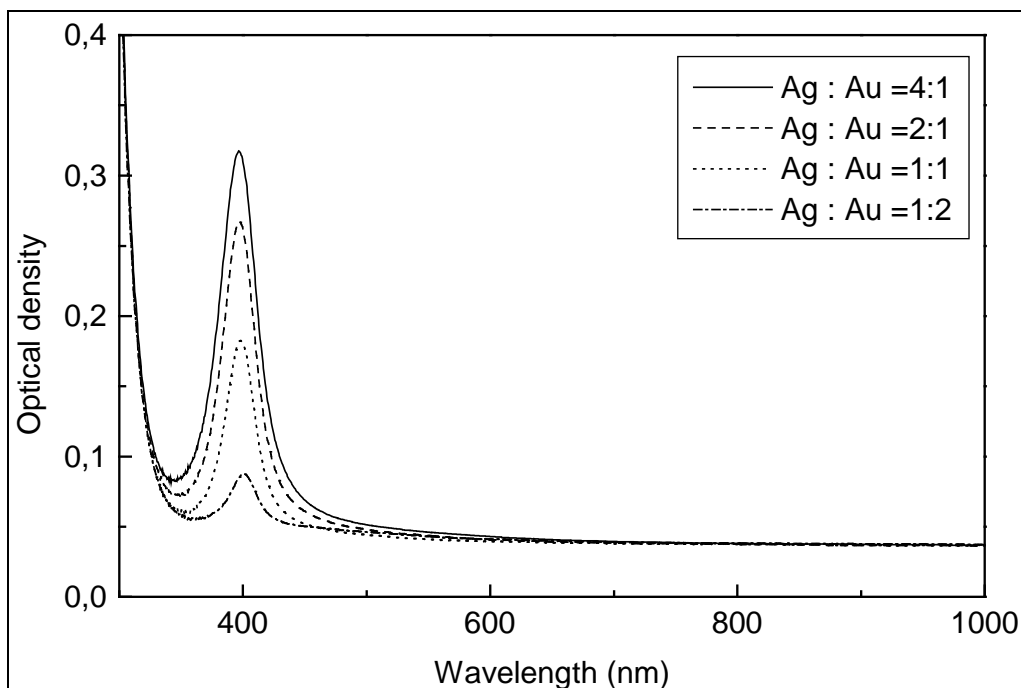
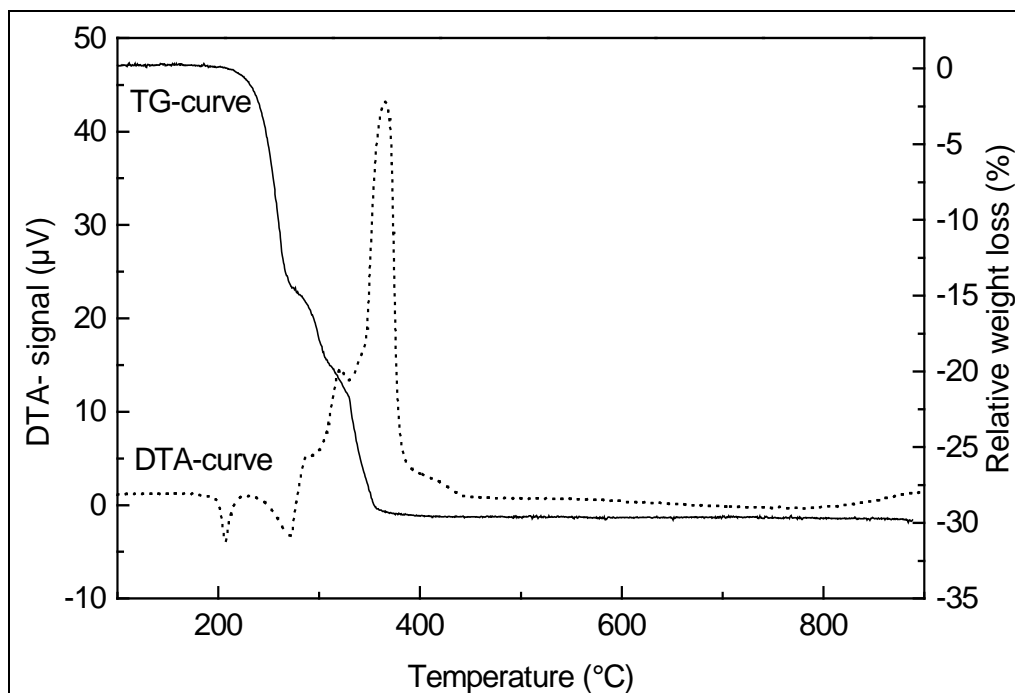


Figure 49: UV-VIS spectra of samples heat treated in air at 400 °C followed by etching in HF solution and heat treatment at 450 °C under reducing atmosphere ($N_2 / H_2 = 92 / 8$, 80 l/h).

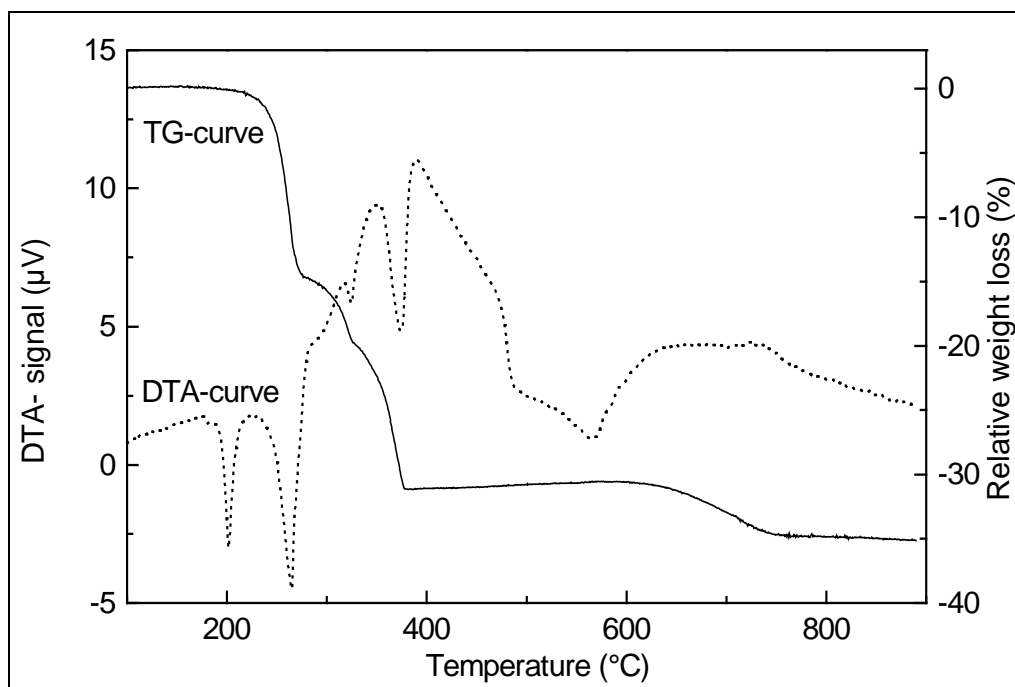
From the above UV-VIS spectra it is clear that in all the cases only one absorption peak corresponding to colloidal silver (at 398 nm) was obtained. The most intense peak was observed for the sample having a molar ratio of Ag : Au = 4 : 1, which gradually decreases with the decreasing molar fraction of silver and the minimum intensity was recorded for the molar ratio Ag : Au = 1 : 2. These results support the assumption that the ionic silver entered into glass gets reduced to colloidal silver on heating under reducing atmosphere.

5.2.1.1.6 DTA-TG Investigations

Lead acetate is known to decompose and to produce lead oxide (PbO) on heating in air above 300 °C. But in the present study samples have been densified in reducing atmosphere in order to stop the reduction of silver to silver oxide. So the question arises how does the behaviour of lead acetate change on heating the samples under reducing atmosphere. For a comparison, DTA-TG investigations of lead acetate were carried out in air and under reducing atmosphere ($N_2 / H_2 = 92 / 8$). DTA-TG curves under both the conditions are shown below in Figure 50.



(a)



(b)

Figure 50: DTA-TG curves of lead acetate in (a) air and (b) under reducing atmosphere.

On comparing the nature of the TG-curves in air and reducing atmosphere, it is clear that the general trend for both of them is almost the same. In air, the weight loss of lead acetate starts at 224 °C and 14% weight loss was observed at 267 °C. At 364 °C

a weight loss of 30% was measured. Whereas under reducing atmosphere also the weight loss starts at 227 °C and a weight loss equal to 14.3% was observed at 271 °C, and 30% weight loss was recorded at 380 °C, which is slightly higher than the same weight loss recorded in air. This slight increase in temperature is justified, as under reducing atmosphere the sample is not getting any oxygen.

However the nature of DTA curves is different in both the cases. In air only one main peak (at 364 °C) was observed, which, based on literature [143], can be assigned to the decomposition of lead acetate in lead oxide. Whereas under reducing atmosphere two peaks located at 349 °C and at 390 °C were observed. As it is clear from both the spectra that the final weight loss till around 400 °C is the same (30%), showing that the final product formed is PbO independent of the atmosphere in which the samples were heated. The peak at 34 °C may be attributed to CO₂ [139] as a product formed by the decomposition of lead acetate, whereas the other peak situated at slightly higher temperature is due to CO [140]. As the sample is heated under reducing atmosphere it will not be getting any oxygen, so the decomposition product will be CO instead of CO₂ in air. However an additional peak was also observed under reducing atmosphere above 610 °C, which is not seen in air and a weight loss of 5% was also observed in between 610 to 750 °C. This loss is due to the reduction of lead oxide in metallic lead, which in fact is not possible in air.

It has been observed in the previous sections that during the heat treatment of the samples under reducing atmosphere above 250 °C, some absorption was observed in the wavelengths ranging from 450 to 700 nm. This was attributed to the incomplete decomposition of the organics under reducing atmosphere. In order to make a comparison, SiO₂ gels containing PVP were first heat treated in an oven at 100 °C for 24h and their DTA-TG investigations were made in air and under reducing atmosphere. The DTA-TG curves are given in the following Figure 51.

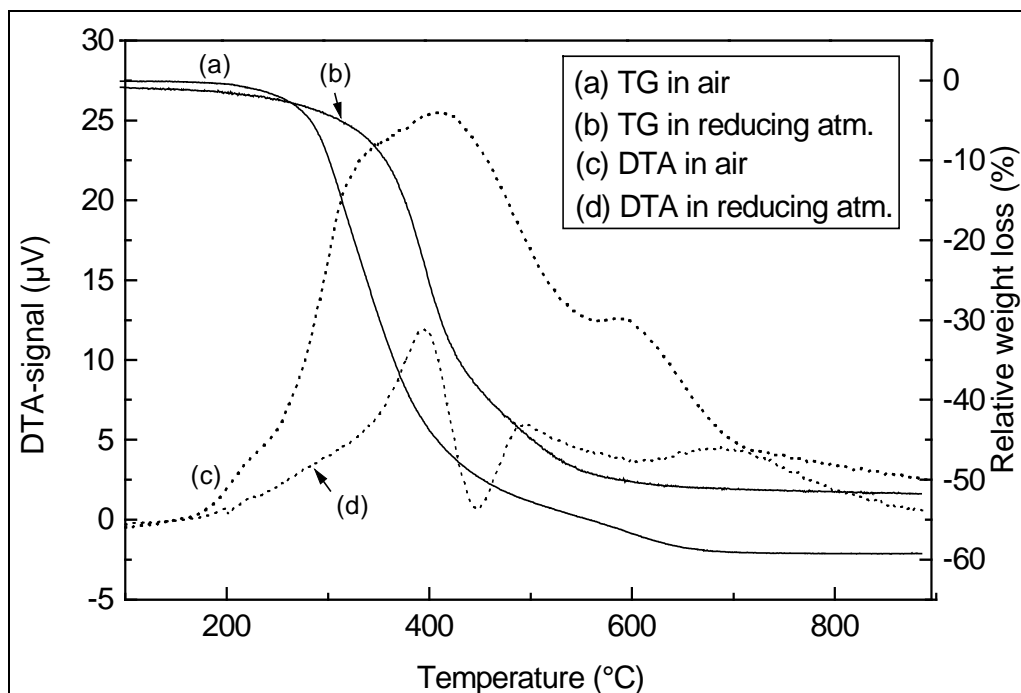


Figure 51: DTA-TG curves of SiO_2 sol containing PVP dissolved in ethanol.

It can be seen from the curves, that in air 40% weight loss is obtained on heating from 275 to 400 °C, on the other hand only 23% weight loss was calculated for heating the same samples under reducing atmosphere. Even at 900 °C, a weight loss of 59% was observed in air, and only 51% weight loss was observed under reducing atmosphere. These experiments also support that the absorption in the wavelength from 400 to 700 nm is due to the incomplete decomposition of organics under the reducing atmosphere.

5.2.1.1.7 HR-TEM characterisation of thin films containing Ag / Au alloy colloids

In order to determine the size and shape of the particles, high resolution transmission electron microscopic (HR-TEM) studies were carried out. Whereas to see the composition of the particles formed, EDX analysis was performed of the thin films containing gold-silver alloy colloids. Samples were prepared using the cross sectional method. Figure 52 shows some high resolution transmission micrographs of Ag / Au alloy colloids.

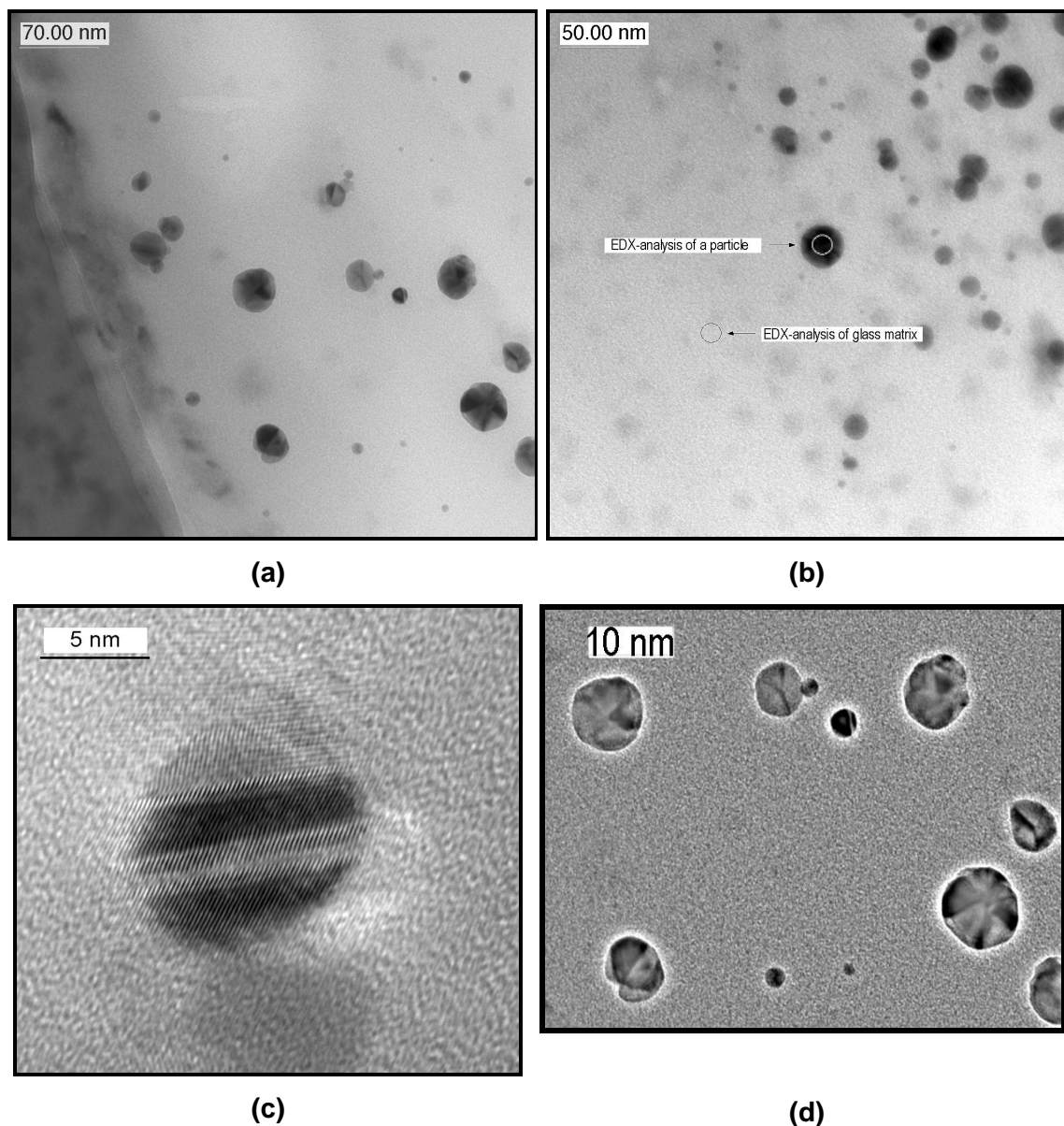


Figure 52: HR-TEM image of colloidal Ag / Au alloy particle (densified at 350 °C under $N_2 / H_2 = 92 / 8$, Ag : Au = 4 : 1) a) Image showing particle distribution b) Some selected regions for EDX analysis c) High resolution micrograph of a single alloy particle d) Some particles having pentagonal structure (Experimental conditions in ch. III, p. 40).

The distribution of alloy particles in the thin films can be seen in Figure 52. Particles with diameters ranging from 8 to 35 nm were observed. In Figure 52 (b) some regions are shown, which are selected for EDX analysis. The high resolution micrograph of a single alloy particle is shown in Figure 52 (c). This figure shows four dark and light zones placed alternatively. This is due to the diffraction contrast of the figure, and can not be attributed to the alloy formation. Figure 52 (d) shows the diffraction contrast of a small area of the film. The figure was obtained by using a high-pass filter, and is the

difference of an original and a Gauss-filtered figure. The pentagonal structure of the nanoparticles is clearly visible in the above figure.

A lattice constant of 2.35 Å was determined from the above. Silver and gold are in fact miscible in all proportions due to almost identical lattice constants [141]. So the lattice plane spacing of 2.35 Å observed in HR-TEM may be attributed either to pure gold and silver or to gold silver alloy. Thus the lattice plane spacing calculated for the individual colloidal particles does not allow to differentiate between these possibilities. Therefore, electron dispersive X- ray analysis (EDX) of individual particles was carried out to estimate their composition, by focusing the electron beam on the individual particles. Some EDX profiles of Ag / Au alloy colloids are shown in Figure 53.

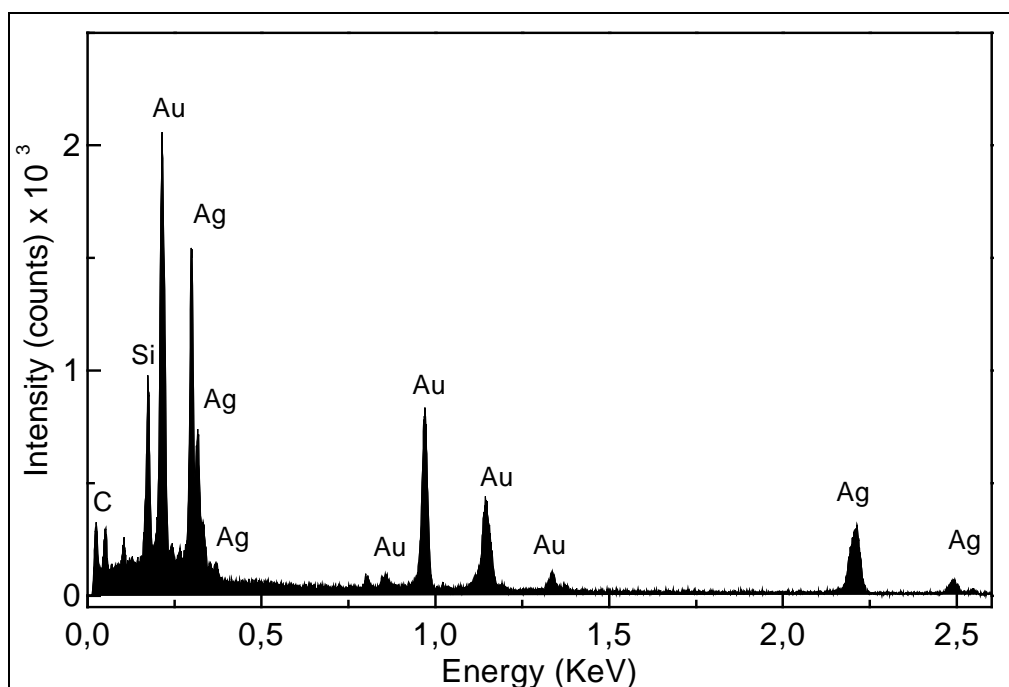


Figure 53: EDX profile of a single Ag / Au alloy particle with molar ratio of 4 : 1 (experimental conditions in ch. III, p. 40).

Figure 53 shows that this particular particle is composed of 81% (atomic) of silver and 19% (atomic) of gold. Keeping in mind that this sample should have a theoretical composition of Ag : Au = 4 : 1, the EDX result is in good agreement. Analysis of several particles showed that the composition varies within $\pm 10\%$, which could be because of experimental errors or it can be attributed to the variation of composition of different particles. Figure A 33 and A 34 in appendix are EDX profiles from a sample with Ag : Au = 2 : 1 and 1 : 2 respectively. The estimated results of 32.4 atom% Ag and

67.6 atom% Au for the molar ratio of Ag : Au = 2 : 1 and 67 atom% Ag and 33 atom% Au for the molar ratio of 1 : 2 are in good agreement with the expected values.

Therefore the EDX analysis of different particle shows that they are bimetallic particles and monometallic particles were not observed. EXD profiles of the glass matrix are shown in appendix (Figure A 35). The EXD measurements on SiO₂ matrix show the presence of Si, O and C only.

5.2.1.1.8 X-ray diffraction characterisation of thin films containing Ag / Au alloy colloids

In order to see if the particles formed in the thin film are crystalline or not, XRD analysis of thin films containing bimetallic colloids of Ag and Au was carried out. The measured diffraction patterns for Ag / Au alloy colloids having molar ratios of Ag : Au = 4 : 1, 2 : 1, 1 : 1 and 1 : 2 are shown below in Figure 54. All the measurements were conducted using CuK α radiation and a graphite monochromator.

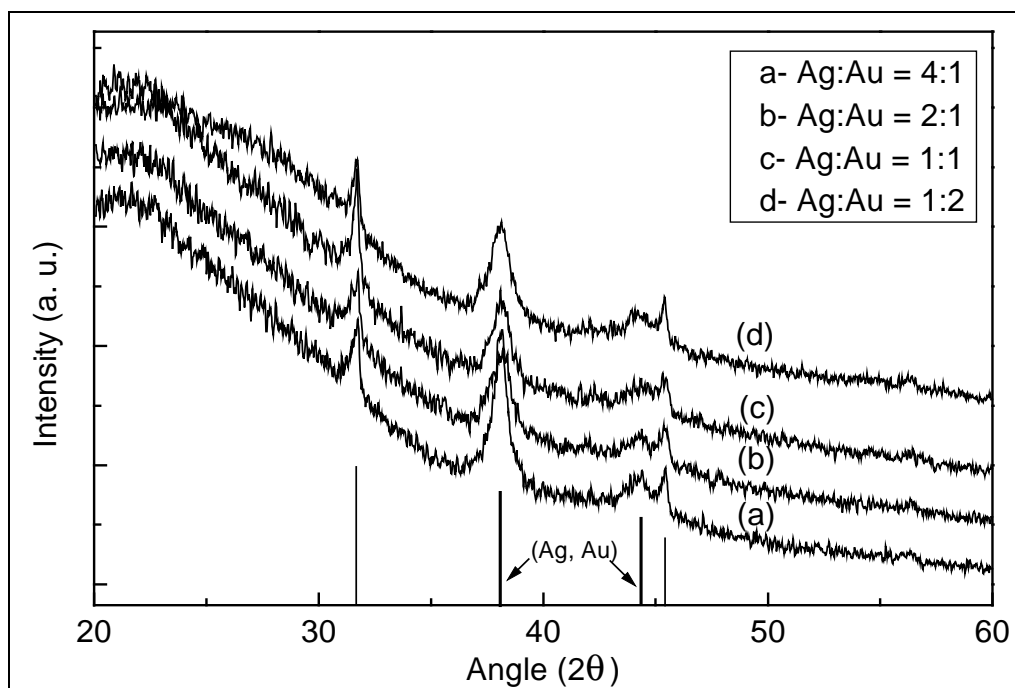


Figure 54: X-ray diffraction patterns of thin films containing Ag / Au alloy colloids with different molar ratios of Ag and Au.

In all the cases in Figure 54 the general behaviour of the diffraction pattern is same, and four peaks are obtained. The peaks corresponding to $2\theta = 38.15^\circ$ and 44.36° may be attributed either to gold, silver or gold / silver alloys. The two additional peaks

corresponding to $2\theta = 31.70^\circ$ and 45.48° may be attributed to sodium chloride, which was formed by the combination of sodium ion (from sodium citrate dihydrate) and chloride ions (from hydrogen tetrachloroaurate and from hydroxylamine hydrochloride). As gold and silver possess almost similar lattice structures, it is difficult to differentiate in between the particles of pure gold, pure silver or gold-silver alloys, only on the basis of X-ray diffraction pattern measurements. Hence the XRD measurements were carried out to determine the colloidal particle size.

These X-ray diffraction patterns were used for the calculation of the crystallite size using Scherrer's equation. The most intense peak corresponding to gold / silver alloy colloids and centred at 38.15° was fitted with the cauchy profile and was used for the particle radius measurements. The particle size calculated using Scherrer's equation of Ag / Au alloy colloids for the different molar ratios of gold and silver are shown in following Table 19.

Table 19: Angle 2θ , corrected half width (β) corresponding to (111) reflex and the crystallite diameter 'd' after the Scherrer's formula for Ag / Au alloy colloids.

Ag:Au	2θ ($^\circ$)	β ($^\circ$)	'd' (nm)
4 : 1	38.067	0.771	15.7
2 : 1	38.091	0.783	15.4
1 : 1	38.100	0.864	13.5
1 : 2	38.098	0.880	13.5

From the table shown above it is clear that the particle size is almost the same in all the cases and is independent of the molar ratio of Ag and Au. The diameter of the crystallites calculated as above is in good agreement with the particle size measured by HR-TEM in above sections.

5.2.1.2 Mixed colloids

It is known from the literature that by dissolving gold and silver salts in a TEOS sol, thin films containing gold and silver colloids can be formed by the thermal reduction of their ions. But the film thickness of the SiO₂ films obtained by this route is very small (< 100 nm) and the optical density of the films was also very small. Spanhel et al. [142] showed that by means of functionalised silanes gold ions can be incorporated in organic-inorganic coatings and can be reduced to gold colloids.

Using this concept Schmitt [143] has studied the thin films containing monometallic noble metal colloids synthesised by the sol-gel route and has studied the influence of different functionalised amino silanes in the formation of colloidal particles. He has obtained interesting colours i.e. ruby from gold, yellow from silver and ruby to green from copper colloids in thick hybrid coatings (up to 1 µm).

In order to achieve the mixed colours of yellow and ruby, gold and silver mixed colloids were synthesised by using sol-gel route. A great problem, which had to be overcome in the synthesis of gold and silver mixed colloids, is the strong reactivity of silver. Addition of a gold containing sol in silver containing sol always led to a precipitate of Ag(I) compounds. To overcome this problem, gold and silver were stabilized with a complexing agent (DIAMO) before mixing with one another.

To synthesise gold / silver mixed colloids, the matrix sol was chosen as GPTS / TEOS, since it is known from other investigations [144] that its short chained organic groups can be completely burnt off without cracking or discolouring coatings of about 1µm in thickness. As a precursor for Au, H[AuCl₄].3H₂O was chosen, since it is well soluble in organic solvents and does not contain additional cations that might disturb the formation of the SiO₂ network in the coatings. Whereas AgNO₃ was used as a precursor of silver due to its solubility in methanol.

In the formation of Ag / Au mixed colloids two different types of substrates were used. These substrates are called as thin (dimensions 10 cm x 2.5 cm x 0.1 cm) and thick glass substrates (dimensions 10 cm x 2.5 cm x 0.2 cm). The motivation behind changing the glass substrates was to make coloured coatings on a wide variety of substrates for the actual applications, and to explore the effects of changing the substrates.

5.2.1.2.1 UV-VIS spectroscopic studies

In order to see if the particles formed are phase separated mixed colloids of Ag and Au, their optical absorption spectra were recorded using Omega 30 UV-VIS spectrophotometer. The UV-VIS spectra of thin films containing Ag / Au mixed colloids having a Ag : Au molar ratio of 1 : 2, as a function of temperature are shown below in Figure 55.

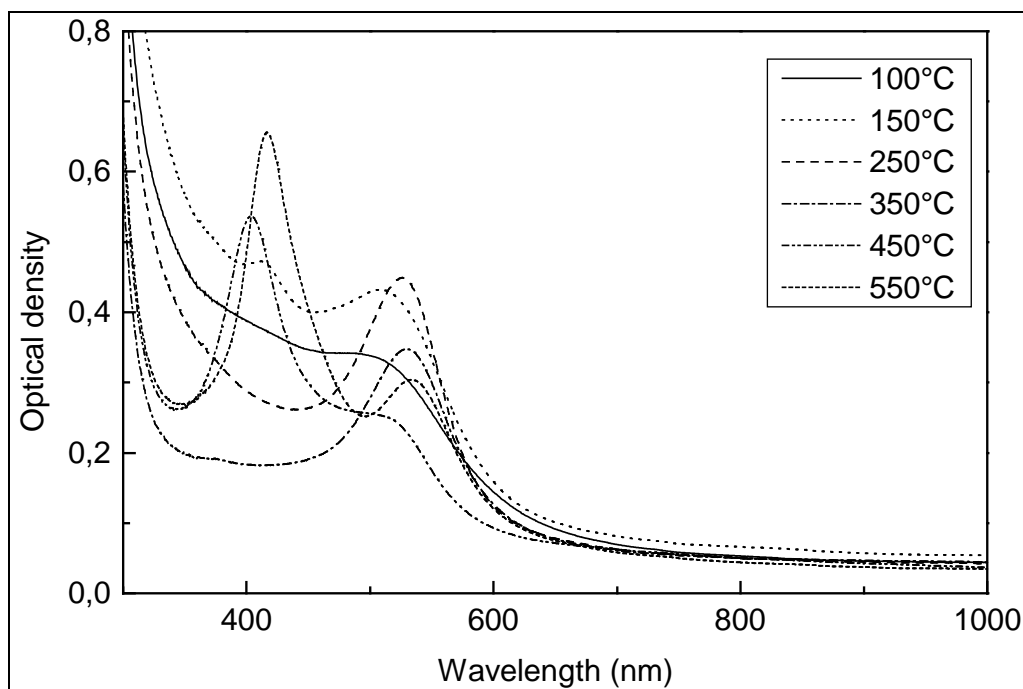


Figure 55: UV-VIS absorption spectra of Ag / Au mixed colloids in PbO-SiO₂ coatings, as a function of densification temperature, Ag : Au = 1 : 2, reference: air, thin glass, experimental conditions in ch. III, p. 43.

It is clear from the above figure that at 100 °C only one peak at 512 nm due to gold was observed, whereas on heating the sample at 150 °C two absorption peaks at 413 nm and 513 nm corresponding to gold and silver were generated. Increasing the temperature to 250 °C results in only one peak at 525 nm due to gold colloids. At 350 °C also only one characteristic peak of gold at 528 nm was observed. Whereas at 450 °C one can again observe both the peaks due to gold and silver at 520 and 404 nm respectively. Heating the sample at 550 °C decreases the optical density of both the peaks.

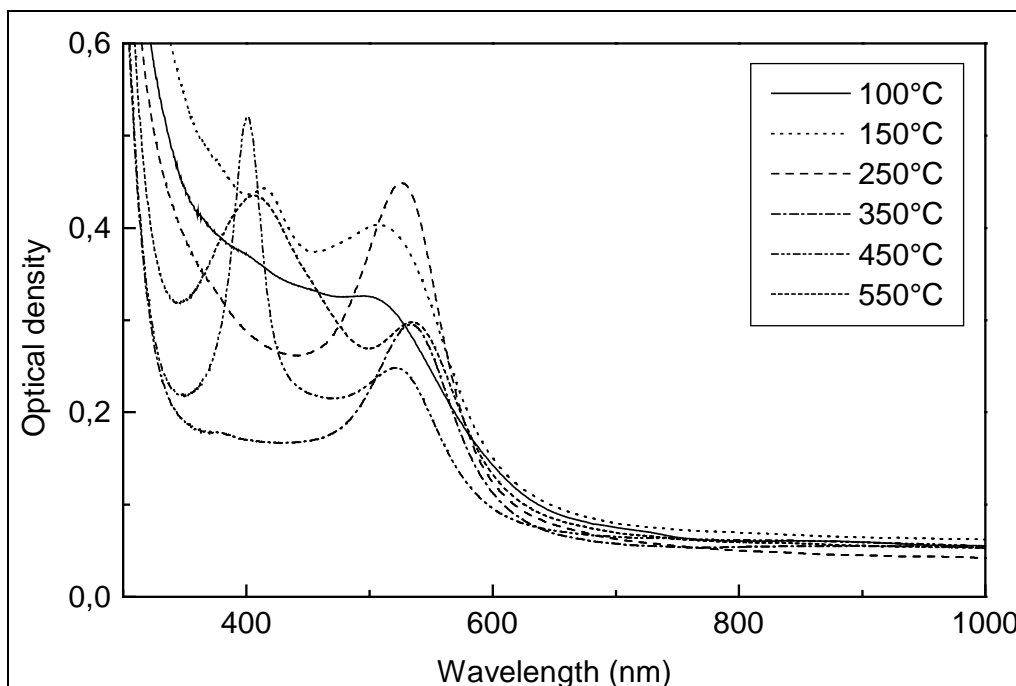


Figure 56: Evolution of Ag / Au mixed colloids peak with the change in heat treatment temperature in PbO-SiO₂ coatings, (Ag : Au = 1 : 2, reference: air, thick glass).

Figure 56 also shows the UV-VIS spectra of the thin films containing Ag / Au mixed colloids as a function of temperature, the only difference is the glass substrate used for the sample preparation are thicker than in the above case. The general trend of the change in the absorption spectra with the temperature is the same in both the cases.

The thickness of the films was measured using a profilometer. For the samples heated at 250 °C, 500 nm thick films were obtained, whose thickness decreases to 360 nm at 350 °C and to 225 nm at 450 °C. A film thickness of 175 nm was measured after the thermal treatment at 550 °C in air.

The UV-VIS spectra of SiO₂ thin films containing Ag / Au mixed colloids having a Ag : Au molar ratio of 1 : 2, as a function of temperature are shown below in Figure 57. This figure shows the UV-VIS spectra of samples formed on thin glass substrates (75 mm x 25 mm x 1 mm).

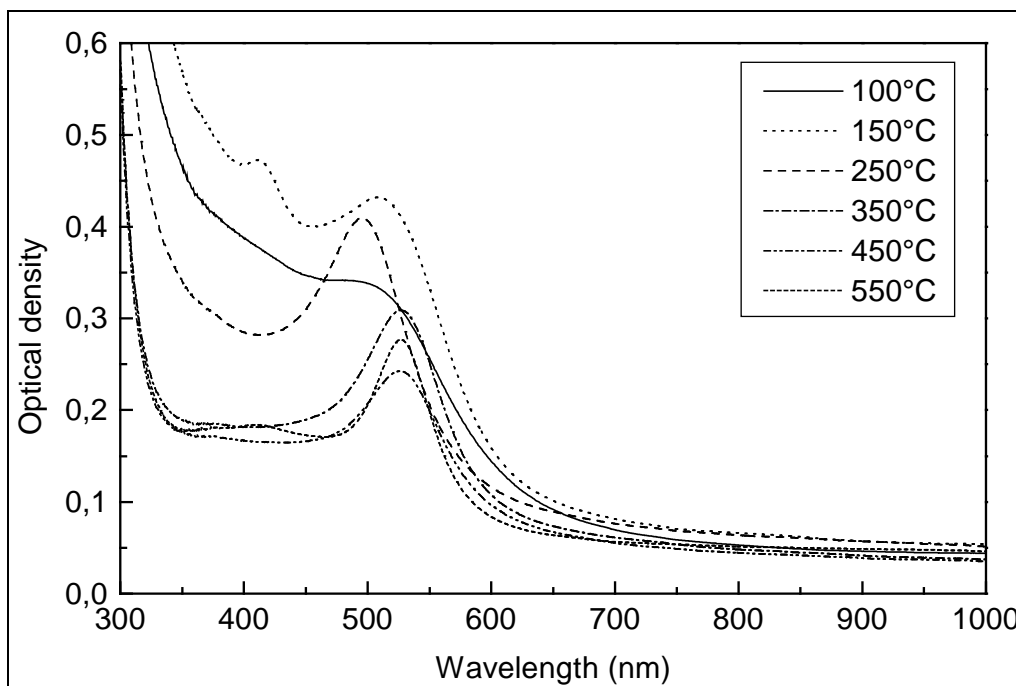


Figure 57: UV-VIS absorption spectra of Ag / Au mixed colloids as a function of temperature of the heat treatment (Ag : Au = 1 : 2, SiO₂ coatings, reference : air, thin glass), experimental conditions can be seen in ch. III, p. 43.

Figure 57 shows only one absorption peak corresponding to colloidal gold at 100 °C. Whereas heating the sample at 150 °C generates two absorption peaks at 413 and 510 nm for colloidal silver and gold respectively. But unlike for the PbO-SiO₂ films only one peak centred at 493 nm was observed for SiO₂ films heat treated at 250 °C. Which shifts to 523 nm on heat treating at 350 °C. The samples heat treated at 450 and 550 °C also did not show any peak corresponding to colloidal silver plasmon absorption.

We have seen in earlier sections that for the gold / silver alloy particles only one absorption peak centred in between pure gold and pure silver was observed, which gradually shifts towards colloidal gold absorption on increasing the molar ratio of gold. The appearance of only one peak at 493 nm for the samples heated at 250 °C may be attributed to the formation of alloy colloids. In order to get a better understanding of the particles formed at this temperature, EDX analysis of the particles was carried out. HR-TEM image of the films and their EDX spectra are given in the later sections.

As it is seen from the above picture that for Ag / Au mixed colloids in SiO₂ thin films an unusual behaviour of absorption peak at 250 °C was observed. So the UV-VIS absorption spectra of thin films densified at 250 °C and containing Ag / Au mixed

colloids having a different proportion of Ag and Au were recorded as function of their molar ratios. The corresponding UV-VIS spectra of these thin films are shown in appendix Figure A 31. It can be seen from the figure that the peak position does not depend much on the molar concentration of Ag and Au. Whereas for the films with a Ag : Au molar ratio of 4 : 1 the peak is positioned at 473 nm, it shifts to 483 nm for the molar ratio of 2 : 1 and 1 : 1 and finally to the 491 nm for the molar ratio of 1 : 2. The observed shift of the peak position with the change in molar ratios of gold and silver is not in good agreement to the calculated (see in *section 5.2.1.1.4*) peak shift for the alloy colloids.

Ehler et al. [145] have also observed that the energy of the resonance absorption peak is nearly independent of alloy composition during the synthesis of bimetallic particles of Ag and Au. They attributed this unusual behaviour to the formation of alloy colloids at the interface between the two metals, and concluded that the optical properties of the Ag / Au alloy formed at the interface of the two metals will certainly be different than those of either of the pure metal films.

Another possibility may be the formation of colloidal particles, which are composed of the segregation of both gold and silver particles. But Toe et al. [98] have shown that as the penetration depth in UV-VIS spectroscopy is much greater than the size of the particles, if the metallic component in the particles indeed segregate, either on the surface or inside the particle, there should be two distinct absorption peaks. Our observation of a single peak thus discards the above assumption and gives a strong indication of homogeneously organised clusters.

Figure 58 shows the UV-VIS spectra of SiO₂ thin films containing Ag / Au mixed colloids with the molar ratio of Ag : Au = 1 : 2. Here the glass substrates used for the samples preparation were thicker (75 mm x 25 mm x 2 mm).

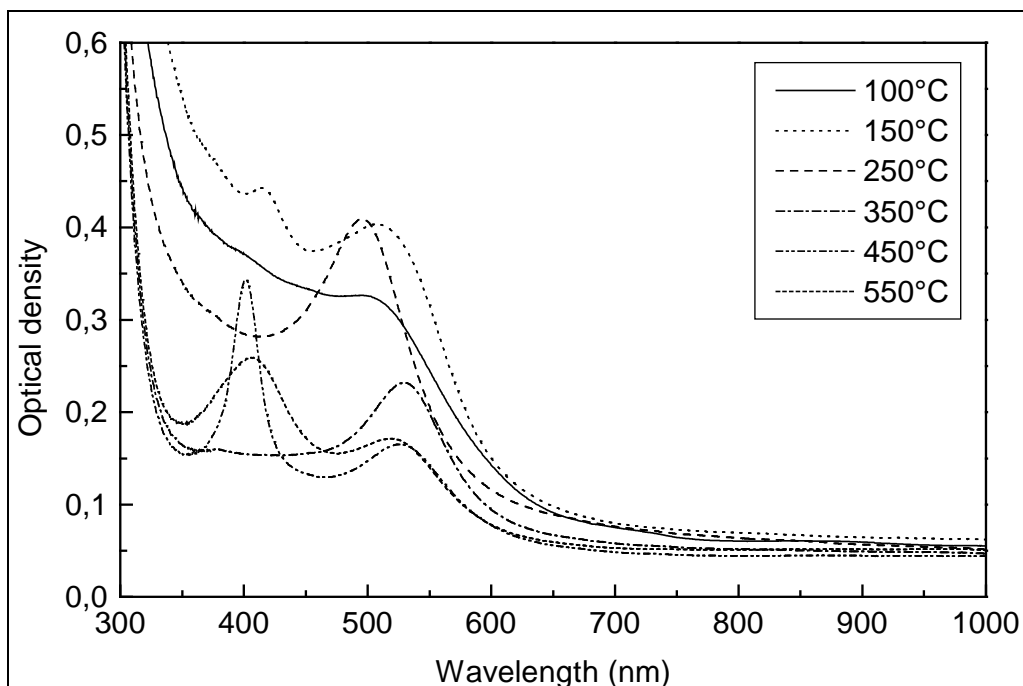


Figure 58: Evolution of Ag / Au mixed colloidal peak with the change in heat treatment conditions, Ag : Au = 1 : 2, SiO₂ coatings, reference : air, (thick glass).

From the above figure it is clear that for the samples heated at 100 and 150 °C the nature of the spectra is almost the same and at 250 °C also only one peak at 493 nm was observed. But unlike thin glass, in the case of thick glass heating of the samples at 450 generates two absorption peaks corresponding to the plasmon peaks of colloidal gold and silver at 527 and 400 nm respectively. Whereas heating at 550 °C decreases the optical density of absorption peaks and also broadens the peak for the silver colloids. This decrease in the optical density with increasing temperature can be attributed to the decrease in film thickness as higher temperatures. These results indicate that the formation of silver colloids on the surface of the glasses is strongly dependent of the type and thickness of the glass substrates used for the sample preparation.

In order to get a better understanding of the bimetallic Ag / Au colloidal particles formed at 250 °C, showing only one absorption peak around 473 - 493 nm, TEM investigations were carried out. HR-TEM micrograph of a thin film containing bimetallic particles of Ag / Au having a molar ratio of Ag : Au = 2 : 1 and heat treated at 250 °C in air has been shown in following Figure 59. Whereas EDX spectra of a particle are shown in Figure 60.

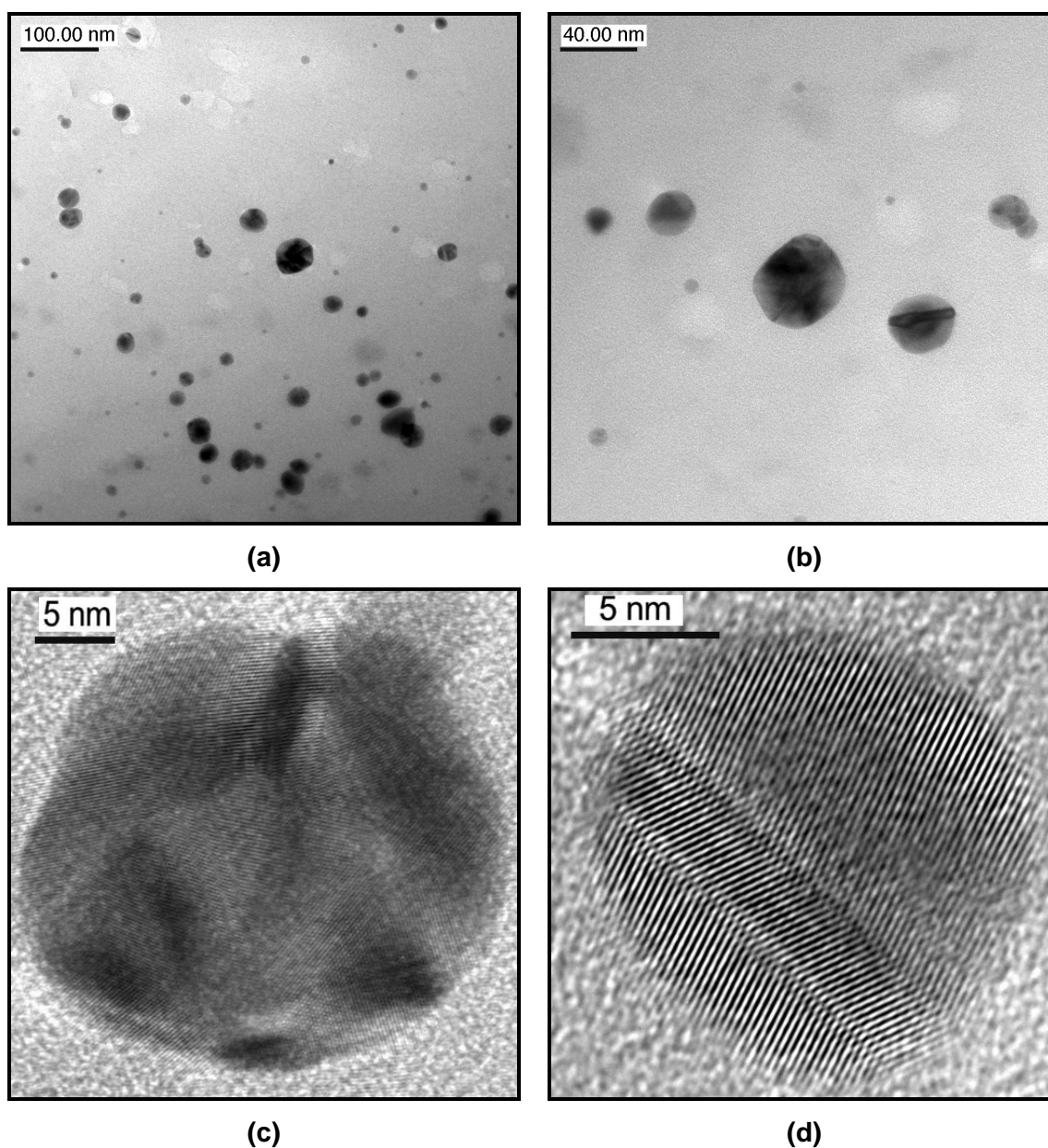


Figure 59: HR-TEM micrograph of thin films containing Ag / Au mixed colloids, heat treated at 250 °C in air for 1h (a) and (b) particles embedded in glass matrix (c) and (d) two particles with high resolution.

Figure 59 shows the distribution of colloidal particles with diameters ranging from 5 nm to 30 nm in a SiO₂ glass matrix. Fourier filtering of an image of a single particle indicated that particles with polycrystalline structures are formed. The possible reason of a very broad particle size distribution can be that the particles are formed by the combination of gold and silver crystallites, not by the alloying of these particles. Due to the practically same lattice dimensions of Ag and Au, this can not be differentiated on the basis of electron microscope only.

In order to determine the composition of the formed colloidal particles at 250 °C, EDX-analysis of some of the particles and glass matrix was also carried out. EDX profiles of a particle selected randomly are shown below in Figure 60.

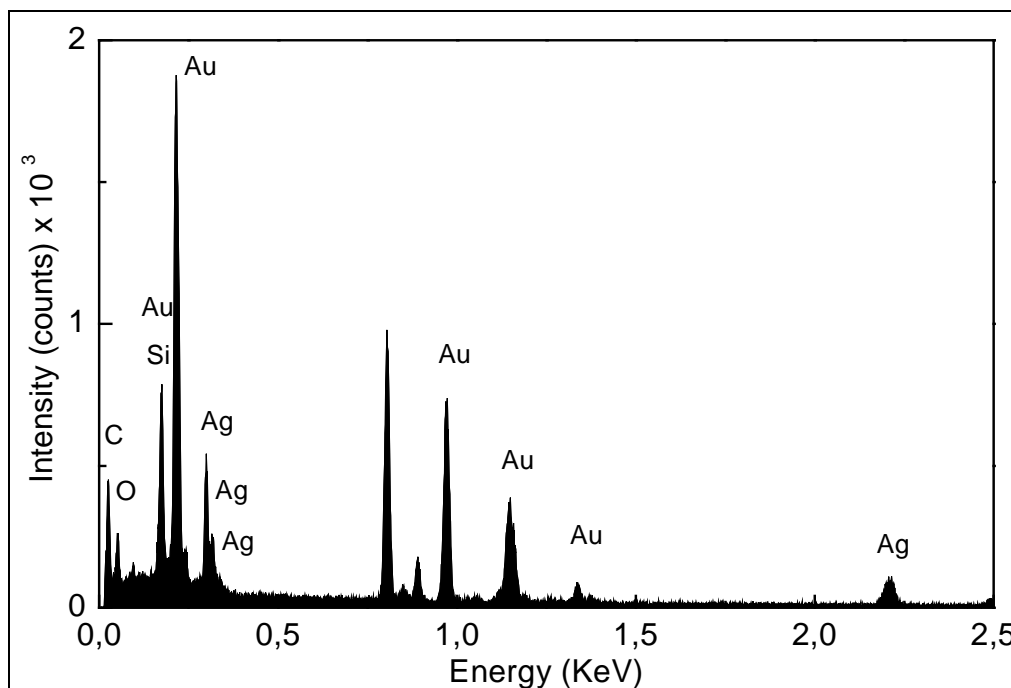


Figure 60: EDX analysis of a Ag / Au bimetallic particle with a molar ratio of Ag : Au = 1 : 2.

EDX analysis of a particle showed the presence of 67.2 atom% of gold and 32.8 atom% of silver. Whereas some other particle selected randomly from the same sample showed an atom% of Ag equal to 35.6 and that of Au equal to 64.4. Presence of Cu peaks in EDX profile is due to the copper grid used for the sample preparation. EDX analysis of matrix however showed the absence of both, gold and silver and the presence of Si, C and O only.

A difference in the formation of Ag / Au mixed colloids can be observed when the UV-VIS absorption spectra of thin films containing different proportions of Ag / Au were recorded as a function of type of the glass substrates. The absorption spectra for thin and thick glass substrates are shown below in Figure 61 and Figure 62 respectively.

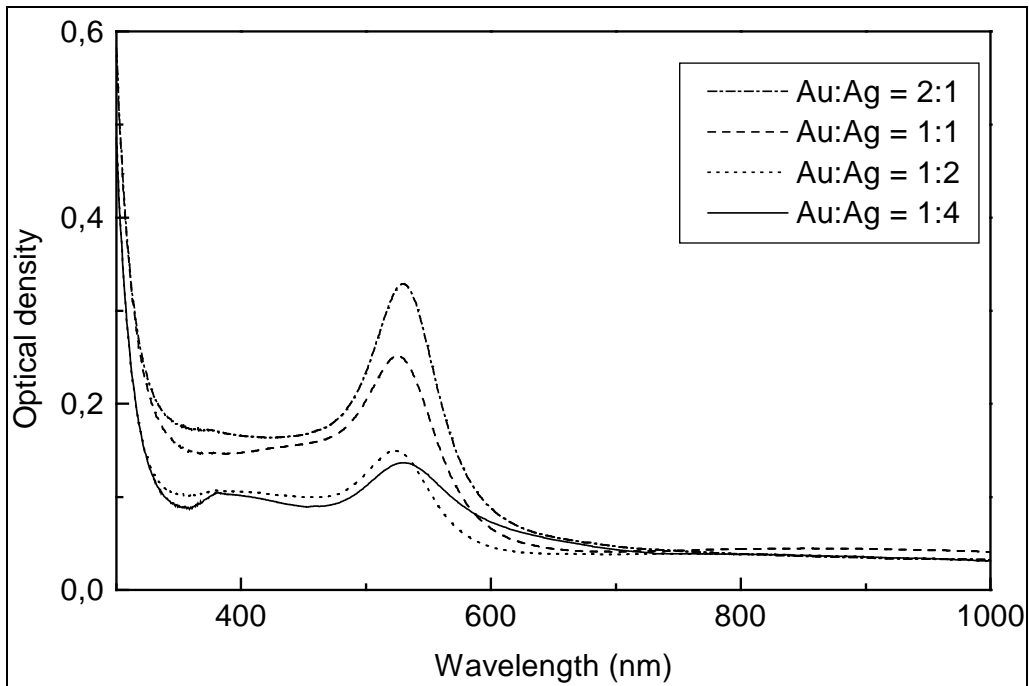


Figure 61: UV-VIS spectra of SiO₂ thin films containing Ag / Au mixed colloids as a function of their molar ratios for the sample heat treated at 450 °C in air, on thin glass substrates, reference: air (experimental conditions in ch. III, p. 43).

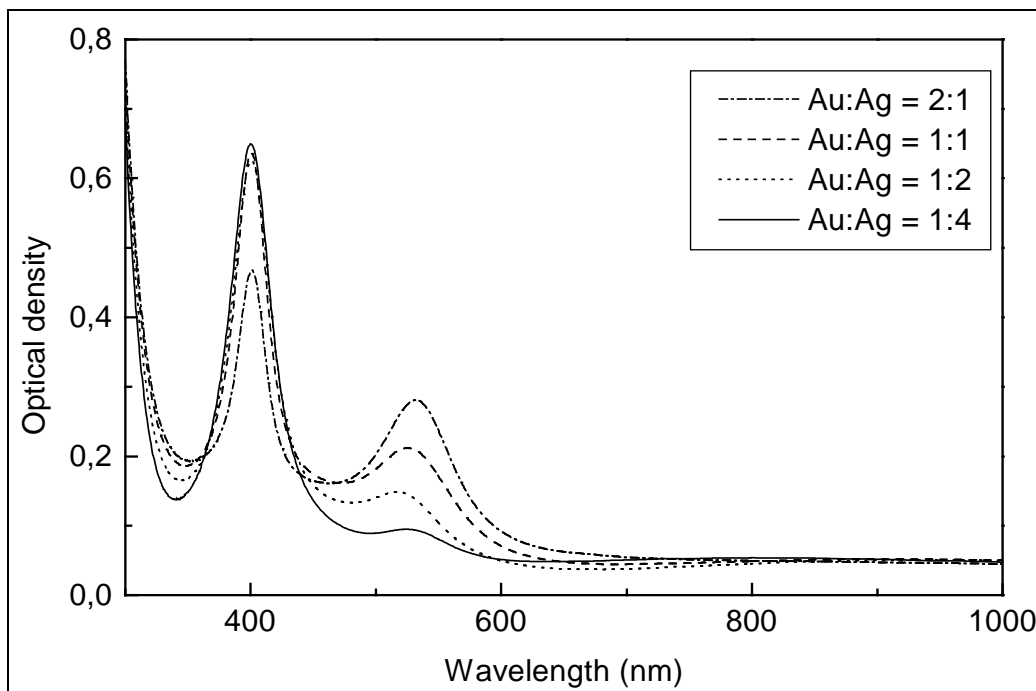


Figure 62: UV-VIS spectra of SiO₂ thin films containing Ag / Au mixed colloids as a function of their molar ratios for the samples heat treated at 450 °C in air, on thick glass substrates, reference: air, (experimental conditions in ch. III, p. 43).

Comparing the UV-VIS spectra of thin films containing Ag / Au mixed colloids synthesised on thin and thick glass substrates, it is clear that for thin glasses only one absorption peak at 520 nm (corresponding to plasmon absorption of gold) was observed. Whereas for thick glasses two peaks positioned at 400 nm and 520 nm (corresponding to silver and gold plasmon absorption respectively) have been observed. The observed UV-VIS spectra clearly indicate the formation of gold colloids only, in the case of thin glasses as substrates, whereas both gold and silver colloids, in the case of thick glasses as substrates. However a shift toward the lower wavelength of absorption peak of gold was observed with the decrease in the molar percentage of gold, this shift may be attributed to the formation of smaller gold colloid particles on decreasing the molar percentage.

It can be said that the appearance of the absorption peak of silver colloids is dependent to the content of tin present on the surface of float glass (this will be shown in the *section 5.2.1.2.3*). In thin glass substrates the tin content will be less and it will not be sufficient to stop the reduction of silver in silver ions. The diffusion of silver ion was studied in the same way as has been done previously. A thin film, heat treated at 450 °C, was etched by 5% HF solution and heat treated again under reducing atmosphere. The formation of silver colloids indicates the diffusion of ionic silver into the substrates. The UV-VIS spectra of etched glasses and those for other proportions of Ag and Au are shown in appendix Figure A 38. The dependence of the intensity of the silver absorption peak on the initial molar percentage of silver is a direct consequence of diffusion of silver inside the glass.

5.2.1.2.2 Calculation of theoretical absorption spectra of Ag / Au mixed colloids

Absorption spectra of thin films containing Ag / Au mixed colloids were calculated using the concept that if the different type of the particles are phase separated in a glass matrix, all of them will show their independent plasmon peaks. The resulting spectra will be the physical addition of the UV-VIS spectrum of the corresponding metal colloids, in which the intensity of the respective plasmon peaks will be proportional to the mixed ratios. Figure 63 shows the calculated extinction spectra for mixed colloids as a function of their molar ratios. Absorption spectra for pure gold and pure silver were calculated for the colloidal volume concentration of 10^{-6} and the refractive index of the matrix was taken as 1.46.

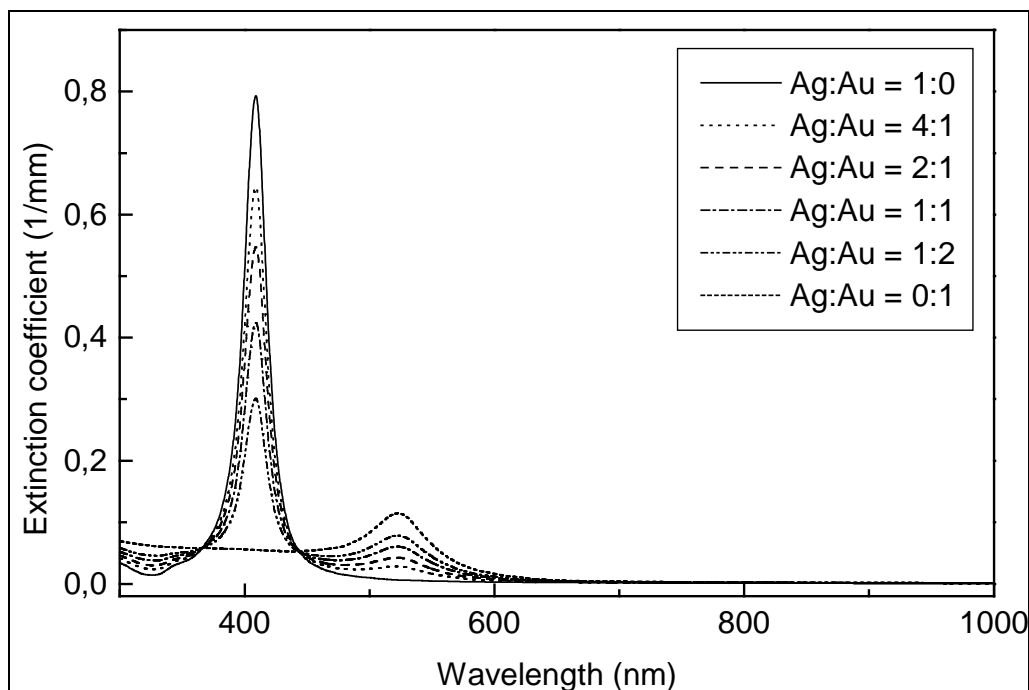


Figure 63: Theoretical absorption spectra of Ag / Au mixed colloids, calculated (Mie theory) by the physical addition of the spectra of colloidal gold and silver at the different proportions. The refractive index of the medium is 1.46, $r = 10$ nm and the volume concentration of colloids 10^{-6} .

Theoretical absorption spectra of Ag / Au mixed colloids show two peaks corresponding to Ag and Au plasmon frequency. The intensity of the peaks is directly proportional to the molar ratios of gold and silver. Comparing the experimentally observed and theoretical spectra it can be said that the appearance of two peaks in present case (see Figure 62), also suggest the formation of mixed colloids of Ag and Au in thin films.

5.2.1.2.3 Effect of the tin content of float glass on the formation of mixed colloids

During the synthesis of gold and silver mixed colloids on the surface of float glass it was observed that the formation of mixed colloids is strongly dependent of the side of the glass substrate. The UV-VIS spectra SiO_2 thin films containing Ag / Au colloids (Ag : Au = 2 : 1), as a function of side of glass substrates, at densification temperature of 450 °C are shown below in Figure 64. The spectra for other molar ratios of Ag and Au are given in appendix Figure A 36.

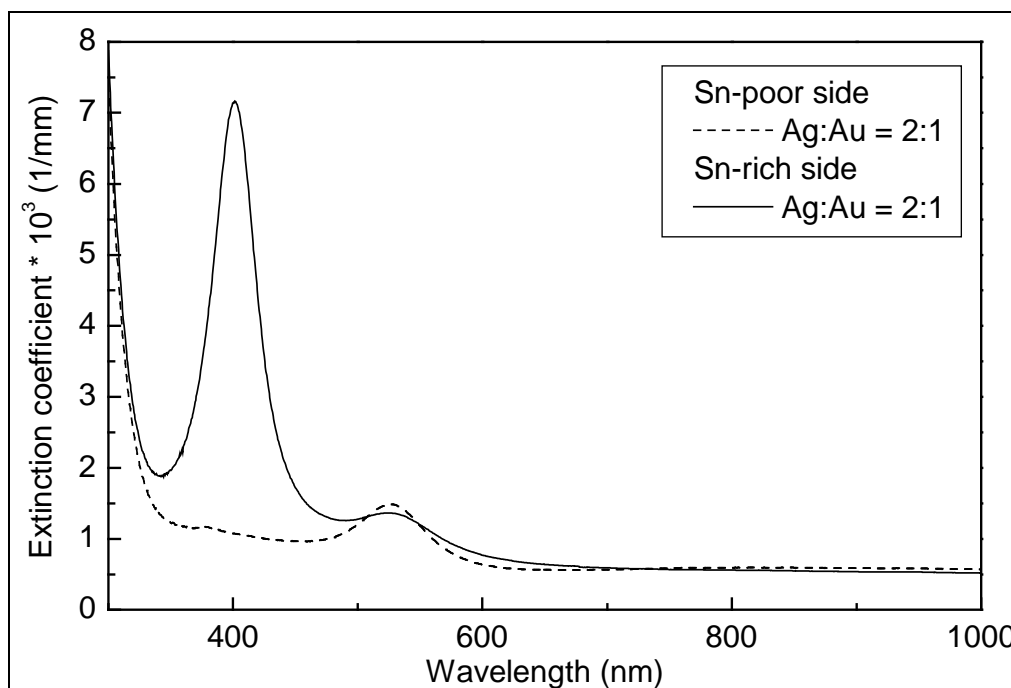
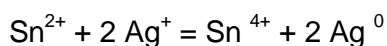


Figure 64: Side dependence of the formation of Ag / Au mixed colloids on thick glass substrates; samples were heated at 450 °C in air.

From the above figure it is clearly seen that one side of the float glass shows only one absorption peak at 525 nm that can be assumed to be colloidal gold. Whereas, the other surface of the glass shows the two peaks at 410 nm and 525 nm belonging to colloidal silver and gold respectively. It is known that the formation of colloidal silver in the near surface region of float glass appears to be closely related to the concentration and chemical state of the tin in the glass surface. Past studies [146, 147] have shown that the concentration of tin at the surface of the tin-rich face of float glass is very high (as much as 30 wt%). The tin concentration decreases rapidly in the first 10 nm of the glass. The tin concentration in the other face of the float glass is very low. Both Seiger [148] and Ernsberger [149] have reported that a large portion of the tin is in the stannous state. Since stannous tin is known to react with ionic silver via the reaction



Ernsberger [149] suggested that the stannous tin in the near surface region of both faces of float glass could react with the silver ions to produce silver colloids.

It is clearly seen from the Figure 64 that the formation of silver colloids is independent to the silver concentration, or the optical density of the spectra for the molar ratios of Ag : Au greater than 1 : 1 is almost the same (see also appendix Figure A 36). It

clearly indicates that the formation of silver colloids is dependent to the tin content of the surface. In order to get a better understanding of this behaviour, the colloidal turnover of the gold and silver containing thin films prepared on the tin rich and tin poor surfaces of the float glass were calculated. In order to evaluate the colloidal turnover the UV-VIS extinction spectra for the mixed colloids were deconvoluted (a deconvoluted curve is shown in appendix Figure A37) and the corresponding spectrum for gold and silver colloids was used for the calculation (rest of the method for the calculation is the same as used for the gold colloids in solutions, *section 5.2.1.1.2*). The calculated turnovers for gold and silver colloids are given below in Figure 65.

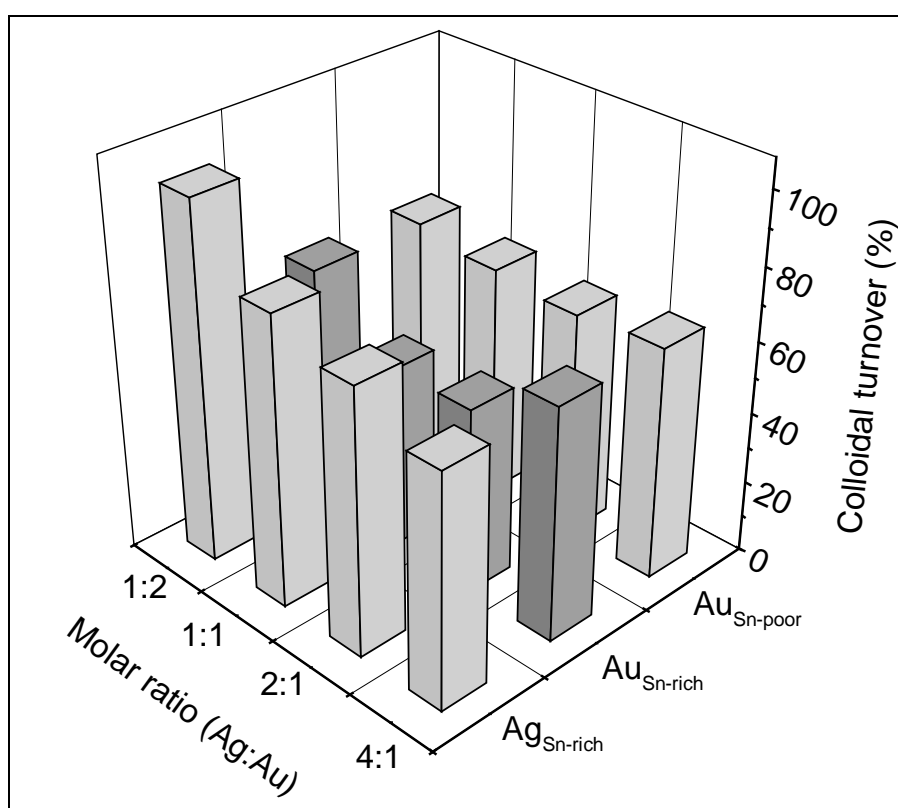


Figure 65: Colloidal turnover of silver and gold colloids in tin rich and tin poor surface of the float glass. All the samples were densified at 550 °C in air, reference: air.

It can be seen from the above figure that the colloidal turnover for Au colloids is almost the same (varying from 65% to 68%) in tin poor side. Whereas formation of both gold and silver took place on the tin rich surface of float glass. The colloidal turnover for gold is varying from 52 to 65%, however a gradual decrease in the colloidal turnover of silver was observed with the increase of molar ratio of silver. Which is 100% for the molar ratio of Ag : Au = 1 : 2, decreases down to 80% for Ag : Au = 1 : 1 and finally

65% for the Ag : Au = 4 : 1. These observations also indicate that the formation of silver colloids is directly dependent on the tin content of float glass.

5.2.1.2.4 Effect of pre-heat treatment of float glass substrates on the formation of Ag / Au mixed colloids

In order to proof this effect of the dependence of colloid formation on the surface, a number of float glass substrates were heated at 500 °C in either H₂ or in air with the rate of 100 K/h and held for 18 h. After cooling them to room temperature samples were prepared by dip coating the substrates. These samples were kept in the furnace and heat treated at 500 °C in air for 1 h. The UV-VIS spectra of the samples recorded at room temperature are shown in Figure 66 and Figure 67.

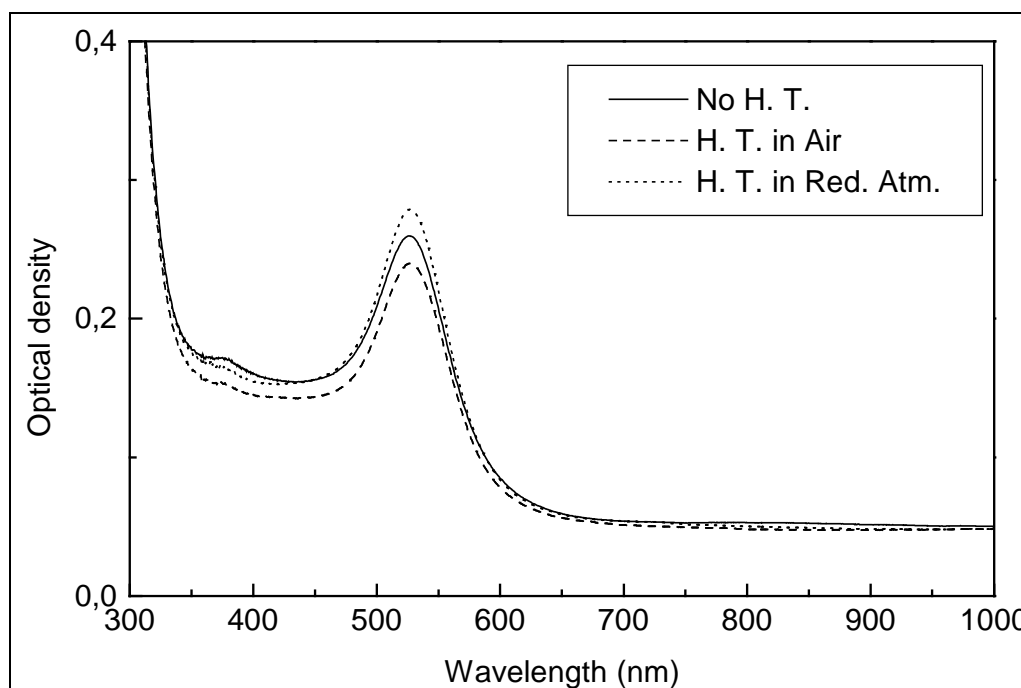


Figure 66: UV-VIS spectra of the thin films (tin poor side) containing gold and silver mixed colloids. Borofloat glass substrates were heat treated under different atmospheres before dip coating.

From the above spectra it is seen that only one peak due to gold colloids is observed. For the samples pre heated in air the observed optical density corresponding to Au colloids is slightly lower than the samples that are not heat treated. Whereas for the samples pre heated in reducing atmosphere (H₂) the observed optical density is slightly higher. This is because as the gold is known to be reduced very fast even without any

reducing agent [2]. So the formation of gold colloids is less dependent of the state of tin (stannous or stannic).

Figure 67 shows UV-VIS spectra of coatings on Sn-rich surface with and without pre-heat treatment.

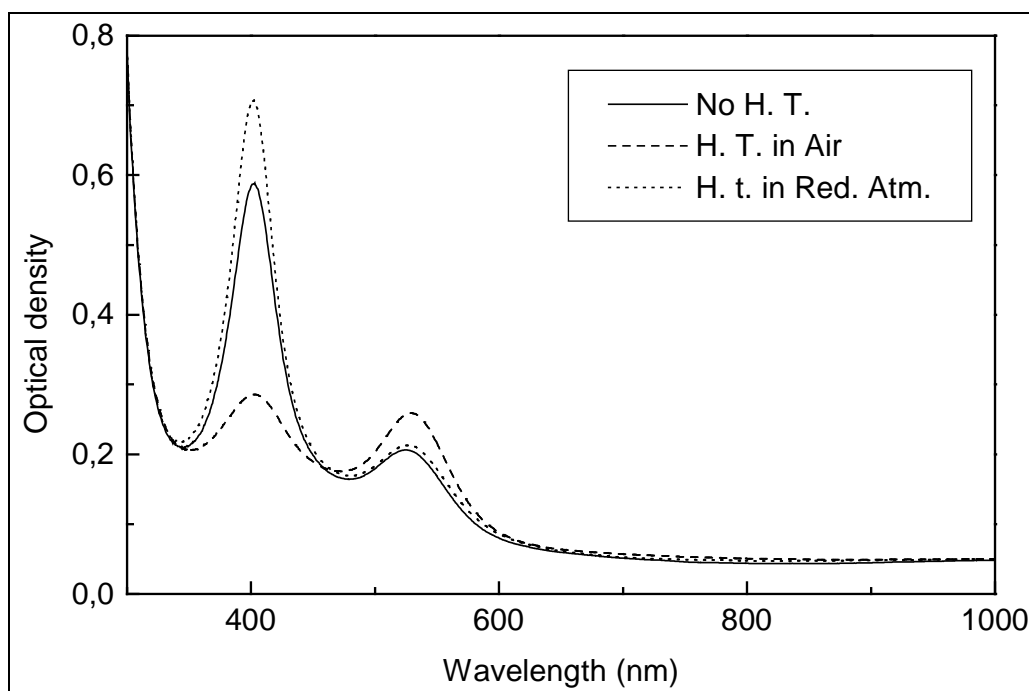


Figure 67: UV-VIS spectra of thin films (on tin rich side) containing gold silver mixed colloids, as a function of pre-heat treatment of glass substrates under different atmospheres.

For the samples without any pre-heat treatment two peaks at 410 nm and 528 nm were observed. The optical density of the peak at 410 nm decreases remarkably on pre-heating the samples in air, whereas it increases on pre-heating the samples under reducing atmosphere ($N_2 / H_2 = 92 / 8$). It means that, the hydrogen pre-treatment increased the silver colloid formation, while the air pre-treatment decreased the silver colloid formation.

This phenomenon appears to be a function of the effect of pre-treatment on the chemical state of the tin. Pre-treatment in a reducing atmosphere may further reduce the tin in the near surface region, which in turn, means that more silver will be reduced during the heat treatment of the samples. Pre-treatment in air results in the oxidation of tin to the stannic state, so that less stannous tin is available to reduce the silver ions.

5.2.1.2.5 HR-TEM characterisation

In order to see the shapes and sizes of the particles formed, HR-TEM characterisation was performed. HR-TEM micrographs of thin film containing Ag / Au mixed colloids, heat treated at 550 °C in air are shown below in Figure 68.

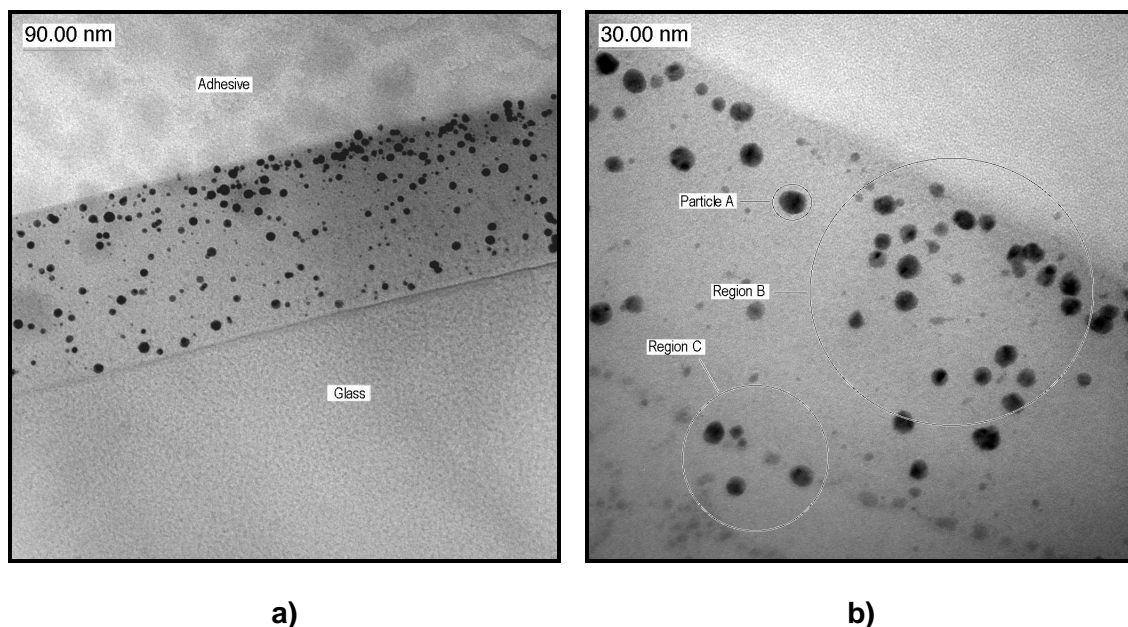
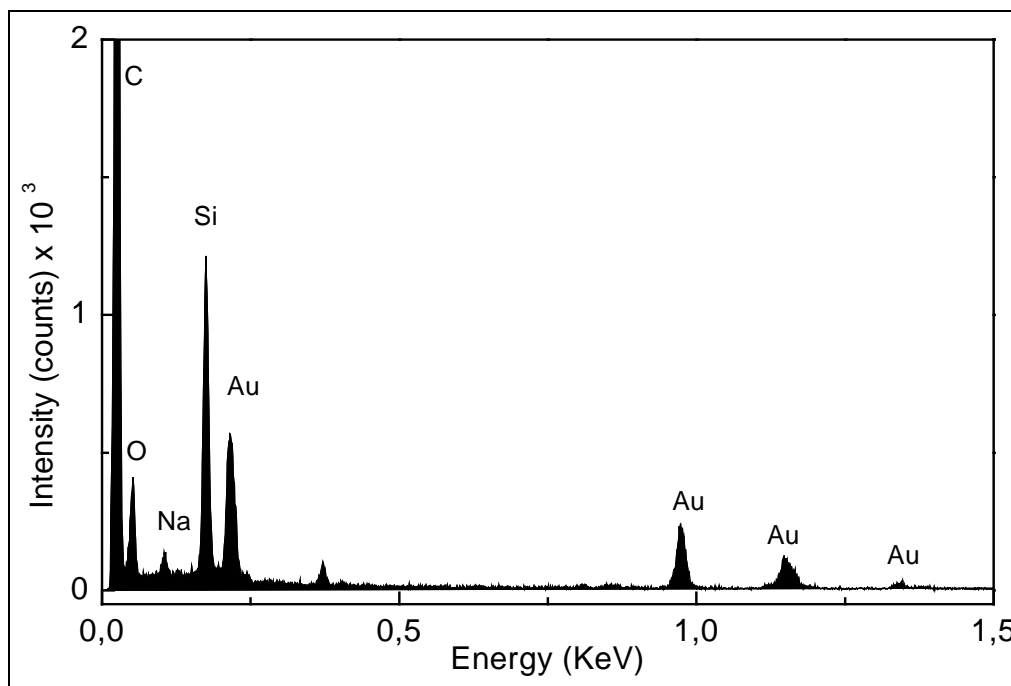


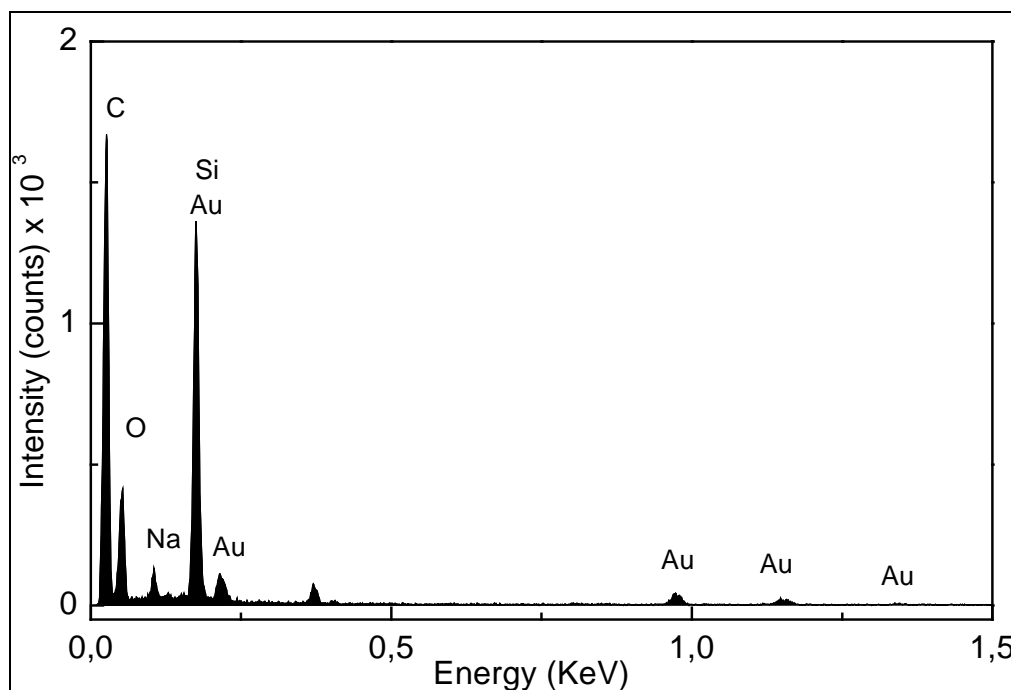
Figure 68: HR-TEM image of thin film containing Ag / Au mixed colloids densified at 550 °C in air (heating rate of 100 K / h for 1 h), (a) Particles distributed in glass matrix and (b) Some selected regions for the EDX measurements.

This figure shows the SiO₂ coating doped with colloidal particles in bright field diffraction contrast. Relatively small particles having a diameter of 1 to 12 nm, which are uniformly dispersed in the glass matrix, are formed. Fourier filtering of an image showed the formation of polycrystalline nanoparticles.

In order to see the composition of the particles formed, their EDX analysis was carried out. Some EDX patterns of some selected regions shown in above Figure 68 are given below in Figure 69.



(a)



(b)

Figure 69: EDX profiles of (a) single particle A, (b) region B shown in Figure 68.

The EDX analysis of a particle labelled as 'A' in Figure 68 (a) is shown in Figure 69 (a), whereas, the analysis of region 'B' shown in Figure 68 (a) is shown in Figure 69 (b). The EDX profiles of a particle 'A' showed the peaks corresponding to gold only, indicating that the particle is not a bimetallic particle but formed of gold only.

Appearance of some other peaks of Si, O, Na and C are coming from the glass matrix and the glass substrate. The EDX profile of the relatively large region 'B' also showed the presence of peaks corresponding to gold, indicating that silver is not even present in the glass matrix in dissolved form.

It has been shown in previous sections that silver on heating in air oxidises and diffuses inside the glass, which reduces at higher temperature to form silver colloids. Since the HR-TEM investigations were from the thin films only, the absence of silver particles in the micrographs is well justified.

5.2.1.2.6 X-ray diffraction characterisation

In order to see the crystalline behaviour of the particles formed and to calculate the size of crystallites using Scherrer's formula X-ray diffraction patterns of thin films containing gold / silver mixed colloids were recorded. Figure 70 shows the XRD patterns of thin films containing Ag / Au mixed colloids as a function of their molar ratios.

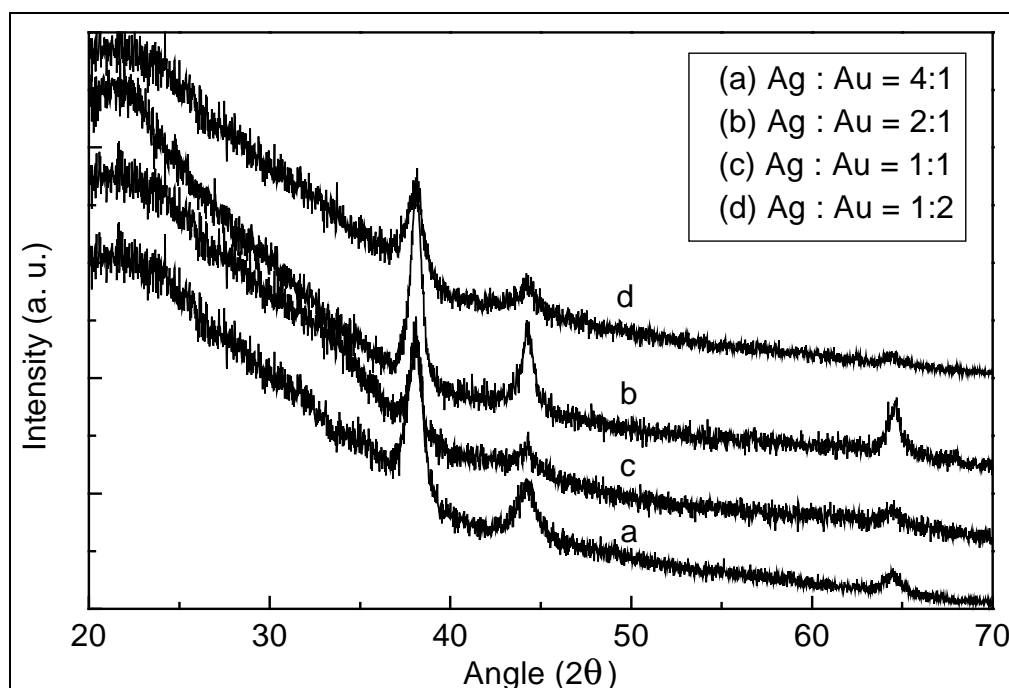


Figure 70: The X-ray diffraction patterns of PbO-SiO₂ thin films containing Ag / Au mixed colloids and densified at 550 °C in air, as a function of their molar ratios.

As the colloids are phase separated mixed colloids of gold and silver the XRD pattern has to be the simple addition of the corresponding XRD patterns of gold and silver. As

the XRD patterns of gold and silver are identical the resulting XDR spectra may be assumed to be because of the addition of gold and silver XRD patterns. These spectra were used for the calculation of particle size using Scherrer's equation. The diameter of the particles 'd' is given below in following Table 20.

Table 20: Angle 2 θ , corrected half width (β) corresponding to (111) reflex and the crystallite diameter 'd' after the Scherrer's formula for Ag / Au mixed colloids.

Ag : Au	2 θ (°)	β (°)	'd' (nm)
4 : 1	38.012	0.675	18.9
2 : 1	38.119	0.919	12.4
1 : 1	38.069	0.699	18.0
1 : 2	38.050	0.921	12.5

Particle sizes calculated as above are in good agreement to the particle size measured using HR-TEM spectroscopy.

5.2.1.3 Summary and conclusion

The synthesis route for the nanocomposite thin films containing alloy- and mixed- colloids of gold and silver by sol-gel method has been developed successfully. Structural and chemical analysis of Ag-Au alloy and mixed nanoclusters in a silica matrix was performed by means of UV-VIS spectroscopy, HR-TEM and EDX. UV-VIS spectroscopy has been successfully applied to differentiate between alloy- and phase separated mixed- colloids of gold and silver.

Thin films containing Ag-Au alloy colloids showed only one absorption peak, the position of which shifts continuously from the absorption maxima of silver to the absorption maxima of gold on increasing the molar ratio of gold in the wavelength range from 410 nm to 530 nm. This allows the tuning of the absorption band (and hence the colour) using glass like films containing nanosized metal colloids. The absorption spectra of Ag / Au mixed colloids on the other hand show two peaks corresponding to the plasmon peak of gold and silver.

The theoretical absorption spectra for the alloy- and mixed- colloids of Ag / Au were also calculated using Mie theory and using an equation given by Baba et al. [97]. A good agreement was found between theoretical and measured absorption spectra of Ag / Au alloy- and mixed- colloids.

Thin films containing bimetallic nanoparticles of Ag / Au

For the synthesis of gold and silver mixed colloids, the formation of silver colloids was found strongly dependent to the surface of the float glass. On the tin rich surface formation of both gold and silver colloids took place whereas on the tin poor surface only the formation of gold colloids was observed. This dependence of the formation of silver colloids was attributed to the presence of tin as a Sn^{4+} state which changes into Sn^{2+} during heat treatment converting the Ag^+ into silver colloids.

5.2.2 Ag / Cu system: Thin films containing alloy- and mixed-colloids

5.2.2.1 Alloy colloids

The sol-gel route has successfully been applied for the preparation of bimetallic particles of Ag / Au in previous section. But the Ag / Cu system would also provide a wider range of tailorability in colours. Therefore, thin films containing bimetallic colloids of silver and copper were also synthesised using the sol-gel route. Experimental details for the synthesis of thin films containing bimetallic colloids of Ag / Cu can be seen in chapter III, page 46.

5.2.2.1.1 Synthesis of colloidal silver containing sol

The synthesis of a sol containing silver colloids was carried out by dissolving PVP in methanol. Methanol was chosen for dissolving PVP since it also has better solubility for silver nitrate. When PVP was dissolved completely, silver nitrate was added to it. A Silver-amine complex was made by the dropwise addition of DIAMO (Ag : DIAMO = 1 : 2). Complexing with DIAMO is necessary since silver is known to react very fast with chlorine and forms a AgCl precipitate. A GPTS / TEOS sol was used as SiO₂ matrix. Finally, NH₂OH.HCl dissolved in methanol was added to the above to obtain colloidal silver containing sol. The addition of PVP is necessary to stop the agglomeration of colloidal particles formed at the end of the process. Mixing of silver in the methanolic solution of PVP turns the colourless and transparent solution into a yellow coloured sol.

As PVP is known as a mild reducing agent [150], it partially reduces ionic silver to colloidal silver. The formation of silver colloids in solution was confirmed by UV-VIS spectroscopy, which shows a characteristic absorption peak for silver at 425 nm [151]. UV-VIS spectra of the silver containing sol after the addition of 1 : 1 and 1 : 2 molar proportions of NH₂OH.HCl as a reducing agent, are shown in Figure A 41 in appendix.

The addition of the NH₂OH.HCl in the molar proportion Ag : NH₂OH.HCl = 1 : 1, gives an absorption peak centred at 415 nm, which becomes stronger on addition of 2 moles of reducing agent per mole Ag, and results in a peak centred at 412 nm. Now the question arises if the addition of 2 mole of reducing agent per mole of Ag is sufficient to reduce all the ionic silver into the colloidal silver or not. Or else, how much ionic silver has been converted to the colloidal silver under this condition.

5.2.2.1.2 Calculation of colloidal turnover of Ag colloids in solution

In order to calculate the percentage of colloidal silver various extinction spectra were calculated using Mie-theory for the silver particles with different radii at a constant colloid volume concentration of 10^{-6} and a constant refractive index of 1.33. After determining the extinction maxima the spectra were integrated from the wavelengths 320 to 1000 nm. These calculations indicated that the proportionality factor ‘f’ for the particles ranging in radii from 1 to 10 nm was nearly independent of the radius of the colloids. The ‘f’ for the silver particles calculated in the same way as in case of Ag / Au colloids is shown below in Table 21.

Table 21: The proportionality factor for the particles of different sizes. ‘Avg’ is the average of the proportionality factor of the particles with radii 3, 5, 8 & 10 nm. $C_{\text{composition}}$ is the colloidal volume concentration calculated assuming that all the silver has converted to colloidal Ag, ρ_S and ρ_{Ag} are the densities of the solution and silver respectively.

Particle size	Proportionality factor ‘f’
Avg	4.62×10^{-8}
20 nm	4.50×10^{-8}
30 nm	4.48×10^{-7}
40 nm	4.41×10^{-7}
ρ_S	1.0 g / cm^3
ρ_{Ag}	10.4 g / cm^3
$C_{\text{composition}}$	17.26×10^{-5}

If proportionality factor ‘f’, and the silver colloid volume used for the synthesis $C_{\text{composition}}$ are known, colloidal turnover can be calculated after calculating the area of extinction spectra of the silver containing sol. The extinction spectrum is shown below in Figure 71.

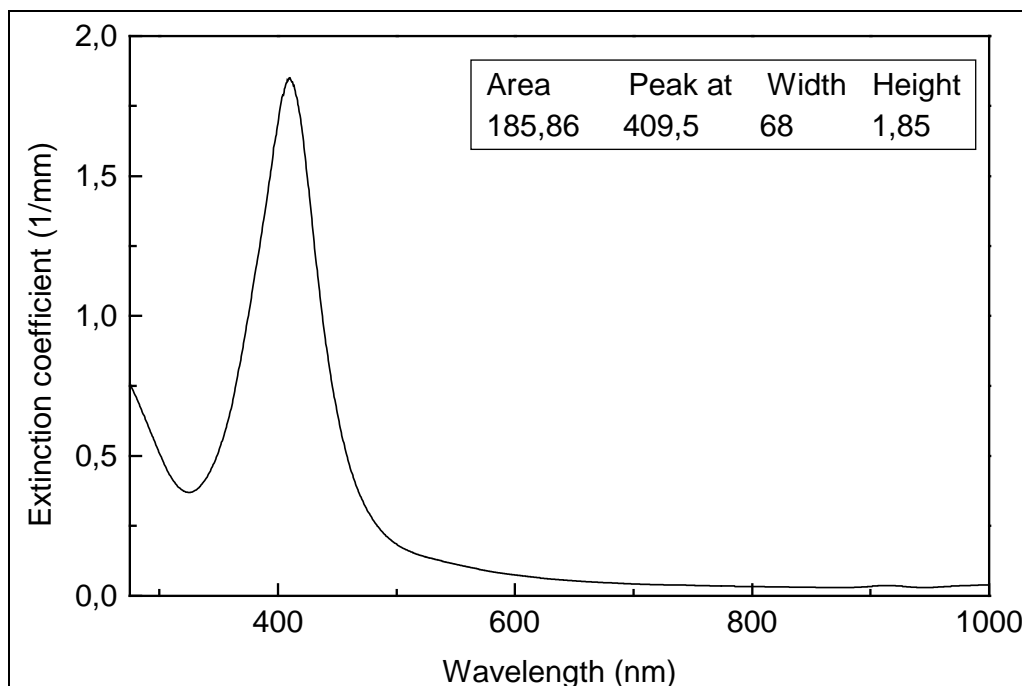


Figure 71: Extinction spectra of a sol containing silver colloids, synthesised by the reduction of Ag ions with ethanolic solution of NH_2OH , Ag : NH_2OH = 1 : 2, the sol was diluted with 20 times water and the thickness of the cuvette used was 2 mm, reference : air.

This extinction spectra was integrated from 320 nm to 1000 nm to calculate the area of the curve. As the sol is diluted 20 times with water the original area of the extinction spectra will be the 20 times of this calculated spectra i.e. $20 \times 185.86 = 3717.2$.

Now the colloidal turnover will be calculated as turnover = $\frac{f \times A}{C_{composition}}$

Using this equation, the turnover for the silver colloids comes out equal to 99.5%, indicating that almost all the ionic silver has been converted into colloidal silver.

5.2.2.1.3 Synthesis of Ag / Cu alloy colloids

In the silver sol prepared as above, copper nitrate (as a DIAMO complex) dissolved in ethanol was added. Sodalime glass substrates were dip-coated using this solution and dried in an oven at 80 °C prior to heat treatment. It is known from the previous studies that the formation of copper colloids takes place on heating the samples containing ionic copper under reducing atmospheres only [152, 153]. Hence the samples prepared as above were heat treated in an oven under reducing atmosphere ($\text{N}_2 / \text{H}_2 =$

92 / 8, 80 l/h) at the temperatures from 150 - 550 °C with the heating rate of 100 K/h, for 1 h.

The thickness of the films heat treated at 350 °C under reducing atmosphere as determined using profilometer was found to be 300 nm, which decreases to 220 nm at 450 °C. Finally, films having the thickness equal to 180 nm were obtained at 550 °C.

5.2.2.1.4 UV-VIS spectroscopic studies

In order to study the optical properties of the thin films containing Ag / Cu alloy colloids, UV-VIS spectroscopic characterisation was carried out. The experimentally observed absorption spectra of thin films containing as a function of Ag : Cu molar ratio at 450 and 550 °C are shown below in Figure 72 and Figure 73 respectively. Whereas the UV-VIS spectra of thin films having different ratios of Ag / Cu heat treated at 350 °C are shown in Figure A 45 in appendix.

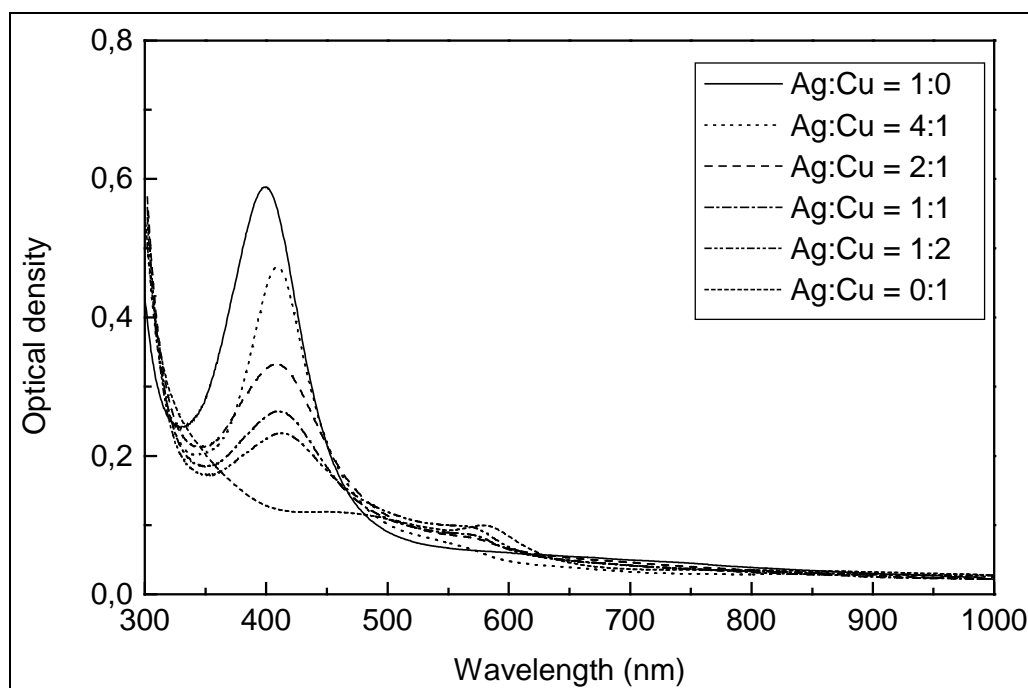


Figure 72: UV-VIS absorption spectra of thin films containing Ag / Cu alloy colloids as a function of their molar ratios for the samples heat treated at 450 °C under reducing atmosphere ($N_2 / H_2 = 92 / 8, 80$ l/h), reference: air, (experimental conditions in ch. III, p. 46).

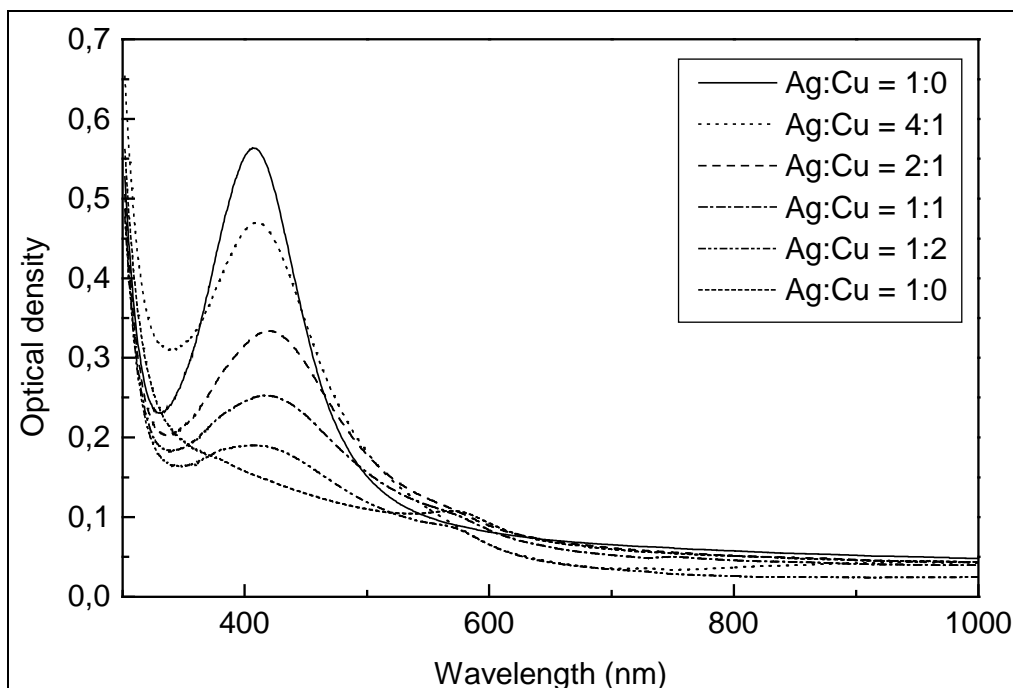


Figure 73: UV-VIS absorption spectra of thin films containing Ag / Cu alloy colloids as a function of their molar ratios for the samples heat treated at 550 °C under reducing atmosphere ($N_2 / H_2 = 92 / 8$, 80 l/h), reference: air, (experimental conditions ch. III, p. 46).

From both these figures one can see two absorption peaks for the Ag : Cu molar ratio $> 4 : 1$. For Ag : Cu molar ratios of 1 : 0 and 4 : 1, only one peak centred at 410 nm was observed which shifts slightly towards higher wavelengths for the Ag : Cu molar ratio of 4 : 1 at 450 °C. For Ag : Cu molar ratios of 2 : 1, 1 : 1 and 1 : 2, a shoulder can also be seen at the position of the colloidal copper plasmon peak which becomes stronger and appears as a clear peak with the increasing concentration of Cu. It is known from the literature that the copper and silver exhibit very limited miscibility in the bulk [154]. So the unreacted copper generates some free copper colloids on heat treating the samples at 450 to 550 °C under reducing atmosphere.

The UV-VIS spectra of thin films containing Ag / Cu alloy colloids with Ag : Cu molar ratio of 1 : 2 as function of temperature are shown below in Figure 74. Whereas the UV-VIS spectra of thin films containing Ag / Cu alloy colloids as a function of temperature for the molar ratio of Ag : Cu = 1 : 1 and 2 : 1 are given in appendix Figure A 43 and A 44.

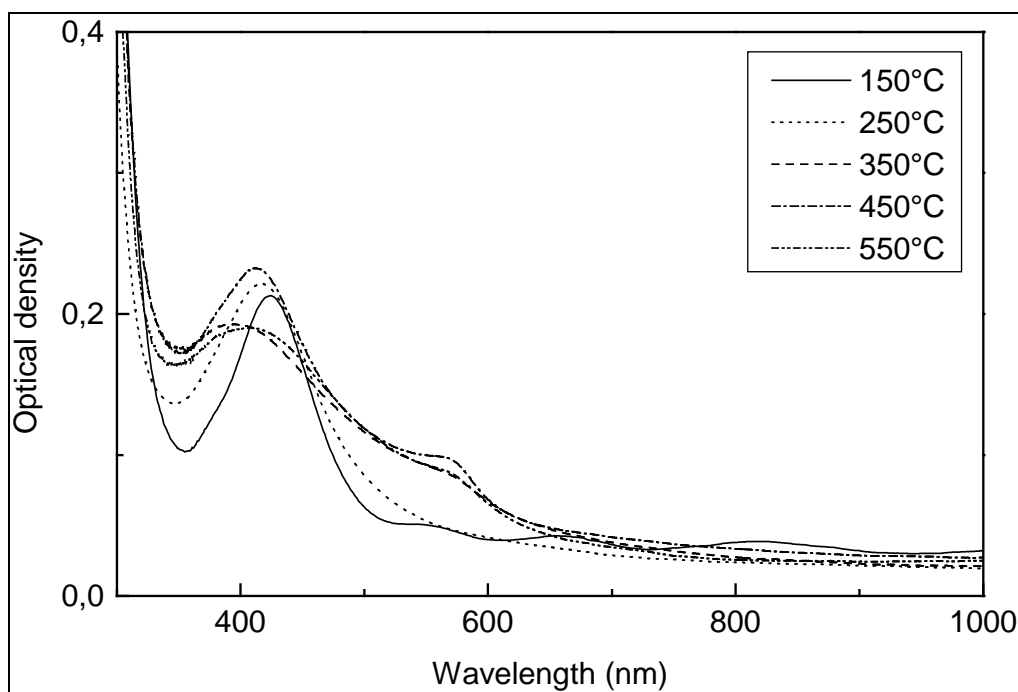


Figure 74: Absorption spectra of SiO₂ thin films containing Ag / Cu alloy colloids (with Ag : Cu = 1 : 2) as a function of temperature, heat treated under reducing atmosphere (N₂ / H₂ = 92 / 8, 80 l/h), reference : air, (experimental conditions in ch. III, p. 46).

The spectra for the sample heat treated at 150 and 250 °C, show only one peak corresponding to plasmon peak of silver, centred around 410-420 nm. Some weak signals located at 558, 660 and 815 nm are due to the Cu²⁺ oxidation states of Cu [155]. As hydroxylaminehydrochloride does not reduce Cu²⁺ into Cu in solution, till 250 °C no peak due to copper colloids was observed. Due to the lower electrode potential of copper (Cu²⁺ / Cu = + 0.35), the formation of copper colloids takes place at temperatures above 250 °C even under reducing atmosphere. For the samples heat treated at 350 °C and 450 °C two absorption peaks are clearly seen located at 410 nm and 580 nm corresponding to the plasmon peak of silver and copper respectively.

The UV-VIS spectra for Ag / Cu alloy colloids are strikingly different from those observed for Ag / Au alloy colloids. In Ag / Au alloy colloids, the absorption edge moves continuously from the absorption edge of one constituent to the other. Which has been attributed to the shift and deformation of a common d-band [99]. For Ag / Cu alloy colloids however there is no continuous modification of the spectrum.

Revory et al. [99, 156] have synthesised Cu-Ag alloy colloids and measured their dielectric constant (imaginary part). They observed two types of absorption spectra, (1)

Cu-rich alloys, for which the imaginary part of ϵ_2 is roughly Cu-like and (2) Ag-rich alloys, for which imaginary part ϵ_2 is roughly Ag like. For small Ag concentration the absorption edge was observed very steep and located at the same energy as in pure Cu (2.15 eV), when C_{Ag} increases it is broadened. This broadening was described due to disorder in these microcrystallites. Since the absorption edge in pure Cu and other noble metals, is mainly determined by transition from the top of the d-bands to the conduction band at fermi level, the upper part of the Cu partial d band must be little affected by alloying with Ag. These observations indicate that the alloying of Ag and Cu will not make any remarkable change in their corresponding absorption spectra. This can be better understood by calculating the theoretical absorption spectra for Ag / Cu alloys.

5.2.2.1.5 Calculation of theoretical absorption spectra of Ag / Cu alloy colloids

In order to get a better understanding of the absorption spectra of the colloidal Ag / Cu alloy particles, a computer simulation of the composition dependence of plasmon frequency was performed. For calculating the absorption spectra of alloy colloids, ϵ_1 (real part of dielectric constant) and ϵ_2 (imaginary part of dielectric constant) were taken to be the 'composition weighted' averages [135] of the bulk dielectric constants of Ag and Cu.

$$\epsilon_i = (1-x) \epsilon_i^{Ag} + x \epsilon_i^{Cu} \text{ for } i = 1, 2$$

To calculate the real part of dielectric constant of alloy colloids, the real part of the bulk dielectric constant of Ag and Cu was used, whereas to calculate the imaginary part, the imaginary part of the bulk dielectric constant of Ag and Cu was used. Theoretical spectra calculated in this way for Ag / Cu alloy colloids are shown below in Figure 75.

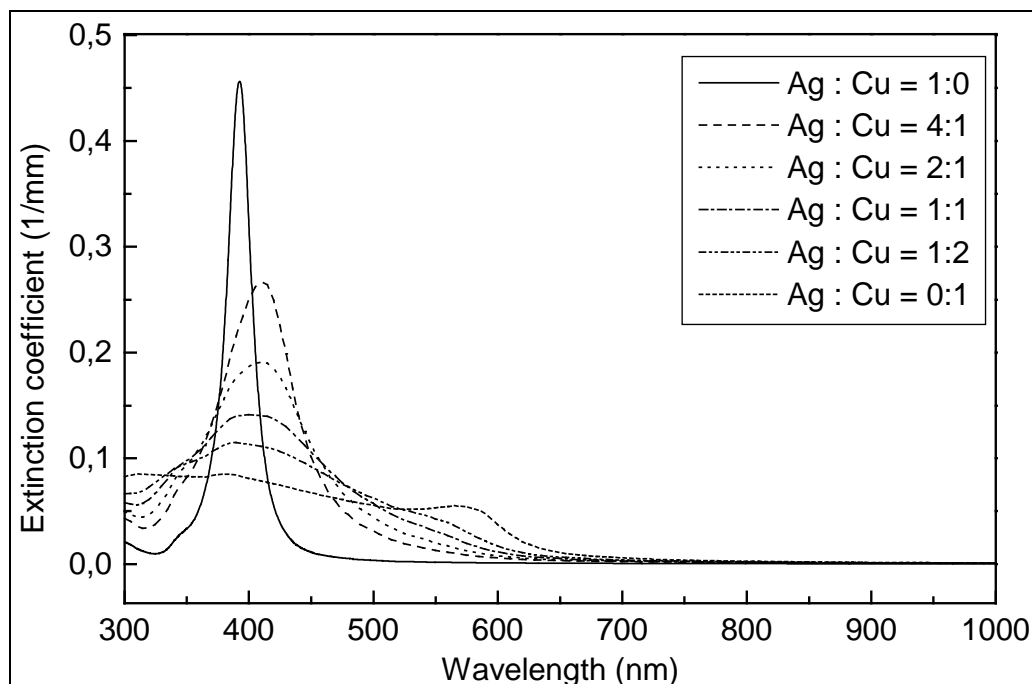


Figure 75: Theoretical extinction spectra of Ag / Cu alloy colloids as a function of their molar ratios, calculated after Mie theory using a computer programme, (particle radius = 10 nm, refractive index of the matrix = 1.46 and total volume concentration of the silver and copper is 10^{-6}).

It is clear from the above calculated spectra that for the samples with Ag : Cu = 1 : 0 only one sharp peak is visible at 393 nm, which is the plasmon peak for colloidal silver. For the samples having Ag : Cu molar ratio of 4 : 1 on the other hand a shift on the peak towards the higher wavelength was observed, and the peak was centred at 411 nm. This red shift is probably attributed to a change of the dielectric function accompanying the formation of composite particles [72]. On increasing the molar percentage of copper this plasmon peak does not shift much and another very weak shoulder like peak appears in the wavelength ranging from 560-575 nm. For the sample containing only copper one absorption peak at 575 nm was observed which is the plasmon peak for colloidal copper. A good agreement was found in between the calculated (Figure 74) and measured (Figure 71 and 72) UV-VIS spectra of SiO₂ thin films containing Ag / Cu alloy colloids.

5.2.2.1.6 HR-TEM characterisation

In order to determine the size and the composition of the particles, high resolution transmission electron microscope (HR-TEM) analysis of thin films containing silver-copper alloy colloids was carried out and their lattice images were observed. Figure 76

and Figure 77 show the Ag / Cu alloy particle size distribution in thin films and the high-resolution micrographs of a single particle of Ag / Cu alloy colloid respectively.

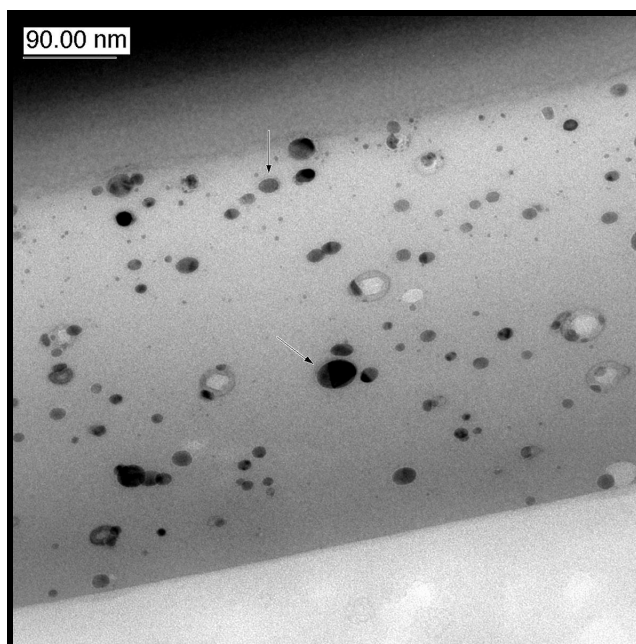


Figure 76: HR-TEM image of colloidal Ag / Cu alloy particles. The samples were densified at 450 °C under reducing atmosphere ($N_2 / H_2 = 92 / 8$) with the heating rate of 100 K/h. Molar ratio of Ag : Cu = 4 : 1 (sample preparation in ch. III, p. 46).

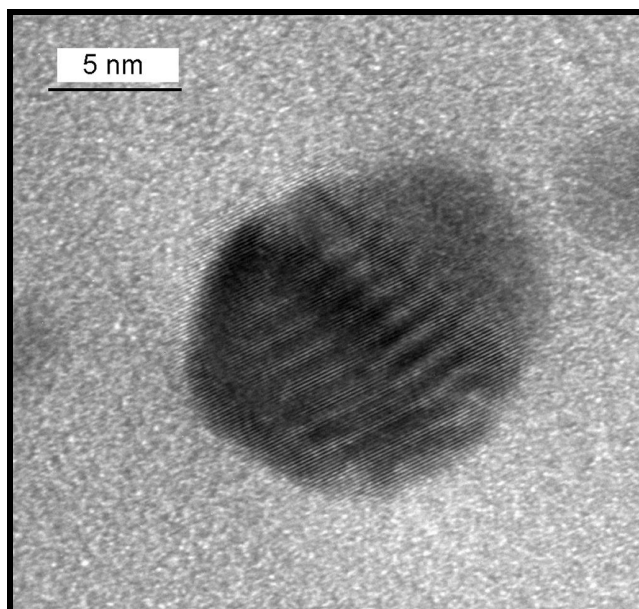


Figure 77: HR-TEM micrograph of a single particle of Ag / Cu alloy (molar ratio = 4 : 1) colloids. The samples were densified at 450 °C under reducing atmosphere ($N_2 / H_2 = 92 / 8$) for 1 h with the heating rate of 100 K/h (sample preparation in ch. III, p. 46).

Figure 76 shows a relatively broad particle size distribution with particle diameters varying from 5 - 40 nm. Figure 77 shows a single particle of Ag / Cu alloy colloid having a diameter of approximately 15 nm.

In order to see the composition of the particles formed, electron dispersive X- ray analysis (EDX) of individual particles was carried out by focusing the electron beam on the particles. EDX profiles of single colloidal Ag / Cu alloy particles is shown below in Figure 78, whereas some others are shown in appendix Figure A 46 and Figure A 47.

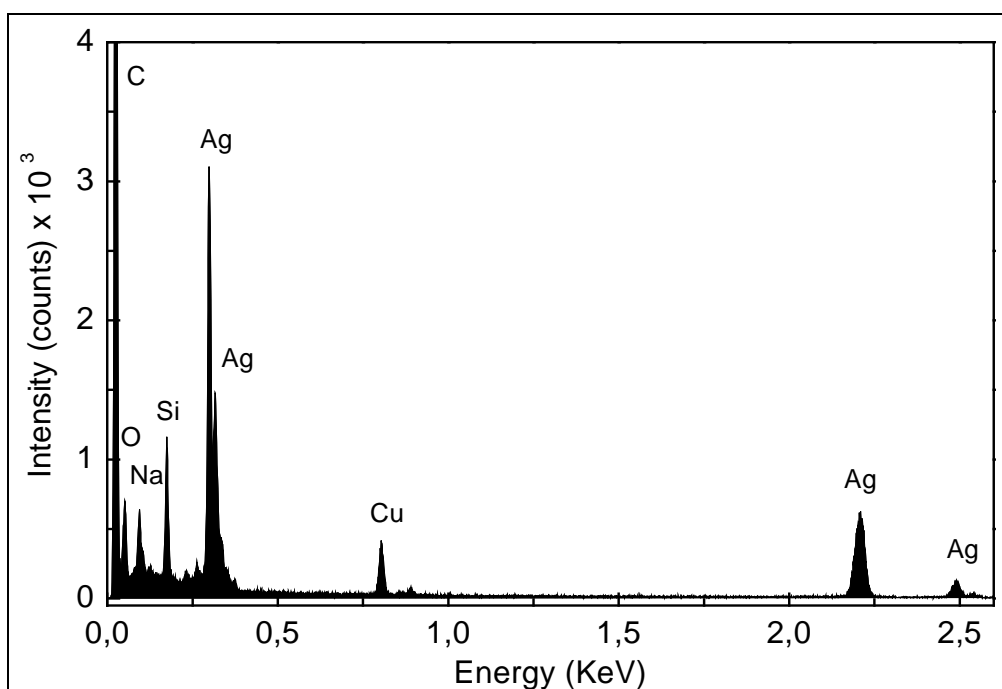


Figure 78: EDX profiles of single Ag / Cu alloy particle (molar ratio of Ag : Cu = 4 : 1).

Above figure shows the EDX profile for a Ag / Cu alloy colloidal particles having a molar ratio of Ag : Cu = 4 : 1. EDX analysis shows the atomic percentage of Ag and Cu equivalent to 83.4% and 16.6% respectively, which is in agreement to the expected values. EDX profiles of some other particles show Ag and Cu equal to 5% and 95% and 95% and 5% (Figure A 46 and Figure A 47). These measurements showed that in some cases the bimetallic particles are either copper rich or silver rich in their composition. This behaviour can be attributed to the limited solubility of silver and copper in the bulk.

5.2.2.1.7 X-ray diffraction characterisation

In order to see the crystalline behaviour of the colloidal Ag / Cu alloy particles and to estimate the crystal size using Scherrer's formula, X-ray diffraction measurements of the thin films containing Ag / Cu alloy colloids were carried out. XRD patterns of thin films heat treated at 450 °C under reducing atmosphere as a function of their molar ratios are given below in Figure 79.

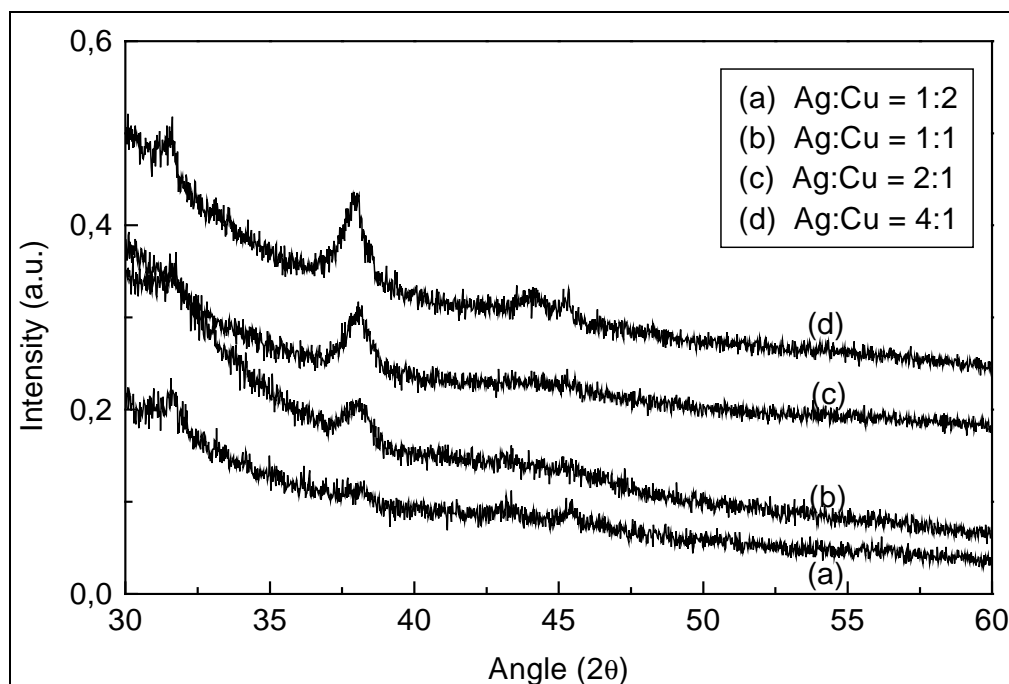


Figure 79: X-ray diffraction patterns of SiO₂ thin films containing Ag / Cu alloy colloids as a function of their molar ratios (experimental conditions in ch. III, p. 46).

The XRD patterns above show three peaks positioned at 2θ equal to 31.7°, 38.0° and 45.48°. These XRD patterns neither match with the literature reported values of silver only nor with copper only. Hence the appearance of these peaks can be attributed to the formation of alloy colloids in thin films. From the recorded XRD patterns, the particle size was calculated using Scherrer's equation. Calculated diameters of the particles as a function of the molar ratio of Ag and Cu are given below in Table 22.

Table 22: Angle 2θ , corrected half width (β) corresponding to most intense peak and particle diameter 'd' after the Scherrer's formula for Ag / Cu alloy colloids.

Ag:Cu	2θ (°)	β (°)	'd' (nm)
4 : 1	37.876	0.894	12.9
2 : 1	38.013	0.948	12.0
1 : 1	37.901	1.449	7.1
1 : 2	38.171	0.732	16.9

Particle size calculated as above using Scherrer's equation is in agreement to the particle size calculated using HR-TEM analysis in *section 5.2.2.1.5*.

5.2.2.2 *Mixed colloids*

To synthesise Ag / Cu mixed colloids, silver nitrate was chosen as silver precursor and copper nitrate as copper precursor. Silver nitrate was dissolved in methanol, DIAMO (Ag : DIAMO = 1 : 2) was used as a complexing agent for silver and GPTS / TEOS sol was added to it. At the same time copper was dissolved in ethanol separately and DIAMO (Cu : DIAMO = 1 : 1) was used as a complexing agent for copper and GPTS / TEOS sol was added. Silver containing sol was added dropwise to copper containing sol. The experimental details for the synthesis of thin films containing different molar ratios of Ag and Cu are given in chapter III, page 48. Glass substrates were dip coated and heat treated under reducing atmosphere in order to get thin films.

The film thickness was measured using a profilometer. For the thin films synthesised as above and heated at 350 °C the thickness was measured to be 280 nm, which reduces to 220 nm at 450 °C and finally to 175 nm at 550 °C. Nanocomposite thin film synthesised as above were characterised by UV-VIS absorption spectroscopy.

5.2.2.2.1 **UV-VIS spectroscopic studies**

The UV-VIS absorption spectra of thin films containing Ag / Cu mixed colloids heated at 450 °C & 550 °C as a function of their molar ratios, are given below in Figure 80 and Figure 81 respectively. Whereas the UV-VIS spectra of thin films heated at 350 °C, as a function of their molar ratios are given in Figure A 48 in appendix.

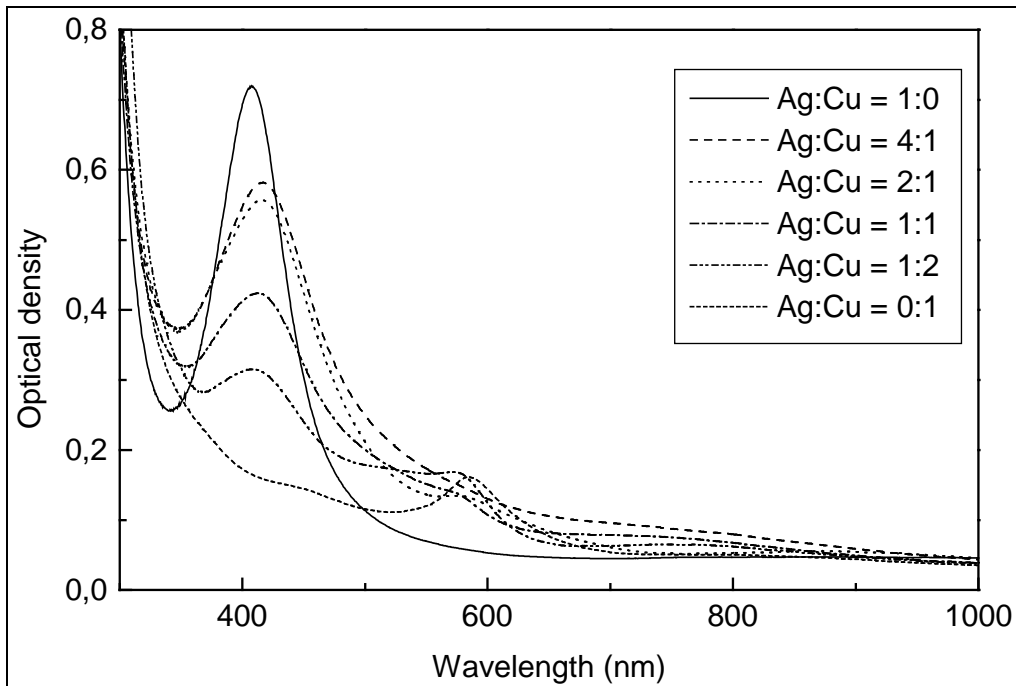


Figure 80: UV-VIS absorption spectra of SiO₂ thin films containing Ag / Cu mixed colloids as a function of their molar ratios, heat treated at 450 °C under reducing atmosphere (N₂ / H₂ = 92 / 8, 80 l/h), reference air.

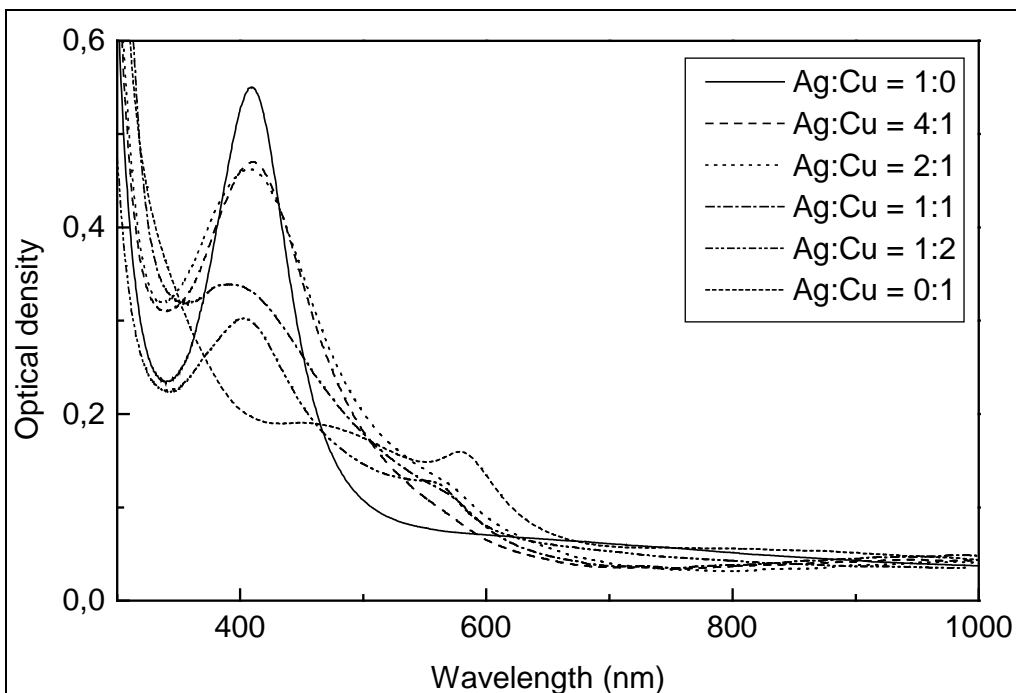


Figure 81: UV-VIS absorption spectra of SiO₂ thin films containing Ag / Cu mixed colloids as function of their molar ratios, heat treated at 550 °C under reducing atmosphere (N₂ / H₂ = 92 / 8, 80 l/h), reference air, (experimental details are in ch. III, p. 48).

It is clearly visible from the above figure that for Ag / Cu mixed colloids heat treated at 450 °C, two peaks were obtained. One due to silver, which is centred around 392 to 409 nm and other due to copper centred around 570 to 579 nm. Whereas at 550 °C silver peak shifts to around 405 - 417 nm and the copper peak to 578 - 587 nm. But both these figures follow a general trend of shifting the plasmon peak due to silver and copper towards the lower wavelength side on decreasing their molar ratios. For example silver peak for Ag : Cu ratio of 4 : 1 is centred at 417 nm and shifts to 405 nm on changing the Ag : Cu ratio to 1 : 2 at 450 °C. At 550 °C the peaks position shift from 409 to 392 nm for the same molar ratios. In the same manner the peak due to copper also shifts from 587 to 570 nm on changing the molar ratio Ag : Cu from 4 : 1 to 2 : 1.

Itakura et al. [72] have synthesised some Ag / Cu mixed colloids having different ratios of Ag : Cu in ethanol. They observed that on increasing the molar ratio of copper, the absorption peak at 400 nm became broader and slightly shifted to longer wavelength. They explained this behaviour on the basis of the electrical interaction taking place between silver and copper. This interaction takes place only when the particles are very close to each other. In present study the behaviour of the shifting of the Ag plasmon peak around 410 nm is reverse to that observed by Itakura et al. This reverse behaviour can be explained by decrease in particle size with decreasing the concentration of silver and copper, which is same as observed by De et al. [157].

5.2.2.2 Calculation of absorption spectra of Ag / Cu mixed colloids

To understand the optical behaviour of the phase separated mixed colloid of Ag and Cu, a semi-quantitative computer simulation of the composition dependence of plasmon frequency using Mie theory was performed. The absorption spectra were calculated for copper and silver for particles with radii 10 nm and the refractive index of the medium 1.46. As the particles are phase separated, we assume that they will not affect the plasmon absorption of each other and their optical absorption spectra will be the simple physical addition of the spectrum of silver and copper. The following Figure 82 shows the calculated absorption spectra of thin films containing different proportions of Ag and Cu.

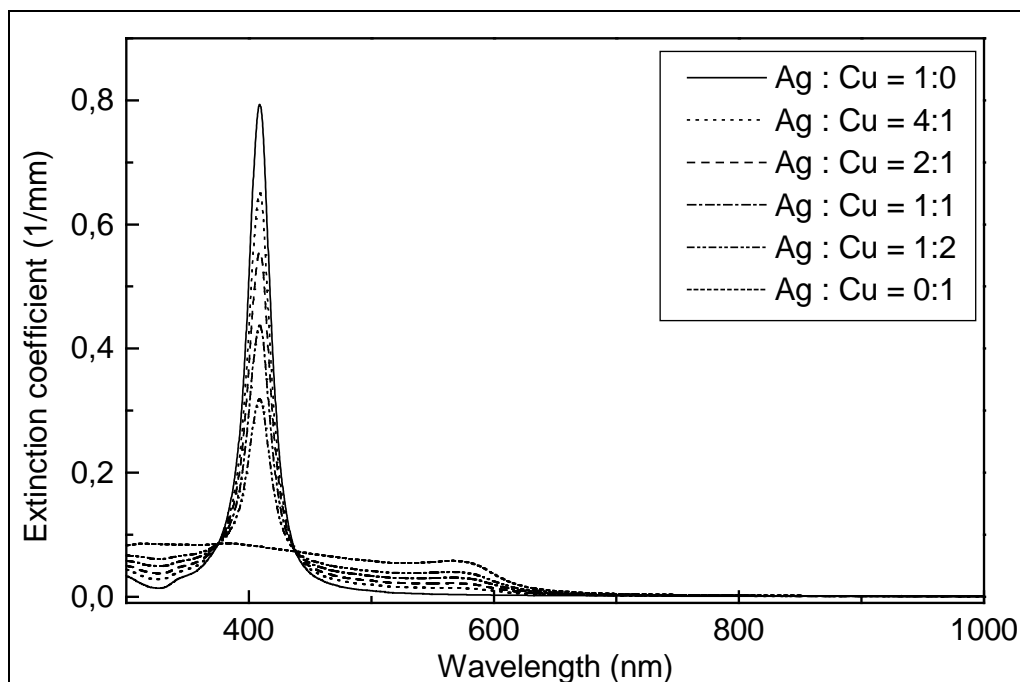


Figure 82: Theoretical UV-VIS absorption spectra of thin films containing Ag / Cu mixed colloids as a function of their molar ratios calculated after Mie theory for particle radii of 10 nm.

Calculated absorption spectra shown in above figure always show two peaks corresponding to Ag and Cu plasmon peaks, except for pure Ag and pure Cu. The intensity of the peaks is directly proportional to the concentration of Ag and Cu. Measured absorption spectra shown above in Figure 80 and Figure 81 for the thin films containing Ag / Cu bimetallic colloids as a function of their molar ratios are in good agreement to the calculated absorption spectra for the Ag / Cu mixed colloids. This observation supports the formation of Ag / Cu mixed colloids in thin films.

The UV-VIS spectra of thin films containing Ag / Cu mixed colloids (Ag : Cu = 1 : 2) as a function of densification temperature are shown below in Figure 83. The spectra for the molar ratio of Ag : Cu = 2 : 1 and 1 : 1 are given in the appendix, Figure A 49 and Figure A 50.

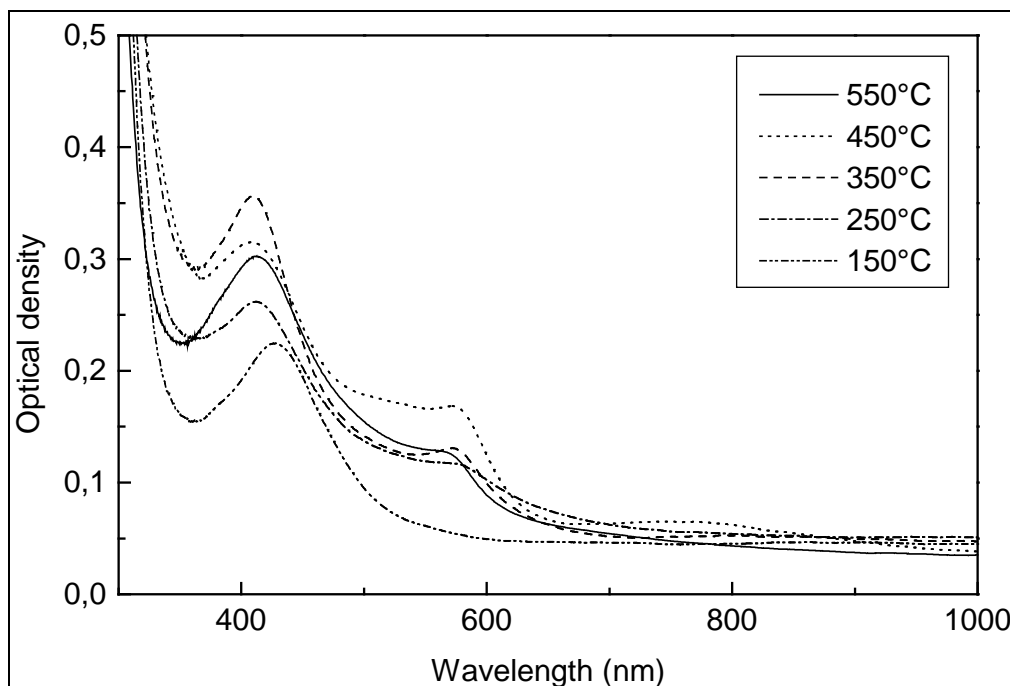
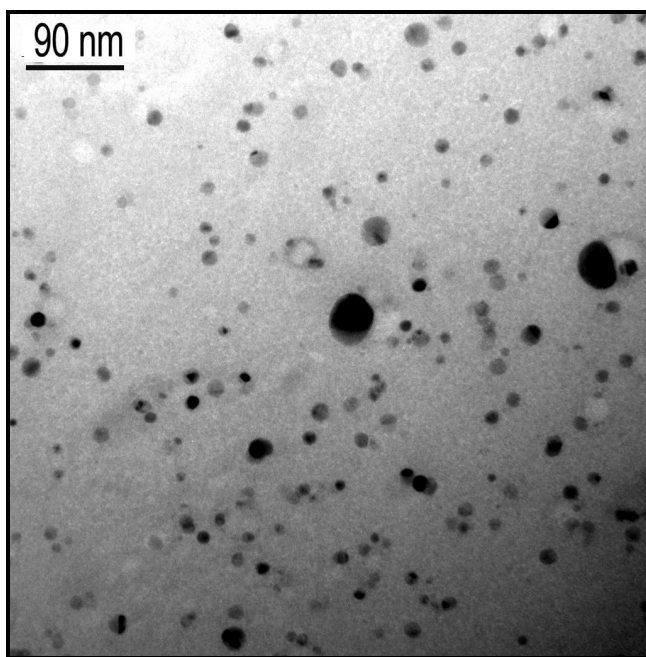


Figure 83: UV-VIS absorption spectra of SiO₂ thin films containing Ag / Cu mixed colloids (Ag : Cu = 1 : 2) as a function of temperature, heat treated under reducing atmosphere (N₂ / H₂ = 92 / 8, 80 l/h), reference : air.

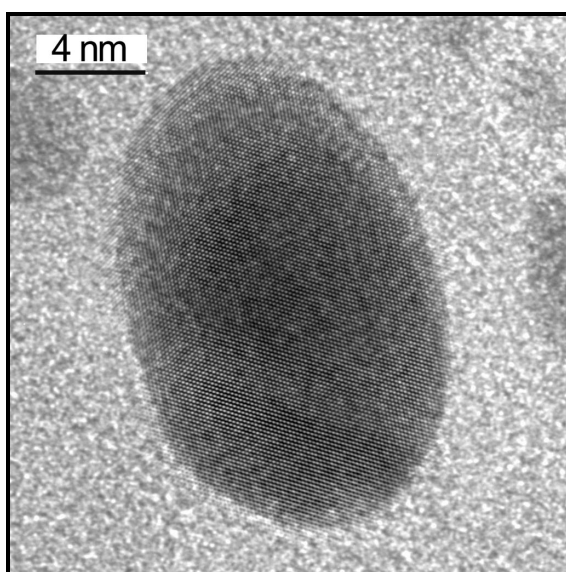
The above figure shows the presence of only one peak at 426 nm, which is the plasmon peak of Ag, on heating the sample at 150 °C. Heating the sample at 250 °C results one more weak peak at 583 nm, which the plasmon peak position of Cu. On heating the samples at 350 °C the plasmon peak intensity due to gold and silver increases, which starts decreasing at 450 °C and 550 °C. This decrease in peak intensities may be attributed to decrease in film thickness at the higher temperatures.

5.2.2.2.3 HR-TEM characterisation

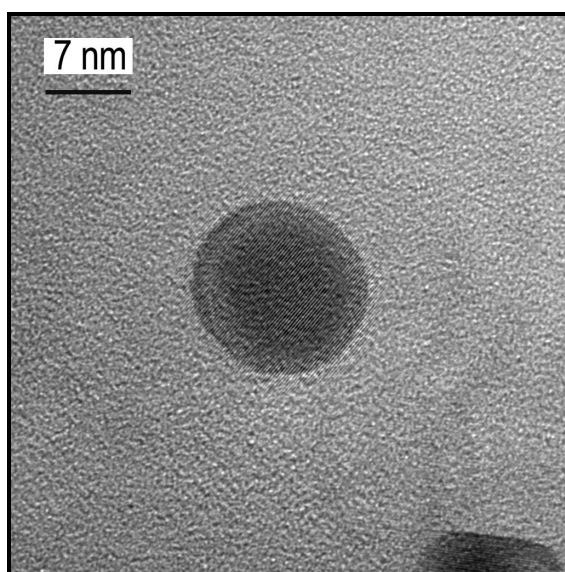
In order to determine the size and shapes of the Ag / Cu mixed colloids formed in thin films, high resolution transmission electron microscopic (HR-TEM) studies were carried out. Whereas, to see the composition of the particles formed, EDX spectra of the different particles were recorded by focussing an electron beam on the single particles. HR-TEM micrograph of Ag / Cu (Ag : Cu = 1 : 2) mixed colloids dispersed in a glass matrix is shown below in Figure 84(a). The high resolution micrograph of two particles selected from the same sample are shown below in Figure 84(b) and (c).



(a)



(b)

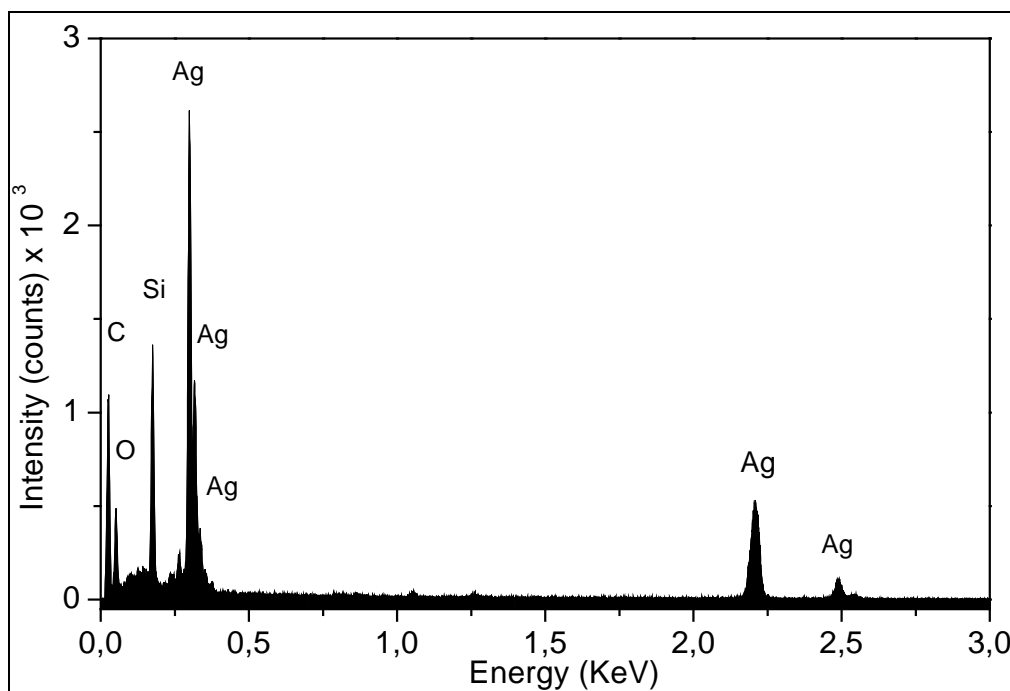


(c)

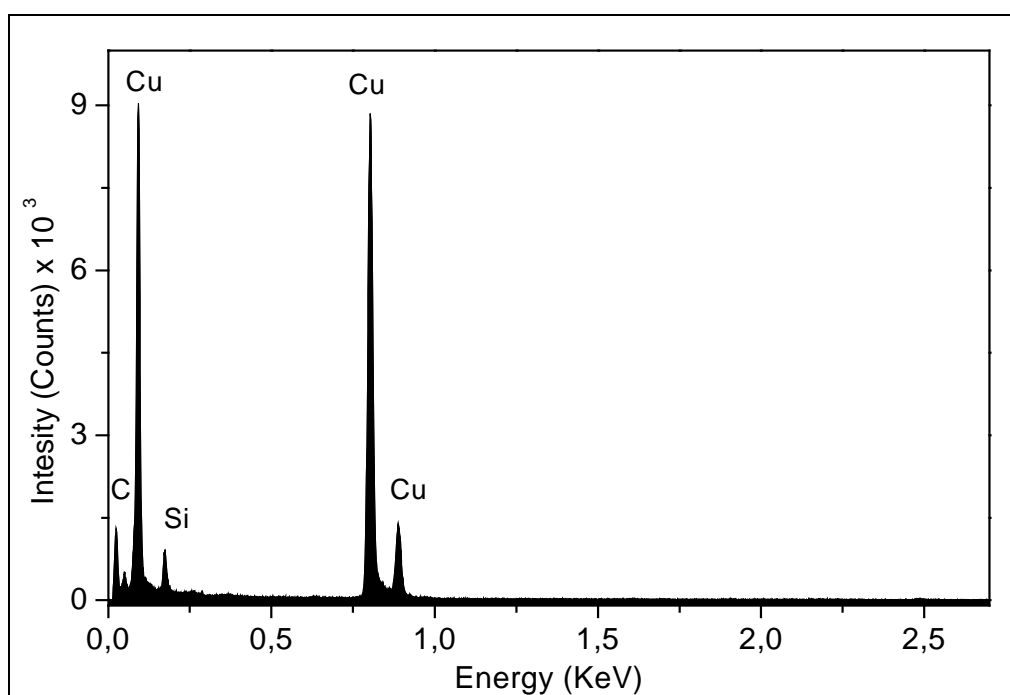
Figure 84: (a) HR-TEM micrograph of Ag / Au mixed colloidal particles dispersed in SiO₂ matrix (b) and (c) HR-TEM micrographs of two different particles selected from the same sample.

Figure 84(a) shows that except a few very big particles, most particles have a diameter ranging from 8 to 20 nm. The average based on 50 particles selected on an area was 15 nm. In order to see if the particles formed in thin film are the phase separated particles of Ag and Cu or not, two particles shown above in Figure 84(b) and (c) were

selected randomly, and their EDX spectra were recorded. The EDX profiles of these two particles are shown below in Figure 85 (a) and (b) respectively.



(a)



(b)

Figure 85: (a) and (b) EDX profiles of two particle shown above in Figure 84(b) and (c) respectively.

From the recorded EDX spectra in Figure 85(a) it can clearly be seen that it does not show any peak due to copper, hence it can be said that this particle is composed of silver only. On the other hand the EDX profiles of the other particle shown in Figure 85 (b) do not show any peak due to silver, but only copper peak is present, indicating that this particle is composed of copper only. Some other additional signals due to Si, O and C in both the spectra are from the SiO₂ matrix and the carbon film used for the sample preparation. These EDX studies prove that the thin film contains the phase-separated particles of copper and silver only.

5.2.2.2.4 X-ray diffraction characterisation

In order to see the crystalline behaviour of the particles of Ag / Cu mixed colloids, X-ray diffraction measurements of the thin films densified at 450 °C under reducing atmosphere were carried out. Scherrer's formula was applied in order to determine the particle size. XRD patterns of thin films as a function of the molar ratio of Ag and Cu are shown below in Figure 86.

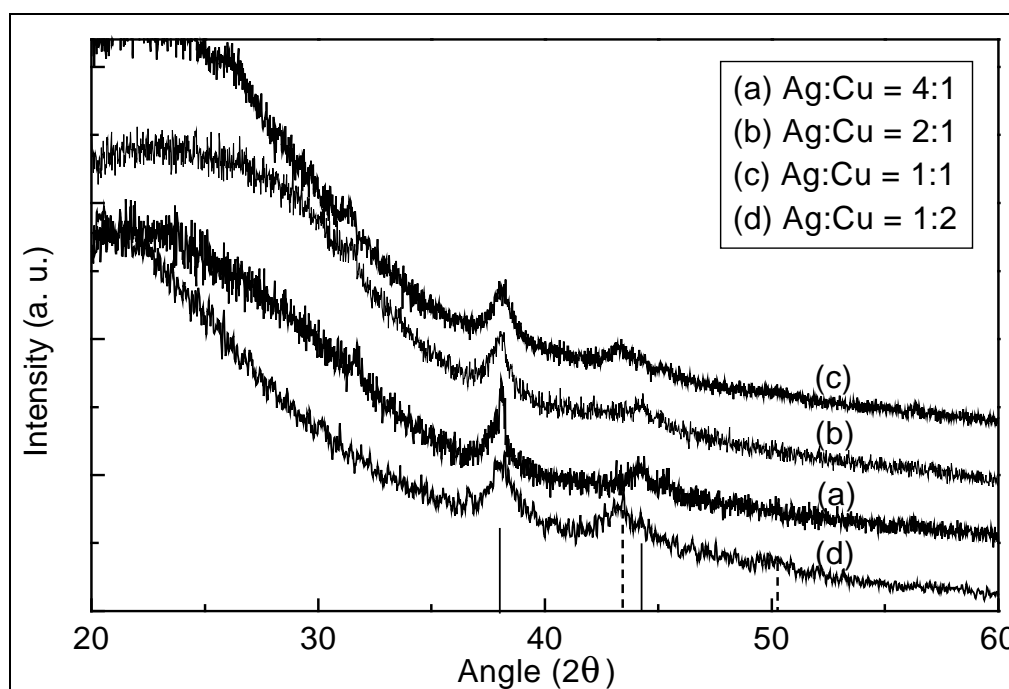


Figure 86: XRD patterns of the SiO₂ thin films containing Ag / Cu mixed colloids heat treated at 450 °C under reducing atmosphere, as a function of their molar ratios. Solid bars in the figure show the literature reported (powder diffraction file no. 4-783 and 4-836) peak positions of Ag and dashed bars show those of Cu.

If the thin films contain phase separated particles of Ag and Cu the XRD patterns should be a simple addition of the XRD patterns of Ag and Cu. From the recorded XRD patterns shown above it is clear that for the sample having Ag : Cu = 4 : 1, two peaks corresponding to the (111) and (200) reflexes of Ag were obtained. The recorded XRD pattern is same for the molar ratio of Ag : Cu = 2 : 1. Whereas increasing the molar ratio to Ag : Cu = 1 : 1 an additional peak corresponding to the (111) reflex of copper at $2\theta = 43.30^\circ$ is also observed. For the samples containing Ag and Cu in a molar ratio of 1:2, all the reflexes corresponding to (111) and (200) of Ag and Cu are obtained. Appearance of the reflexes of Ag and Cu both also supports the presence of phase separated mixed colloids of Ag and Cu in these films.

Using the most intense reflex in XRD pattern of Ag / Cu mixed colloids the particle size was determined using Scherrer's formula. Calculated particle diameters have been listed in following Table 23 as a function of the molar ratio of Ag and Cu.

Table 23: Angle 2θ , corrected half width (β), corresponding to (111) reflex of Ag and Cu and particles diameter 'd' after the Scherrer's formula for Ag / Cu mixed colloids.

Ag : Cu	for Ag colloids			for Cu colloids		
	2θ (°)	β (°)	'd' (nm)	2θ (°)	β (°)	'd' (nm)
4 : 1	37.930	0.605	22.2	n.c.	n.c.	n.c.
2 : 1	37.700	1.504	6.8	n.c.	n.c.	n.c.
1 : 1	37.968	1.454	7.1	43.238	0.984	11.6
1 : 2	38.022	0.964	11.7	43.311	0.938	12.3

The crystallites size calculated as above is in good agreement to the particles size measured using HR-TEM analysis.

5.2.2.3 Summary and Conclusions

Synthesis of nanocomposite thin films containing alloy- and mixed- colloids of gold and copper by sol-gel route has been done successfully. Structural and chemical analysis of Ag-Cu alloy and mixed nanoclusters in a silica matrix was performed by means of UV-VIS spectroscopy, HR-TEM and EDX.

The theoretical absorption spectra for the Ag / Cu alloy- and mixed- colloids were also calculated using Mie theory. A good agreement was found in between theoretical and measured absorption spectra of alloy- and mixed- colloids.

Opposite to Ag / Au alloy colloids, UV-VIS spectra of Ag / Cu alloy colloids showed two plasmon peaks for the molar ratio of Ag : Cu > 4 : 1, corresponding to Ag and Cu plasmon resonance. This was due to the limited miscibility of silver and copper in bulk. Opposite to the bimetallic colloids of Ag / Au, it is not possible for the bimetallic colloids of Ag / Cu to differentiate in between phase separated mixed colloids and alloy colloids, only on the basis of their UV-VIS spectra measurements.

VI CONCLUDING REMARKS

Sol-gel process has successfully been applied for the synthesis of nanocomposite thin films containing $\text{CuCl}_x\text{Br}_{1-x}$ ($x = 1-0$) nanocrystals and bimetallic colloids of noble metals. In the first part of this work, it has been studied that copper could be stabilised as Cu^+ as acid soluble halocuprate complex in solution, in the presence of acetonitrile. These complexes decompose during heat treatment and form copper halide nanoparticles. UV-VIS spectroscopy confirmed the formation of acid soluble halocuprate complexes like CuX_2^- and CuX_3^{2-} ($X = \text{Cl}, \text{Br}$) and their decomposition during the heat treatment to CuCl and CuBr . The presence of high intensity $Z_{1,2}$ and Z_3 exciton peaks in UV-VIS spectra confirmed the formation of Cu halide nanocrystals.

The nanocomposite thin films containing CuCl , CuBr and $\text{CuCl}_x\text{Br}_{1-x}$ were characterised with the help of X-ray diffraction measurements. For nanocomposites containing copper chloride heat treated at 150°C in a UV-IR beltron machine (at 1200 W), particles with average diameter of 11 nm were formed, and their lattice constant was determined to be 5.42 \AA . For copper bromide the particles with the average diameter of 14 nm were formed under the same conditions and the lattice constant was determined to be 5.68 \AA . Cubic, gamma- and nantokite- phases were observed for (CuBr) and (CuCl) nanoparticles respectively.

In order to synthesise $\text{CuCl}_x\text{Br}_{1-x}$ nanoparticles in thin films, chloride ions were stepwise substituted by bromide ions. It was observed that the addition of HBr shifted the peak towards the higher wavelength and characteristic peaks corresponding to $\text{CuCl}_x\text{Br}_{1-x}$ ($0 < x < 1$) were observed. Subsequent addition of HBr finally produced the peaks corresponding to CuBr indicating the complete substitution of chloride by bromide ions.

The absorption edge was observed to be shifted from 371 nm (for pure CuCl) to 411 nm (for pure CuBr) for $\text{CuCl}_x\text{Br}_{1-x}$ nanoparticles. These experiments confirmed that the position of the absorption edge can favourably be shifted by the substitution of chloride ions by bromide ions. It was observed that the copper halide films are very sensitive to oxygen and copper oxidises from Cu^+ to Cu^{+2} on standing in air. Therefore further research has to be conducted in order to find an impervious matrix, which prohibits the reduction of cuprous to cupric ions, thus opening the fields of applications like UV-VIS filters with sharp edge and non-linear optics.

In the second part a new sol-gel route for the synthesis of nanocomposite thin films containing alloy- and mixed- colloids of silver / gold and silver / copper has been developed successfully. In this work the particles formed by the solid solutions of Ag / Au or Ag / Cu are termed as Ag / Au- or Ag / Cu- '*alloy colloids*' respectively. The particles formed by the mixing of phase separated individual particles of Ag / Au or Ag / Cu are termed as Ag / Au- or Ag / Cu- '*mixed colloids*' respectively. UV-VIS spectroscopy, HR-TEM and EDX studies were performed for the structural and chemical analysis of alloy- and mixed- nanoclusters in a silica matrix.

For Ag-Au alloy colloids only one absorption peak was observed in their UV-VIS spectra, the position of which shifts continuously from the absorption maxima of silver (410 nm) to the absorption maxima of gold (530 nm) on increasing the molar ratio of gold. This allows the tuning of the absorption band (and hence the colour) using glass like films containing nanosized metal alloy colloids. The absorption spectra of Ag / Au mixed colloids on the other hand show two peaks corresponding to the plasmon peak of gold and silver. These observations showed that UV-VIS spectroscopy can be used as a very good tool to differentiate between alloy- and phase separated mixed- colloids of gold and silver.

For the synthesis of gold and silver mixed colloids, the formation of silver colloids was found strongly dependent to the surface of the float glass. On the tin rich surface, formation of both gold and silver colloids took place whereas on the tin poor surface, only the formation of gold colloids was observed. This dependence of the formation of silver colloids was attributed to the presence of tin as a Sn^{4+} state which changes into Sn^{2+} during heat treatment converting the Ag^+ into silver colloids.

Opposite to Ag / Au alloy colloids, UV-VIS spectra of Ag / Cu alloy colloids showed two plasmon peaks for the molar ratio of Ag : Cu > 4 : 1, corresponding to Ag and Cu plasmon resonance. This was due to the limited miscibility of silver and copper in bulk. Opposite to the bimetallic colloids of Ag / Au, it is not possible for the bimetallic colloids of Ag / Cu to differentiate in between phase separated mixed colloids and alloy colloids, only on the basis of their UV-VIS spectra measurements.

The theoretical absorption spectra for the alloy- and mixed- colloids of Ag / Au and Ag / Cu were also calculated using Mie theory and using an equation given by Baba et al. [97]. A good agreement was found between theoretical and measured absorption spectra of alloy- and mixed- colloids of Ag / Au and Ag / Cu.

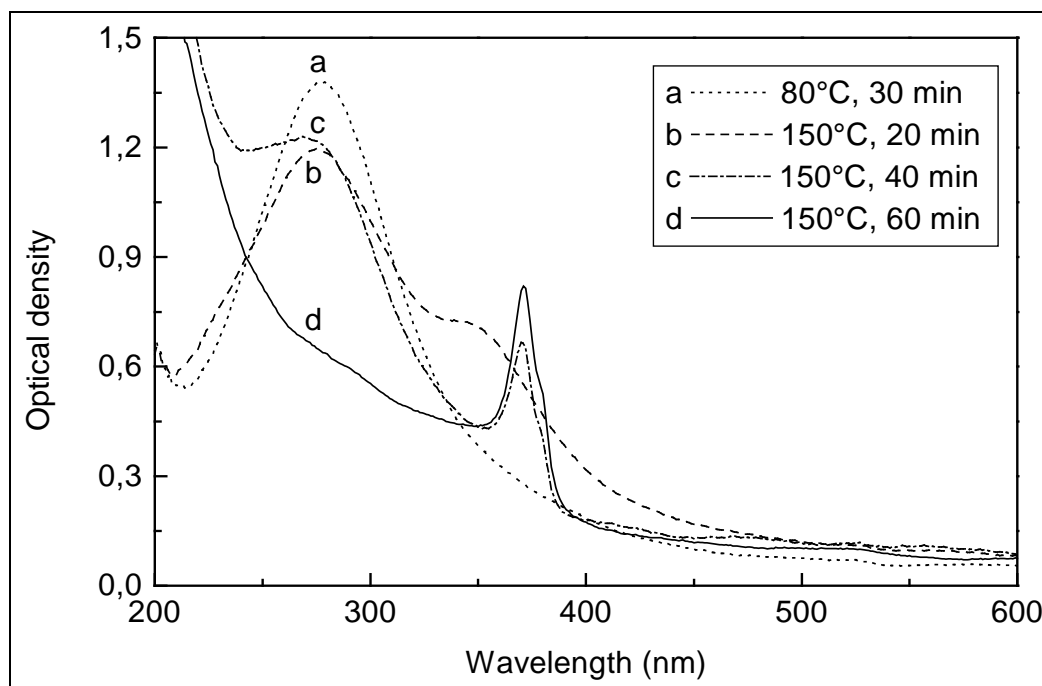
VII APPENDIX

Figure A 1: UV-VIS absorption spectra of thin films containing CuCl nanoparticles as a function of heat treatment conditions, (a) dried in an oven at 60°C, heated in an oven at 150 °C for (b) 20 min (c) 40 min (d) 60 min.

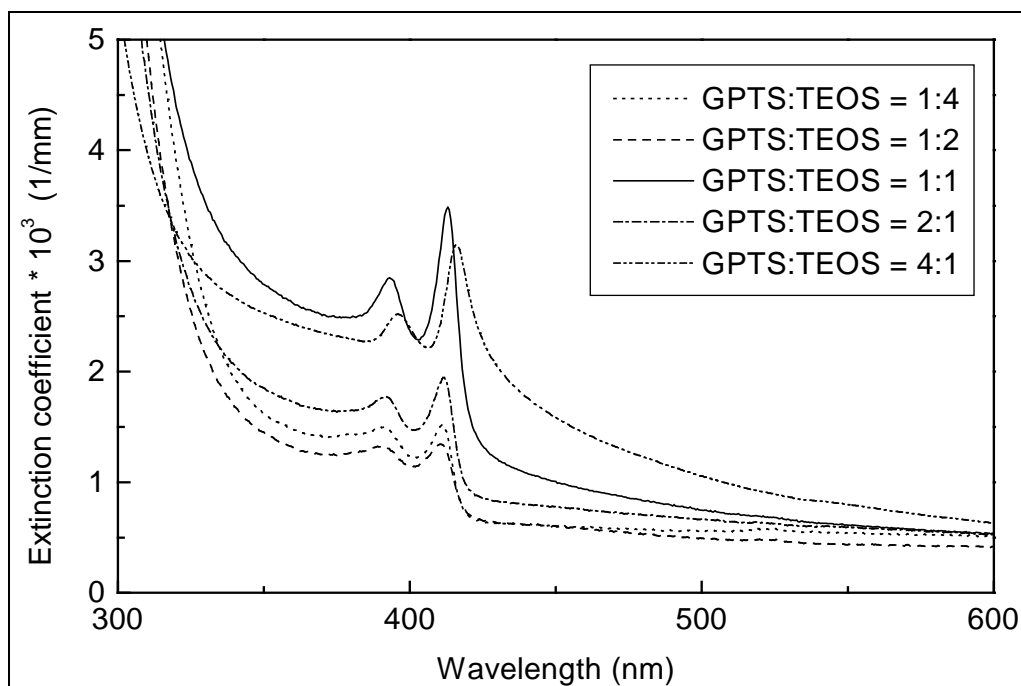


Figure A 2: UV-VIS absorption spectra of CuBr nanocomposite films synthesised using different GPTS / TEOS ratios. (Films were densified at 150 °C / 4 min in UV-IR beltron machine) reference: air.

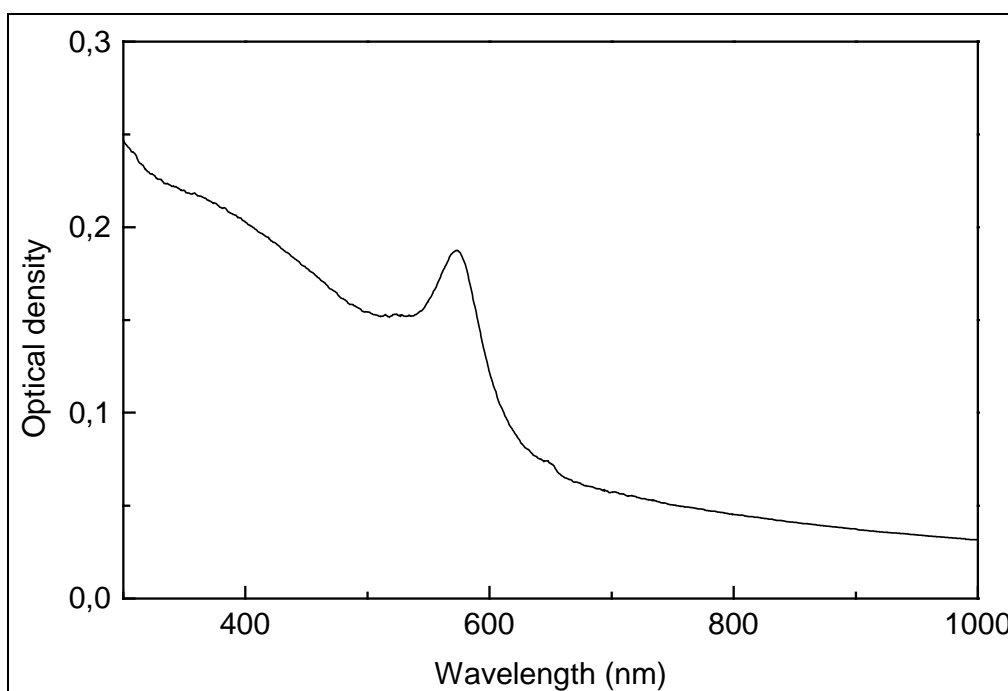


Figure A 3: UV-VIS spectra of thin film containing CuCl nanoparticles heat treated under reducing atmosphere at 450 °C ($N_2 / H_2 = 92 / 8$, 80 l/h) after heat treatment in air for 3 h at 250 °C; reference: air.

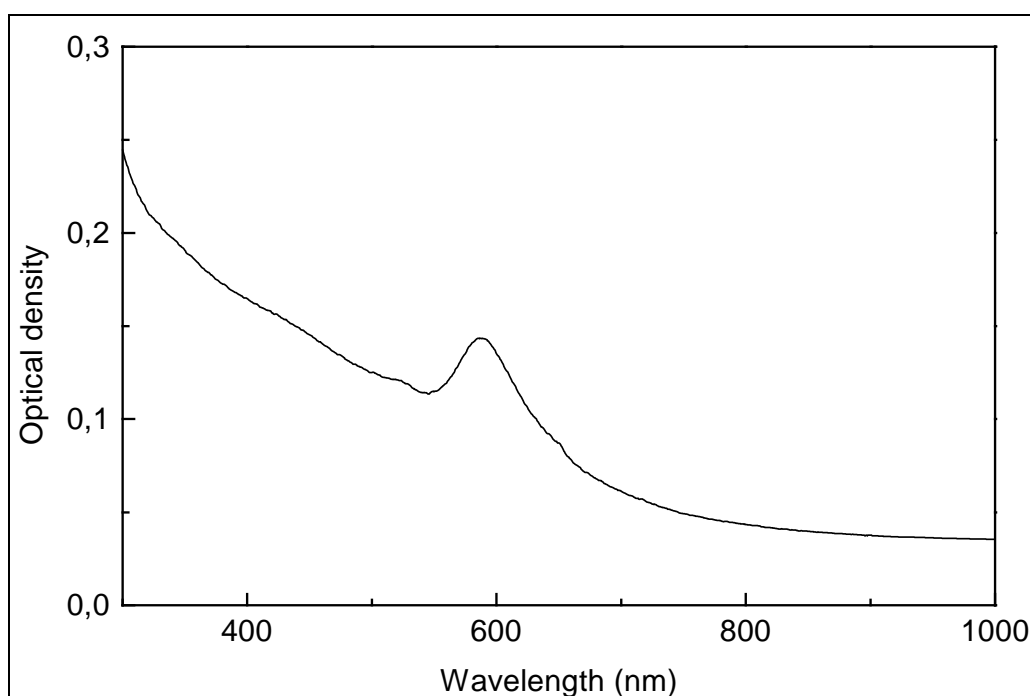


Figure A 4: UV-VIS spectra of thin film containing CuBr nanoparticles heat treated under reducing atmosphere at 450 °C ($N_2 / H_2 = 92 / 8$, 80 l/h) after heat treatment in air for 3 h at 250 °C; reference: air.

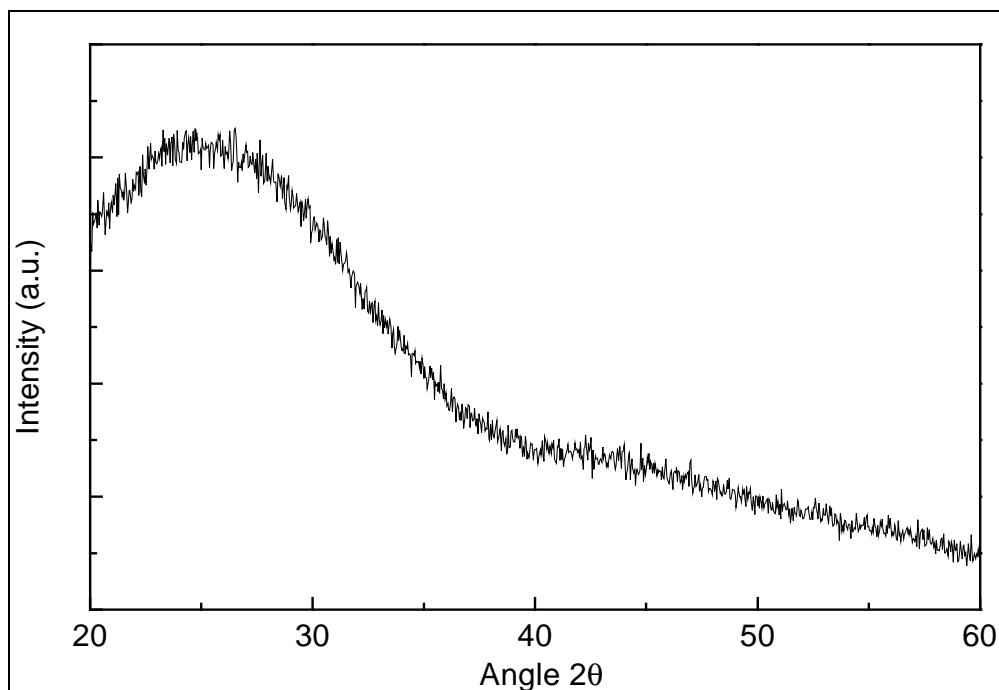


Figure A 5: X-ray diffraction pattern of thin film containing CuCl after heat treatment in air at 250 °C for 3 h.

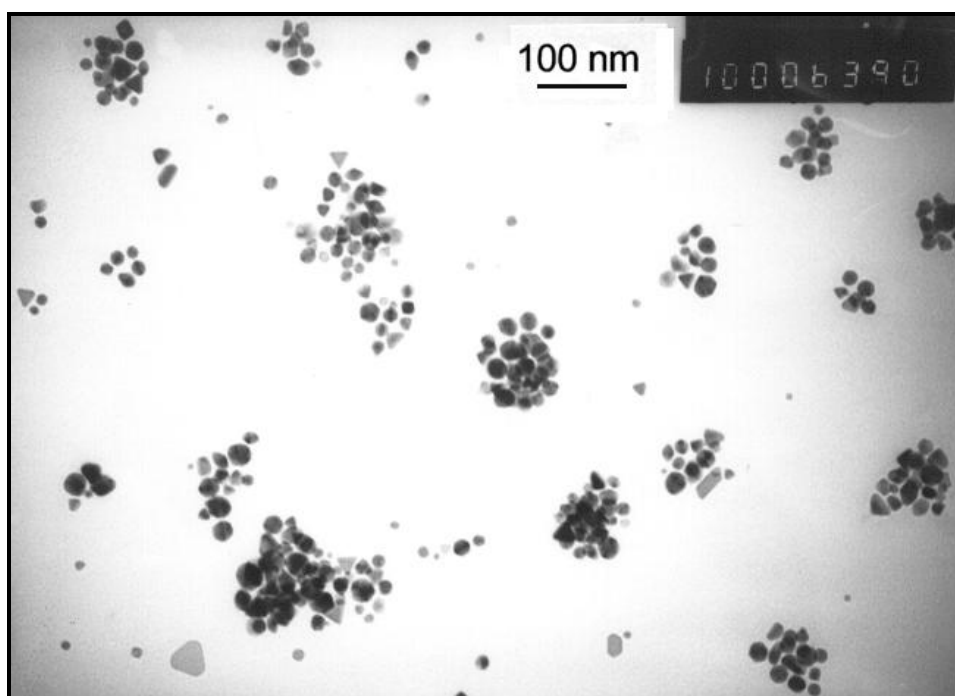


Figure A 6: TEM micrograph of colloidal gold particles in solution after 10000 times magnification.

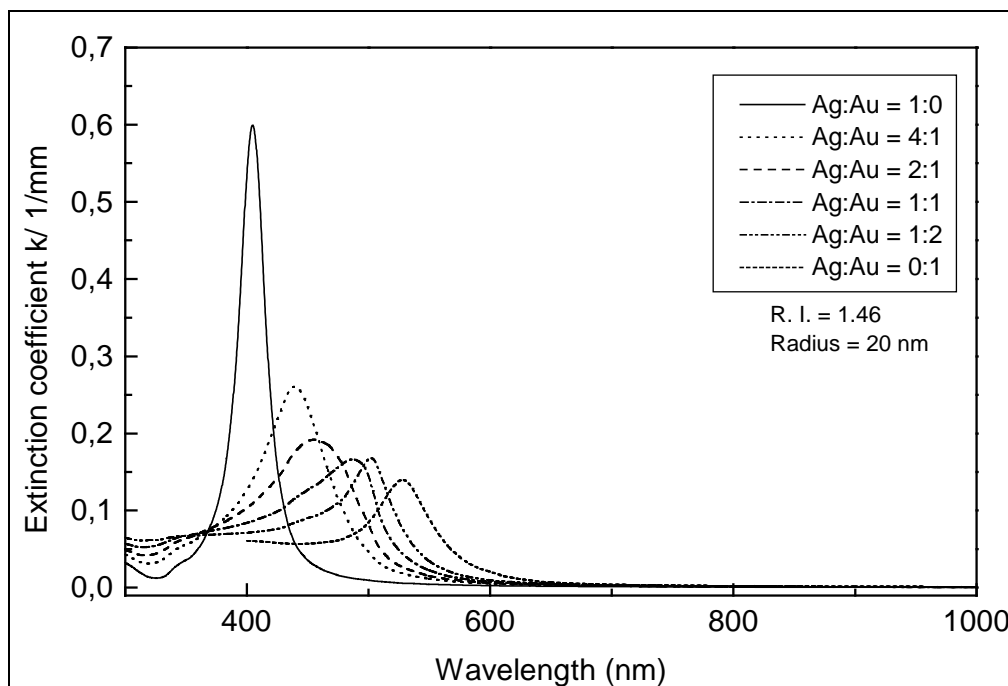


Figure A 7: Theoretical extinction spectra of Ag / Au alloy colloids as a function of their molar ratios after Mie-theory, using a computer simulation programme. Colloid volume concentration is 10^{-6} and the refractive index of the matrix is 1.46.

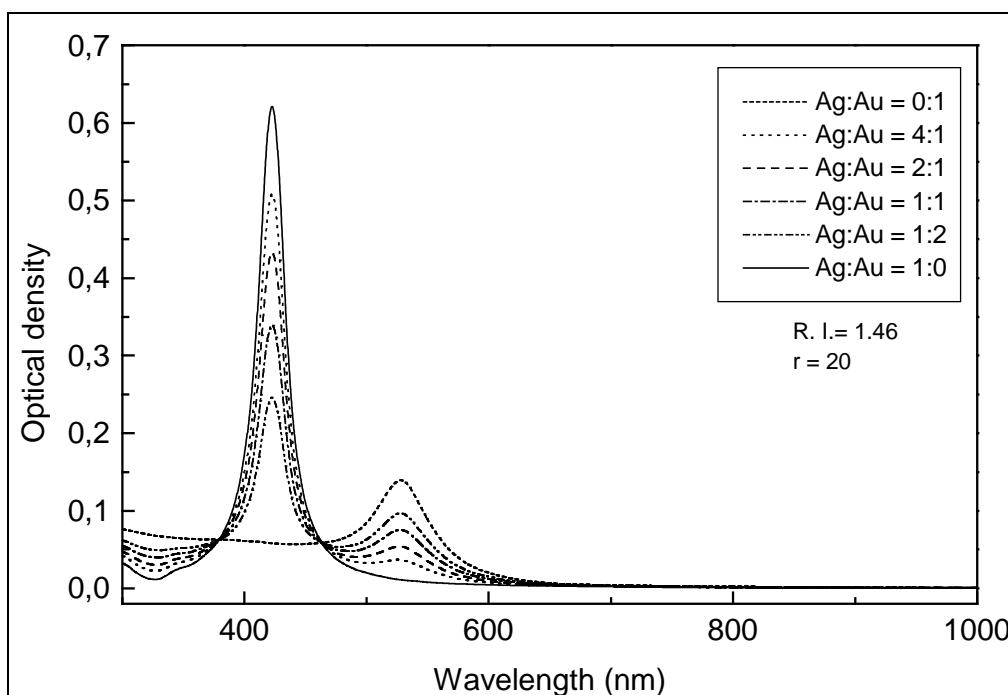


Figure A 8: Theoretical extinction spectra of Ag / Au mixed colloids having different molar ratio of Ag : Au after Mie-theory using a computer programme, for a total colloidal volume concentration of 10^{-6} and refractive index of matrix 1.46.

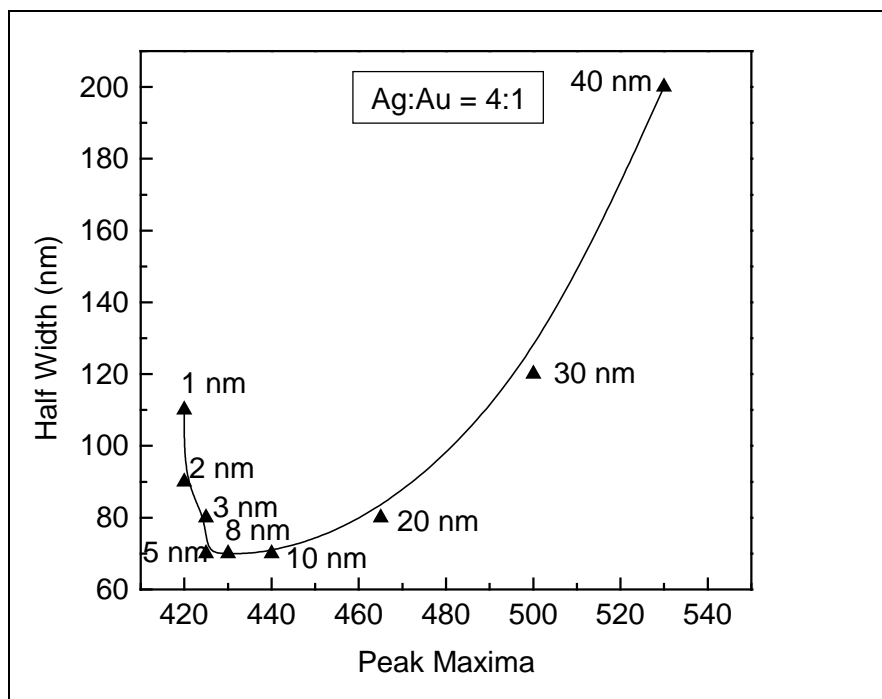


Figure A 9: Peak position and half width of calculated spectra for different radii of Ag / Au alloy particles in a medium with refractive index of 1.46 and the Ag : Au = 4 : 1.

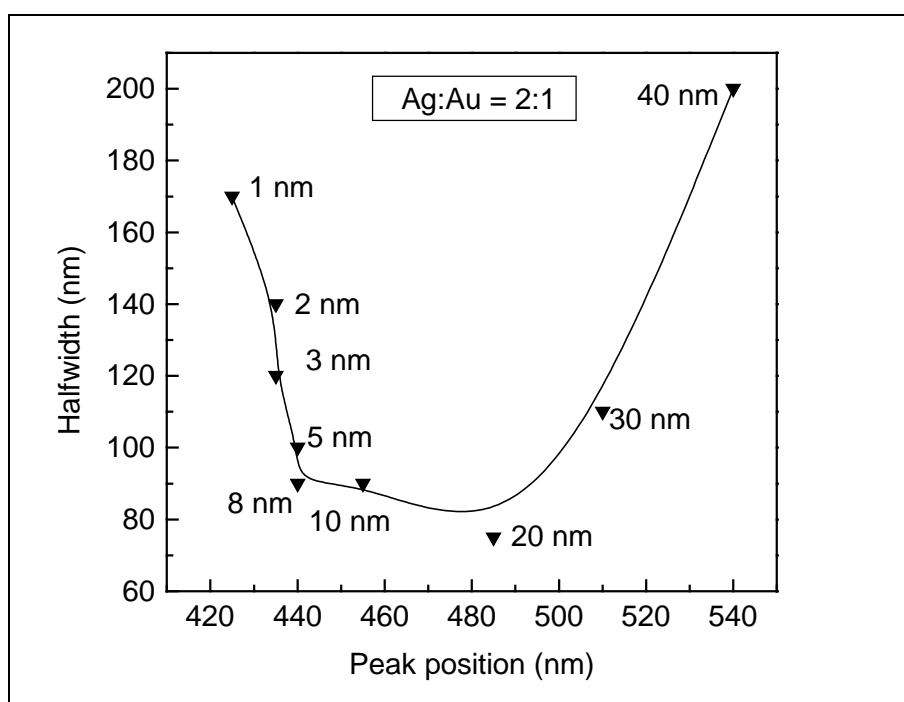


Figure A 10: Peak position and half width of calculated spectra for different radii of Ag / Au alloy particles in a medium with refractive index of 1.46 and the Ag : Au = 2 : 1.

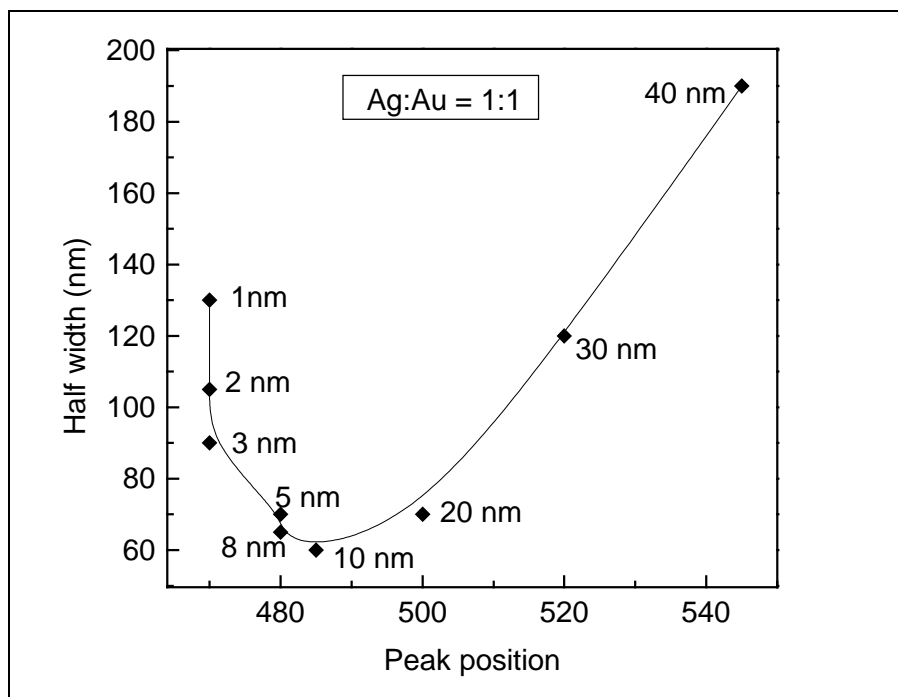


Figure A 11: Peak position and half width of calculated spectra for different radii of Ag / Au alloy particles in a medium with a refractive index of 1.46 and the Ag : Au = 1 : 1.

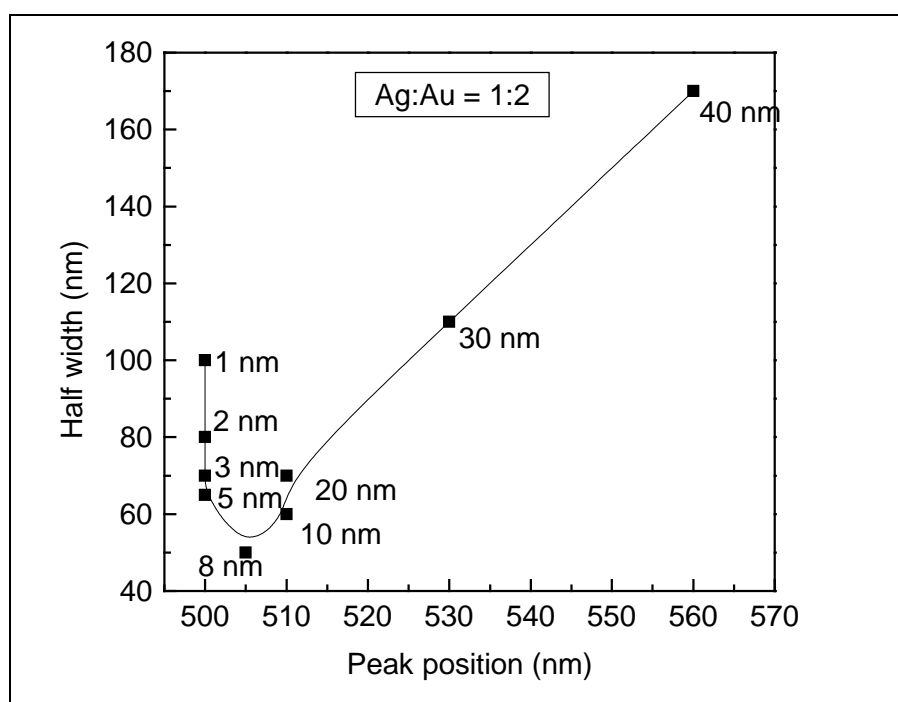


Figure A 12: Peak position and half width of calculated spectra for different radii of Ag : Au alloy particles in a medium with refractive index of 1.46 and the Ag : Au = 1 : 2.

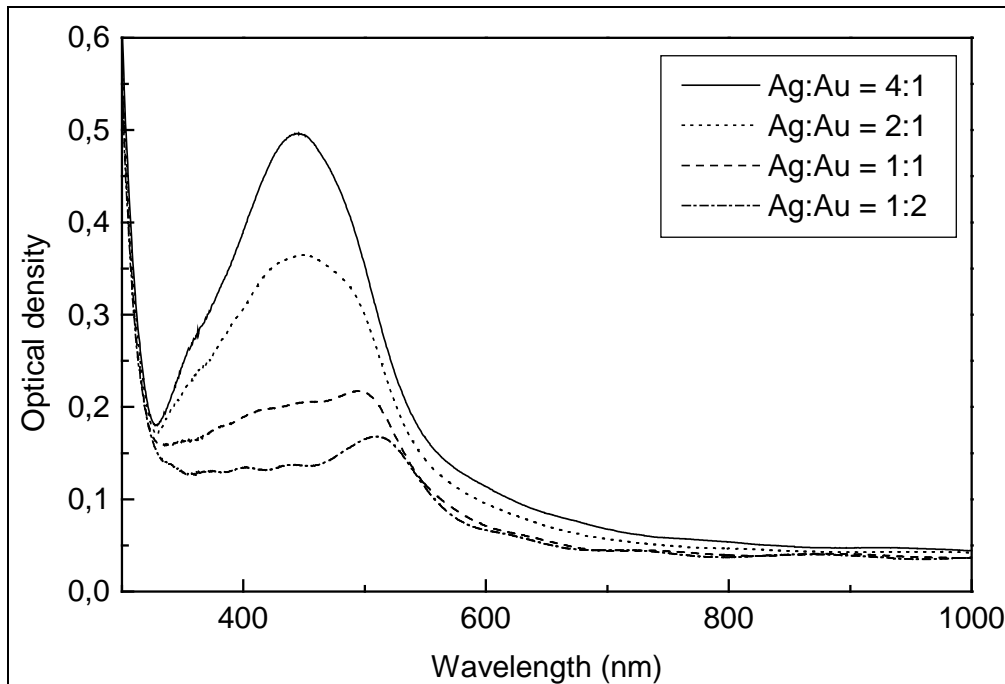


Figure A 13: Measured absorption spectra of PbO-SiO₂ thin films containing Ag / Au alloy colloids as a function of their molar ratios, heat treated at 50 °C under reducing atmosphere (N₂ / H₂ = 92 / 8, 80 l/h); reference: air.

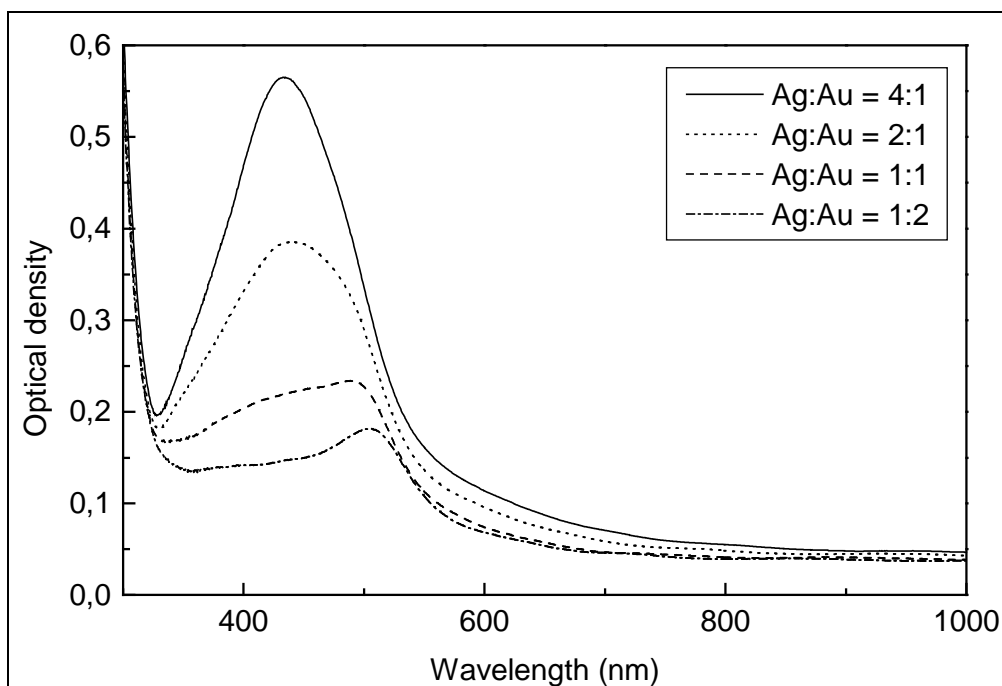


Figure A 14: Measured absorption spectra of PbO-SiO₂ thin films containing Ag / Au alloy colloids as a function of their molar ratios, heat treated at 150 °C under reducing atmosphere (N₂ / H₂ = 92 / 8, 80 l/h); reference: air.

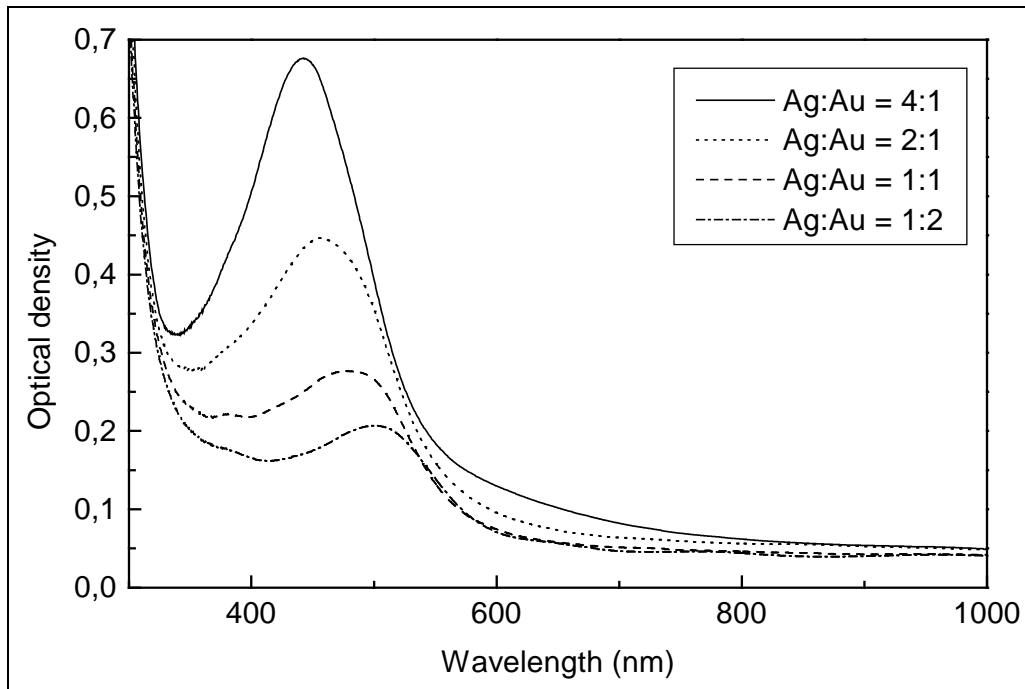


Figure A 15: Measured absorption spectra of PbO-SiO₂ thin films containing Ag / Au alloy colloids as a function of their molar ratios, heat treated 250 °C under reducing atmosphere (N₂ / H₂ = 92 / 8, 80 l/h); reference: air.

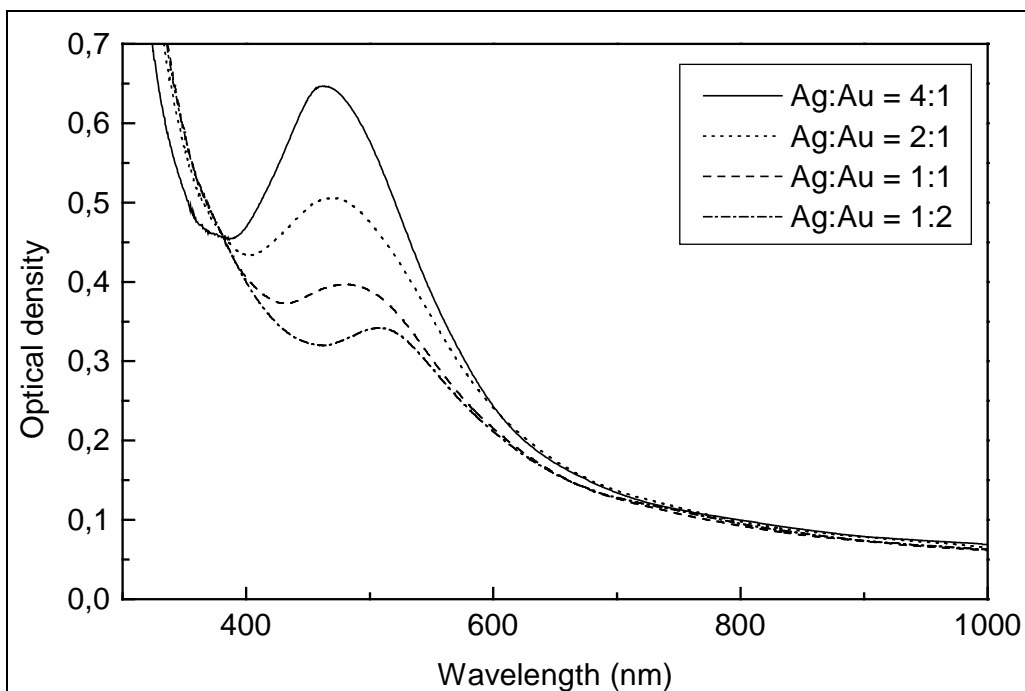


Figure A 16: Measured absorption spectra of PbO-SiO₂ thin films containing Ag / Au alloy colloids as a function of their molar ratios, heat treated at 450 °C under reducing atmosphere (N₂ / H₂ = 92 / 8, 80 l/h); reference: air.

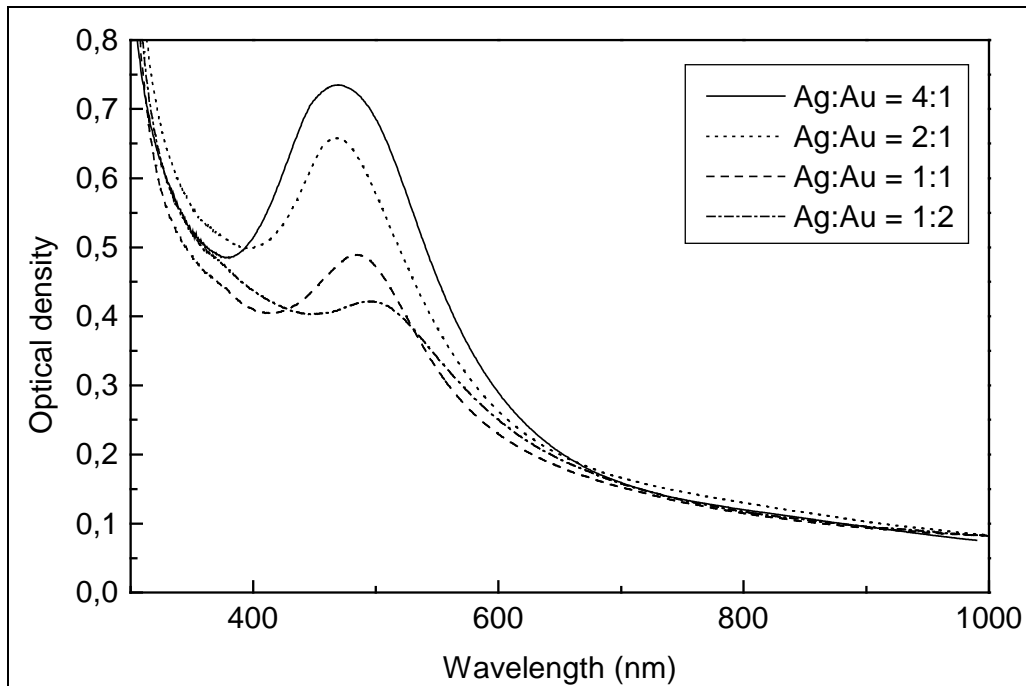


Figure A 17: Measured absorption spectra of PbO-SiO₂ thin films containing Ag / Au alloy colloids as a function of their molar ratios, heat treated at 550 °C under reducing atmosphere (N₂ / H₂ = 92 / 8, 80 l/h); reference: air.

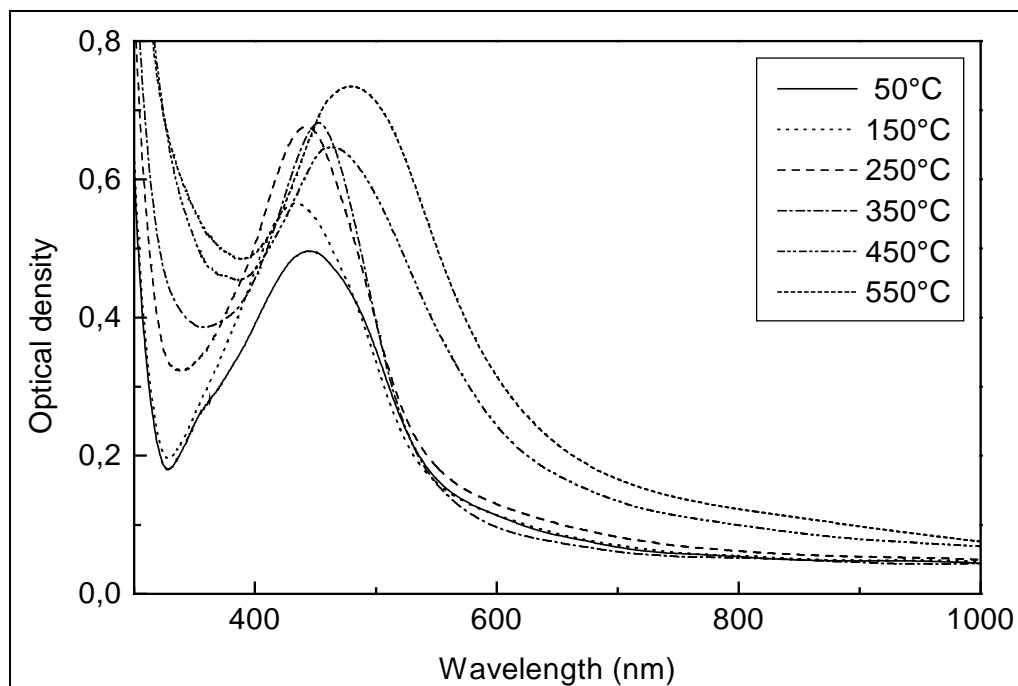


Figure A 18: Measured absorption spectra of PbO-SiO₂ thin films containing Ag / Au alloy colloids as a function of densification temperature, at a constant molar ratio of Ag : Au = 4 : 1 (densified under N₂ / H₂ = 92 / 8, 80 l/h); reference: air.

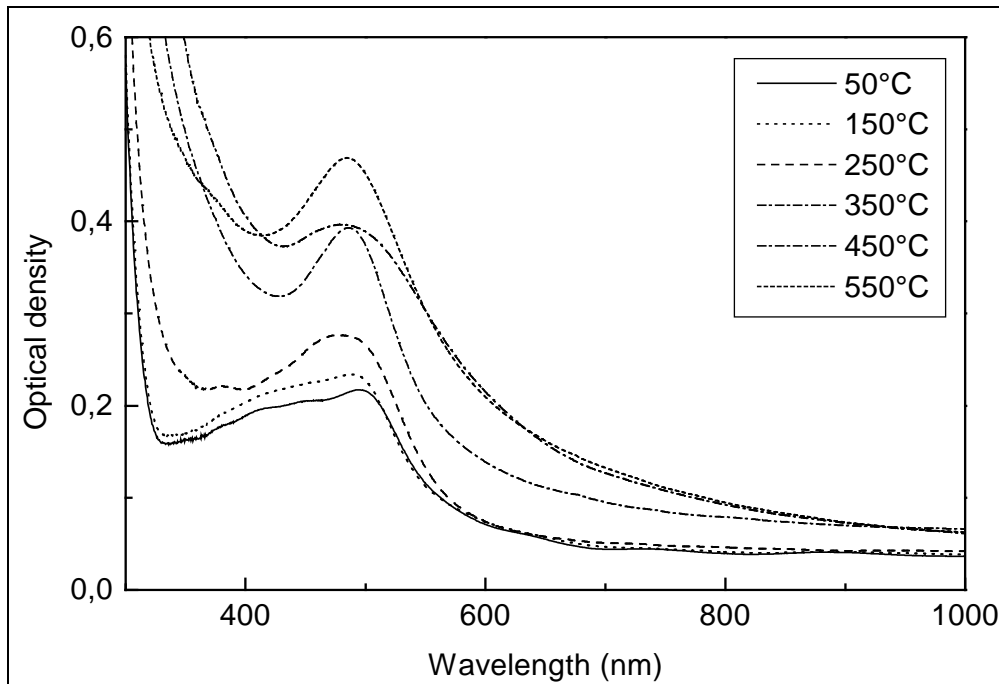


Figure A 19: Measured absorption spectra of PbO-SiO₂ thin films containing Ag / Au alloy colloids as a function of densification temperature, at a constant molar ratio of Ag : Au = 1 : 1 (densified under N₂ / H₂ = 92 / 8, 80 l/h); reference: air.

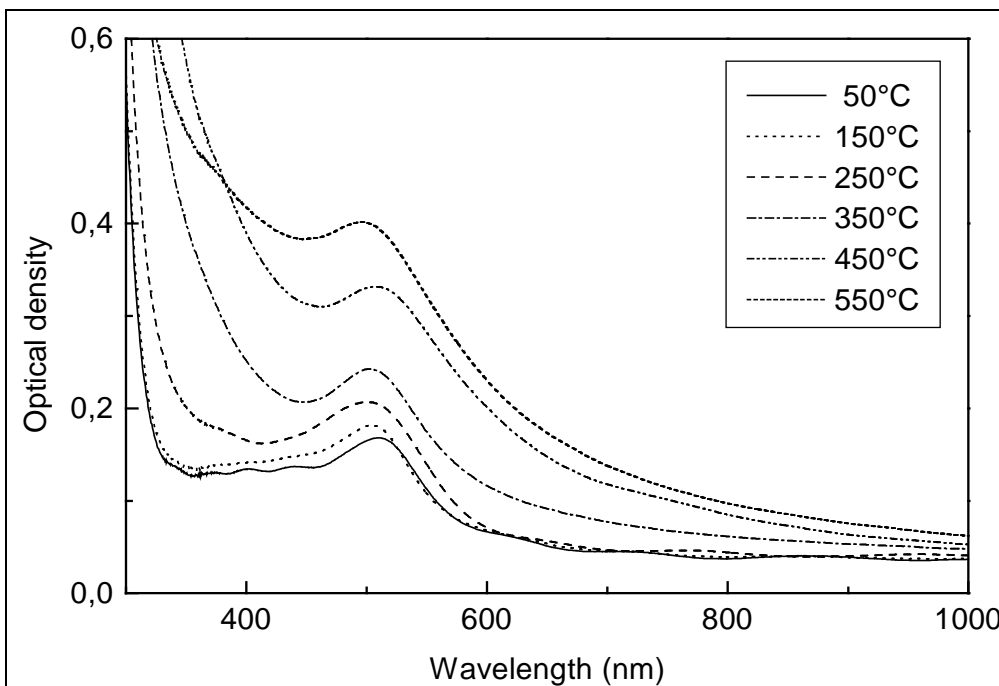


Figure A 20: Measured absorption spectra of PbO-SiO₂ thin films containing Ag / Au alloy colloids as a function of densification temperature, at a constant molar ratio of Ag : Au = 1 : 2 (densified under N₂ / H₂ = 92 / 8, 80 l/h); reference: air.

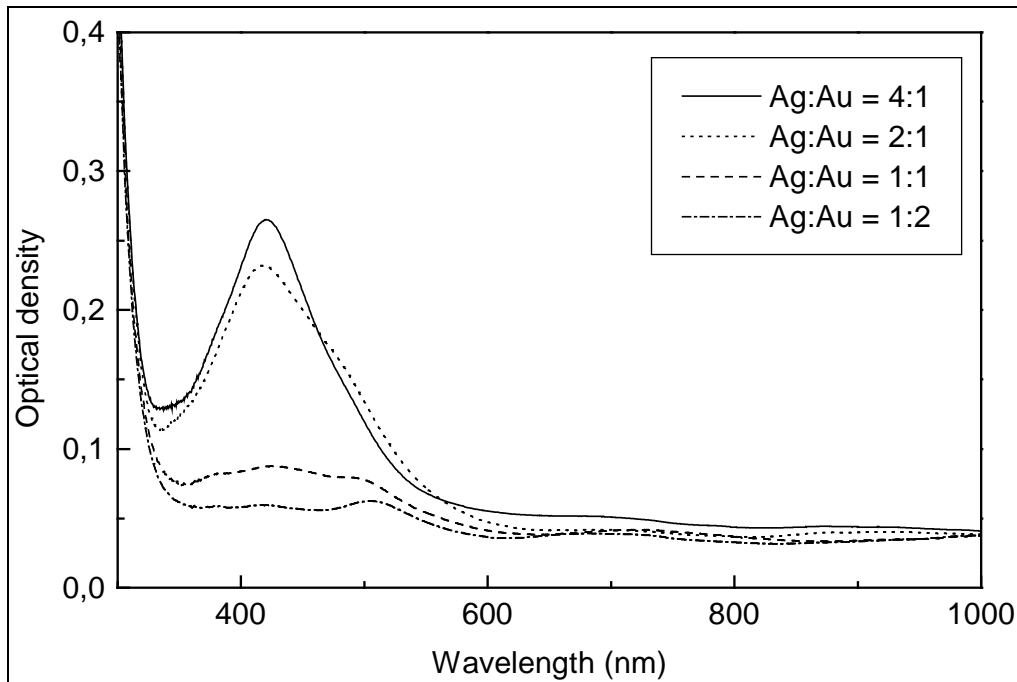


Figure A 21: Measured absorption spectra of SiO₂ thin films containing Ag / Au alloy colloids as a function of their molar ratios, heat treated at 50 °C under reducing atmosphere (N₂ / H₂ = 92 / 8, 80 l/h); reference: air.

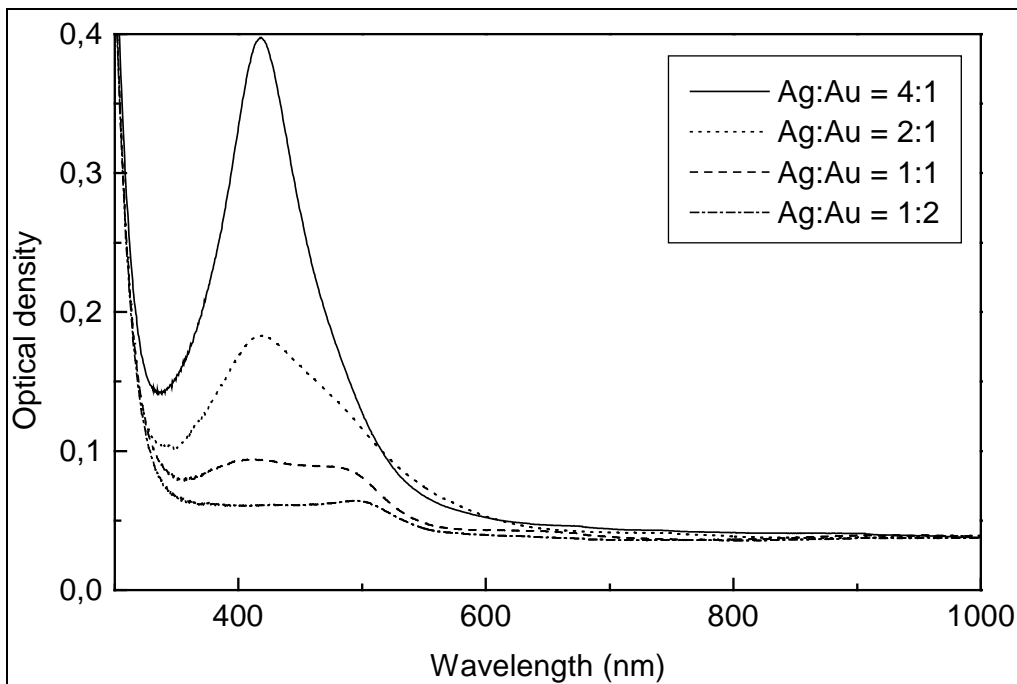


Figure A 22: Measured absorption spectra of SiO₂ thin films containing Ag / Au alloy colloids as a function of their molar ratios, heat treated at 150 °C under reducing atmosphere (N₂ / H₂ = 92 / 8, 80 l/h); reference: air.

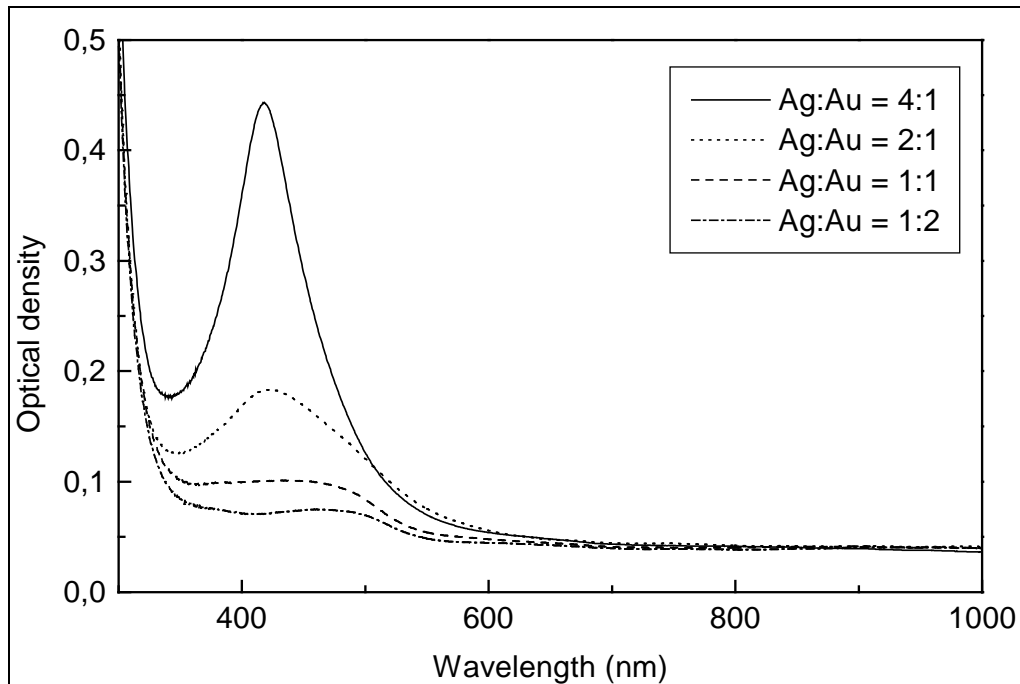


Figure A 23: Measured absorption spectra of SiO₂ thin films containing Ag / Au alloy colloids as a function of their molar ratios, heat treated at 250 °C under reducing atmosphere (N₂ / H₂ = 92 / 8, 80 l/h); reference: air.

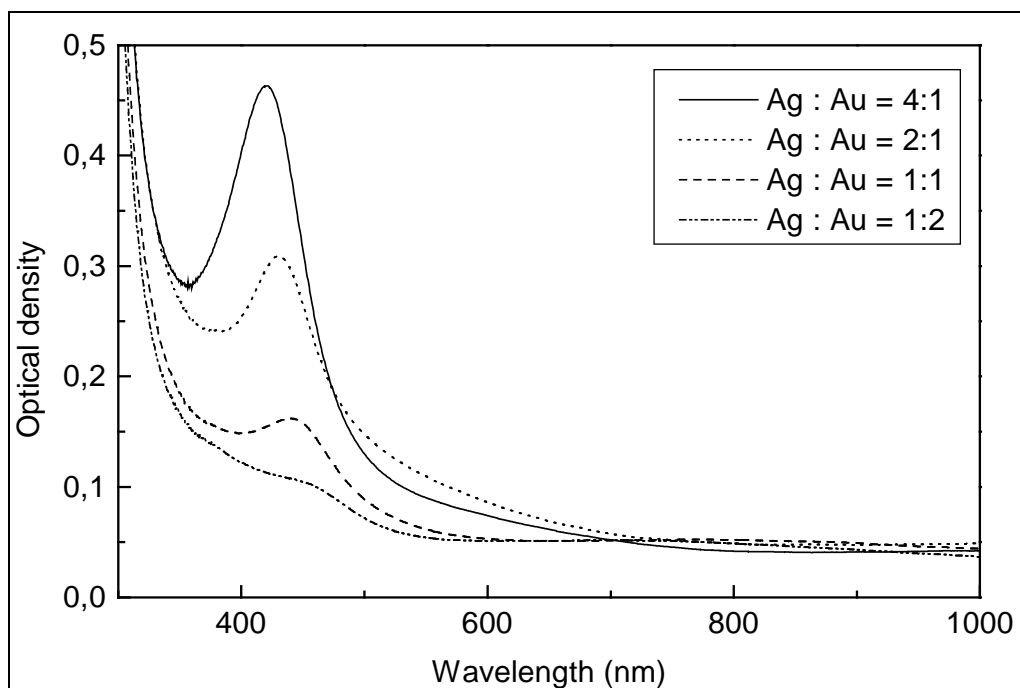


Figure A 24: Measured absorption spectra of SiO₂ thin films containing Ag / Au alloy colloids as a function of their molar ratios, heat treated at 450 °C under reducing atmosphere (N₂ / H₂ = 92 / 8, 80 l/h); reference: air.

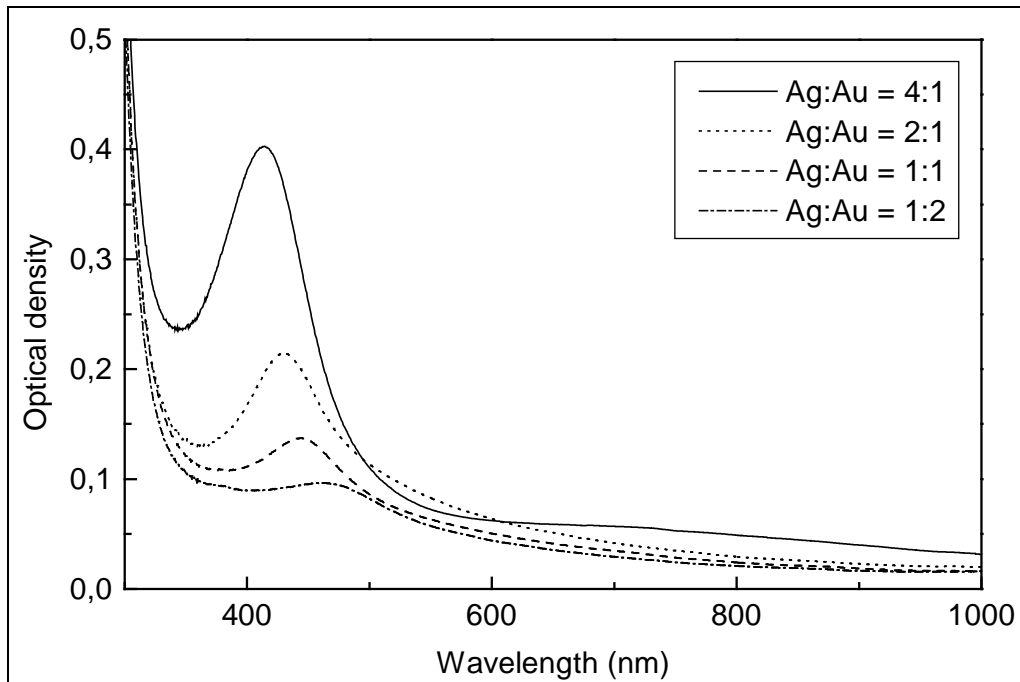


Figure A 25: UV-VIS absorption spectra of SiO_2 thin films containing Ag / Au alloy colloids heat treated at 550 °C under reducing atmosphere ($\text{N}_2 / \text{H}_2 = 92 / 8$, 80 l/h), as a function of their molar ratios; reference: air.

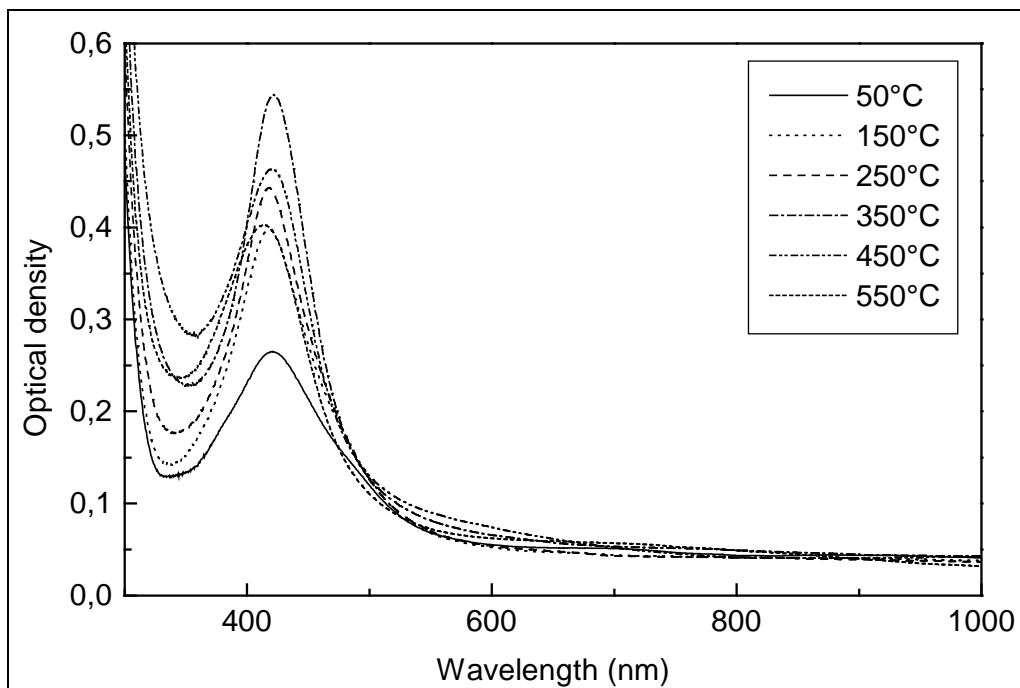


Figure A 26: UV-VIS absorption spectra of SiO_2 thin films containing Ag / Au alloy colloids (Ag : Au = 4 : 1) heat treated under reducing atmosphere ($\text{N}_2 / \text{H}_2 = 92 / 8$, 80 l/h), as a function of densification temperature; reference: air.

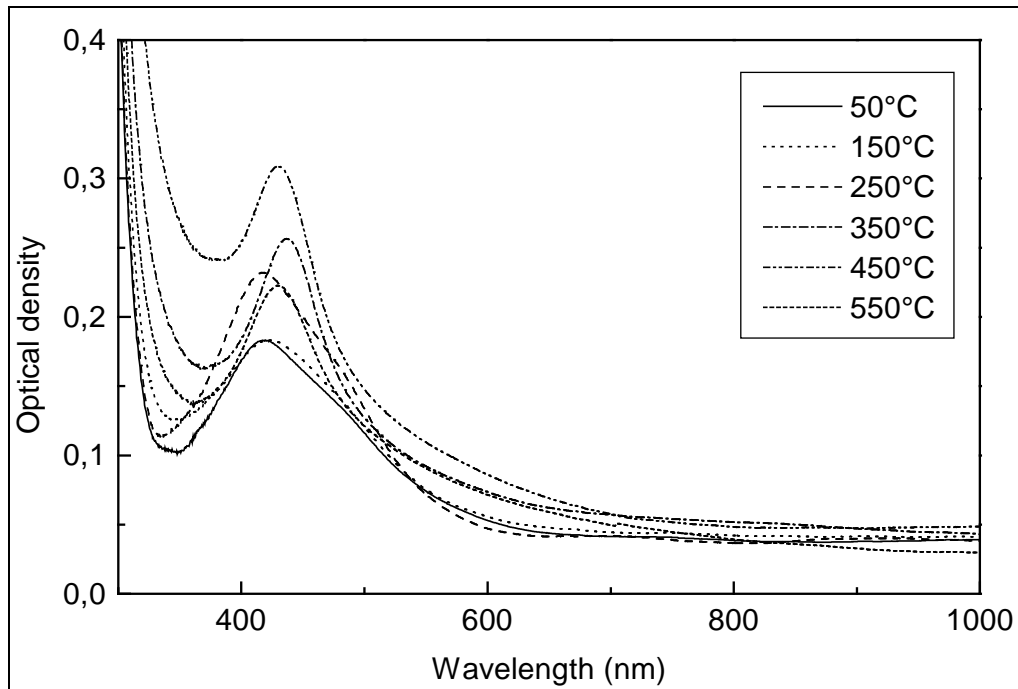


Figure A 27: UV-VIS absorption spectra of SiO₂ thin films containing Ag / Au alloy colloids (Ag : Au =2 : 1) heat treated under reducing atmosphere (N₂ / H₂ = 92 / 8, 80 l/h), as a function of densification temperature; reference: air.

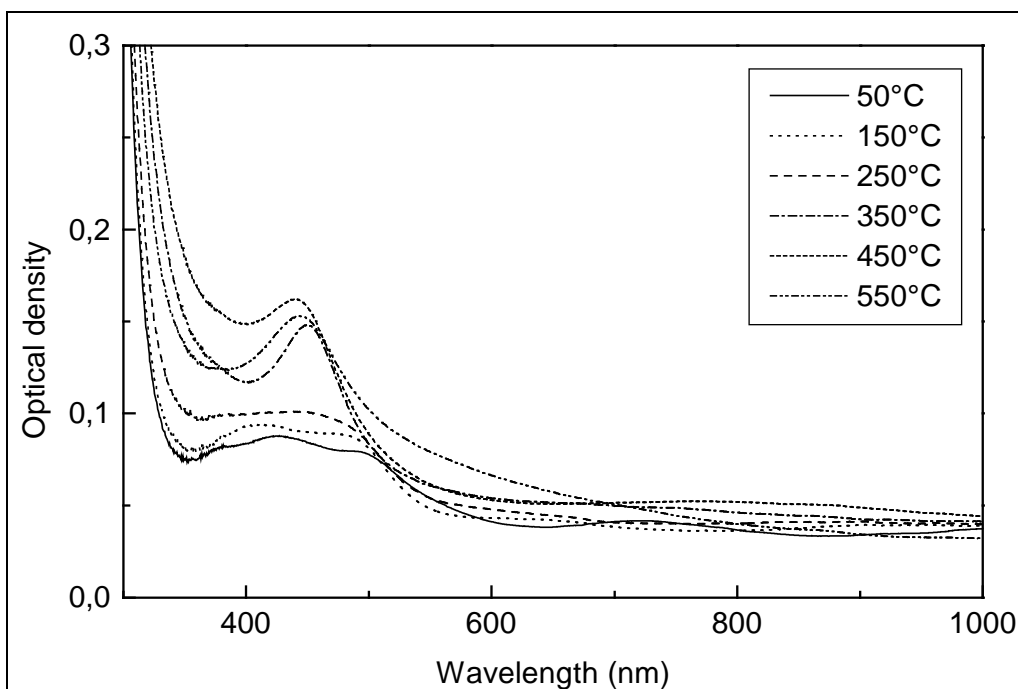


Figure A 28: UV-VIS absorption spectra of SiO₂ thin films containing Ag / Au alloy colloids (Ag : Au =1 : 1) heat treated under reducing atmosphere (N₂ / H₂ = 92 / 8, 80 l/h), as a function of densification temperature; reference: air.

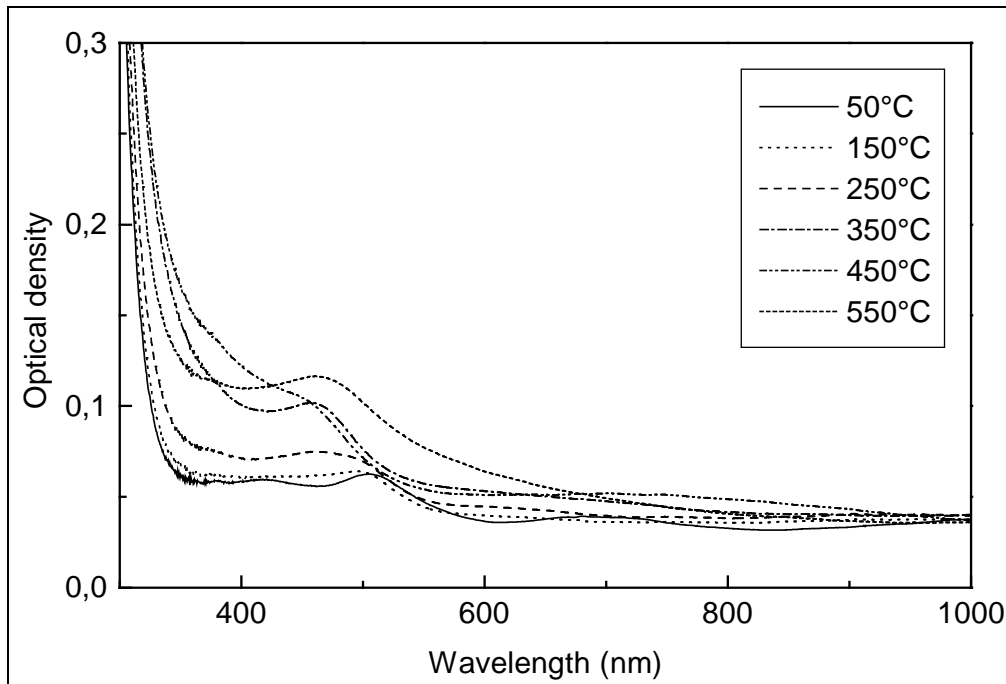


Figure A 29: UV-VIS absorption spectra of SiO₂ thin films containing Ag / Au alloy colloids (Ag : Au = 1 : 2) heat treated under reducing atmosphere (N₂ / H₂ = 92 / 8, 80 l/h), as a function of densification temperature; reference: air.

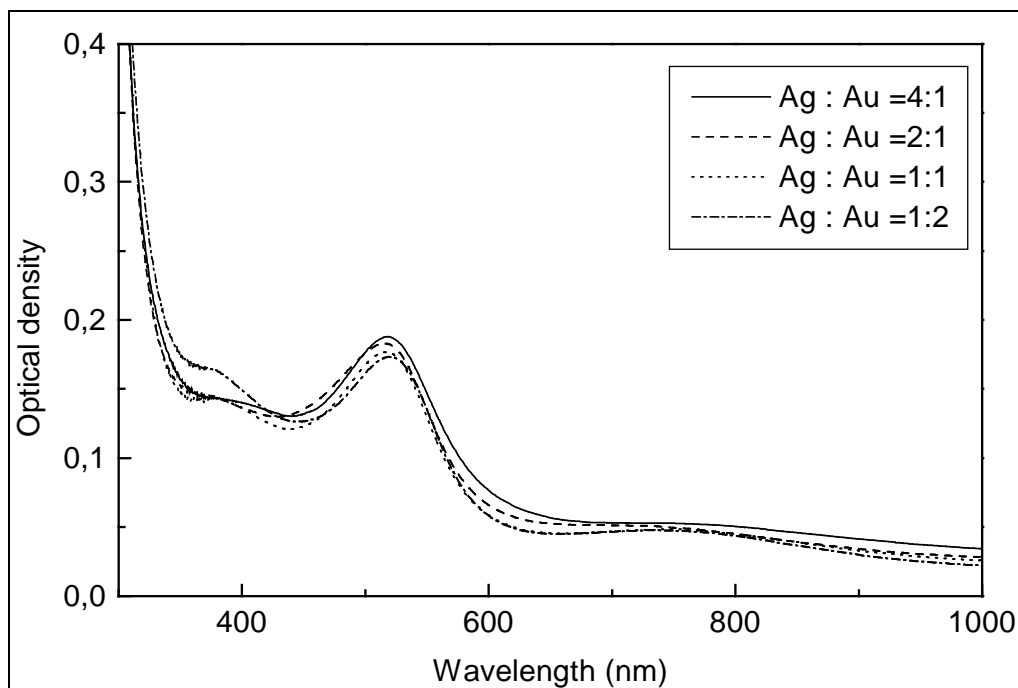


Figure A 30: UV-VIS spectra of SiO₂ thin films containing Ag / Au after heat treating the samples at 400 °C in air for 1 h with the heating rate of 100 K/h; reference: air.

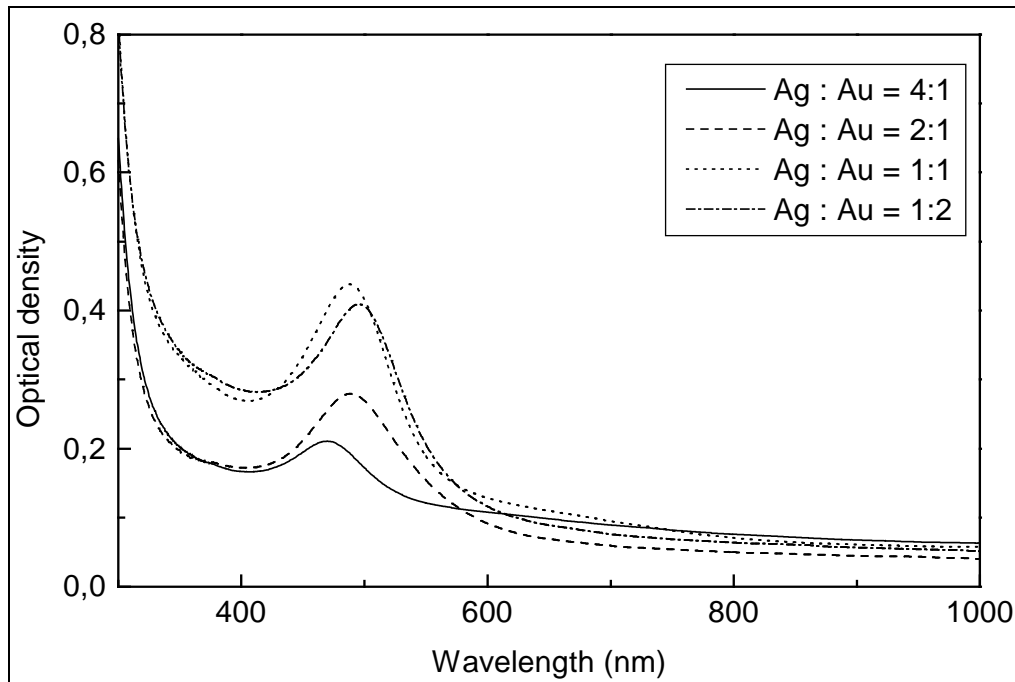


Figure A 31: UV-VIS absorption spectra of thin films containing Ag / Au mixed colloids heat treated at 250 °C in air, as a function of their molar ratios; reference: air.

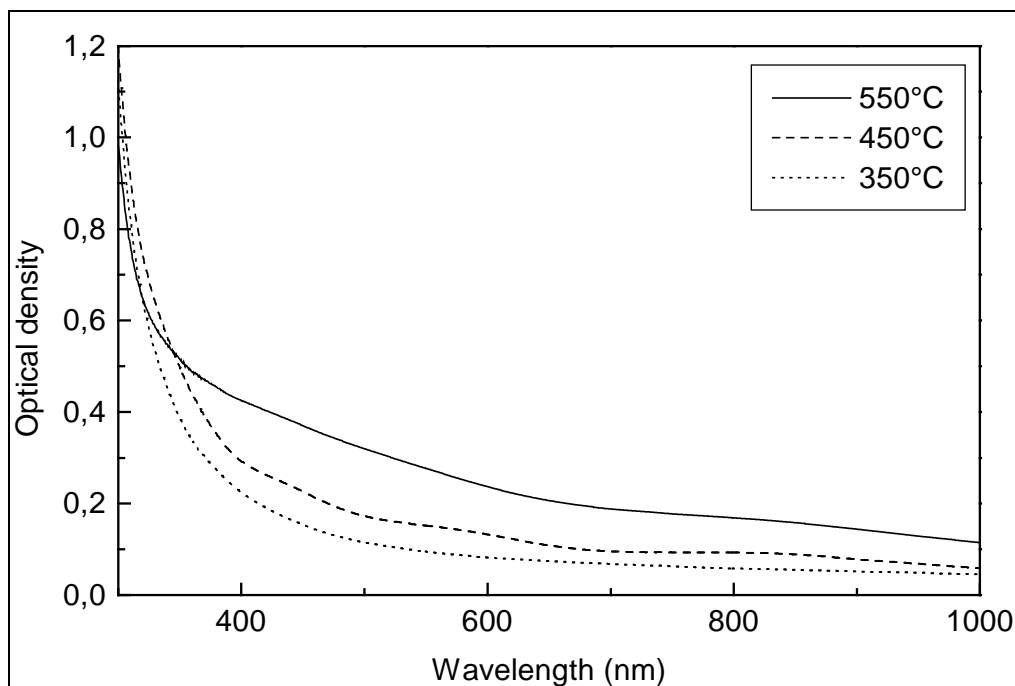


Figure A 32: UV-VIS spectra of reference coatings from matrix sol only, for the Ag / Au alloy colloids, densified under reducing (N₂ / H₂ = 92 / 8, 80 l/h) atmosphere.

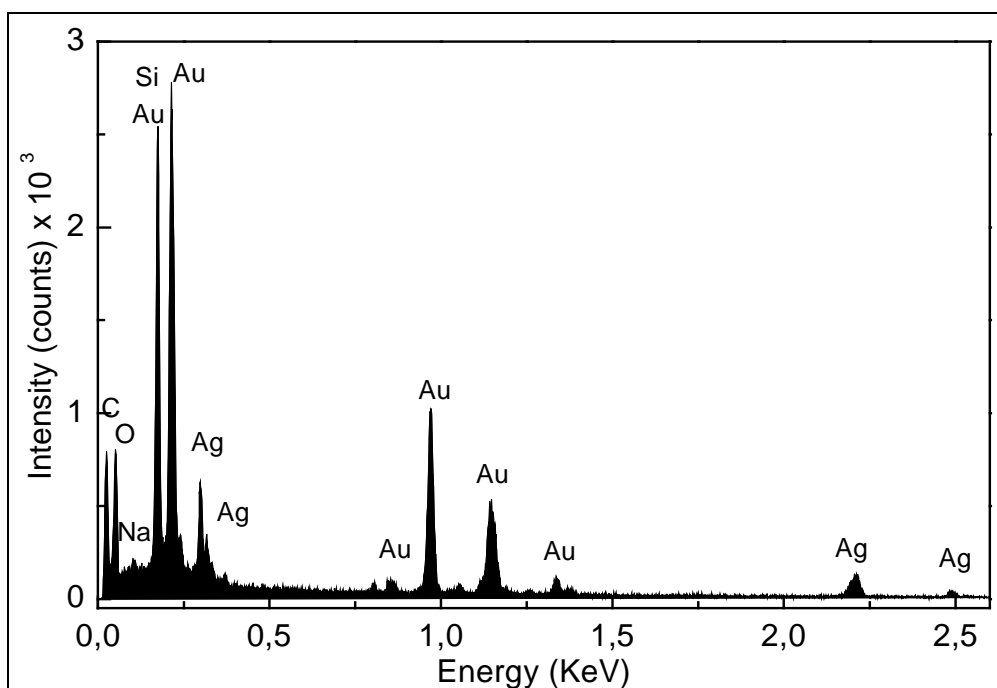


Figure A 33: EDX profiles of a single Ag / Au colloidal alloy particle with a molar ratio of Ag : Au = 2 : 1, analysis showed 67% (atom) Ag and 33% (atom) Au.

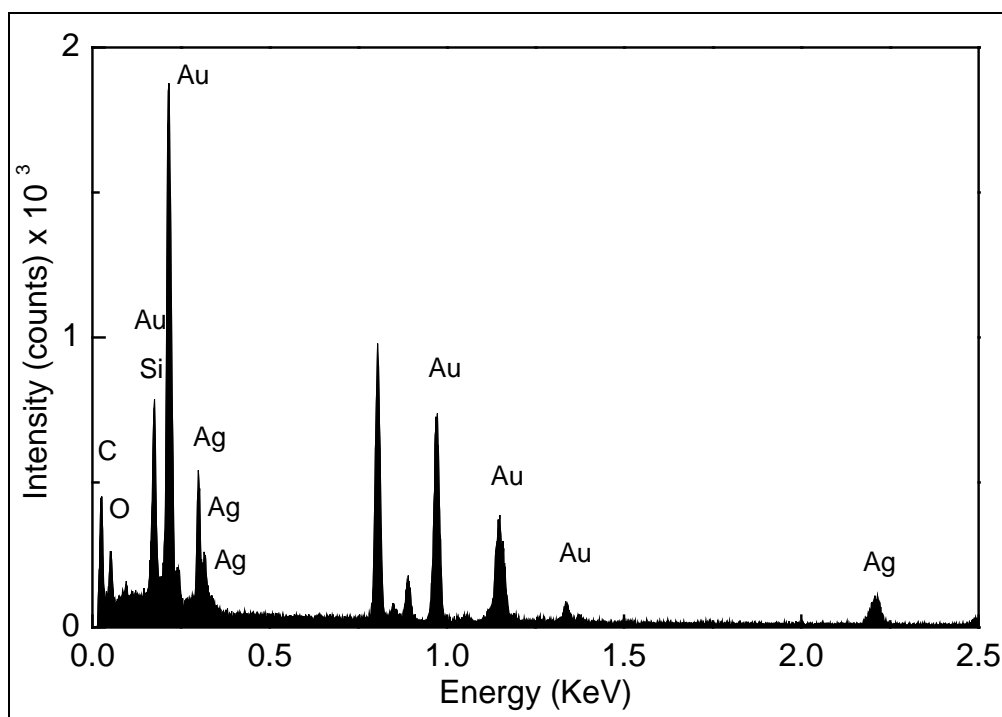


Figure A 34: EDX profiles of a single Ag / Au colloidal alloy particle with a molar ratio of Ag : Au = 1 : 2, analysis showed 32.4% (atom) Ag and 67.7% (atom) Au.

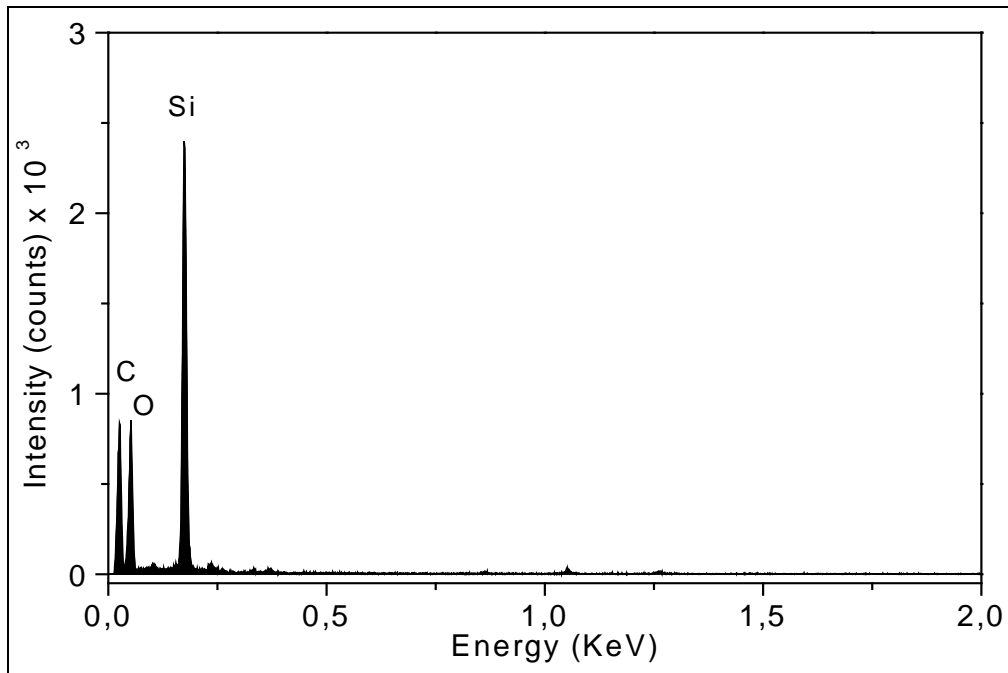


Figure A 35: EDX analysis of SiO₂ glass matrix containing Ag / Au alloy colloids showing the signals due to C, O and Si only, the film was densified at 450 °C.

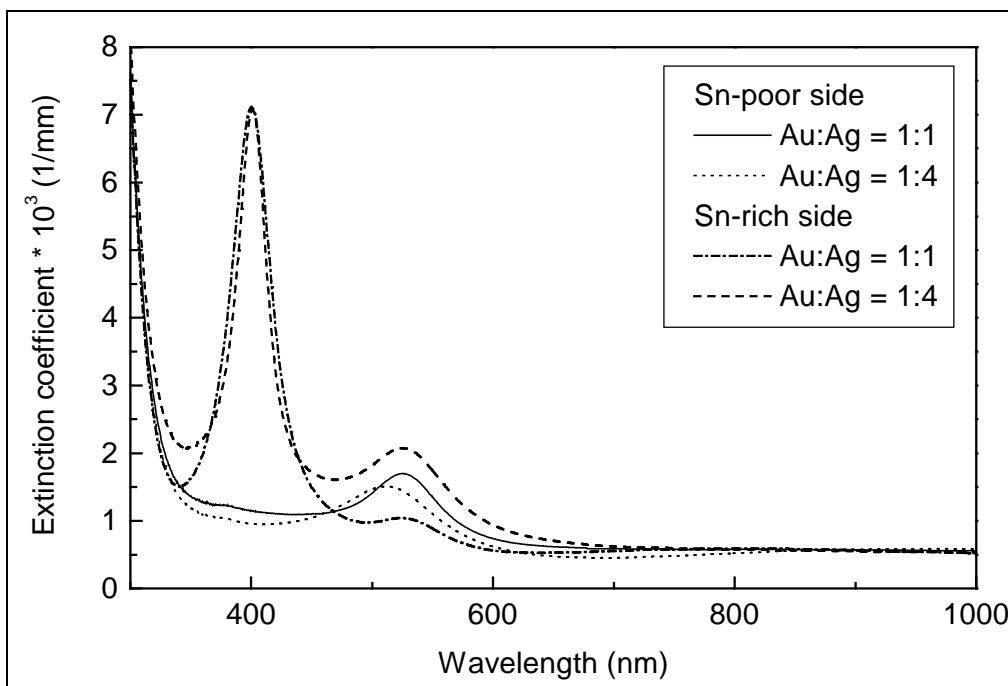


Figure A 36: Surface dependence of the formation of Ag / Au mixed colloids in SiO₂ thin films, all the samples were heat treated in air at 550 °C; reference : air.

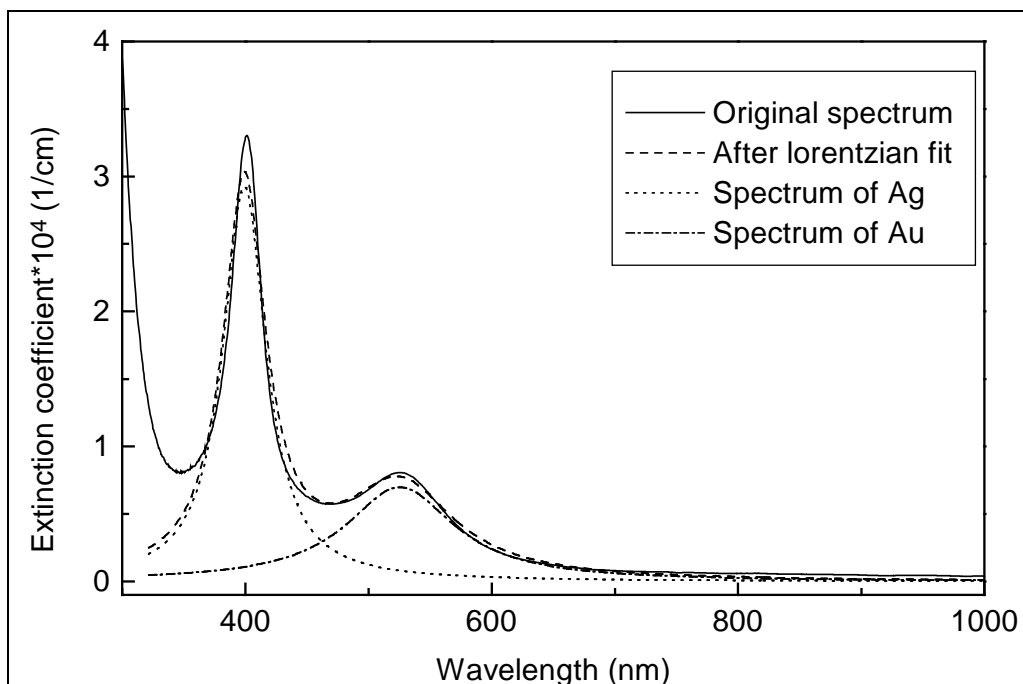


Figure A 37: Deconvolution of a UV-VIS spectra of thin films containing Ag / Au mixed colloids.

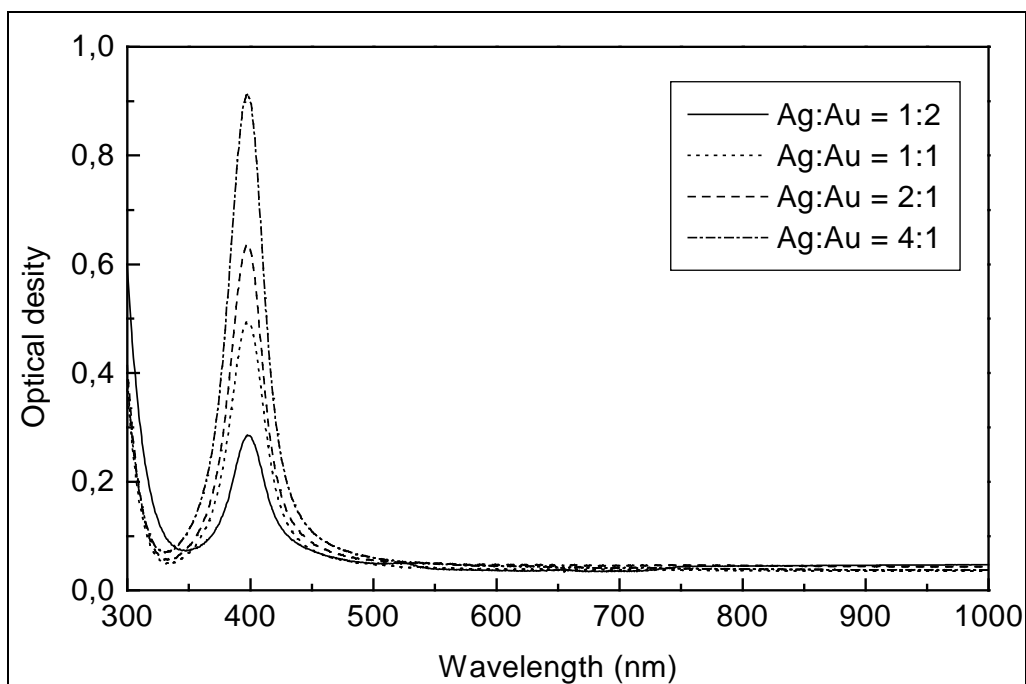


Figure A 38: UV-VIS absorption spectra of thin films containing Ag : Au mixed colloids as a function of their molar ratios, heat treated under reducing atmosphere at 450 °C. (after densifying in air at 450 °C the film was etched with 5% HF solution and the etched samples were re-heated under reducing atmosphere for 1 h); reference : air.

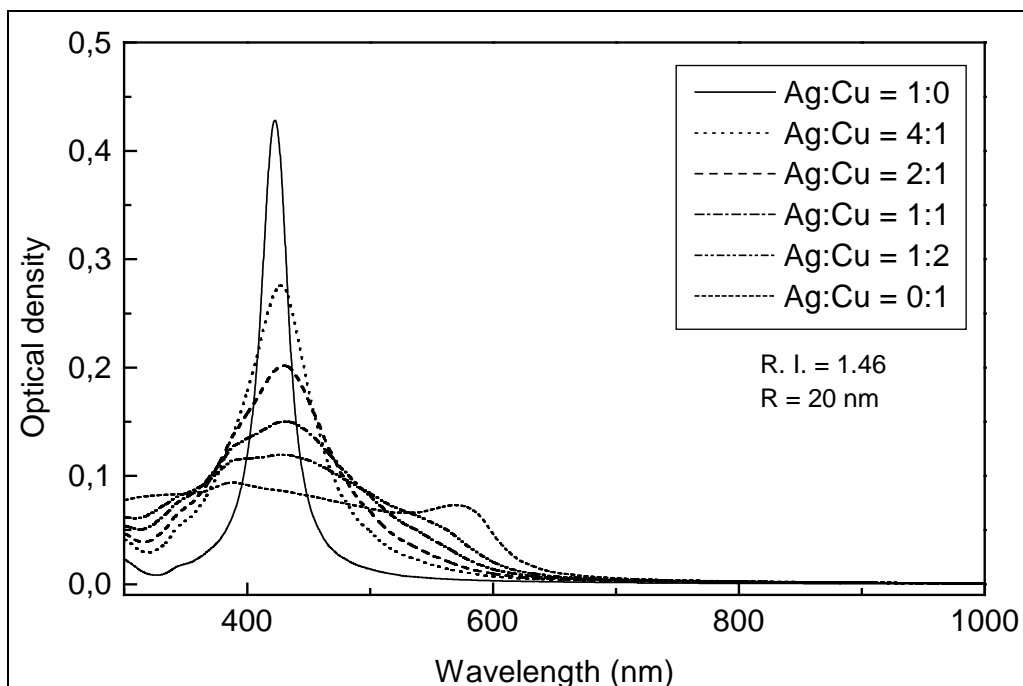


Figure A 39: Calculated extinction spectra of Ag / Cu alloy colloids as a function of their molar ratio after Mie-theory using a computer programme, for a total colloid volume concentration of 10^{-6} and refractive index of matrix 1.46, radius =20 nm.

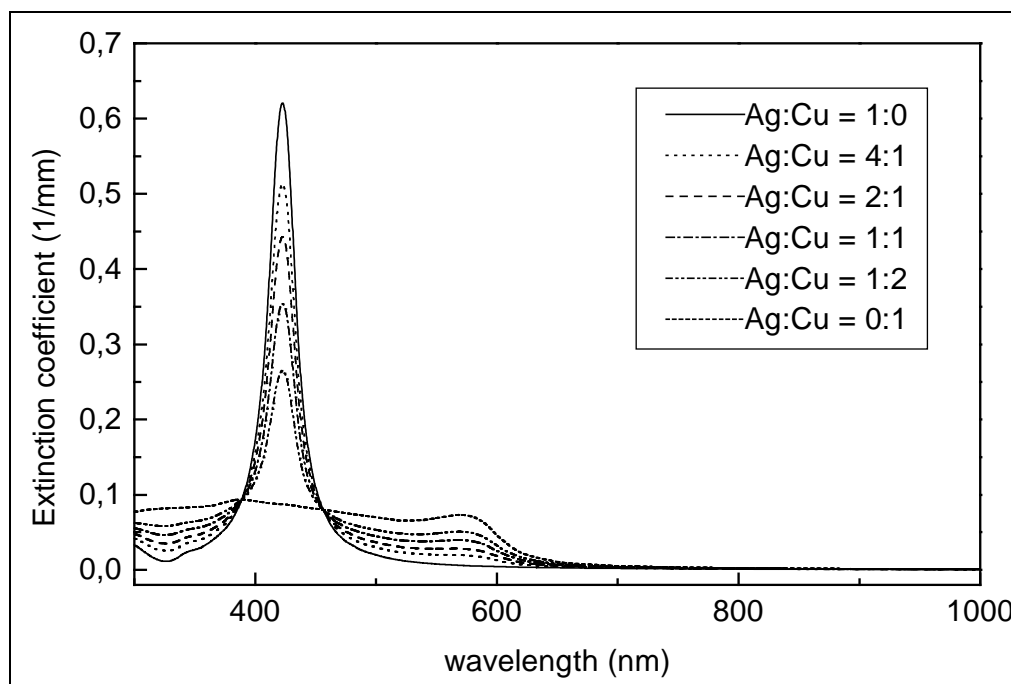


Figure A 40: Calculated extinction spectra of Ag / Cu mix colloids as a function of their molar ratios, after Mie-theory using a computer programme, for a total colloidal volume concentration of 10^{-6} and refractive index of matrix 1.46, $r = 20$ nm.

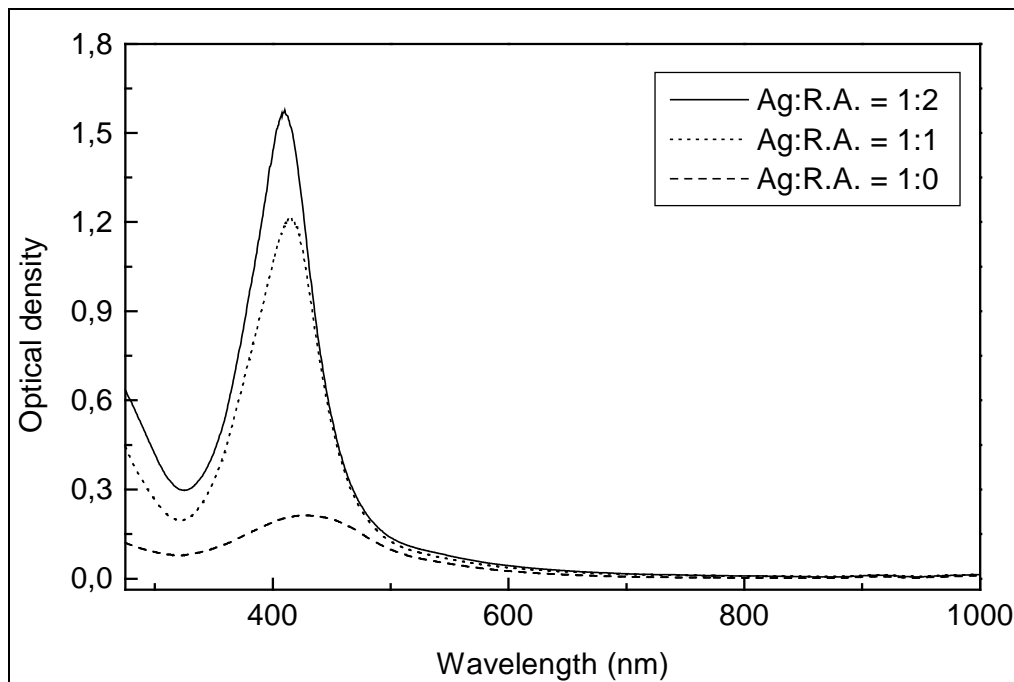


Figure A 41: Change in plasmon peak due to silver as a function of the change in molar ratio of hydroxylamine hydrochloride as reducing agent.

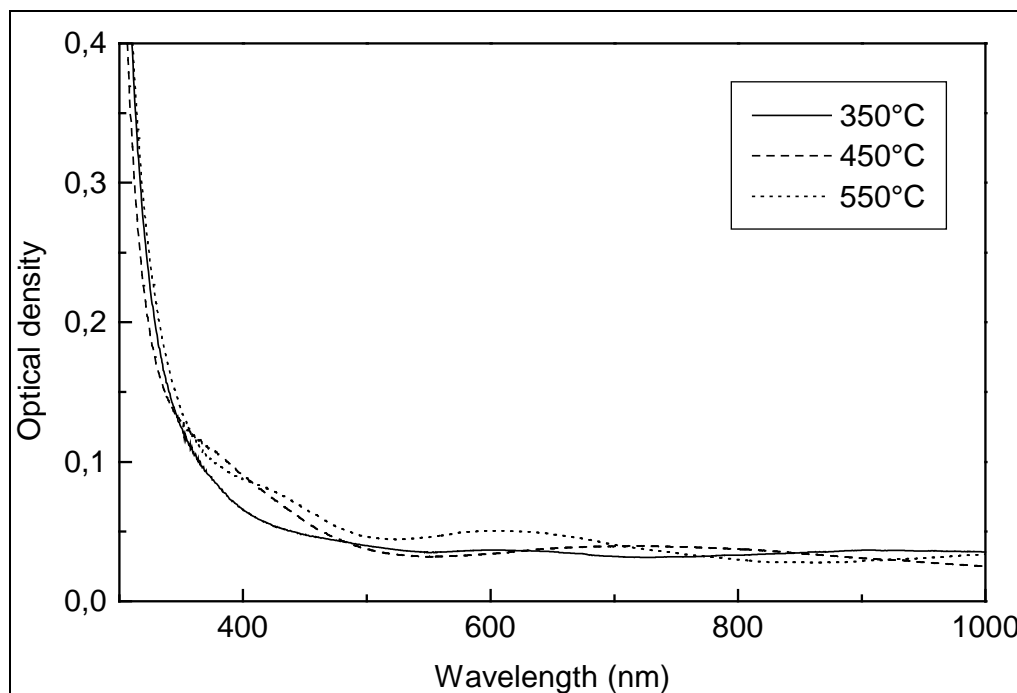


Figure A 42: UV-VIS spectra of reference coatings from matrix sol only for the Ag/Cu alloy colloids, densified under reducing ($N_2/H_2 = 92/8$, 80 l/h) atmosphere.

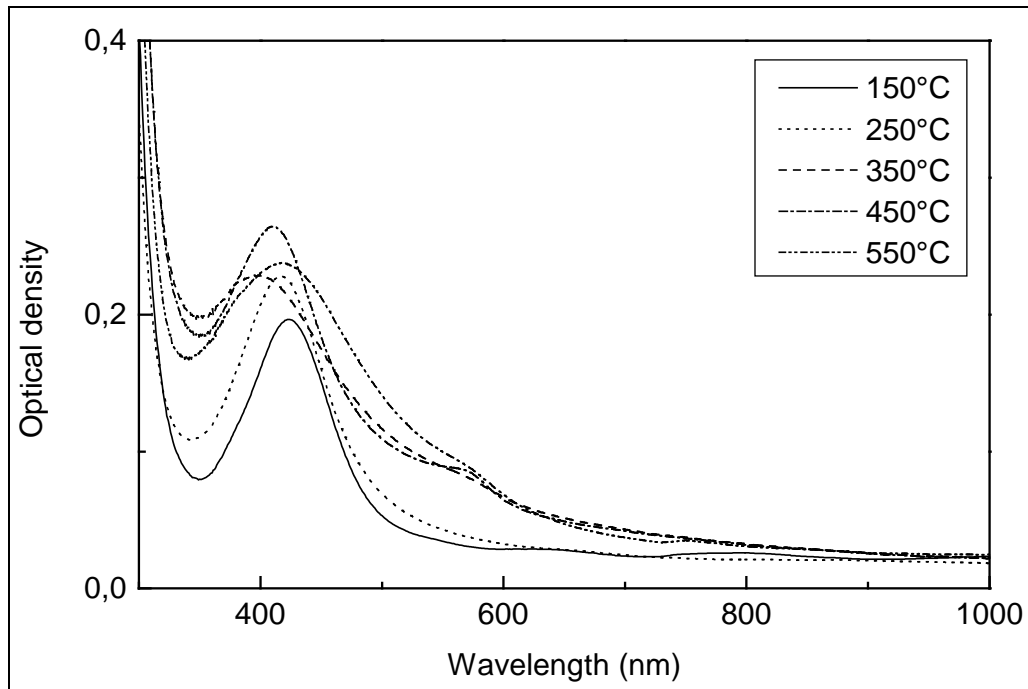


Figure A 43: UV-VIS absorption spectra of SiO₂ thin films containing Ag / Cu (molar ratio of Ag : Cu = 1 : 1) alloy colloids heat treated under reducing atmosphere (N₂ / H₂ = 92 / 8, 80 l/h), as a function of temperature; reference : air.

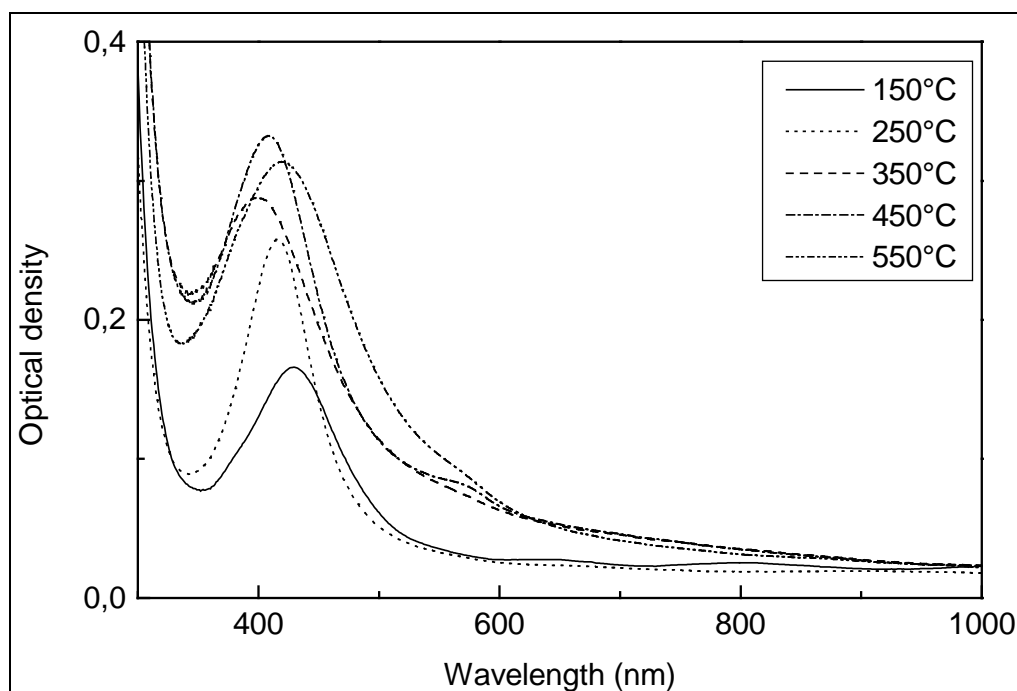


Figure A 44: UV-VIS absorption spectra of SiO₂ thin films containing Ag / Cu (molar ratio of Ag : Cu = 2 : 1) alloy colloids heat treated under reducing atmosphere (N₂ / H₂ = 92 / 8, 80 l/h), as a function of temperature; reference : air.

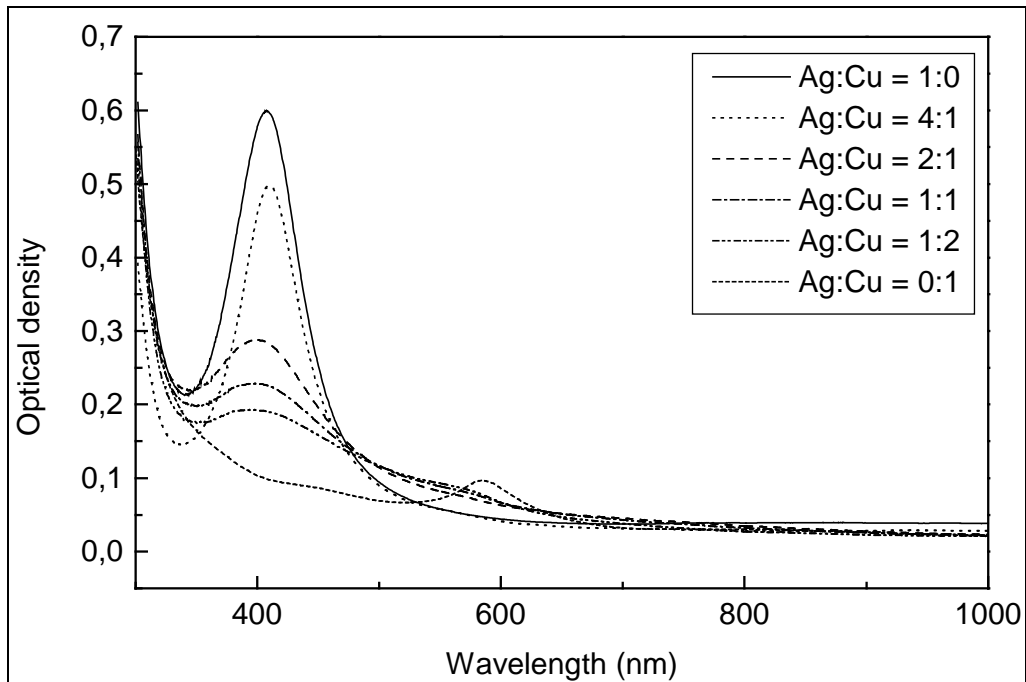


Figure A 45: UV-VIS absorption spectra of thin films containing Ag / Cu alloy colloids as a function of their molar ratios for the samples heat treated at 350 °C under reducing atmosphere ($N_2 / H_2 = 92 / 8$, 80 l/h); reference : air.

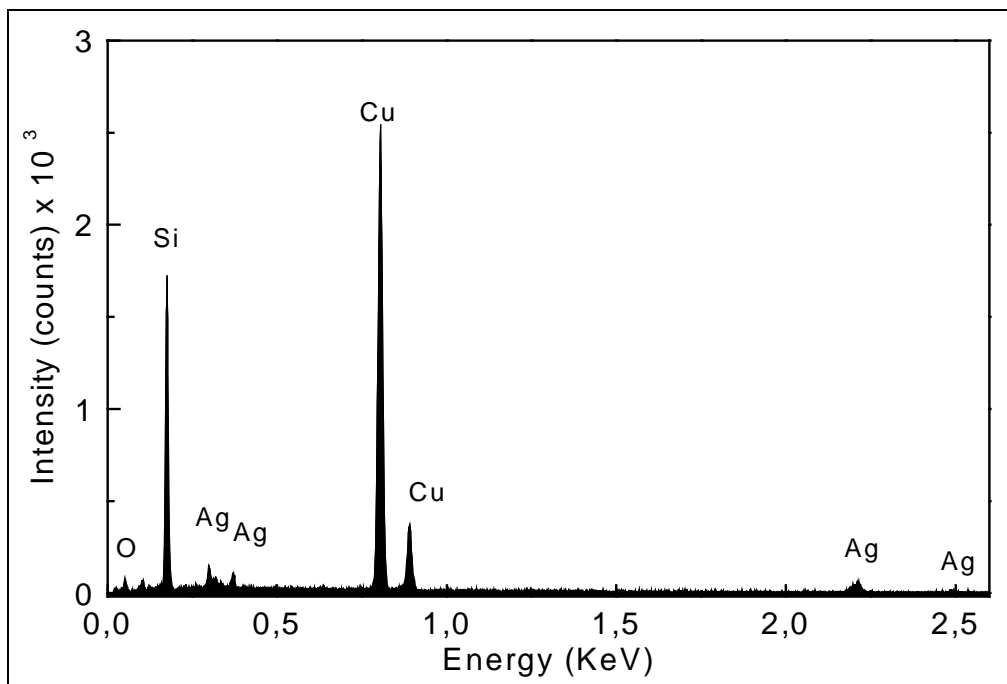


Figure A 46: EDX profiles of a Cu rich Ag / Cu colloidal alloy particle with a molar ratio of Ag : Cu = 1 : 1, analysis showed 94 atom% Cu and 6 atom% Ag.

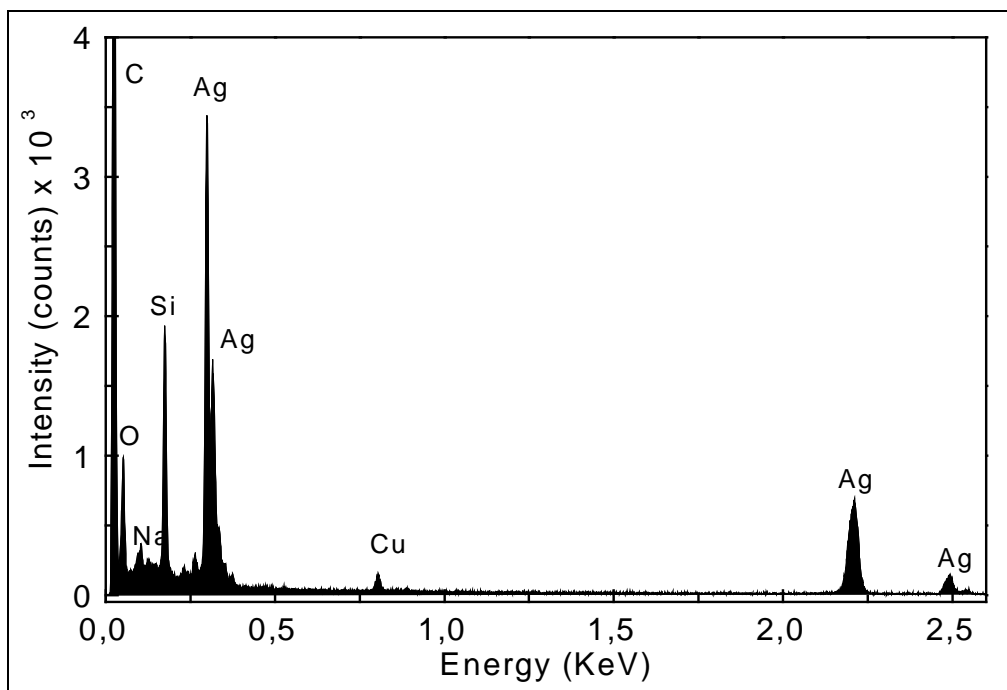


Figure A 47: EDX profiles of a Ag rich Ag / Cu colloidal alloy particle with a molar ratio of Ag : Cu = 1 : 1, analysis showed 94.8 mole% Ag and 5.2 mole% Cu.

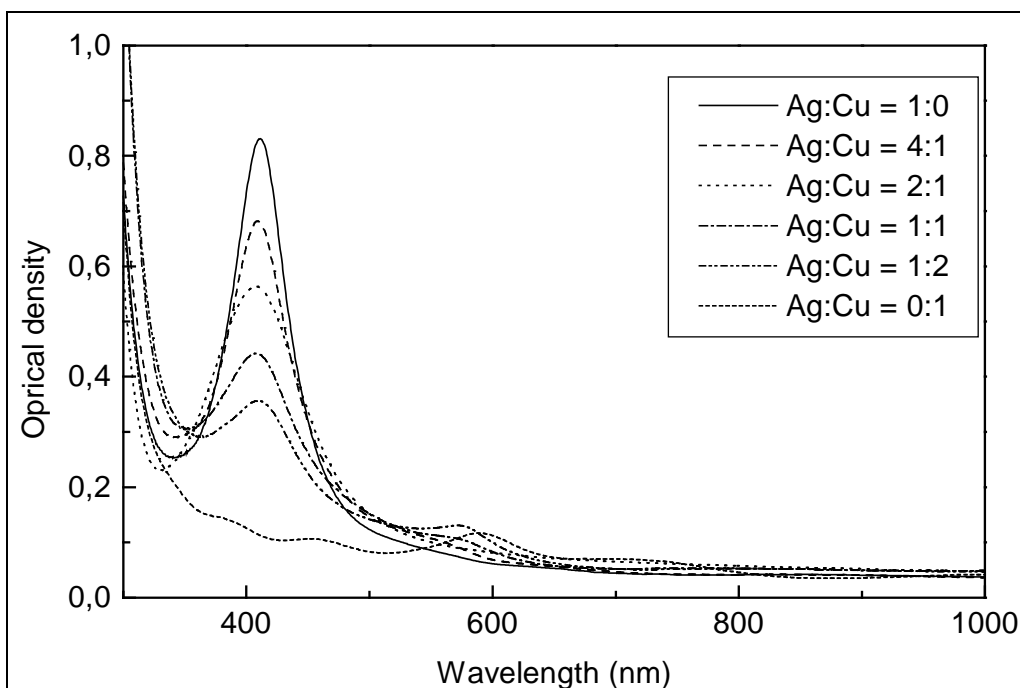


Figure A 48: UV-VIS absorption spectra of SiO₂ thin films containing Ag / Cu mixed colloids heat treated at 350 °C under reducing atmosphere (N₂ / H₂ = 92 / 8, 80 l/h), as a function of their molar ratios; reference: air.

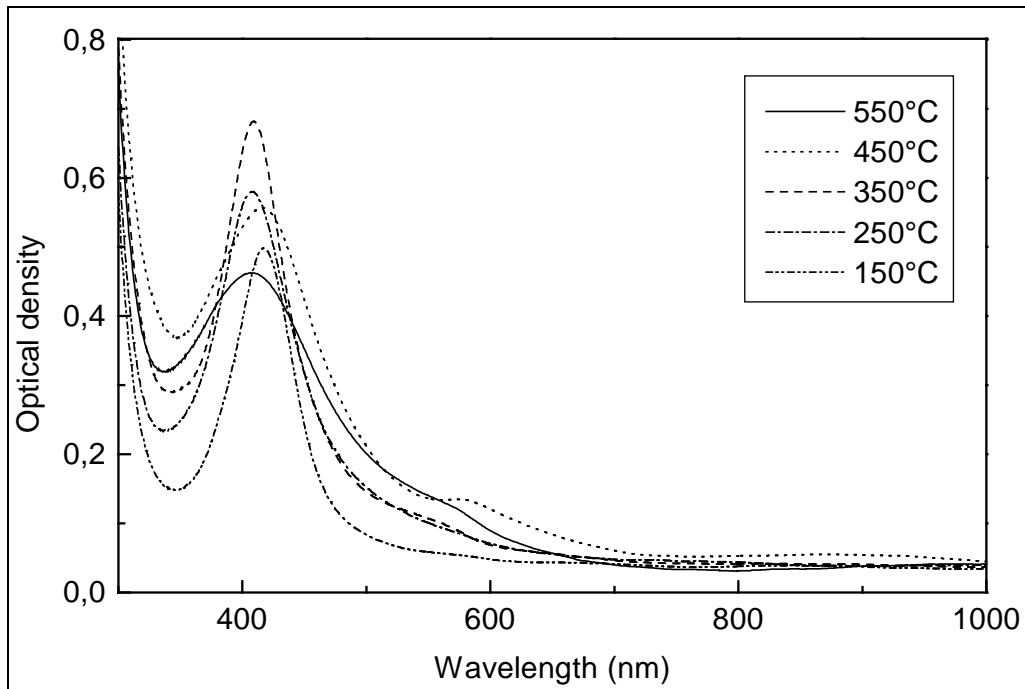


Figure A 49: UV-VIS absorption spectra of SiO₂ thin films containing Ag / Cu mixed colloids (molar ratio of Ag : Cu = 2 : 1) heat treated under reducing atmosphere (N₂ / H₂ = 92 / 8, 80 l/h), as a function of temperature, reference : air.

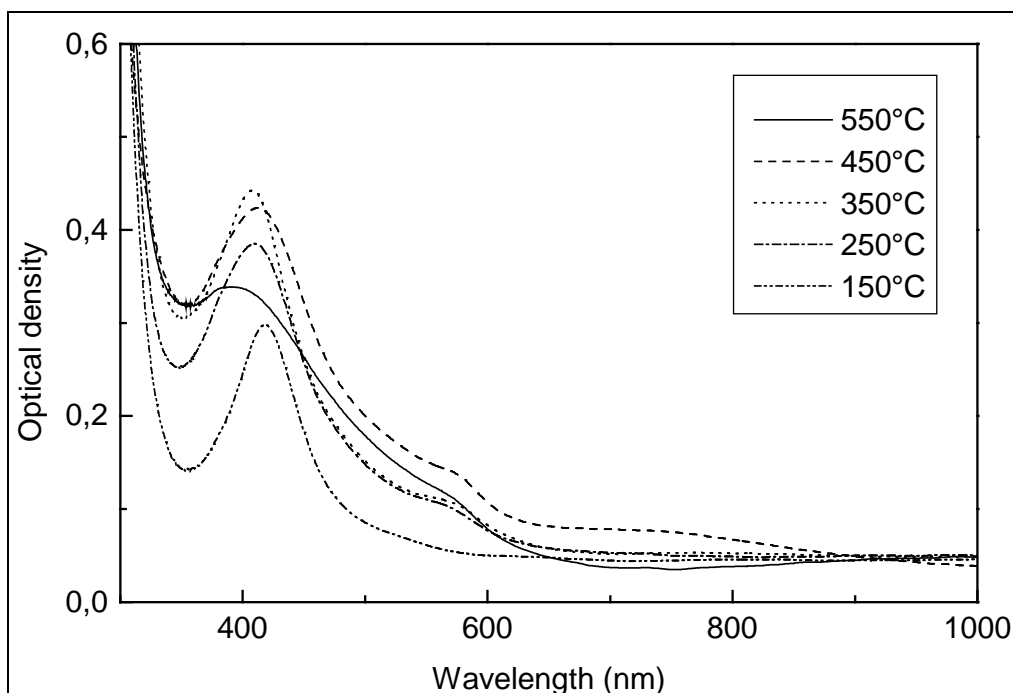


Figure A 50: UV-VIS absorption spectra of SiO₂ thin films containing Ag / Cu mixed colloids (molar ratio of Ag : Cu = 1 : 1) heat treated under reducing atmosphere (N₂ / H₂ = 92 / 8, 80 l/h), as a function of temperature; reference : air.

VIII REFERENCES

-
1. Encyclopaedia of Chemical Technology, Third Edition, Vol. **11**, p. 807
 2. Weyl, W.A., 'Coloured Glasses' Sheffield Soc. Glass Tech. 1951.
 3. Mie, G., Ann. Phys., **25** (1908) 377.
 4. Stooky, S.D. and Araujo, R.J., Appl. Optics, **7** (1969) 777.
 5. Mennig, M. and Berg, K.- J., Mat. Sci. Eng., **B(9)** (1991) 421.
 6. Kreibig, U., Physik Z., **224** (1969) 307.
 7. Sinzig, J., Radtke, U., Quinten, M. and Kreibig, U., Z. Phys. D, **26** (1993) 242.
 8. Hosono, H., Abe, Y., Lee, Y.L., Tokizaki, T. and Nakamura, A., Appl. Phys. Lett., **61** (1992) 2747.
 9. Hanamura, E., Oyo Butsuri, **59** (1990) 352
 10. Takada, T., Yano, T., Yasumori, A., Yamane, M. and Mackenzie, J.D., The 32nd Glass & Photonics Materials Meeting Osaka, 26-26 November 1999, p. 67.
 11. Nogami, M., Ozaki, K., Nagasaka, K. and Nakamura, A., The 37th Spring Meeting of Japan Applied Physics, 31a-N-1, 1990.
 12. Corning Glasses Nos. 2403 to 2434 and 3480 to 3486.
 13. Schott Glasses Nos. RG 610 to RG 715 and OG 5515 to OG 590.
 14. Vogel, W., Chemistry of Glass (translated by N. Kreidle), The American Ceramic Society Inc., Columbus, OH, 1985, p. 163.
 15. Jain, R.K. and Lind, R.C., J. Opt. Soc. Am., **73** (1983) 647.
 16. Yumoto, J., Fukushima, S. and Kubodera, K., Opt. Lett., **12** (1987) 832.
 17. Sakka, S. and Yoko, T., 'Structure and Bonding- 77, Edited by - Reisfeld, R. and Jorgensen, C.K', Springer- Verlag Berlin Heidelberg 1992, p. 89.
 18. Remillard, J.T. and Steel, D.G., Opt. Lett., **13** (1988) 30.
 19. Jerominek, H., Pigeon, M., Patela, S., Jakubezyk, Z., Delisle, C. and Trembley, R., Jl. of Appl. Phys., **63** (1988) 957.
 20. Paul, A., 'Chemistry of Glasses, Second Edition', Chapman & Hall, p. 116.
 21. Brinker, C.J. and Scherer, G.W., 'Sol-Gel Science: The Physics and Chemistry of Sol-Gel Science', (Academic Press, New York, 1990).
 22. Jones, P.W., 'Fundamental Principles of Sol-Gel Technology (The Institute of Metals, London, 1989)'.
'
 23. Hench, L.L. and West, J.K, Chem. Rev., **90** (1990) 33.

-
24. Ekimov, A.I., and Onushchenko, A.A., JETP Letter, **40** (1989) 1136.
 25. Efros, A.I. and Efros, A.A., Fiz. Tekhn. Polupr., **16** (1982) 1209.
 26. Davydov, A.S., Kvantova mekhanika, F. M. (1969) 149.
 27. Lifshitz, I.M. and Slesov, V.V., Zh. Eksp. Teor. Fiz., **88** (1969) 1490.
 28. Seitz, F., The Modern Theory of Solids (Mc. Graw-Hill, New York, 1940) p. 448.
 29. Goldman, A., Phys. Rev., **129** (1963) 69.
 30. Ekimov, A.I., Onushchenko, A.A., Pluhin, A.G. and Efros, A.I., Zh. Eksp. Teor. Fiz., **88** (1985) 1490.
 31. Ekimov, A.I., Efros, A.I. and Onushchenko, A.A., Solid State Comm., **56 (11)** (1985) 921.
 32. Goto, T., Takakashi, T. and Ueta, M., JI. of Phys. Soc. of Japan, **24(2)** (1968) 314.
 33. Ruller, J.A., Williams, G.M. and Friebele, E.J., Ceramic Transactions, Vol. **28**, (1992) 499, Solid-State Optical Materials.
 34. Lifshitz, M. and Slezov, V.V., JI. Expt. Theor. Phys., **35** (1952) 1479.
 35. Kadono, K. and Tanaka, H., Science and Technology of New Glasses, Proceedings of the international conference on science and technology of new glasses, Zenkyoren Building, Tokyo, October 16-17, (1991) p. 223.
 36. Sugimoto, N., Yamamoto, M., Manabe, T., Ito, S., Tokizaki, T., Kataoka, T. and Nakamura, A., Science and Technology of New Glasses, Proceedings of the international conference on science and technology of new glasses, Zenkyoren Building, Tokyo, October 16-17, (1991) p. 394.
 37. Tsunetomo, K., Shimizu, R., Kawabuchi, A., Kitayama, H. and Osaka, Y., Jap. JI. of App. Phys., **30(4B)** (1991) L764.
 38. Nogami, M., Zhu, Yi- Q., Tohyama, Y. and Nagasaka, K., J. Am. Ceram. Soc., **74 (1)** (1991) 238.
 39. Nogami, M., Zhu, Yi- Q. and Nagasaka, K., JI. of Non-Cryst. Solids, **134** (1991) 71.
 40. Reisfeld R., and Minti, H., JI. of Sol-Gel Science and Technology, **2** (1994) 641.
 41. Facht, R., Müller, M. and Bürger, H., JI. of Sol-Gel Science and Technology, **11** (1998) 197.
 42. Cardona, M., Physical Review, **129(1)** (1963) 69.
 43. Kato, Y., Yu, C.I. and Goto, T., JI. Phys. Soc. of Japan, **28(1)** (1970) 104.

-
44. Takahashi, T. and Goto, T., *Jl. Phys. Soc. of Japan*, **25(2)** (1968) 461.
 45. Toyozawa, Y., *Jl. Phys. Chem. Solids*, **25** (1964) 59.
 46. Ruller, J.A., Ginther, R.J., Williams, G.M., Justus, B.L., Camopillo, A.J. and Friebele, E.J., *Ceramic Transactions*, Vol-**14** (1990) 151.
 47. Mie, G., *Ann. Phys.*, **25** (1908) 377.
 48. Kreibig, U., *Jl. Phys. F*, **4** (1974) 999
 49. Henglein, A., *Jl. Phys. Chem.*, **97** (1993) 5457.
 50. Doyle, W.T., *Phys. Rev.*, **111** (1958) 1067.
 51. Matsuoka, J., Mizutani, R., Nasu, H. and Kamiya, K., *Jl. of Cer. Soc. Japan*, **100** (1992) 599.
 52. Matsuoka, J., Mizutani, R., Kaneko, S., Nasu, H., Kamiya, K., Kadano, K., Sakaguchi, T. and Miya, M., *Jl. of Cer. Soc. Japan*, **101** (1993) 51.
 53. Kozuka, H. and Sakka, S., Presented at Ann. Mtg. Ceram. Soc. Jpn., May 1992.
 54. Innocenzi, P., Kozuka, H. and Sakka, S., *Jl. of Sol-Gel Science and Technology*, **1** (1994) 305.
 55. Johnson, B.F.G., and David, R., in *Comprehensive Inorganic Chemistry 3* [Pergamon, New York, (1973) 129].
 56. Schubert, U., Amberg-Schwag, S., Breitscheider, B. and Schmidt, H., US patent 07/482.860 (1990).
 57. Mennig, M., Spanhel, L., Betzholz, S. and Schmidt, H., *Jl. Non-Cryst. Solid*, **147 & 148** (1992) 326.
 58. Mennig, M., Schmitt, M. and Schmidt, H., *Jl. of Sol-Gel Sci. Tech.*, **8** (1997) 1035.
 59. Vogel, H., *Glasshemie* (Springer, Berlin, 1992).
 60. Burkhart, T., Mennig, M., Schmidt, H. and Licciulli, A., *Better Ceramics Through Chemistry, VI-MRS Symp. Proc.* **346** (1994) 779.
 61. Spanhel, L., Mennig, M. and Schmidt, H., *Sol-Gel Glass Surface Archaeometry Education*, (1992) S 9.
 62. Mennig, M., Schmitt, M., Becker, U., Jung, G. and Schmidt, H., *SPIE Vol.* **2288** *Sol-Gel Optics III* (1994) 130.
 63. M. Mennig, U. Becker, M. Schmitt and H. Schmidt, 8th CIMTEC proceeding Florenz, 01.07.1994 - 04.07.1994.

-
64. Nogami, M., Abe, Y., *Jl. of Mat. Res.*, **10 (10)** (1995) 2648
 65. Toshima, N. and Wang, Y., *Langmuir*, **10** (1994) 4574.
 66. Wang, Y. and Liu, H., *Polym. Bull.*, **25** (1991) 139.
 67. Esumi, K., Shiratori, M., Ishizuka, H., Tano, T., Torigoe, K. and Meguro, K., *Langmuir*, **7** (1991) 457.
 68. Sato, T., Kuroda, S., Takami, A., Yonezawa, Y. and Hada, H., *Appl. Organo. Chem.*, **5** (1991) 261.
 69. Harada, M., Asakura, K., Ueki, Y. and Toshima, N., *Jl. Phys. Chem.*, **96** (1992) 9730.
 70. Toshima, N., Harada, M., Yamazaki, Y. and Asakura, K., *Jl. Phys. Chem.*, **96** (1992) 9927.
 71. Vasan, H.N. and Rao, C.N.R., *Jl. Mater. Chem.*, **5(10)** (1995) 1755.
 72. Itakura, T., Torigoe, K. and Esumi, K., *Langmuir*, **11** (1995) 4129.
 73. Wang, Y., Gui, L. and Tang, Y., *Chin. Jl. Chem.*, **12** (1994) 11.
 74. Morriss, R.H. and Collins, L.F., *The Jl. of Chem. Phys.*, **41 (11)** (1964) 3357.
 75. Aden, A.L. and Kerker, M., *Jl. Appl. Phys.*, **22** (1951) 1242.
 76. Mulvaney, P., Giersig, M. and Henglein, A., *Jl. Phys. Chem.*, **97** (1993) 7061.
 77. Mulvaney, P., *Langmuir*, **12** (1996) 788.
 78. Schlüter, M., *Z. Phys.*, **250** (1972) 87
 79. Ripken, K., *Z. Phys.*, **250** (1972) 228.
 80. Papavassiliou, G.C., *Jl. Phys. F. Met. Phys.*, **6** (1976) L103.
 81. Fukutani, H. and Sueoka, O., "In Optical Properties of Electronic Structure of Metal and Alloys", Abeles, F., Ed., Wiley New York, 1966, p. 565.
 82. Baddeley, C.J., Jefferson, D.A., Lambert, R.M., Ormerod, R.M., Rayment, T., Schmid, G. and Walker, A.P., *Mat. Res. Soc. Symp. Proc.*, Vol. **272** (1992) 85.
 83. Lee, A.F., Baddeley, C.J., Hardcare, C., Ormerod, R.M., Lambert, R.M., Schmid, G. and West, H., *Jl. Phys. Chem.*, **99** (1995) 6096.
 84. Bradley, J.S., Hill, E.W., Klein, C., Chaudret, B. and Duteil, A., *Chem. Mater.*, **5** (1993) 254.
 85. Esumi, K., Tano, T., Torigoe, K. and Meguro, K., *Chem. Mater.*, **2** (1990) 564.
 86. Mulvaney, P., Giersig, M. and Hanglein, A., *Jl. Phys. Chem.*, **96** (1992) 10419.
 87. Liz-Marzan, L.M., and Philipse, A.P., *Jl. Phys. Chem.*, **99** (1995) 15120.

-
88. West, R.C., Handbook of Chemistry and Physics, 56th ed., CRC Press: Cleveland. OH. 1975; p D-141.
 89. Silvert, P.-Y., Vijayakrishnan, V., Vibert, P., Herrera-Urbena, R., Elhsissen, K.T., Nanostructured Materials, **7(6)** (1996) 611.
 90. Torigoe, K. and Esumi, K., Langmuir, **9** (1993) 1664.
 91. Torigoe, K., Nakajima, Y. and Esumi, K., JI. Phys. Chem., **97** (1993) 8304.
 92. Aihara, N., Torigoe, K. and Esumi, K., Langmuir, **14** (1998) 4945.
 93. Yonezawa, T. and Toshima, N., JI. Chem. Soc. Faraday Trans., **91(22)** (1995) 4111.
 94. Hirai, H., Chawanya, H. and Toshima, N., JI. Macromol. Sci. Chem., **A13** (1979) 727
 95. Magruder III, R.H., Osborne Jr., D H. and Zuhr, R.A., JI. of Non-Cryst. Solids, **176** (1994) 299.
 96. Ehler, T.T. and Noe, L. J., Langmuir, **11** (1995) 4177.
 97. Baba, K., Okuno, T. and Miyagi, M., JI. Opt. Soc. Am., **B (12)** (1995) 2372.
 98. Teo, B.K., Keating, K. and Kao, Y.-H., J. Am. Chem. Soc., **109** (1987) 3494.
 99. Rivory, J. and Theye, M. L., Le JI. de Physique Letters, **36** (1975) L-129.
 100. Nilsson, P.O., Lindau, I. and Hagström, S.B.M., Phys. Rev. B, **1(2)** (1970) 498
 101. Gonellaa, F. Mattei, G., Mazzoldi, P., Spizzo, F., Quaranta, A. and De, G., Philo. Maga. B, **76(4)** (1997) 615.
 102. Mennig, M., Schmitt, M., Schmidt, H., Berg, K.-J., Postendorfer, J., Fundamentals of Glass science and Technology Vol. XXIII (1993) 357.
 103. West, A. R., 'Solid state chemistry and its applications', John Wiley & Sons, New York 1984.
 104. Thompson-Russel, K.C., and Edington, J.W., 'Practical Electron Microscopy in Material Science, Monograph, Interpretation of Transmission Electron Micrographs,' N. V. Philips, Eindhoven, 1974.
 105. Peters, D.G. and Caldwell, R.L., Inorganic Chemistry, **6** (1967) 1478.
 106. Cotton, F.A. and Wilkinson, G., Advanced Inorganic Chemistry, p. 906.
 107. Ekimov, A.I., Efros, A.L. and Onushchenko, A.A., Solid State Communications, **56** (1985) 921.
 108. Powder Diffraction File, Inorganic Phases, page 184 & 185.
 109. Ullmanns Encyclopedia of Industrial Chemistry, Vol. **A7** Page 573.

-
110. Powder Diffraction File, Inorganic Phases, Page 185.
 111. Ullmann's Encyclopedia of Industrial Chemistry, Vol. **A7**, p. 587.
 112. Sugasaka, K. and Fujii, A., Bull. of Chem. Soc. of Japan, **49(1)** (1976) 82.
 113. Kaifu, Y. and Komatsu, T., Phys. Stat. Sol. **(b)48**, (1971), K125.
 114. Garro, N., Cantarero, A., Cardona, M., Ruf, T., Göbet, A., Lin, C., Reimann, K., Rübenacke, S. and Steube, M., Solid State Communications, **98(1)** (1996) 27.
 115. Ringeissen, J., Coret A. and Nikitine, S., Localized Excitations in Solids (Plenum Press), p. 297 (1968).
 116. Toyozawa, Y., Progr. Theory. Phys., **27** (1962) 89.
 117. Powder Diffraction File, Inorganic Phases, page 184 & 185.
 118. Figgies, B.N., Introduction to Ligand Field (Wiley, New York, 1966) p. 306.
 119. Concise Inorganic Chemistry, J. D. Lee, P. 825 (1996).
 120. Toyozawa, I., JI. Phys. Chem. Solids, **25** (1964) 59.
 121. Börnstein, L., Numerical Data and Fundamental Relationship in Science and Technology, II-VI Compounds, New Series III 17b, Ed. O. Madelung, Springer Verlag, Berlin 1982.
 122. Yashima, M., Ishizawa, N. and Yoshimura, M., JI. Am. Ceram Soc., **75(6)** (1992) 1550.
 123. Hirai, H., Nakao, Y., Toshima, N., JI. Macromol. Sci. Chem., **A12** (1979) 1117.
 124. Meguro, K., Nakamura, Y., Hayashi, Y., Torizuka, M., Esumi, K., Bull. Chem. Soc. Japan, **61** (1988) 347.
 125. Turkevich, J., Stevenson, P.C. and Hiller, J., Disc. Faraday Soc., **11** (1951) 55.
 126. Kreibig, U. and Fragstein, C.V., Z. Physik, **224** (1969) 307.
 127. Quinten, M., Ph.D. thesis, Universität des Saarlandes, Saarbrücken (1989).
 128. Brown, K.R. and Natan, M.J., Langmuir, **14** (1998) 726.
 129. Bohren, C.F. and Hoffman, D.R., Absorption and Scattering of Light by Small Particles, Wiley: New York, 1983.
 130. Scholze, H., 'Glas- Natur, Structure und Eigenschaften', Springer Verlag Berlin 1988.
 131. Strawbridge, I. and James P.F., British Ceramic Proceedings, **38** (1986) 251.
 132. James P.F., Chen, M. and Jones, F.R., JI. Non-Cryst. Solids, **155** (1993) 99.
 133. Kalleder, A., Ph.D. Thesis, Saarbrücken 1998.
 134. Mie, G., Ann. Phys., **25** (1908) 377.

-
135. Fukutani, H. and Sueoka, O., In Optical Properties and Electronic Structure of Metals and Alloys, F. Abeles, Ed. Wiley, New York, 1966.
 136. Mulvaney, P., Langmuir, **12** (1996) 788.
 137. Morris, R.H. and Collins, L.F., The JI. of Chem. Phys., **41(11)** (1964) 3357.
 138. Baba, K., Okuno, T. and Miyagi, M., JI. Opt. Soc. Am., **B (12)** (1995) 2372.
 139. Teleshova, A.S., Teleshov, E.N. and Pravednikov, A.N., Vysokomol. Soedin (1995) 2372.
 140. Teleshova, A.S., Teleshov, E.N. and Pravednikov, A.N., Vysokomol AB **10(13)** (1971) 2309, Engl. Trans. Polym. Sci. USSR, **13** (1971) 2593
 141. LeBlanc, M. and Erlen, W., Ann. Phys, **16** (933) 321.
 142. Spanhel, L., Mennig, M. and H. Schmidt, Bol. Soc. Esp. Ceram. Vid. 31-C Vol **7** (1992) 268.
 143. Schmitt, M., Ph.D. thesis, Saarbrücken 1998.
 144. Schmidt, H., Multifunctional inorganic organic composite sol-gel coatings for glass surfaces, Proc. PACRIM meeting, Nov. 7-10, 1993, Honolulu, Hawaii.
 145. Ehler, T.T. and Noe, L.J., Langmuir, **11** (1995) 4177.
 146. Baitinger, W.E., French, P.W. and Swart, E.L., JI. Non-Cryst. Solids, **38-39** (1980) 749.
 147. Colombin, L., Charlier, H., Jelli, A., Debras, G. and Verbist, J., JI. Non-Cryst. Solids, **38-39** (1980) 551.
 148. Seiger, J.S., JI. Non-Cryst. Solids, **19** (1975) 213.
 149. Ernsberger, F.M., US Patent 4 155 735 (1979).
 150. Silvert, P-Y., Urbina, R.H., Duvauchelle, N., Vijaykrishnan, V. and Elhsissen K. T., JI. Mater. Chem., **6(4)** (1996) 573.
 151. De, G., Licciulli, A., Massaro, C., Tapfer, L., Catalana, M., Battaglin, G., Meneghini, C. and Mazzoldi, P., JI. of Non-Cryst. Solids, **194** (1996) 225.
 152. Mennig, M., Schmitt, M., Kutsch, B. and Schmidt H., SPIE Vol. **2288**, Sol-gel Optics III (1994) 120.
 153. De, G., Gusso, M., Tapfer, L., Catalano, M., Gonella, F., Mattei, G., Mazzoldi P. and Battaglin, G., JI. of Appl. Phys., **80(12)** (1996) 6734.
 154. Hansen, M., Constitution of Binary Alloys, 2nd ed., McGraw-Hill, New York, 1958, p. 18.
 155. Cable, M. and Xiang, Z.D., Phys. and Chem. Glasses, **33** (1992) 154.

156. Rivory, J., Physical Review B, **15(6)** (1977) 3119.
157. De, G., JI. of Sol-Gel Science and Technology, **11** (1998) 289.